

**The Evolution of Shell Form
in
Tropical Terrestrial Microsnails**

Liew Thor Seng

Disclaimer

This thesis is not issued for purposes of Zoological nomenclature and is not published within the meaning of the International Code of Zoological Nomenclature (1999: Article 8).

The Evolution of Shell Form in Tropical Terrestrial Microsnails

Proefschrift

**ter verkrijging van
de graad van Doctor aan de Universiteit Leiden,
op gezag van Rector Magnificus prof.mr. C.J.J.M. Stolker,
volgens besluit van het College voor Promoties
te verdedigen op woensdag 18 juni 2014
klokke 11.15 uur**

door

**Liew Thor Seng
geboren te Johor Bahru (Maleisië)
in 1980**

Promotiecommissie

Promotor

Prof. dr. M. Schilthuizen

Overige leden

Prof. dr. C.J. ten Cate

Prof. dr. P.M. Brakefield (University of Cambridge)

Prof. dr. E.F. Smets

Prof. dr. G.J. Vermeij (University of California)

Dr. W. Renema (Naturalis Biodiversity Center)

© Liew Thor Seng



Creative Commons Attribution License (CC BY 4.0).

ISBN 978-90-9028246-6

PhD thesis Leiden University. An electronic version of this dissertation is available at <https://openaccess.leidenuniv.nl>

The thesis printed by GVO printers & designers B.V.



The research presented in this thesis was supported by the Netherlands Organization for Scientific Research (NWO, grant no. 819.01.012).

Contents

Nederlandse Samenvatting	7
Chapter 1 Introduction and Summary	13
Chapter 2 A cybertaxonomic revision of the micro-landsnail genus <i>Plectostoma</i> Adam (Mollusca, Caenogastropoda, Diplommatinidae), from Peninsular Malaysia, Sumatra and Indochina	19
Chapter 3 On growth and form of a heteromorphic terrestrial snail: <i>Plectostoma concinnum</i> (Fulton, 1901) (Mollusca: Caenogastropoda: Diplommatinidae)	113
Chapter 4 A method for quantifying, visualising, and analysing gastropod shell form	137
Chapter 5 Association between shell morphology of micro-land snails (genus <i>Plectostoma</i>) and their predator's predatory behaviour	165
Chapter 6 An ontogenetic perspective on the evolution of shell size and shell shape in the land snail genus <i>Plectostoma</i>	195
References	217
Curriculum Vitae	245

Nederlandse Samenvatting

De Mollusca vormen een belangrijk fylum van het dierenrijk. De eerste mollusken verschenen gedurende het Cambrium, en heden ten dage is het, na de Arthropoda, in omvang het tweede dierlijke fylum met meer dan 100 000 recente soorten (Bieler, 1992; Brusca and Brusca, 2003). De klasse Gastropoda neemt 80% van de recente soorten van de Mollusca voor haar rekening. Ondanks deze soortenrijkdom is een gegeneraliseerde schelpbouw bij slakken gehandhaafd vanwege behoudende ontwikkelingsprocessen. Alle huisjesslakken groeien in één richting doordat de mantelrand schelpmateriaal toevoegt aan de mondrand. De groeisnelheid van de schelp kan variëren. Deze ontogenese van de schelp, of eigenlijk deze ontogenese van de mondopening, veroorzaakt de algemene spiraalvorm van schelpen. De feitelijke vorm van de spiraal kan echter variëren door verschillen in de aspecten van deze mondopening-ontogenese, met name de snelheid en richting van het afzetten van schelpmateriaal om de mondopening, de grootte en vorm van de mondopening (d.w.z. de mantelrand), en de totale duur van de schelp-ontogenese. De interactie tussen deze ontwikkelingsparameters heeft een grote variatie in schelpvormen veroorzaakt. Taxonomen en evolutiebiologen proberen nu de evolutie van deze veelheid van vormen te karakteriseren en te begrijpen.

De variabiliteit in schelpvorm is een van de hoekstenen van de taxonomie van de Gastropoda. Gewoonlijk is de variabiliteit van de schelpen van soorten van hetzelfde genus vrij gering, en taxonomen beschrijven soorten vaak op basis van subtiele verschillen van de kenmerken van de schelp, zoals de grootte, de verhouding van de hoogte tot de breedte, de richting van de winding, de sculptuur van het schelpoppervlak, of de morfologie van de mondopening. De soorten van verscheidene genera van landslakken, zoals *Plectostoma* en *Opisthostoma* (Diplommatinidae), vertonen echter een grotere variatie in schelpvormen. Deze grotere variatie is voornamelijk te danken aan de laatste winding, die bij sommige soorten onregelmatig gebogen is (van Benthem Jutting, 1952; Vermeulen, 1991; Vermeulen, 1994). Dergelijke verschillen vormen een uitdaging voor het nauwkeurig beschrijven en vergelijken van de schelpen, omdat het bepalen van homologiën en synapomorfiën bij deze schelpen problematisch is (van Benthem Jutting, 1952).

In **Hoofdstuk 2** worden de niet-Borneose soorten van *Plectostoma*, die meer variatie in schelpvorm vertonen dan de Borneose soorten, gereviseerd. De schelpkenmerken worden getaxiseerd op basis van ontwikkelingshomologieën, genetische en 3D-morfometrische gegevens. Dit leidt ertoe dat het subgenus *Plectostoma* de status van zelfstandig genus krijgt, gebaseerd op de genetische en oecologische gegevens. Dit hoofdstuk suggereert dat er meer biologisch informatieve schelpkenmerken kunnen worden verkregen als men de schelp beschouwt als een versteende ontogenie dan wanneer men de schelp opvat als een vast geometrisch voorwerp.

In **Hoofdstuk 2** wordt voorts aangetoond dat de schelpvormen van *Plectostoma* en de verschillende mondopening-ontogeneses op een kwalitatieve manier kunnen worden geanalyseerd en vergeleken. Het blijft echter onbekend hoe veranderingen in het ontogenese-

profiel van de mondopening een specifieke schelpvorm veroorzaken. De situatie wordt gecompliceerd door het feit dat de grootte en vorm van een schelp ook nauw verbonden zijn aan de groeisnelheid van de schelp. Er zijn maar weinig onderzoeksgegevens bekend over hoe het mondopening-ontogeneseprofiel en de groeisnelheid van de schelp samen de vorm van de schelp bepalen. Dit is omdat groei en vorm moeilijk gelijktijdig te kwantificeren en te bestuderen zijn.

Daarom wordt in **Hoofdstuk 3** geprobeerd dit hiaat op te vullen door te onderzoeken hoe groei en vorm veranderen gedurende de ontogenese van één speciale soort, *Plectostoma concinnum*. Bij deze soort bestaat de schelp uit drie delen: de regelmatig gewonden spiraalfase, de insnoeringsfase die de overgang vormt naar de laatste fase, die van de afwijkend gewonden tuba. Er wordt een nieuw gedefinieerde ontogenese-as gebruikt waarmee gelijktijdig de verbanden tussen en de veranderingen in groeisnelheid en het profiel van de mondopeningsontogenese kunnen worden geanalyseerd. Er wordt aangetoond hoe de veranderingen in de mondopeningontogenese-profielen met betrekking tot vorm van de mondopening, grootte en groeirichting, en de veranderingen in groeisnelheid, verbonden zijn met verschillende schelpvormen gedurende verschillende perioden van de schelp-ontogenese. Met andere woorden, de schelpvorm kan gekwantificeerd worden als een mondopeningsontogenese-profiel. Dit hoofdstuk benadrukt ook het feit dat, hoewel plausible functies van mantelrand en de columellaire spier opgemaakt kunnen worden uit de registratie van mondopeningsontogenese-profielen vastgelegd in een schelp, het toch van belang is de anatomie en werking van deze organen te bestuderen om de onderliggende mechanismen die de profielen veroorzaken te begrijpen.

De resultaten van **Hoofdstuk 3** benadrukken ook de beperkingen van de traditionele lineaire meting en de geometrische morfometrie bij de kwantificatie van de schelpvorm. Hoewel deze kwantificatiemethoden meetbare vormverschillen tussen schelpen kunnen opleveren, kunnen deze verschillen nauwelijks rechtstreeks vanuit het aspect van mondopeningsontogenese worden afgeleid. Lineaire metingen enerzijds leveren de absolute grootte van een schelp maar kunnen de vorm van de gewonden schelp niet bevatten. Geometrische morfometrie (GM) anderzijds, levert informatie over de vorm van een schelp door homologe punten, lijnen of oppervlakten te vergelijken. Echter kunnen deze homologieën, of ze nu betrekking hebben op de ontwikkeling, de evolutie of de geometrie, niet universeel worden gedefinieerd voor verschillende schelpvormen en voor verschillende onderzoeken. Geometrische morfometrie werd ontwikkeld door Bookstein (1977, 1980) die het idee van Thompson (1917: Hoofdstuk 17, "On the theory of transformations, or the comparison of related form") formaliseerde. Ironisch genoeg heeft Thompson (1917) schelpvormen niet met zijn eigen methode vergeleken, terwijl recente biologen GM snel hebben geadopteerd om schelpvormen te vergelijken. In plaats daarvan gebruikte Thompson een logaritmische spiraal benadering, wat er op kan duiden dat hij zich bewust was van de beperkingen van de aanpak van schelpvorm analyse met GM.

Met het oog op deze beperkingen werd een methode om de slakkenhuisvorm te kwantificeren, te visualiseren en te analyseren ontwikkeld in **Hoofdstuk 4**. Het zou niet mogelijk geweest zijn om deze methode, die is gebaseerd op ideeën van theoretische

modellering van de schelpvorm en uit **Hoofdstuk 3**, te ontwikkelen zonder de ontwikkeling van moderne technologie van grafische apparatuur voor computers, flexibele 3D software voor modellering, en 3D scanning instrumenten. Om te beginnen werd de topologie van de schelp herzien in overeenstemming met de mondopeningsontogenese. Vervolgens werden de mondopeningsontogenese-profielen afgeleid uit berekening van de baan van de mondopeningsgroeï, de vorm van de mondopening en de ontogenese-as. Tenslotte werden de overeenkomsten tussen schelpvormen bepaald door hun mondopeningsontogenese-profielen te vergelijken. De onderliggende veranderingen in mondopeningsontogenese-profielen die de verschillen tussen schelpvormen hebben veroorzaakt kunnen met deze methode onderzocht worden. Daarenboven kan het netwerkmodel van de hertopologiseering worden gebruikt voor functioneel-morfologische analyse en voor de evaluatie van theoretische modellen van schelpen. Bovendien kan de similariteitsmatrix voor schelpen gebaseerd op de mondopeningsontogenese-profielen geanalyseerd worden samen met andere afstandsmatrices zoals fylogenetische afstand, geografische afstand of milieu-afstand.

Nadat de groei en vorm van morfologisch gevarieerde en ongewone schelpen geanalyseerd werd in de twee voorafgaande hoofdstukken worden nu de functionele aspecten van de meer opvallende eigenschappen van de schelpen van *Plectostoma*-soorten onderzocht, zoals daar zijn de geprononceerde radiale sculptuur en de vervormd-gedraaide tuba. Over het algemeen genomen dienen de schelpen van landslakken voor bescherming tegen predatie en uitdroging. Van zeeslakken is bekend dat schelpkenmerken gelijkend op die van *Plectostoma* een functie hebben om predatie tegen te gaan (Vermeij, 1993; Allmon, 2011). Daarom wordt in **Hoofdstuk 5** onderzocht of deze eigenschappen van de *Plectostoma*-schelp aanpassingen kunnen zijn die dienen als verdediging tegen een van haar bekende predators namelijk de naaktslak *Atopos*.

Atopos naaktslakken hebben twee strategieën om hun prooi te overheersen, namelijk naar binnen dringen door de mondopening van de schelp en een gat boren in de schelp. Op deze manieren vallen ze *Plectostoma concinnum*, *P. cf. ornatum*, *P. fraternum* en andere, nauw verwante, soorten aan in Sabah, Maleisisch Borneo. Het gedraaide tubadeel van de schelpen van deze slakken is een effectieve verdediging tegen een aanval door middel van binnendringen via de mondopening. Echter, als de naaktslak er niet in slaagt via de mondopening binnen te dringen, zal ze overgaan op de strategie van het boren in de schelp, die meer energie kost. Er zijn aanwijzingen dat de naaktslak er de voorkeur aan geeft om gaten te boren in schelpen zonder sculptuur. In ieder geval garanderen noch de verbogen tuba, noch de geprononceerde sculptuur richels de overleving van een slak. Nadere analyse onthult dat het ontbreken van volledige effectiviteit van deze anti-predatie schelpeigenschappen zou kunnen worden veroorzaakt door een functionele balans tussen beide kenmerken onder selectiedruk van twee verschillende predatiestrategieën.

In **Hoofdstukken 2-5** wordt belicht hoe de schelpvormen van *Plectostoma* kunnen verschillen tussen de soorten, hoe de schelpvorm kan veranderen tussen verschillende ontwikkelingsstadia van een soort, en hoe de eigenschappen van verschillende schelpkenmerken een anti-predatie functie kunnen hebben. Een van de overgebleven vraagstukken is hoe de *Plectostoma* schelpvormen zijn veranderd en verschillende vormen

hebben aangenomen in de loop van de evolutie. De overdadige convergente en parallelle evolutie van de schelpvormen bij de Gastropoda is algemeen bekend. Veel studies hebben dit patroon onderzocht vanuit het gezichtspunt van het belang van aanpassing van de schelp vorm. Dit vooronderstelt functionaliteit van de schelp als reactie op selectiedruk. In feite zijn evolutionaire veranderingen in schelpvorm alleen mogelijk als de onderliggende schelpontogenese ook verandert. Er is echter een schaarste aan onderzoeken die de evolutie van de schelpvorm proberen te begrijpen in het licht van de noodzakelijke veranderingen van de schelpontogenese.

In **Hoofdstuk 6** wordt de evolutie van de schelpvormen bij *Plectostoma* onderzocht vanuit het gezichtspunt van de schelpontogenese. om te beginnen worden mondopeningsontogenese-profielen opgesteld zoals in **Hoofdstuk 3** en **Hoofdstuk 4**, en worden schelpkenmerken vastgesteld zoals in **Hoofdstuk 2**, en tenslotte wordt de fylogenie van *Plectostoma* soorten gereconstrueerd. De gegevens van alle drie deze bronnen worden vergeleken, en de patronen van kenmerkevolutie voor schelpvorm vanuit een *morphospace*-perspectief besproken. De resultaten suggereren dat de fylogenetische historie de veranderingen in de schelpontogenese, en de resulterende schelpvormen bij *Plectostoma* niet beperken. Voorts kunnen soorten met een overeenkomstige schelpvorm een eigen unieke mondopeningsontogenese-profiel hebben, terwijl bepaalde aspecten van de ontwikkeling van schelpgrootte een conservatief ontwikkelingsprogramma tussen de soorten behouden.

Samenvattend onthult dit proefschrift verscheidene tot nu toe onbekende aspecten van de schelpvormen bij *Plectostoma*, betreffende ontwikkelingshomologieën, het ontogenese-profiel van de mondopening, hun functie om predatie tegen te gaan, en evolutionaire patronen van schelpkenmerken en ontogenetische *morphospace*-evolutie. In feite zijn dit vraagstukken waar biologen al eeuwen op studeren met het doel om de schelpvormen beter te beschrijven en het begrip van de evolutie van de schelpvorm te verbeteren. In veel wetenschapsgebieden hebben verbeterde technieken nieuwe methodes geleverd om klassieke vraagstellingen aan te pakken. Dit geldt ook voor dit proefschrift. De 3D-technologie die in ieder hoofdstuk van dit proefschrift intensief gebruikt is, heeft nieuwe dimensies geopend in de manier waarop deze klassieke vraagstukken benaderd kunnen worden, en levert belangrijke inzichten op voor de bestudering van de schelpvorm.

Chapter 1

Introduction and summary

Thesis Outline

Mollusca form an important animal phylum that first appeared in the Cambrian, and today is, after Arthropoda, the second largest animal phylum, with more than 100,000 extant species (Bieler, 1992, Brusca and Brusca, 2003), with the class Gastropoda accounting for 80% of the extant species in the Mollusca. Despite its species-richness, a generalised gastropod shell architecture is maintained because of conserved developmental processes. All of the shelled-gastropods grow by adding, in a unidirectional accretionary way, shell material with the mantle edge organ, usually at different deposition rates around the existing aperture. This shell ontogeny, or to be more specific aperture ontogeny, gives the general spiral form for the shells. However, spiral forms can vary when there are changes in any one of the aspects in the aperture ontogeny profiles, namely, the rate and direction of shell deposition around the aperture, size and shape of the aperture (i.e. mantle edge), and the total length of the shell ontogeny processes. The interplays between these developmental parameters have generated a great diversity in shell form, for which taxonomists and evolutionary biologist are now trying to accurately characterise and to understand with regard to its evolution.

The variability in shell form is one of the cornerstones of gastropod taxonomy. Usually, shell form variability between species at genus level is quite small, and taxonomists frequently describe a species based on subtle differences in shell characters, such as size, height-width proportions, coiling direction, shell surface ornamentation, or aperture morphology. However, species in several land snail genera, such as *Plectostoma* and *Opisthostoma* (Diplommatinidae), exhibit a greater diversity in shell forms, largely due to the last whorl, which, in some species is coiled irregularly (van Benthem Jutting, 1952; Vermeulen, 1991; Vermeulen, 1994). Such disparity, poses a challenge to describe and compare the shell accurately, because homologisation and the determination of shell synapomorphies in these taxa is problematic (van Benthem Jutting, 1952).

In **Chapter 2**, I revise non-Borneo *Plectostoma* species, which are more diverse in their shell form than Bornean *Plectostoma*. I appraise the shell characters on the basis of developmental homology, genetic and 3D morphometric data. As a result, the subgenus *Plectostoma* is elevated to genus status based on the genetic and ecological data, and 10 new *Plectostoma* species are described together with the existing 21 species, based on the redefined shell characters and genetic data. This chapter suggests that more biologically informative shell characters can be obtained when the shell is viewed as a petrified ontogeny, rather than as a solid geometrical object.

The shell forms of *Plectostoma* and their underlying aperture ontogeny differences can be characterised and compared in a qualitative manner as shown in **Chapter 2**. However, it remains unknown how changes in the aperture ontogeny profile may generate a particular shell form. To complicate matters further, the size and shape of a shell are known to have a close association with the shell growth rate. Thus, few empirical data are available on how the aperture ontogeny profiles and shell growth rates determine shell form because growth and form are difficult to quantify and examine simultaneously.

Hence, I attempt to fill this gap in **Chapter 3** by examining how growth and form change along the shell ontogeny in one particular species, *Plectostoma concinnum*. Its shell consists of three shell parts: the regularly-coiled spire phase, the transitional constriction phase, and the distortedly-coiled tuba phase. I use a newly defined ontogeny axis to simultaneously analyse the associations between and changes in growth rates and aperture ontogeny profile. As a result, I show how the changes in the aperture ontogeny profiles in terms of aperture shape, size and growth trajectory, and the changes in growth rates, are associated with different shell forms at different stages of the shell ontogeny. In other words, shell form can be quantified as an aperture ontogeny profile. This chapter also highlights the fact that while a plausible roles for mantle edge and columellar muscle can be inferred from the record of aperture ontogeny profiles contained in a shell, it is important to study the anatomy and behaviour of these two organs to understand the underlying mechanisms that create the profiles.

The outcome of **Chapter 3** also highlights the limitation of the traditional linear measurement and geometric morphometrics in the quantification of shell form. While these quantification methods can provide measurable form differences between shells, these differences can hardly be interpreted directly from the aspect of aperture ontogeny. Linear measurements, on the one hand, give absolute size of a shell but cannot capture the shape of the spiral shell. Geometric morphometrics (GM), on the other hand, provide shape information of a shell by comparing homologous landmark points, lines or surfaces. However, these homologies, either developmental, evolutionary or geometric cannot be universally defined across different shell forms, different species, and different studies. Geometric morphometrics was developed by Bookstein (1977, 1980) who formalised the idea of Thompson (1917: Chapter 17, “On the theory of transformations, or the comparison of related form”). Ironically, while recent biologists have quickly adopted GM to compare shell forms, Thompson (1917) himself did not compare shell forms with his own transformation method, instead using a logarithmic spiral approach, which may suggest he was aware of the limitations in addressing shell shape analysis with GM.

In view of these limitations, I develop a new method for quantifying, visualising and analysing gastropod shell form in **Chapter 4**. I would not have been able to develop this method, which is based on ideas from theoretical modelling of shell form and from **Chapter 3**, without the development of state-of-the-art technology in computer graphic hardware, flexible 3D modelling software, and 3D scanning instrumentation. First, the shell was retopologised according to the aperture ontogeny. Then, the aperture ontogeny profiles were extracted by calculation of aperture growth trajectory, aperture form and ontogeny axis. Lastly, the similarities between shell forms were determined by comparing their aperture ontogeny profiles. The underlying changes in the aperture ontogeny profile that have caused the differences between shell forms can be examined with this method. Moreover, the reopotologised shell mesh model can be used for functional-morphological analysis and for the evaluation of theoretical shell models. In addition, the similarity matrix for shells as based on the aperture ontogeny profiles can be analysed together with other distance matrixes, such as phylogenetic distance, geographical distance or environmental distance.

After the growth and form of morphologically diverse and unusual shells have been analysed in the preceding two chapters, I examine the functional aspects of the more striking shell traits in *Plectostoma* species, such as the protruding radial ribs and the distortedly-coiled tuba. In general, land snail shells serve for protection against predation and desiccation. In marine snails, shell traits similar to those in *Plectostoma* are known to have anti-predation function (Vermeij, 1993; Allmon, 2011). Hence, in **Chapter 5**, I explore whether these *Plectostoma* shell traits may act as defensive adaptations against one of its identified predators, namely the slug *Atopos*.

Atopos slugs have two predatory strategies, namely, shell-apertural entry and shell-drilling, to attack *Plectostoma concinnum*, *P. cf. inornatum*, *P. fraternum*, and other closely-related species in Sabah, Malaysian Borneo. The twisted tuba part of the shells of these snails is an effective defensive trait against shell-apertural entry attack. However, when the slug fails to enter the shell via the aperture, it will shift to the energetically more costly shell-drilling strategy. I found indications that the slug prefers to drill holes on shell surfaces without ribs. In any case, the twisted tuba and the protruding ribs do not guarantee the survival of the snails. Further analysis reveals that the lack of full effectiveness of these anti-predation shell traits may be caused by a functional trade-off between both traits under selection by two different predatory strategies.

In **Chapters 2 – 5**, I give insight into how *Plectostoma* shell forms can differ between species, how shell forms change between different developmental stages in a species, and how the properties of different shell traits can have anti-predation functionality. One of the remaining questions is how the *Plectostoma* shell forms have changed and diversified in the course of evolution. The rampant convergent and parallel evolution in shell form in the Gastropoda is well known. Many studies have investigated this pattern from the perspective of adaptive significance of the shell forms, which implies shell functionality under selection pressures. In fact, evolutionary changes in shell form are only possible when the underlying shell ontogeny changes as well. However, there is a scarcity in studies that aim at understanding shell form evolution with respect to the required changes in their ontogeny.

In **Chapter 6**, I investigate the evolution of shell forms in *Plectostoma* from the viewpoint of shell ontogeny. First, I obtain aperture ontogeny profiles as in **Chapter 3** and **Chapter 4**, characterise the shell characters as in **Chapter 2**, and finally estimate the phylogeny of *Plectostoma* species. I collate all these three data sources, and discuss the patterns of character evolution for shell form from an ontogenetic morphospace perspective. The results suggest that the phylogenetic history does not constrain changes in shell ontogeny, and the resultant *Plectostoma* shell forms. Also, species that are similar in shell shape may have their individually unique aperture ontogeny profile, while certain developmental aspects of shell size retain a conserved developmental program among species.

Summary

In summary, this thesis reveals several hitherto unknown aspects of *Plectostoma* shell forms, in terms of the developmental homology, the aperture ontogeny profile, anti-predation functionality, and evolutionary pattern in shell characters and ontogenetic morphospace evolution. In fact, these are the issues that have been targeted by biologists for centuries in order to improve the way shell shape is characterised and to improve understanding of shell form evolution. In many scientific fields, technology advancement has offered a new way to address old questions. This is also true for this thesis. The 3D technology that has been used intensively in every chapter of this thesis has, to some extent, opened new dimensions in the way we address these old questions, and provides important insight in the study of shell form.

Hence, I suggest three topics for future studies, which are essential to improve our understanding of the evolution of gastropod shell form:

- *Which shell characters should be used in the taxonomy?*
When the taxonomy of snail taxa relies heavily on the shell characters, it is important that the chosen shell characters represent certain biological information in terms of developmental, ecological, or functional aspects of the shell.
- *What are the roles of anatomy, behaviour, and development of snail columellar muscle and mantle edge in the determination of the snail's shell form?*
In order to understand the development and evolution of a gastropod solid shell, the animal's soft body organs, particularly the mantle edge that produces the shell and the columellar muscle that supports the shell, must be understood.
- *What are the quantifiable biological and physical properties of different shell forms and how do these quantitative properties influence a snail's fitness?*
The current state of 3D technology, in terms of hardware and software, allows not only comparisons of the geometrical shape of a shell form, but it also allows comparisons of the biological and physical properties of a shell form in an accurate and quantitative manner. Thus, these quantified biological and physical properties should be used in the functional, ecological and phylogenetic analysis of the shell forms.

Chapter 2

A cybertaxonomic revision of the micro-landsnail genus *Plectostoma* Adam (Mollusca, Caenogastropoda, Diplommatinidae), from Peninsular Malaysia, Sumatra and Indochina

(*ZooKeys* 393:1–107, <http://dx.doi.org/10.3897/zookeys.393.6717>)

Thor-Seng Liew^{1,2,3,4, †}, Jaap Jan Vermeulen^{1,5, ‡}, Mohammad Effendi bin Marzuki^{6, §}, and Menno Schilthuizen^{1,2,3, §}

1 Naturalis Biodiversity Center, P.O. Box 9517, 2300 RA Leiden, The Netherlands.

2 Institute Biology Leiden, Leiden University, P.O. Box 9516, 2300 RA Leiden, The Netherlands.

3 Institute for Tropical Biology and Conservation, Universiti Malaysia Sabah, Jalan UMS, 88400, Kota Kinabalu, Sabah, Malaysia.

4 Rimba, 4 Jalan 1/9D, 43650, Bandar Baru Bangi, Selangor, Malaysia.

5 jk.artandscience, Lauwerbes 8, 2318 AT, Leiden, The Netherlands.

6 102, Jalan Muut, Kampung Sekaan Besar, 96250 Matu, Sarawak, Malaysia.

† <http://zoobank.org/7D912940-C78C-4E43-9BBA-F0A49E360028>

‡ <http://zoobank.org/F3BCEB3D-0214-45BB-9A37-FCDC9AD1B36B>

§ <http://zoobank.org/F93444BE-BC25-46E1-85CB-EE1A7231AFA8>

| <http://zoobank.org/683D0AB7-CDD8-4FAA-94B6-436F3BFB8873>

Author Contributions

Conceived and designed the experiments: T-SL. Performed the experiments: T-SL. Analyzed the data: T-SL, JJV. Contributed reagents/materials/analysis tools: T-SL, JJV, MEM, MS. Wrote the paper: T-SL, JJV, MS, MEM.

Appendix

(<http://dx.doi.org/10.6084/m9.figshare.830412>)

Abstract

Plectostoma is a micro land snail restricted to limestone outcrops in Southeast Asia. *Plectostoma* was previously classified as a subgenus of *Opisthostoma* because of the deviation from regular coiling in many species in both taxa. This paper is the first of a two-part revision of the genus *Plectostoma*, and includes all non-Borneo species. In the present paper, we examined 214 collection samples of 31 species, and obtained 62 references, 290 pictures, and 155 3D-models of 29 *Plectostoma* species and 51 COI sequences of 19 species. To work with such a variety of taxonomic data, and then to represent it in an integrated, scaleable and accessible manner, we adopted up-to-date cybertaxonomic tools. All the taxonomic information, such as references, classification, species descriptions, specimen images, genetic data, and distribution data, were tagged and linked with cyber tools and web servers (e.g. Lifedesks, Google Earth, and Barcoding of Life Database). We elevated *Plectostoma* from subgenus to genus level based on morphological, ecological and genetic evidence. We revised the existing 21 *Plectostoma* species and described 10 new species, namely, *P. dindingsensis* sp. n., *P. mengaburensis* sp. n., *P. whitteni* sp. n., *P. kayiani* sp. n., *P. davisoni* sp. n., *P. relauensis* sp. n., *P. kubuensis* sp. n., *P. tohchinyawi* sp. n., *P. tenggekensis* sp. n., and *P. ikanensis* sp. n. All the synthesised, semantic-tagged, and linked taxonomic information is made freely and publicly available online.

Introduction

The purpose of this paper is twofold. Firstly, we demonstrate an updated workflow that uses several free tools to semantically tag and link different types of information during taxonomic revision. This approach allows the taxonomist to manage information in a more effective manner, making good quality data accessible and scaleable, which is essential for the taxonomist himself, future taxonomists and other users. Secondly, we revise the taxonomy of the genus *Plectostoma* based on the materials that have been accumulated since the last revision on the *Plectostoma* species of this region about five decades ago (van Benthem-Jutting, 1952, 1961). We revised the non-Bornean *Plectostoma* by using the redefined description of shell characters, which are better suited for the representation of the shell ontogeny and shell form. These shell character descriptions constitute a species hypothesis for each species, which is then discussed in terms of its genetic variation and biogeography.

Therefore, in this introduction section, we briefly review current issues in taxonomy, especially on the importance of taxonomic data management. After that, we introduce the taxonomy history of the genus *Plectostoma* and the taxonomic problems of the genus. In the methodology section, we describe in detail the procedure to incorporate cybertaxonomy tools in the taxonomic revision workflow. Finally, we discuss the taxonomy of the genus *Plectostoma* in the results and discussion sections.

Current issues in taxonomy

Taxonomy is arguably man's oldest profession and an important fundamental discipline for many other biological fields (Hedgpeth, 1961; Wilson, 2004). It helps us to inventory the

biodiversity on earth by naming each classified group of organisms that shares certain attributes based on, for example, genetic and morphological evidence. However, the taxa names are not necessarily maintained in perpetuity, as classifications can be changed when more specimens and novel attributes are examined and compared. In fact, the continuous improvement of the existing classification scheme of any taxon is a fundamental characteristic in taxonomic science. As a result, a taxon name is a summary of hundreds of years' of taxonomists' attempts to classify biodiversity.

Despite this long history, only a small fraction of biodiversity has been named (Mora et al., 2011). Certainly, more resources (money, time and taxonomists) are needed to describe the remaining unknown biodiversity. For example, Carbayo and Marques (2011) estimated that over two hundred billion US dollars are needed to describe the remaining ca. 5.5 million undescribed species. They indicate that half of the cost is to be invested on training taxonomists and project budgets. Although it is not being discussed in Carbayo and Marques (2011), it is not hard to imagine that a significant proportion of the amount were spent on travelling to various museums for studying type specimens and other samples, compiling literature and maintaining all this information. Even if there were no financial constraint, given the current pace in describing species (ca. 18000 species per year, see Zhang, 2008), about 400 years are still needed to describe all the species, which translates into 10 generations of taxonomists (Padial et al., 2010).

All organisms could eventually be scientifically described, but there are several pressing contemporary issues that could affect the advancement of taxonomy as a science. Firstly, the population of taxonomists is declining (Wägele et al., 2011), which will directly reduce the pace of species discovery and capacity building for future taxonomists. Secondly, the majority of taxonomic resources (e.g. type materials, literature, expertise) are centralised in developed countries, whereas the remaining undescribed species are concentrated in developing countries (Rodrigues et al., 2010). Neither taxonomists from developed countries nor taxonomists from developing countries can work effectively without having both biodiversity and taxonomic resources readily available to be integrated. Thirdly, many unnamed species are likely to go extinct under the current rates of habitat destruction in biodiversity hotspots (Giam et al., 2011). Thus, taxonomists have to find ways to be able to work more effectively and accelerate the pace of species discovery.

Several proposals to improve the practice of taxonomy have been published (e.g. Webb et al., 2010; Wägele et al., 2011; Miller et al.; 2012). One of these suggests that taxonomists embrace the information and internet technologies in their routine workflow. This is particularly relevant because taxonomy is a data-rich science and taxonomists have to deal with all past taxonomic works, in terms of literature, collection data, genetic data, and ecology, that have been accumulated over hundreds of years. Thus, computer and internet technologies have become important tools to manage all these taxonomic data, especially regarding data storage, dissemination, and retrieval.

Over the past few years, many web-based databases have been developed to accommodate almost all kinds of the data that taxonomists deal with. For example, museum specimen data are held in the Global Biodiversity Information Facility (<http://www.gbif.org>, Edwards, 2004), morphology data (images) in Morphbank (<http://www.morphbank.net>), genetic data in the Barcoding of Life Database (<http://www.barcodinglife.com>, Ratnasingham & Hebert, 2007) and GenBank (<http://www.ncbi.nlm.nih.gov/genbank>, Benson et al., 1997), nomenclature data in ZooBank (<http://zoobank.org>, Pyle & Michel, 2008), and literature in the Biodiversity Heritage Library (<http://www.biodiversitylibrary.org>, Gwinn & Rinaldo, 2009). Although the need to use these facilities to improve taxonomy has been emphasised (e.g. Maddison et al., 2012; Wheeler et al., 2012; Miller et al., 2013), the majority of taxonomists has yet to join this movement. This hesitance may be caused by taxonomists' fear for investing extra work to supply the data, and their doubt of the usefulness of these poorly integrated databases.

Recently, tools have become available for managing and integrating various types of taxonomic data by using either top-down approaches (e.g. Encyclopedia of Life <http://eol.org>, Wilson, 2003) or bottom-up approaches (e.g. Lifedesks <http://www.lifedesks.org>, offered by EOL; Scratchpads <http://scratchpads.eu>, Smith et al., 2009). The top-down mechanism acts as an automatic data aggregator that harvests and pools semantic-tagged information from different databases. The bottom-up mechanism, on the other hand, acts as quality controller that checks, links and tags the different types of taxonomic data. Obviously, the key factor that determines the success of cybertaxonomy and the main challenge of these integration processes is the quality of the underlying taxonomic data (Parr et al., 2012).

Many data in the databases are outdated (e.g. nomenclature change), incorrect due to the limitation of technology (e.g. automation text extraction, Page, 2011) or human error (e.g. misidentification, Yesson et al., 2007), and not linked or semantic-tagged. In fact, taxonomists spend much of the time in their careers to validate, link and tag all the existing and new taxonomic information. Thus, their contribution to the quality control of the data is essential. However, each database has its unique needs, standards, and format for the data and thus it might require taxonomists to do redundant work, such as uploading and key in the same data in different formats as required by the database.

In addition to the possible redundant efforts that need to be spent, it is not very clear how taxonomists as data suppliers would benefit most from such databases. In view of this, we demonstrate a working example of how these existing databases and platforms can be incorporated into revisionary taxonomic study processes, which begin with managing new specimen information, then establishing identity (literature study and examination of specimens in museum collections), and then writing taxonomic treatises (Winston, 1999). Our working example consists of a revision of the taxonomy of the genus *Plectostoma* of Peninsular Malaysia, Indochina and Sumatra (i.e. non-Bornean) by using cybertaxonomy tools during the entire revisionary taxonomy process. With these cybertaxonomy tools, we show that various kinds of taxonomic information can be semantically tagged, linked and integrated in a more user-friendly interface (Penev et al., 2011). In addition, we demonstrate

that using this technology and these databases could facilitate the hypothesis-testing nature of taxonomic research that deals with vast amounts of different kinds of information (e.g. Sluys, 2013). The validated, linked and tagged data that are generated during the taxonomic revision in turn facilitates forthcoming taxonomy studies that will be conducted by future taxonomists. Finally, all this species information is made readily available and accessible for other users such as ecologists and conservationists, especially for those who have limited budget and are from developing countries.

An overview of Genus *Plectostoma*'s taxonomy history

The study of *Opisthostoma* sensu stricto and *Plectostoma* started during the English colonisation in India and North Borneo in the 1860s (Blanford & Blanford, 1860; Adam, 1865b). All early collections were made by English officers, who later described the species themselves or sent their collections to other malacologists for species identification and publication. Until 1880, there was only one *Plectostoma* species known – *Plectostoma decrespignyi* from Labuan, North Borneo. Between the 1880s and 1900s, A. H. Everett, C. Hose and S. Beddome collected more *Plectostoma* specimens from North Borneo and Sarawak, where they were working as either British colonial administrators or naturalists. Based on these specimens, a total of 20 *Plectostoma* species were eventually described from Borneo (Godwin-Austen, 1889, 1890; Boettger, 1893; Smith, 1893b, 1894, 1904, 1905a; Fulton, 1901). Many of these were originally described under *Plectostoma*, which was considered a subgenus of *Opisthostoma*.

After the intensive malacological documentation in Borneo in the late 19th and early 20th century, more material of *Plectostoma* was collected in Sarawak and Sabah during explorations which principally had a different purpose, by the geologist G.E. Wilford and his associates in 1960s, by soil scientists K. Auffenberg and D.K. Dorman in the late 1980s, and by the botanist J.J. Vermeulen in the 1980s and early 1990s. All of this material was revised by Vermeulen (1994), under the genus *Opisthostoma*, which resulted in the description of 27 new *Plectostoma* species from Borneo. Since the 2000s, *Plectostoma* has attracted more interest, also regarding its phylogeny and evolution (Schilthuizen, 2003, 2006; Webster et al., 2012) and ecology (Schilthuizen et al., 2003a, 2005).

In addition to the Bornean *Plectostoma*, two other *Plectostoma* species were described from Southern Thailand and Southern Vietnam in the 1900s (Sykes, 1903; Dautzenberg & Fischer 1905). Between the 1930s and 1960s, M.W.F. Tweedie (then director of the Raffles Museum of Singapore) collected many *Plectostoma* specimens during explorations of Peninsular Malaysia. These specimens were later described as 13 new *Plectostoma* species (Tomlin, 1938, 1948; van Benthem-Jutting, 1952, 1961). The research on the taxonomy of non-Bornean *Plectostoma* ceased in the 1960s with the retirement of Tweedie and the death of van Benthem-Jutting. However, ecological investigations of one *Plectostoma* species – *P. retrovertens* – had started in 1960s by A.J. Berry, a professor at University Malaya (Berry, 1961, 1962, 1963, 1964, 1966).

No publications on *Plectostoma* from Peninsular Malaysia appeared between 1966 and 1996, but many *Plectostoma* specimens were collected by Geoffrey W. H. Davison, mainly from the state of Kelantan, and other localities in Malaysia (e.g. Davison & Kiew, 1990). In 1996, *Plectostoma klongsangensis* was described from Southern Thailand (Panha, 1997). After that, four new species were described from Southern Thailand and Peninsular Malaysia (Maassen, 2001). One year later, the first *Plectostoma* from Sumatra – *Plectostoma kitteli*, was described by Maassen (2002).

To sum up, a total of 69 *Plectostoma* are currently known. The hotspots of *Plectostoma* diversity are the Malay Peninsular (including the southern part of Thailand) and Borneo, harbouring 19 and 48 species, respectively. In addition, one species is known from Sumatra and another from Southern Vietnam.

Current taxonomic status of *Plectostoma* from Indochina, Sumatra and Peninsular Malaysia

The last revision of the non-Bornean *Plectostoma* species was done by van Benthem-Jutting (1952, 1961). It is important to note that she described 10 new species on the basis of shell characters from only 21 samples from 16 locations. However, it is problematic to use conventional shell descriptions in this genus. The striking shell form of *Plectostoma* has attracted the attention of malacologists, but it also poses a challenge to describe the shell accurately. As mentioned by Benthem-Jutting (1952), "... it is evident that in such irregular shells ... the measurements can only be given approximately, and never indicate the real proportion of the shell..." and "...after comparing over and over again did I succeed in checking the points of difference [between species], but even then it remained difficult to bring the true nature of these minor details into adequate words". To date, Vermeulen's (1994) approach in describing the *Plectostoma* shell is the most comprehensive, but it is still difficult to recognise the species from the written description alone.

As mentioned in the taxonomic history section above, additional *Plectostoma* specimens were collected by Geoffrey W. H. Davison in Peninsular Malaysia in the 1990s. Furthermore, we collected more specimens, including living ones for genetic study, during field trips to Peninsular Malaysian limestone hills between 2010 and 2011. These *Plectostoma* specimens are valuable to improve the taxonomy of *Plectostoma* in Peninsular Malaysia. Thus, it is timely to revise the non-Bornean *Plectostoma* based on these recently collected specimens by re-examining the species hypotheses formed on the basis of shell morphology. In addition, we also update the knowledge of *Plectostoma* regarding conservation status, distribution, and genetics.

Materials and methods

Data resources

The data underpinning the analysis reported in this paper are deposited in the Figshare Repository at <http://dx.doi.org/10.6084/m9.figshare.830412>.

Taxonomic data mining, storing and tagging (Appendix 1)

Literature. In addition to traditional searching of, for example, the Zoological Record, we also searched for the terms “Geothauma, Plectostoma and Opisthostoma” in Google Scholar (on 21st November 2012) and the Biodiversity Heritage Library (on 19th November 2012). A URL link to the full-text article was provided as listed in bibliography whenever possible (e.g. from <http://www.biodiversitylibrary.org>). Each of the articles was tagged with the relevant *Plectostoma* taxon names. All the relevant references were catalogued as individual contents in bibliography of the *Opisthostoma* Lifedesks pages (<http://opisthostoma.lifedesks.org/biblio>). All the relevant bibliography metadata of each article were entered and stored according to the standard data entries of BibTeX (<http://www.bibtex.org/>) as implemented in Lifedesks. Furthermore, the bibliography metadata can be exported as BibTeX formatted file (.bib), which all the tagged metadata can be retrieved and reused. For video tutorials, see Appendix 1(1&2).

Nomenclature information and classification. After the relevant literature was identified, the relevant taxon names were extracted and organised by using the classification tool (tree editor) of Lifedesks (for detailed descriptions of the methodology, see: <http://help.lifedesks.org/classification/edit>). The classification and nomenclature information can be downloaded and saved according to the DarwinCore standard as xml file. For video tutorials, see Appendix 1(3).

Species information. In addition, the original species descriptions and important notes from the literature were imported to individual species pages as quotations (for detailed descriptions of the methodology, see: <http://help.lifedesks.org/quickstart>). New and unpublished data, together with the information extracted from literature were managed and stored in the relevant chapters under the headings of ‘Overview’, ‘Conservation’, ‘Description’, ‘Ecology and Distribution’, ‘Evolution and Systematics’, and ‘Relevance’ of each species webpage. As all the information was tagged accordingly in the form of xhtml format, the data of each species can be retrieved and reused. For video tutorials, see Appendix 1(4).

Managing museum collections data. As common curation practice, each collection (i.e. one museum lot) consists of a specimen or multiple specimens, which are kept either dry (empty shells) or wet (shells with animals preserved in ethanol) that were collected at a single sampling occasion, for example from a particular location at a particular day/time. In this study, each collection is regarded as a sample. For each sample, there are two categories of information that can be extracted, namely the physical properties and metadata of the samples.

For the physical properties of the samples, we recorded the exact number of shells or (for samples >10 shells) categorised the samples into four categories of sample size: 1) > 10 (10–24 shells); 2) > 25 (25–49 shells); 3) > 50 (50–100 shells); and 4) > 100 (>100 shells). We also obtained shell morphology data as follows. Whenever possible, each registered

collection was photographed. The images for each unique collection were imported into Lifedesks as an individual content. Each of the images was then linked with the species name. For video tutorials, see Appendix 1(5).

Metadata consisted of collection reference number, collector information, collecting date, and locality of each sample. This information was published in Lifedesks as image description, except for the collection reference number, which was published as image caption. In addition to presenting collection data in a tabular format (Appendix 2), we also published the collection data in a more interactive manner, which can be used in Google Earth.

Whenever possible, location data of the collections were georeferenced. When the location description in the specimen label or in the publication was not clear, the itinerary of the collectors or expedition which had been published in other types of publication (e.g. maps and reports) was consulted. After the exact limestone hill where the collection had been made was identified, it was verified in Google Earth, after which the latitude and longitude were obtained. Although the coordinates as obtained from Google Earth are of high accuracy, they might be too accurate and lack an uncertainty estimate (Mesibov, 2012). Thus, the coordinates that we report here should be interpreted as the location of the limestone hill and not the exact spot where the specimens were collected.

A Keyhole Markup Language (KML) file, which comprises the location, images, and collection reference number of each of the museum collections, was created by using Google Earth Spreadsheet Mapper v3.0 (<http://www.google.com/earth/outreach/tutorials/spreadsheet3.html>). For the data input for the spreadsheet (Template4), the species name was used for “Folder name”, and collection reference number for “Placemark Name”; the concatenation of species name and collection reference number for “Title”; URL of each collection’s original image in Lifedesks was named “Image URL”; detailed collection data as “Paragraph Text”. After that, the data in Spreadsheet Mapper were converted into a KML file, which allows semantic-tagged collection information to be retrieved and reused. When the KML file is opened in Google Earth, each of the museum collection (specimens) is shown as a single landmark on the virtual earth. For video tutorials, see Appendix 1(6).

Specimen repositories

BMNH - Natural History Museum (previously known as British Museum (Natural History)), London, United Kingdom.

BOR – BORNEENSIS collection, Institute for Tropical Biology and Conservation, Universiti Malaysia Sabah, Kota Kinabalu, Malaysia.

RMNH – Naturalis Biodiversity Center (previously known as Rijksmuseum van Natuurlijke Historie), Leiden, the Netherlands

V – Jaap Vermeulen’s private collection, Leiden, the Netherlands.

YSC – Chen Yansen’s private collection, Medan, Sumatra, Indonesia.

ZMA – Naturalis Biodiversity Center (previously known as Zoological Museum of Amsterdam), Leiden, the Netherlands.

Establishing identity and revising the collection data

In the routine of conventional taxonomic revision practice, samples are sorted into groups (e.g. morphospecies) based on their morphology and distribution. Then, each group is assigned to an existing species name – when the morphology, distribution and/or other important characteristics fit with the species' morphological description and distributional range as mentioned in the literature; or a newly designed species name – when the characteristics do not fit to any of the named species. In some cases, different species identities may have been assigned to the same specimen by multiple taxonomists. Thus, for each specimen, the collection data (morphology, distribution, genetics and others) are immutable, but the species name is mutable.

The key of this process is the taxonomists, who gather, integrate, sort and analyse, not only the biological specimens, but diverse and vast amounts of information from hundreds of specimens (Sluys, 2013). This task has become more challenging for taxonomists and their successors because of the accumulative nature of taxonomic information. Thus, taxonomists have been using information technology to assist their routine work since the 1980s (Heywood, 1974; Maxted, 1992). However, the potential of information technology to be used by taxonomists remains underexploited, except for data storage. In fact, in addition to data storage, this technology can improve the efficiency and effectiveness of taxonomists in integrating, sorting, analysing and disseminating the information from the specimens.

As mentioned above, all key information from specimens and literature was digitised and tagged. Here, we integrated different types of information for different processes in taxonomy revision. For the specimen sorting process, we used a KML file to link and present the unique collection number, images and location data for each specimen. Each museum collection was shown on Google Earth as a landmark and these landmarks were sorted into respective species folders. When each landmark was selected (by clicking it), the information of the morphology (as shown in images), location (text description and map), and other relevant information was visible to the user (taxonomist). Species identification can be done in a single platform (i.e. Google Earth), where the morphological variation within a species or between the specimens across the genus' geographical range can be examined. Based on this information, the species identity of the landmark (specimen) was determined by either keeping the landmark in the same species folder or moving to the other species folder. Likewise, whenever the coordinate of a specimen location was wrong, the landmark was edited by moving it to the correct location. Whenever necessary, the specimen itself was examined. For video tutorials, see Appendix 1(7).

After all the collection species identifications and location data in the KML file were verified and corrected, the data in the KML file were extracted with a customised Python script to update the data in Spreadsheet mapper and image species link in Lifedesks for all specimens in an automatic manner. This saved much time compared to the traditional laborious method of manually updating the collection database specimen by specimen after sorting and

identification. Lastly, the taxonomic content was written in Lifedesks and then exported to the appropriate format and layout for publication. For video tutorials, see Appendix 1(8).

Since the information was stored and tagged digitally, a simple program can be customised to retrieve, integrate and process the data from many different online/offline databases and files. In our case, we used scripting language Python 2.7.3 (<http://www.python.org>). Its “urllib” and “re” modules were used to retrieve information from Internet resources and searching for patterns in text. In the same way, additional specimen information from Lifedesks (i.e. image pages) can be integrated into the KML file. Simultaneously, the literature and species information compiled in Lifedesks can be retrieved easily when necessary.

Species delimitation

The application of a species concept in *Plectostoma* has been particular problematic. Nowadays, the most widely accepted species concepts (e.g., the biological species concept; Mayr 1942) include some aspect of genetic and/or reproductive cohesion. Such species concepts are, however, difficult to apply in taxa like *Plectostoma*, where all species and populations are restricted to isolated limestone outcrops. This island-like (allopatric) distribution pattern suggests very limited gene flow between populations. Furthermore, it would be impractical to verify experimentally “potential interbreeding” for each population, as *Plectostoma* populations occur in hundreds of different limestone outcrops.

Previous species circumscriptions in this genus have been mainly based on a morphological species concept. In gastropods, this is common practice. However, shell shape or even some shell structures, such as rib intensity, can be genetically variable and/or phenotypically plastic under different environmental conditions (e.g. Berry, 1962; Kemp & Bertness, 1984). Nevertheless, when the intra- and inter-specific variations in shells are understood (see below “Morphological analysis”), a morphological species concept may be used as one of the guidelines in species delimitation.

Finally, the phylogenetic species concept (sensu Cracraft, 1983 – “A species is the smallest diagnosable cluster of individual organism within which there is a parental pattern of ancestry and descent”) also cannot be used in the case of *Plectostoma* species, again because of their populations’ allopatric distribution on isolated limestone outcrops. The deposition age of Peninsular Malaysian limestone ranges from the Ordovician to the late Triassic (ca. 480 mya – 200 mya). Though the exact time at which the limestone outcrop was exposed is unknown, van Benthem-Jutting (1960) believed this began to happen after the Cretaceous - ca. 140 mya. Given the fact that *Plectostoma* species have been found on relatively young, Miocene age, limestone (ca. 24 mya – 5 mya) in Borneo, it is likely that *Plectostoma* species will have colonised limestone hills in Peninsular Malaysia soon after the limestone hills were exposed. Hence, populations of the same *Plectostoma* species on each isolated limestone hill could have been separated for a long time and thus these isolated populations would appear as a several deeply diverged lineages in the phylogenetic tree (Liew TS, unpublished data). In

view of this, the blind application of a phylogenetic species concept could inflate the number of species in *Plectostoma*.

Because of these problems, in this study, we have used elements of different species concepts for the delimitation of *Plectostoma* species. First we used a set of shell characters for initial morphological species delimitation. These groups were then checked for their distribution ranges. Whenever more than one of these morphological species was found at the same hill, we examined the genetic dissimilarity (in DNA barcode, COI) between these sympatric morphological species. In addition, the intra-specific genetic divergence was examined among several geographically separated populations of the same species (see below “COI Barcoding”). By reciprocal illumination from the morphological, genetic and distribution data, we determined for each species a set of characters that is stable within a species and diagnosable between *Plectostoma* species. We applied the same approach to the Bornean species (Liew et al., *in prep*).

Morphological analysis

In conventional conchology, shell descriptions and measurements are mainly made based on the standard apertural view of the shell. In this view, the shell is positioned so that the columella is vertical and the shell is rotated around this columella axis until the aperture faces the user. After the apertural view of the shell is set, the shell linear measurements are taken and descriptions of other shell characters are made (see, e.g., Vermeulen, 1994). However, the irregularity in the orientation of the aperture of *Plectostoma* shells, caused by the distortion in the shell coiling hinder this traditional conchological approach.

We feel that in *Plectostoma* the usefulness of this traditional approach is limited because of the presence of the tuba that deviate from the coiling axis of the spire. The varying length and coiling mode of the tuba prevent any standardisation of the ‘frontal’ view of the spire (Figure 1; see also Sasaki (2010), who refers to “different direction in shell-mouth opening”). Nevertheless, all previous authors use this method to describe and illustrate *Plectostoma* shells. Here, we proposed a better approach to describe the shells of this, conchologically unusual, genus.

In *Plectostoma*, the only part of the shell that can serve as a landmark to determine a frontal view, while at the same time fixing the position of both the spire as well as the tuba, is not the aperture, but the constriction, the point where the spire ends and the tuba begins, and operculum rests. Therefore, we determined the frontal view of the shell as follows: the shell is held with the coiling axis of the spire vertical and with the operculum perpendicular to the line of view, on the right side (because all *Plectostoma* shells are dextral). Left lateral view, back view and right lateral view are obtained by turning the shell 90°, 180°, and 270° from this starting point (Figure 1). Accordingly, all the shell characters were described based on this positioning scheme.

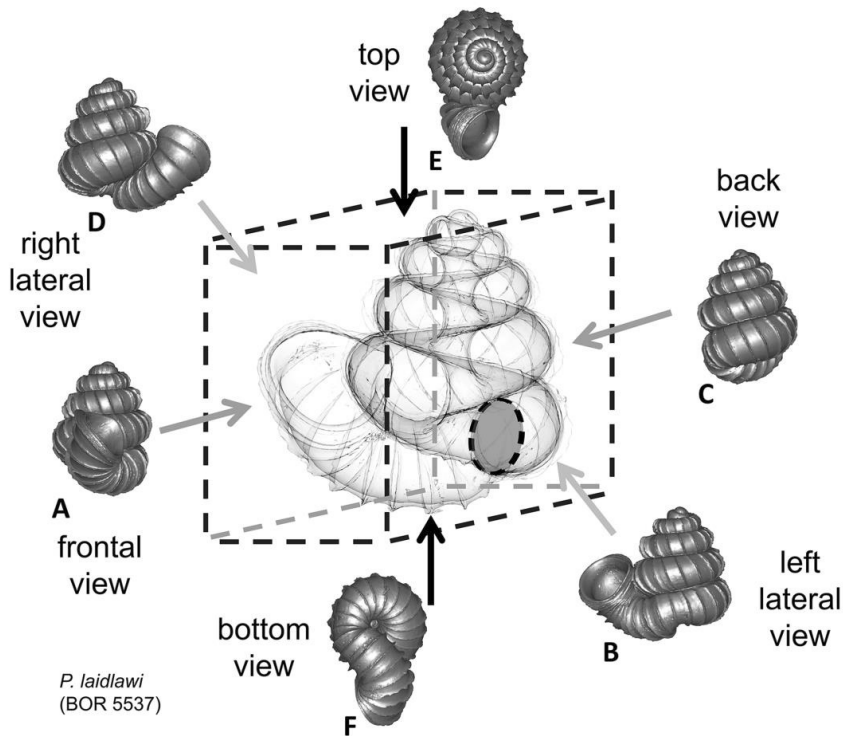


Figure 1. Six shell views. The shaded circle is the operculum. The frontal view (perpendicular on the operculum) was set as reference perspective for the other views: back, right lateral, left lateral, top, and bottom. the basal spire that consist of the last two whorls of the spire, and the apical spire that consist of the remaining spire whorls.

Specimen images and 3D models. To examine the shell morphology, at least one digital 3D model of each species was obtained. We used microcomputed X-ray tomography (CT) to obtain 3D models of *Plectostoma* shells. For each species, several empty shells and ethanol-preserved shells with the soft body inside, spanning the morphological variation breadth, were selected. Microcomputed tomography was carried in a high-resolution micro-CT scanner (SkyScan, model 1172, Aartselaar, Belgium). 3D models were created from the reconstructed images with the manufacturer's software CT Analyser ver. 1.12.0.0 (Skyscan©) and saved as digital polygon mesh objects (*.ply). The 3D models were then simplified by quadric edge collapse decimation (to ca. 200,000 faces) as implemented in the program MeshLab ver. 1.3.2 (Cignoni et al., 2008).

The position and orientation of the 3D digital shell was manipulated so that the shell columella was in parallel with the z-axis and the operculum outer side was visible from a user perspective (Figure 1, Appendix 1(9)). Then, the outer operculum view of the shell was regarded as frontal view. After that, the field of view of the 3D model was set to orthographic, and an image was taken for each of the six perspectives: frontal view (A), left lateral view (B), back view (C), right lateral view (D), top view (E), and bottom view (F). In addition, two images were made of the constriction teeth of the parietal (G) and basal (H)

inner shell whorl after clipping of the 3D model. All manipulation and imaging was done with MeshLab ver.1.3.2 (Cignoni et al., 2008). Thus, a total of eight images were made for each species (A – H). For video tutorials, see Appendix 1(10).

Shell characters and descriptions. The shell is an accretionary exoskeleton of the snail. The overall shape of the shell, which resembles a 3D spiral, results from changes in the curvature and torsion during the shell accretionary process, and form changes in aperture form during

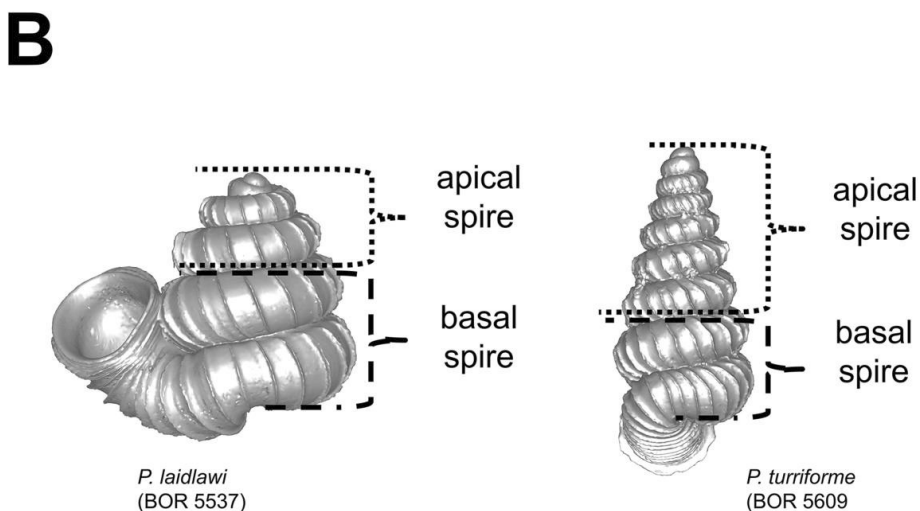
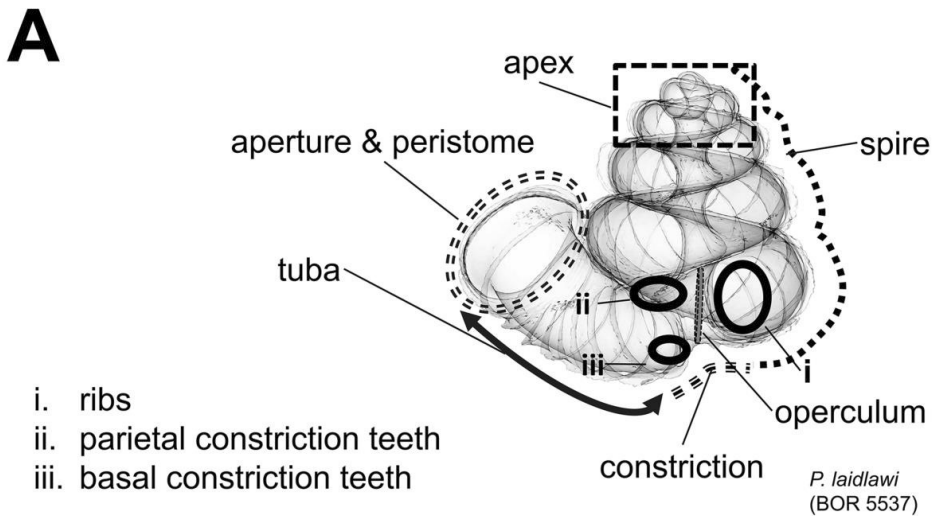


Figure 2. Morphological terminology and shell measurements. **A** shell part terminology as used in the species descriptions is shown in an example shell; **B** Two shell examples show the basal spire that consist of the last two whorls of the spire, and the apical spire that consist of the remaining spire whorls.

shell growth (Okamoto, 1988). However, the exact quantifications of these changes might exceed the requirements of the practical purpose of this taxonomic paper. Therefore, we used traditional linear measurements to quantify the shell form, in a way that these measurements abstract the shell ontogeny and its 3D spiral properties.

After the six views of a shell were determined as described (Figure 1), the shell whorls were described for each of six major parts, according to the shell ontogeny order: (1) apex – protoconch and the first teleoconch (Figure 2A, and 3); (2) apical spire – the whole teleoconch except the last 1 1/2 whorls before the constriction (Figure 2B, and 4); (3) basal spire – the last 1 1/2 whorls before the constriction (Figure 2B, and 5); (4) constriction – the narrowest transitional part of the whorl between spire and tuba (Figure 2A, 6, and 7); (5) tuba whorl – teleoconch after the constriction (Figure 2A, and 8); and (6) aperture and peristome (Figure 2A, 9, and 10). The first three parts constitute the shell spire, for which size and shape were quantified from the left lateral view. The height, width and number of whorls of the shell were measured and counted from the spire (Figure 11A, and B). In addition to the description of the general shell form, we recorded the shell surface ornamentations, namely, (7) fine spiral striation (Figure 12), and (8) distinct radial ribs (Figures 2A and 13).

(1) Apex – Ranges from “distinctly convex”, via “moderately convex”, to “slightly convex” (Figure 3). The slightly convex apex has a teleoconch that grows with less torsion and greater curvature than the protoconch, and vice versa in the distinctly convex apex.

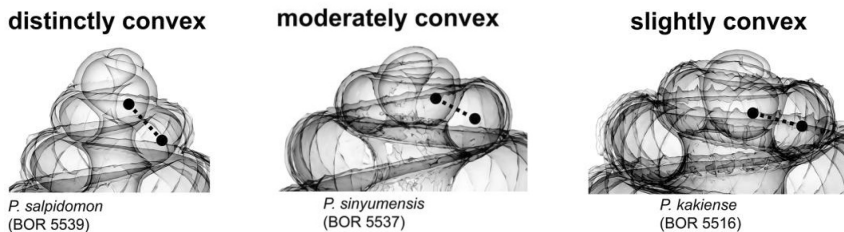


Figure 3. Apex forms in shell left lateral view. The degree of shell apex depression results from the growth regime of the teleoconch after the protoconch.

(2) Apical spire – Similar to the apex form, less torsion and greater curvature in shell growth produce a “depressed conical” apical spire, and the reverse produces an “oblong conical” apical spire. The oblong and depressed conical shape of the spire can be estimated by measuring the ratio between the apical spire height and width (Figure 4).

(3) Basal spire – The curvature of the basal spire determines the final form of the spire. The width of the spire base is related to how tightly the basal spire whorl coils towards the shell columella, and to the whorl width. The basal spire shape categories, namely, conical, ovoid, and ellipsoid, can be estimated by comparing the difference between two whorl width measurements from three consecutive whorl peripheries (Figure 5). This measurement is

made at both the left and the right side of the shell, in left lateral view. The spire umbilicus may be open, partially closed or totally closed by the tuba.

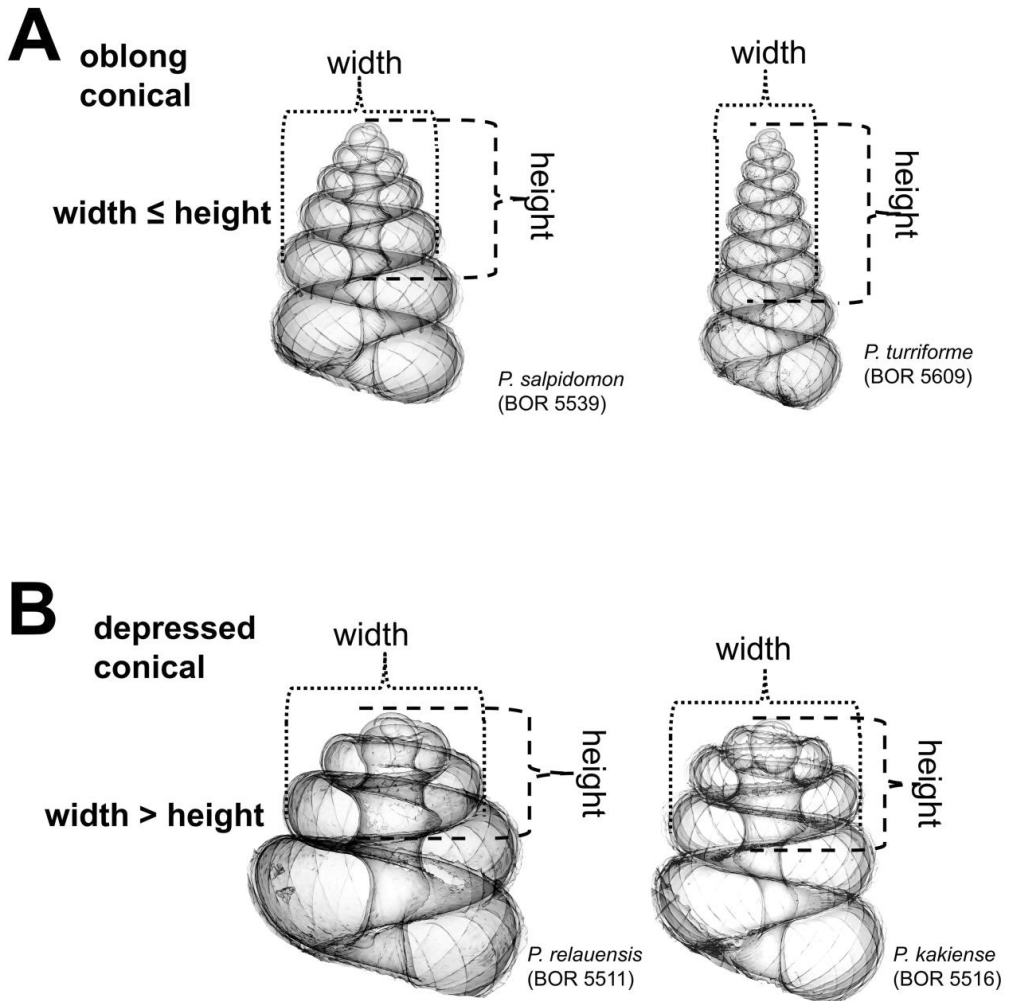


Figure 4. Two basic forms of apical spire whorls: **A** oblong conical; **B** depressed conical.

(4) Constriction –The constriction is a short transitional and narrow part of the whorl between the spire and tuba (Figure 2A). This is the furthest point to where the snail can retract into the shell and where the operculum rests (Figure 1, and 2A). Inside the constriction of some species, there are calcareous structures that protrude from the inner shell wall – constriction teeth (Figure 6 and 7). The number, shape, and location of the constriction teeth are taxonomically informative characters.

(5) Tuba – It is difficult to describe the variable forms of tuba in words. For the sake of convenience, we categorised the tuba into three coiling regimes, which represent how many times torsion changes drastically. These are: type 1 – no drastic changes in torsion at the

beginning of the tuba as compared to the spire; type 2 – drastic changes in torsion at the beginning and midway of the tuba; and type 3 – drastic changes in torsion at the beginning of tuba (Figure 8). In addition to the coiling regime, the overall shell form is also determined by the final tuba length. However, estimation of tuba length is difficult. Hence, we quantified the tuba length by estimating the ratio of the tuba periphery length on the one hand, and the spire last whorl periphery length on the other. In addition, we estimated the proportion of the tuba that attaches to the spire. Finally, the difference between tuba forms can also be determined by comparing the shell perspective where the aperture opening is best visible.

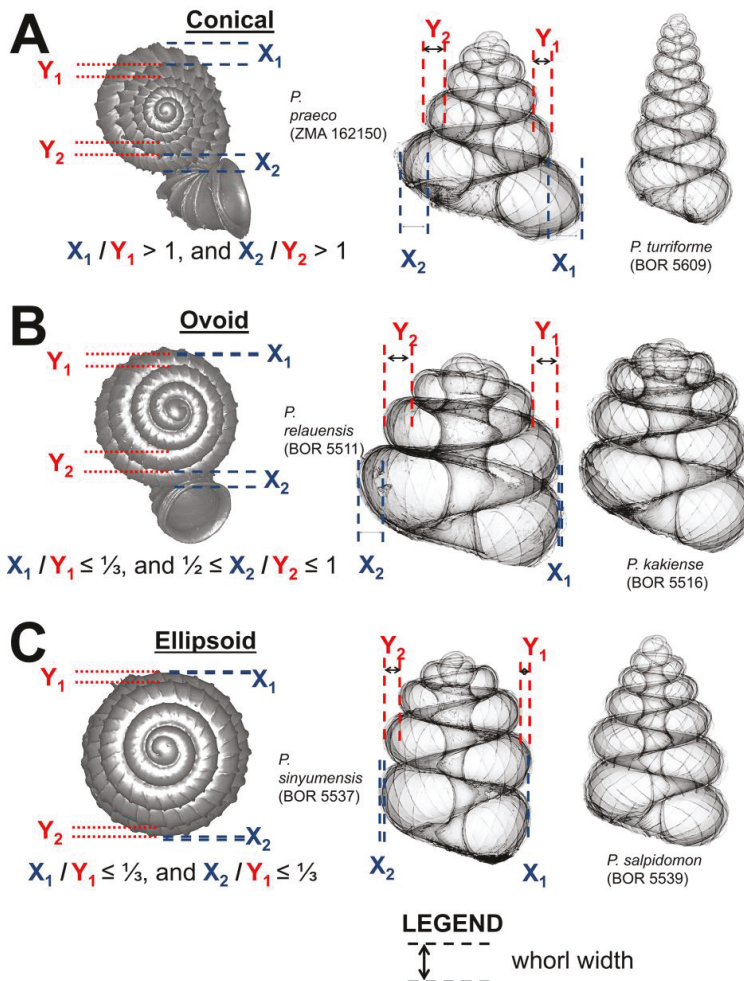


Figure 5. Three basic forms of shell spire basal whorls in left lateral view. Panels from left to right of each of the shell forms: quantifications of the shell form in top view; example of the shell form with a low number of whorls in left lateral view; example of the shell form with a higher number of whorls in left lateral view. **A** conical; **B** ovoid; **C** ellipsoid.

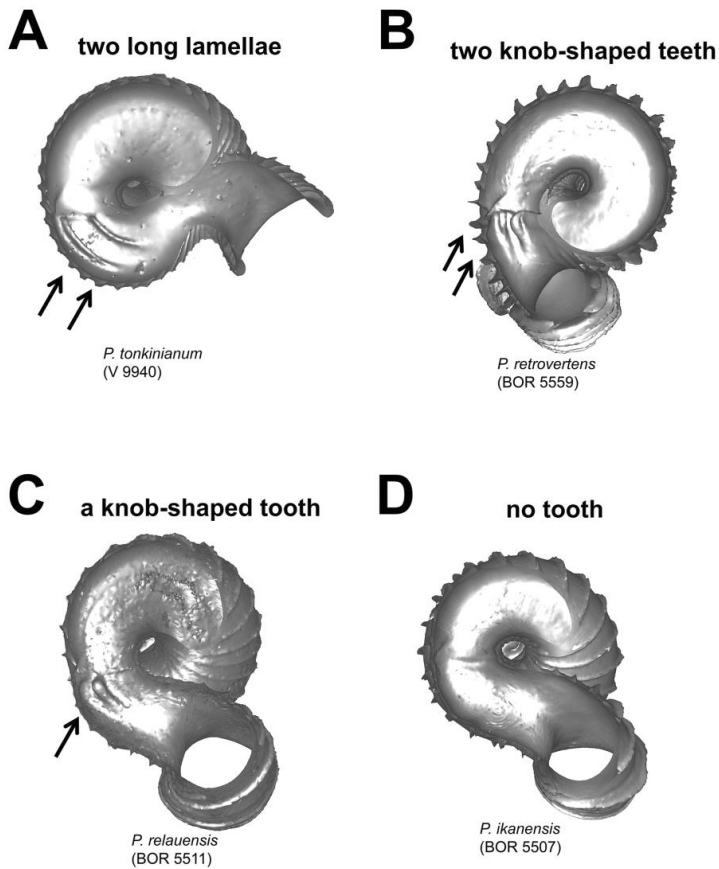


Figure 6. Different types of parietal constriction teeth before the operculum resting site, in bottom view. **A** two long lamellae run parallel to the whorl growing direction; **B** two short ridges run parallel to the whorl growing direction, each knob-shaped at one end; **C** a single ridge runs parallel to the whorl growing direction, knob-shaped at one end; **D** no tooth.

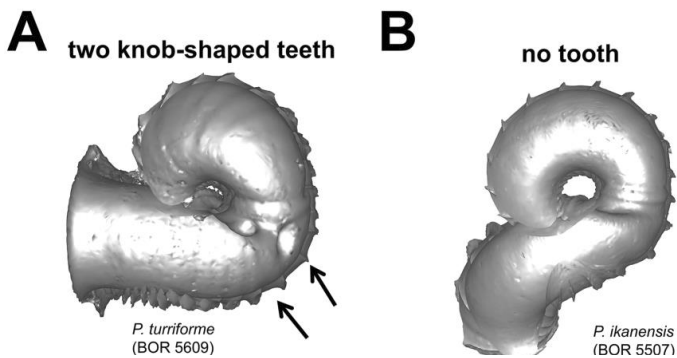


Figure 7. Different types of basal constriction teeth in top view. **A** two teeth after operculum resting site: one ridge runs parallel to the whorl growing direction; the other ridge has a knob at one end and runs perpendicular to the whorl growing direction; **B** no tooth.

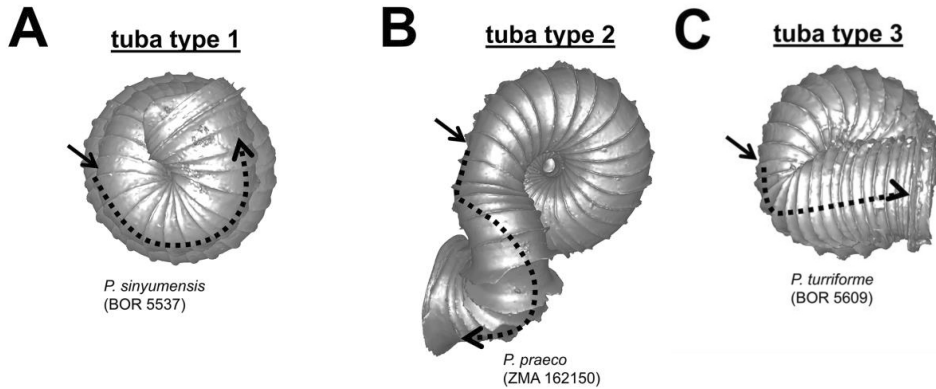


Figure 8. Different tuba coiling regimes in bottom view. **A** tuba type 1 – tuba coiling as regularly as the spire last whorl; **B** tuba type 2 – tuba gradually coiling downward and then in a different direction; **C** tuba type 3 – tuba bent abruptly. Arrows point to the constriction.

(6) Aperture and peristome – Before we characterise the aperture form, we define the anatomical position of the aperture according to the orientation of the animal inside (Figure 9). Our definitions for the four areas of aperture side correspond to the conventional terminology used for the aperture of a regularly coiling shell: Anterior = palatal side, posterior = columellar side, right lateral = parietal side and left lateral = basal side. The convenient way to recognise these aperture areas is by identifying the posterior area where it has the densest ribs (Figure 9B). After that we describe and compare the shape of the aperture and the outer peristome (Figure 10). The shell has either a simple or a double peristome, and this character is species specific in *Plectostoma*. The prominence and shape of the outer peristome is described by how much the outer peristome is projected at the anterior, posterior, and both lateral sides, as compared to the inner peristome (Figure 10A).

(7) Spiral lines – Spiral line sculpture on the shell is composed of a row of granulated micro-structures. The intensity of the spiral lines depends on the size of these micro-structures. In general, Thick spiral lines should be visible under the dissecting microscope at 50× magnification (Figure 12A), whereas thin spiral lines are hardly visible at 50× magnification, but are visible at 100× magnification (Figures 12A and B, Appendix 3). Thick spiral lines are more widely spaced (< 7 lines per 100 μm) than thin lines (> 10 lines per 100 μm). Thin lines may be present in between sparse thick lines (Figure 12A), but on living snails these may fade away when the snail ages and may be hardly visible in old empty shells.

(8) Radial ribs – Radial ribs are produced by a change of shell ontogeny in both shell accretion direction and aperture dimensions. During rib formation, the shell material accretion direction around the aperture changes from longitudinal to orthogonal; meanwhile, aperture size increases and probably aperture shape changes. Thus, the formation of each rib represents a discontinuity in shell growth in the longitudinal direction and a change of the aperture shape and size. In view of these, three characters can be observed in the radial ribs.

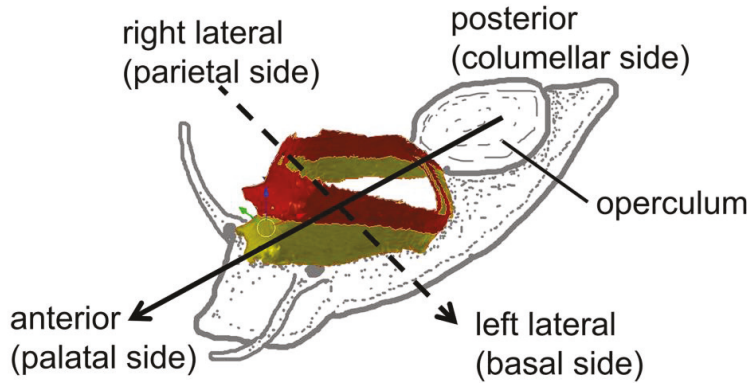
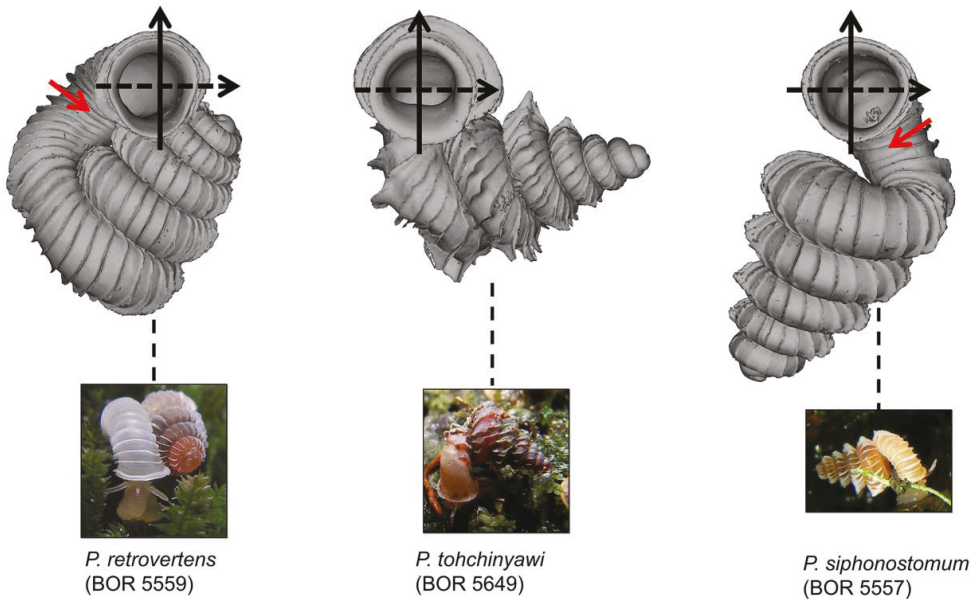
A**B**

Figure 9. Positioning scheme for the description of aperture and peristomes. **A** anterior, posterior, right and left lateral sides of aperture and peristome are defined according to the orientation of the shell relative to the active animal; **B** Three shell examples showing the defined positions of aperture and peristome. Red arrows point to the aperture area with the densest ribs.

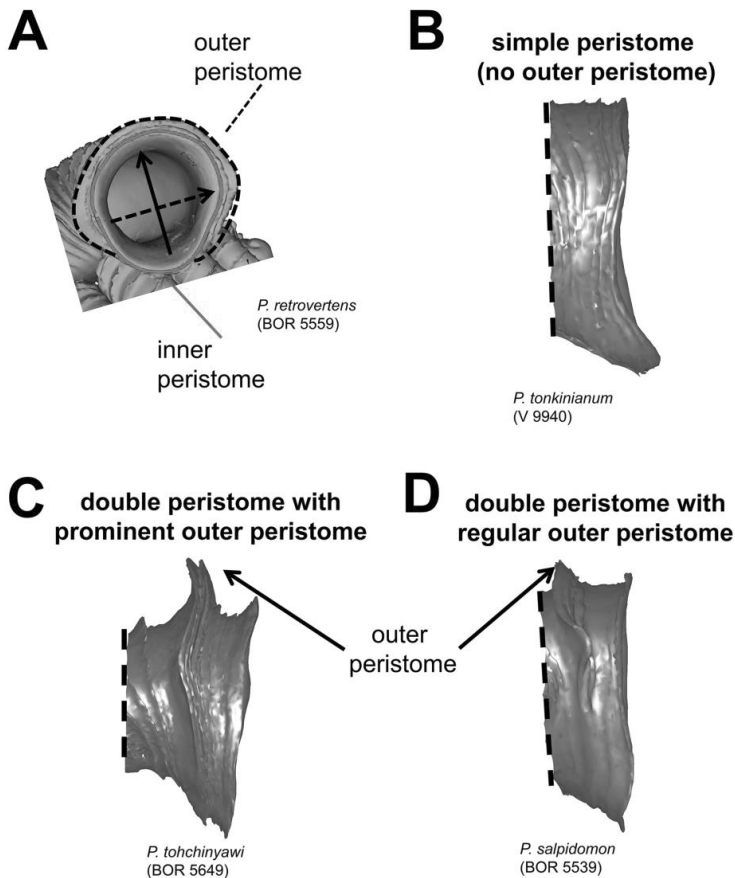


Figure 10. Aperture and peristome forms. **A** outer and inner peristome; **B** Simple aperture without outer peristome; **C** aperture with double peristomes in which the outer peristome is prominent; **D** aperture with double peristomes in which the outer peristome is equally prominent as the inner.

The first character is the total number of ribs and the spacing between them on the shell. The number of ribs for a species can be highly variable between different individuals. The ribs are not evenly distributed on the shell surface; for example, the spacing between ribs consistently increases from the apex to the last whorl of the spire (Appendix 4). In view of this, we describe the rib density as the number of ribs within 1 mm on the whorl above the shell constriction in left lateral view (Figure 13A).

The second character is the intensity of the ribs in terms of length and thickness. Generally, rib length is related to the spacing between the ribs; for example, the greater the spacing (whorl length) before the rib, the longer the rib projects from the whorl periphery (Liew T.S., unpublished data). Thus, the lengths of the ribs, from the apex to the last whorl of the shell, change in a trend similar to the rib spacing. Besides, the thickness of ribs can vary between species, but less so within species. The thickness of the ribs depends on the number of shell layers and the thicker the ribs, the more likely it is that ribs persist in old shells (Figure 13B).

The third character is the form of the ribs. As mentioned above, each radial rib on a *Plectostoma* shell was actually a deformed aperture during shell ontogeny. Thus, a more biologically meaningful way to describe the radial ribs is to compare the rib edge form (deformed aperture) to the whorl before the rib (regular aperture). The rib form can be either the same or different in the spire and tuba parts of the shell. As is the case with the aperture and peristome, the rib edge is either slightly or distinctly projected at its anterior side (i.e. at whorl periphery) as compared to the lateral sides (hereafter “rib plate”). In addition, the shape of the rib plate can be straight, slightly curved, or single-humped (Figure 13C). Although thinner ribs are easily abraded in old shells, at least the rib plate form can be inferred from the abraded scar at the whorl periphery (Figure 13B).

Finally, we noticed variation among species in the rib inclination, which can be estimated with respect to the coiling axis. However, it is difficult to quantify this inclination accurately. Nevertheless, we add this character into the description of the shell in a qualitative manner in the terms of orthoclin (i.e. ribs are almost straight with respect to the collumella, as in *Plectostoma christae* and *P. siphonotomum*), prosoclin (i.e. ribs are distinctly tilted with respect to the collumella, as in *P. tohchinyawi* and *P. salpidomon*).

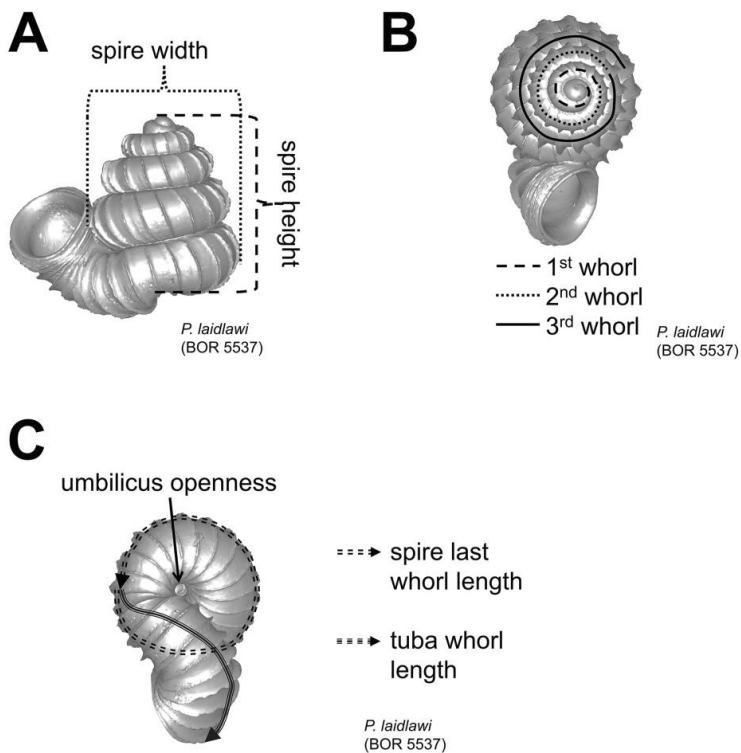


Figure 11. Shell measurements. **A** height and width of spire; **B** number of whorls; **C** spire last whorl length, tuba whorl length and umbilicus openness.

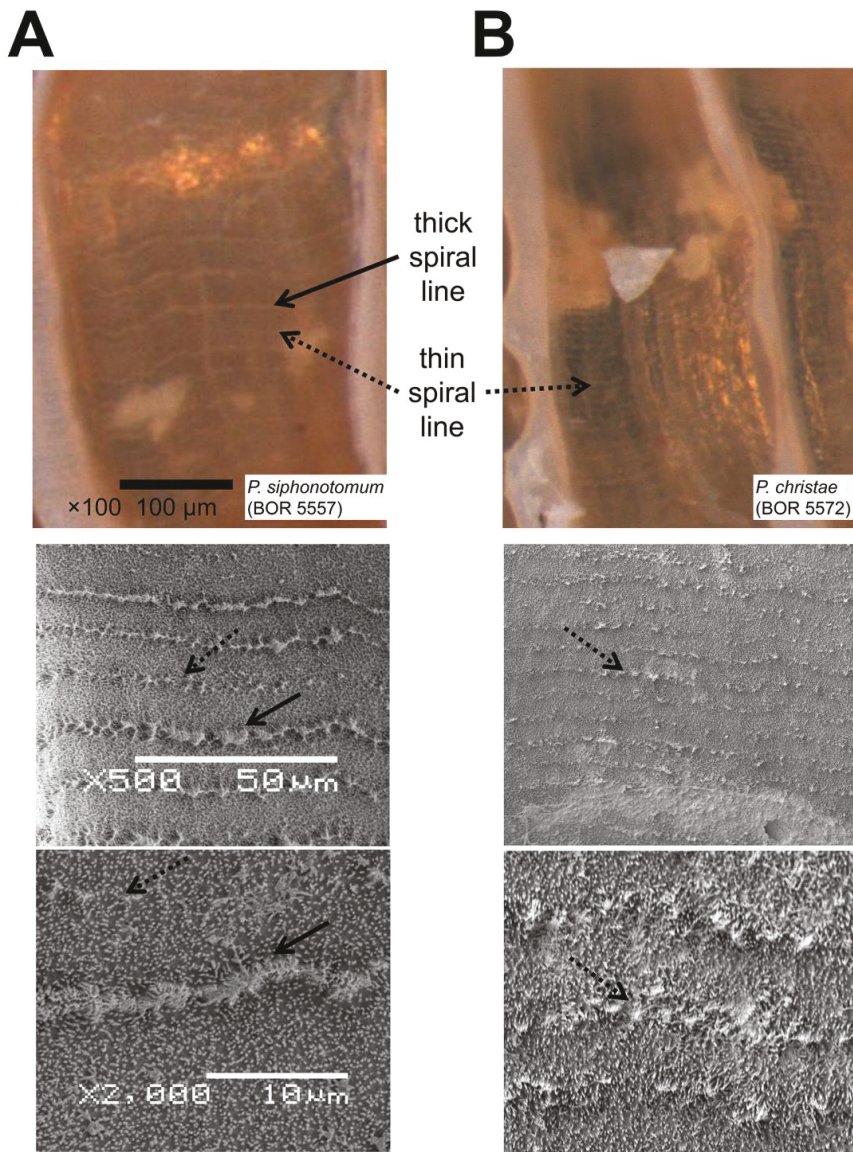


Figure 12. Spiral lines on the shell surface are shown in, from top to bottom, $100 \times$ magnification under the dissecting microscope, $500 \times$ and $2000 \times$ magnification under scanning electron microscope. **A** shell with both thick and thin spiral lines; **B** shell with only thin spiral lines. Each corresponding image in **A** and **B** is at the same scale.

In brief, shells of all species were described following a template consisting of three major elements (Table 1). First, the shell was described in several parts which represent the chronology of the shell ontogeny. Second, we defined a set of characters that can be determined in each shell part. Lastly, we described each character in either a quantitative or quantitative manner. We regard this template as a morphological model for the taxonomy of the genus *Plectostoma*, and each element in this template may be updated by future taxonomists when necessary. We present the final description of each species in a uniform telegraphic format (e.g. semantic-tagged by bold text, and colon “:”) so that these

morphological data can be mined effectively. By doing this, we hope to reduce the redundant process where species descriptions are done de novo each time a taxonomist revises the same taxa (Deans et al., 2012).

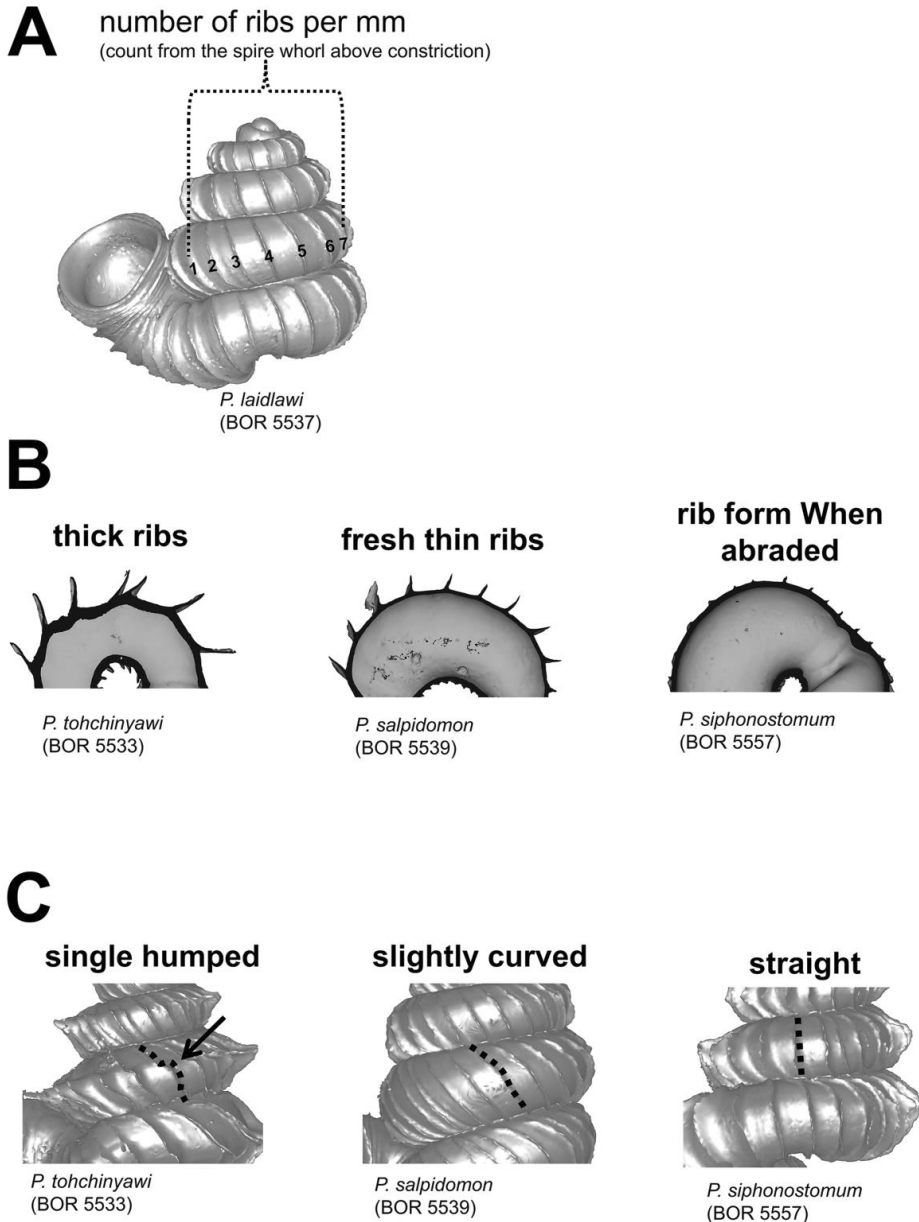


Figure 13. Radial ribs. **A** measurement of number of ribs per mm at the whorl above the constriction in left lateral view; **B** rib intensity, from left to right: thick ribs, thin ribs, and abraded ribs; **C** three different rib shapes, from left to right: single-humped, slightly curved and straight.

Table 1. Format for species shell description.

Shell parts (Figure 2)	Characters for shell part†	Descriptions (see section “Morphological analysis” for details).
Apex.	Shape: #.	Figure 3.
Spire.	Height: #.	Figure 2.
	Width: #.	Figure 4.
	Number of whorls: #.	Figure 5.
	Apical spire shape: #.	Figure 11.
	Basal spire shape: #.	
Constriction.	Whorl periphery: #.	
	Umbilicus: #.	
	Parietal teeth: #.	Figure 6.
Tuba.	Basal teeth: #.	Figure 7.
	Coiling direction: # and aperture visible in # view.	Figure 1.
	Tuba whorl length in proportion to spire last whorl: #.	Figure 8.
	Proportion of tuba that attaches to spire: #.	Figure 11.
Aperture and peristome.	Peristome: #.	Figure 9.
Spiral lines.	Outer peristome shape: #.	Figure 10.
	Thick lines: #.	Figure 12.
Radial ribs.	Thin lines: #.	
	Rib density: # ribs per mm.	
	Rib intensity: #.	
	Shape: #.	Figure 13.
	Inclination: #.	

† “#” is the description for each shell character for figure 1–13.

Digital model. Pictures are more effective than verbal descriptions for shell morphology. However, it is not feasible to have hundreds of pictures taken for each perspective of a shell. Many non-linear characteristics of a shell cannot effectively be represented by 2D images. Thus, an interactive 3D model shell improves the dissemination of morphological information. Presenting 3D models in digital publication has started five years ago (Ruthensteiner & Heß, 2008), and since then more taxonomists have taken the initiative to embed 3D models in e-papers. However, in this paper we have refrained from embedding 3D models in the paper itself, since this limits further analysis by readers. Instead, we provide sets of 3D data in *.blend files, which consist of all 3D models and which can be opened in Blender ver. 2.63 (www.blender.org). The 3D models in the blend file can be exported to *.ply format, which can be opened in MeshLab ver. 1.3.2 (Cignoni et al., 2008). Both Blender and MeshLab are freeware and can be used to analyse the 3D model further (e.g. measurements, modification, etc). For video tutorials, see Appendix 1(11 and 12).

Conservation status assessment

We propose the conservation status for each species by following IUCN Red List Criteria and guidelines (IUCN Standards and Petitions Subcommittee, 2013). We assess the conservation status based on our fieldwork in Malaysia between the year 2010 and year 2013 and the information obtained from the museum collections.

Molecular phylogeny and COI barcoding

Taxon sampling. A total of 27 ingroup taxa of the genus *Opisthostoma* (n=11) and *Plectostoma* (n=16) were included in this study: six *Opisthostoma* species from Borneo, five *Opisthostoma* from Peninsular Malaysia, nine *Plectostoma* species from Borneo, and seven *Plectostoma* from Peninsular Malaysia. All of these ingroup taxa were selected on the basis of their distribution and shell forms which are representative for about 150 species in both genera. In addition to the ingroup taxa, eight outgroup taxa were included in the phylogenetic analysis. Sequence data for these outgroup taxa, which include three genera of the Diplommatinidae and a species of the Cochlostomatidae, were obtained from Webster et al. (2012). The details of these specimens and the Genbank accession numbers are listed in Table 2.

DNA extraction, PCR and sequencing. DNA extraction was done for each specimen (entire animal and its shell), with the E.Z.N.A. Mollusc DNA kit (OMEGA bio-tek). We followed the manufacturer's extraction protocol. After extraction, PCR was carried out to amplify four regions, namely, 16S (mitochondrial, Palumbi, 1996), COI (mitochondrial, Folmer et al., 1994), 28S (nuclear, Park & Foighil, 2000), and 18S (nuclear, Stothard et al., 2000). We used the PCR reactions and programs of Webster et al. (2000). Positive PCR products were sequenced by MacroGen sequencing service (MacroGen Inc., Europe).

Table 2. Details of the taxa used for phylogenetic analysis and DNA barcoding.

no	Species	Voucher codes	Locality (Country, state, location, Lat, Long)	Genbank accession no.			
				COI	16S	18S	28S
1	<i>Cochlostoma septemspirale</i> (Wagner, 1897)	RMNH.MOL.119825	Switzerland.	HM753326	HM753497	HM753423	HM753367
2	<i>Arintia paricostata</i> (Vermeulen, 1996)	RMNH.MOL.119779	Malaysia, Sabah.	n.a.	HM753500	HM753441	HM753384
3	<i>Diplommatina canaliculata</i> (Moellendorff, 1886)	RMNH.MOL.119783	Malaysia, Pahang.	HM753338	HM753504	HM753445	HM753388
4	<i>Diplommatina gomantongensis</i> (Smith, 1894)	RMNH.MOL.119800	Malaysia, Sabah.	HM753342	HM753509	HM753451	HM753394
5	<i>Diplommatina rubicunda</i> (Von Martens, 1864)	RMNH.MOL.119819	Malaysia, Sabah.	HM753363	HM753520	HM753477	HM753417
6	<i>Diplommatina rubra</i> (Godwin Austen, 1889)	RMNH.MOL.119797	Malaysia, Sabah.	HM753346	HM753514	HM753456	HM753399
7	<i>Palaina alba</i> (Beddome, 1889)	RMNH.MOL.119810	Belau, Peleliu.	HM753354	HM753531	HM753469	HM753409
8	<i>Palaina striolata</i> (Crosse, 1866)	RMNH.MOL.119812	Belau, Ngerেকেbesang.	HM753356	HM753533	HM753470	HM753410
9	<i>Opisthostoma haitlei</i> Solem, 1964	n.a.	Malaysia, Sabah, 5.536, 118.213.	KC250856	KC250897	KC250923	KC250948
10	<i>Opisthostoma holzmarkii</i> Thompson, 1978	BOR 5580	Malaysia, Sarawak, 3.804, 113.78.	KC250871	KC250912	KC250937	KC250962
11	<i>Opisthostoma</i> sp.	BOR 5561	Malaysia, Sarawak, 4.044, 114.815.	KC250876	KC250917	KC250942	KC250967
12	<i>Opisthostoma brachyacrum</i> (Thompson, 1978)	BOR 5548	Malaysia, Sarawak, 1.319, 110.291.	KC250874	KC250915	KC250940	KC250965
13	<i>Opisthostoma brachyacrum</i> (Thompson, 1978)	BOR 5593	Malaysia, Sarawak, 3.804, 113.78.	KC250873	KC250914	KC250939	KC250964

Table 2. (continued)

14	<i>Opisthostoma</i> sp.	BOR 5561	Malaysia, Sarawak, 4.044, 114.815.	KC250878	KC250920	KC250945	KC250970
15	<i>Opisthostoma vermiculum</i> Clements & Vermeulen, 2008	BOR 5526	Malaysia, Perak, 4.55, 101.131.	n.a.	KC250910	n.a.	n.a.
16	<i>Opisthostoma paulucciae</i> Crosse & Nevill, 1879	BOR 5558	Malaysia, Pahang, 4.487, 101.976.	KC250866	KC250907	n.a.	n.a.
17	<i>Opisthostoma tenuicostatum</i> van Benthem Jutting, 1952	BOR 5525	Malaysia, Kelantan, 5.09, 102.22.	KC250869	n.a.	KC250935	KC250960
18	<i>Opisthostoma playcephalum</i> van Benthem Jutting, 1952	BOR 5576	Malaysia, Pahang, 3.908, 103.147.	KC250864	KC250905	KC250931	KC250956
19	<i>Opisthostoma tenerum</i> van Benthem Jutting, 1952	BOR 5577	Malaysia, Pahang, 3.984, 103.144.	KC250861	KC250902	KC250928	KC250953
20	<i>Plectostoma mirabile</i> (Smith, 1893)	n.a.	Malaysia, Sabah, 5.531, 118.071.	KC250867	KC250908	KC250933	KC250958
21	<i>Plectostoma obliquedentatum</i> (Vermeulen, 1994)	BOR 5607	Malaysia, Sabah, 4.726, 116.615.	KC250880	KC250922	KC250947	KC250972
22	<i>Plectostoma hosei</i> (Godwin-Austen, 1890)	BOR 5592	Malaysia, Sarawak, 3.804, 113.78.	KC250860	KC250901	KC250927	KC250952
23	<i>Plectostoma austeni</i> (Smith, 1894)	BOR 5589	Malaysia, Sarawak, 1.311, 110.293.	KC250863	KC250904	KC250930	KC250955
24	<i>Plectostoma wallacei busauense</i> (Smith, 1893)	BOR 5545	Malaysia, Sarawak, 1.323, 110.3.	KC250875	KC250916	KC250941	KC250966
25	<i>Plectostoma stellastibis</i> (Vermeulen, 1994)	BOR 5588	Malaysia, Sarawak, 3.804, 113.78.	KC250858	KC250899	KC250925	KC250950
26	<i>Plectostoma pulchellum</i> (Godwin-Austen, 1890)	BOR 5563	Malaysia, Sarawak, 4.044, 114.815.	KC250857	KC250898	KC250924	KC250949
27	<i>Plectostoma cookei</i> (Smith, 1894)	BOR 5591	Malaysia, Sarawak, 3.804, 113.78.	n.a.	KC250918	KC250943	KC250968
28	<i>Plectostoma grandispinosum</i> (Godwin-Austen, 1889)	BOR 5590	Malaysia, Sarawak, 3.804, 113.78.	KC250879	KC250921	KC250946	KC250971
29	<i>Plectostoma christae</i>	BOR 5509	Malaysia, Kelantan, Limestone hill on the	KC420288	n.a.	n.a.	n.a.

Table 2. (continued)

	(Maassen, 2001)									
30	<i>Plectostoma christae</i> (Maassen, 2001)	BOR 5505		right hand side of the road no. 8 direction to Gua Musang, opposite to Quarry Damai, 4.896, 102.137.	KC420287	n.a.	n.a.	n.a.	n.a.	n.a.
31	<i>Plectostoma christae</i> (Maassen, 2001)	BOR 5505		Malaysia, Kelantan, Bukit Sejuk near Quarry Damai, along the road no. 8 from Gua Musang to Kuala Krai, 4.905, 102.121.	KC420294	n.a.	n.a.	n.a.	n.a.	n.a.
32	<i>Plectostoma christae</i> (Maassen, 2001)	BOR 5506		Malaysia, Kelantan, Bukit Sejuk near Quarry Damai, along the road no. 8 from Gua Musang to Kuala Krai, 4.905, 102.121.	KC420305	n.a.	n.a.	n.a.	n.a.	n.a.
33	<i>Plectostoma christae</i> (Maassen, 2001)	BOR 5506		Malaysia, Kelantan, Limestone hills 'Ciku 2', in the FELDA plantation Ciku 2, 4.924, 102.177.	KC420303	n.a.	n.a.	n.a.	n.a.	n.a.
34	<i>Plectostoma christae</i> (Maassen, 2001)	BOR 5572		Malaysia, Kelantan, Limestone hills 'Ciku 2', in the FELDA plantation Ciku 2, 4.924, 102.177.	KC420271	n.a.	n.a.	n.a.	n.a.	n.a.
35	<i>Plectostoma christae</i> (Maassen, 2001)	BOR 5509		Malaysia, Kelantan, Limestone hill on the right hand side of the road no. 8 direction to Gua Musang, opposite to Quarry Damai, 4.896, 102.137.	KC420298	n.a.	n.a.	n.a.	n.a.	n.a.
36	<i>Plectostoma christae</i> (Maassen, 2001)	BOR 5505		Malaysia, Kelantan, Bukit Sejuk near Quarry Damai, along the road no. 8 from Gua Musang to Kuala Krai, 4.905, 102.121.	KC420269	n.a.	n.a.	n.a.	n.a.	n.a.
37	<i>Plectostoma crassipupa</i> (van Benthem Jutting, 1952)	BOR 5512		Malaysia, Kelantan, Limestone hill near Kampung Paloh, on the right hand side of the road no 8 to Gua Musang, 4.992, 102.228.	KC420304	n.a.	n.a.	n.a.	n.a.	n.a.
38	<i>Plectostoma crassipupa</i> (van Benthem Jutting, 1952)	BOR 5512		Malaysia, Kelantan, Limestone hill near Kampung Paloh, on the right hand side of the road no 8 to Gua Musang, 4.992, 102.228.	KC420273	n.a.	n.a.	n.a.	n.a.	n.a.
39	<i>Plectostoma davisoni</i> sp. n.	BOR 5515		Malaysia, Kelantan, Limestone hill in rubber estate (Ulu Kumbang FELCRA), 4.69, 101.989.	KC420295	n.a.	n.a.	n.a.	n.a.	n.a.
40	<i>Plectostoma davisoni</i> sp. n.	BOR 5508		Malaysia, Kelantan, Limestone hill on the right hand side of the road D29, km 17 from Jelawang to Gua Musang, 4.985, 101.965.	KC250872	KC250913	KC250938	KC250963		
41	<i>Plectostoma davisoni</i> sp. n.	BOR 5508		Malaysia, Kelantan, Limestone hill on the right hand side of the road D29, km 17 from Jelawang to Gua Musang, 4.985, 101.965.	KC420264	n.a.	n.a.	n.a.	n.a.	n.a.

Table 2. (continued)

42	<i>Plectostoma dindingsis</i> sp. n.	BOR 5612	Malaysia, Pahang, Dinding, 3.846, 102.378.	KC420285	n.a.	n.a.	n.a.
43	<i>Plectostoma ikanensis</i> sp. n.	BOR 5504	Malaysia, Kelantan, Gua Ikan. Loc 1, 5.353, 102.026.	KC420286	n.a.	n.a.	n.a.
44	<i>Plectostoma ikanensis</i> sp. n.	BOR 5507	Malaysia, Kelantan, Gua Ikan. Loc 1, 5.353, 102.026.	KC420302	n.a.	n.a.	n.a.
45	<i>Plectostoma ikanensis</i> sp. n.	BOR 5504	Malaysia, Kelantan, Gua Ikan. Loc 1, 5.353, 102.026.	KC420301	n.a.	n.a.	n.a.
46	<i>Plectostoma ikanensis</i> sp. n.	BOR 5504	Malaysia, Kelantan, Gua Ikan. Loc 1, 5.353, 102.026.	KC250862	KC250903	KC250929	KC250954
47	<i>Plectostoma ikanensis</i> sp. n.	BOR 5507	Malaysia, Kelantan, Gua Ikan. Loc 1, 5.353, 102.026.	KC420278	n.a.	n.a.	n.a.
48	<i>Plectostoma ikanensis</i> sp. n.	BOR 5504	Malaysia, Kelantan, Gua Ikan. Loc 1, 5.353, 102.026.	KC420268	n.a.	n.a.	n.a.
49	<i>Plectostoma kakiense</i> (Tomlin, 1948)	BOR 5516	Malaysia, Perlis, Kaki Bukit, 6.645, 100.202.	KC420265	n.a.	n.a.	n.a.
50	<i>Plectostoma tohchinyawi</i> sp. n.	BOR 5533	Malaysia, Terengganu, Tasik Kenyir. Gua Bewah, 4.851, 102.723.	KC420289	n.a.	n.a.	n.a.
51	<i>Plectostoma tohchinyawi</i> sp. n.	BOR 5533	Malaysia, Terengganu, Tasik Kenyir. Gua Bewah, 4.851, 102.723.	KC420307	n.a.	n.a.	n.a.
52	<i>Plectostoma kaibuensis</i> sp. n.	BOR 5519	Malaysia, Perlis, Bukit Kubu. Loc 3, 6.404, 100.144.	KC420272	n.a.	n.a.	n.a.
53	<i>Plectostoma kaibuensis</i> sp. n.	BOR 5519	Malaysia, Perlis, Bukit Kubu. Loc 3, 6.404, 100.144.	KC420270	n.a.	n.a.	n.a.
54	<i>Plectostoma laidlawi</i> (Sykes, 1902)	BOR 5510	Malaysia, Kelantan, Limestone hill in Kampung Bayu. About 337 km from Kuala Lumpur by road no. 8, 5.09, 102.22.	KC420279	n.a.	n.a.	n.a.
55	<i>Plectostoma laidlawi</i> (Sykes, 1902)	BOR 5510	Malaysia, Kelantan, Limestone hill in Kampung Bayu. About 337 km from Kuala Lumpur by road no. 8, 5.09, 102.22.	KC420300	n.a.	n.a.	n.a.
56	<i>Plectostoma laidlawi</i> (Sykes, 1902)	BOR 5571	Malaysia, Kelantan, Limestone in FELDA Ciku 4, 5.043, 102.196.	KC420275	n.a.	n.a.	n.a.
57	<i>Plectostoma mengaburensis</i> sp. n.	BOR 5574	Malaysia, Pahang, Sri Jaya, Gunung Mengapur, 3.731, 102.821.	KC420299	n.a.	n.a.	n.a.
58	<i>Plectostoma mengaburensis</i> sp. n.	BOR 5574	Malaysia, Pahang, Sri Jaya, Gunung Mengapur, 3.731, 102.821.	KC420267	n.a.	n.a.	n.a.
59	<i>Plectostoma palnihelix</i> (van Benthem Jutting, 1952)	BOR 5520	Malaysia, Pahang, Bukit Serdam, 3.83, 101.927.	KC250877	KC250919	KC250944	KC250969

Table 2. (continued)

60	<i>Plectostoma palmihelix</i> (van Benthem Jutting, 1952)	BOR 5520	Malaysia, Pahang, Bukit Serdam, 3.83, 101.927.	KC420283	n.a.	n.a.	n.a.
61	<i>Plectostoma relauensis</i> sp. n.	BOR 5511	Malaysia, Kelantan, Taman Negara, Sungai Relau Station. Gua Gajah, 4.642, 102.063.	KC420277	n.a.	n.a.	n.a.
62	<i>Plectostoma retrovertens</i> (Tomlin, 1938)	BOR 5559	Malaysia, Pahang, Bukit Chintamanis, 3.446, 102.014.	KC420297	n.a.	n.a.	n.a.
63	<i>Plectostoma salpidomon</i> (van Benthem Jutting, 1952)	BOR 5539	Malaysia, Pahang, Kenong Rimba Park. Gunung Kesong, 4.194, 102.177.	KC420276	n.a.	n.a.	n.a.
64	<i>Plectostoma salpidomon</i> (van Benthem Jutting, 1952)	BOR 5542	Malaysia, Pahang, Kenong Rimba Park. Gunung Tangkup, 4.194, 102.177.	KC420296	n.a.	n.a.	n.a.
64	<i>Plectostoma salpidomon</i> (van Benthem Jutting, 1952)	BOR 5541	Malaysia, Pahang, Kenong Rimba Park. Gunung Telahup, 4.194, 102.177.	KC420266	n.a.	n.a.	n.a.
65	<i>Plectostoma salpidomon</i> (van Benthem Jutting, 1952)	BOR 5569	Malaysia, Pahang, Gua Bama, 4.194, 101.967.	KC420280	n.a.	n.a.	n.a.
66	<i>Plectostoma salpidomon</i> (van Benthem Jutting, 1952)	BOR 5569	Malaysia, Pahang, Gua Bama, 4.194, 101.967.	KC250868	KC250909	KC250934	KC250959
67	<i>Plectostoma senex</i> (van Benthem Jutting, 1952)	BOR 5575	Malaysia, Pahang, Gua Charas, 3.908, 103.147.	KC250859	KC250900	KC250926	KC250951
68	<i>Plectostoma sinumensis</i> (Maassen, 2001)	BOR 5537	Malaysia, Pahang, Gunung Jebak Puyuh, near Gunung Senyum, 3.7, 102.453.	KC420291	n.a.	n.a.	n.a.
69	<i>Plectostoma sinumensis</i> (Maassen, 2001)	BOR 5537	Malaysia, Pahang, Gunung Jebak Puyuh, near Gunung Senyum, 3.7, 102.453.	KC250870	KC250911	KC250936	KC250961
70	<i>Plectostoma siphonostomum</i> (van Benthem Jutting, 1952)	BOR 5513	Malaysia, Kelantan, Taman Negara, Sungai Relau Station. Gua Gajah, 4.642, 102.063.	KC420292	n.a.	n.a.	n.a.
71	<i>Plectostoma siphonostomum</i> (van Benthem Jutting, 1952)	BOR 5513	Malaysia, Kelantan, Taman Negara, Sungai Relau Station. Gua Gajah, 4.642, 102.063.	KC420274	n.a.	n.a.	n.a.
72	<i>Plectostoma siphonostomum</i> (van Benthem Jutting, 1952)	BOR 5557	Malaysia, Pahang, Limestone hill on the left hand site of the road no. 8 toward Kuala Lipis. Near Kampung Chegar Perah I and II	KC420306	n.a.	n.a.	n.a.

Table 2. (continued)

74	<i>Plectostoma siphonostomum</i> (van Benthem Jutting, 1952)	BOR 5557	FELDA, 4.487, 101.976. Malaysia, Pahang, Limestone hill on the left hand site of the road no. 8 toward Kuala Lipis. Near Kampung Chegar Perah I and II FELDA, 4.487, 101.976.	KC420293	n.a.	n.a.	n.a.
75	<i>Plectostoma siphonostomum</i> (van Benthem Jutting, 1952)	BOR 5557	Malaysia, Pahang, Limestone hill on the left hand site of the road no. 8 toward Kuala Lipis. Near Kampung Chegar Perah I and II FELDA, 4.487, 101.976.	KC250865	KC250906	KC250932	KC250957
76	<i>Plectostoma whitteni</i> sp. n.	BOR 5536	Malaysia, Terengganu, Tasik Kenyir. Gua Taat, 4.842, 102.721.	KC420284	n.a.	n.a.	n.a.
77	<i>Plectostoma whitteni</i> sp. n.	BOR 5536	Malaysia, Terengganu, Tasik Kenyir. Gua Taat, 4.842, 102.721.	KC420282	n.a.	n.a.	n.a.
78	<i>Plectostoma umbilicatum</i> (van Benthem Jutting, 1952)	BOR 5503	Malaysia, Pahang, Gua Tongkat, 3.891, 102.473.	KC420281	n.a.	n.a.	n.a.
79	<i>Plectostoma umbilicatum</i> (van Benthem Jutting, 1952)	BOR 5503	Malaysia, Pahang, Gua Tongkat, 3.891, 102.473.	KC420290	n.a.	n.a.	n.a.

Phylogenetic inferences. Alignment of sequences was done with Bioedit ver 7.1.3 (Hall, 1999) and adjusted manually. The final aligned data matrix consists of 2241 positions, of which 2092 can be aligned unambiguously (Appendix 17). The remaining 149 characters (91 from 16S and 58 from 28S) were excluded from further analysis. Mr.Modeltest ver. 2.3 (Nylander, 2004) was used to select the most appropriate model, based on the Akaike Information Criterion (AIC) for 16S, 18S and 28S, and as well as each of the three codon positions for COI. The best fits were: the GTR+I+ Γ model for 16S, 28S, COI(2nd codon) and COI(3rd codon); the GTR+ Γ for COI(1st codon); and the SYM+I+ Γ for 18S.

Three phylogenetic analyses were done, namely, Bayesian inference (BI), Maximum Likelihood analysis (ML), and Parsimony analyses (PA). Bayesian inference was run in MrBayes ver. 3.2.1 (Huelsenbeck & Ronquist, 2001) with the following setting: mcmc ngen=5000000; nchains=4; samplefreq=100; average deviation of split frequencies < 0.01; and a burn-in value of 25%. A Maximum Likelihood analysis was run using RaxML ver. 7.2.6 (Stamatakis, 2006) as implemented on CIPRES portal ver. 2.2 (Miller et al., 2010) on all the genes together, with 1000 rapid bootstraps using GTR + U. The data was divided into six partitions, all analyzed with a GTR substitution model. The Parsimony analyses were run using PAUP ver. 4.0b (Swofford, 1998). Gaps were set as fifth character state. A bootstrapped heuristic search with 1000 bootstrap replicates, and 10 random addition sequence heuristic search replicates, with no rearrangement limit per replicate was carried out, with 50% as the minimum bootstrap support included.

COI Barcoding. As mentioned above, the shell morphology alone may not be sufficient to delimit many species that have greater morphological variation within species. Thus, in addition to shell morphology, we sought another way to make the decision about the species delimitation. DNA barcoding is used to provide more insight into the species delimitation for gastropods (Boeters & Knebelberger, 2012; Puillandre et al., 2012). Therefore, we sequenced COI (mitochondrial, Folmer et al., 1994) for standard DNA barcoding analysis for a greater number of individuals than we used for the phylogenetic analysis. In total, we obtained COI sequences from 51 individuals, which comprise 19 species (including 8 new species) (Table 2). Then, the pairwise genetic distances for all the 51 sequences were computed by using Kimura 2-parameters in MEGA5 (Tamura et al., 2011).

Genetic data repository. The collection information for the specimens used were uploaded, stored and managed in Barcoding of Life Database (BOLD, <http://www.boldsystems.org>, Ratnasingham & Hebert, 2007). After that, all DNA sequences were uploaded to NCBI GenBank (<http://www.ncbi.nlm.nih.gov/genbank>, Benson et al., 1997) via BOLD. Genetic data deposited in GenBank can be retrieved easily with the Python tool Biopython (e.g. Module “Entrez”) (<http://biopython.org>, Cock et al., 2009).

Results and Discussion

Taxonomic data depository and cybertaxonomy

While uploading the data of 31 species, 62 references, 214 collections, 290 pictures, and 31 species pages to Lifedesks, they were simultaneously tagged and linked to each other (Figure 14). The textual information can be downloaded and accessed offline in the xhtml format (source code) (Figures 15). Similarly, the taxonomic information that was used in creating the KML file can be retrieved in KML format (source code) (Figures 15, Appendix 5). In addition to the taxonomic data, a total of 155 3D models of 29 *Plectostoma* species were constructed, which belong to 86 samples. For the ease of specimen and species comparison, all 3D models were saved in ten separate .blend files, each containing 20 layers (Appendix 6 – 15). The 3D models (i.e. specimens) that belong to the same species were saved in the same layer.

Most taxonomists will have established their own workflow when working with taxonomic data. However, often only fractions of such data are published in a taxonomic revision paper. Thus, extra work would be needed to upload the data to online data platforms whenever a taxonomic revision is done in a traditional manner (i.e. not using cybertaxonomic tools). Here, we demonstrated that, in fact, no extra works is required if a cybertaxonomic workflow is adopted. Taxonomists themselves, who maintain, tag, link and create the data will benefit most by using these cybertaxonomy tools. For example, with some existing tools, such as Google Earth, the information can be integrated, explored and analysed in an interactive way, which will increase the efficiency of the taxonomic methodology (sensu Figure 1 in Sluys, 2013; Appendix 5).

Furthermore, all textual information is preserved, and can be simply accessed in raw format. In other words, this information is not locked and can be retrieved and integrated with very basic programming skills (such as Python) even when the desirable platform (internet) and software are not available. More importantly, adopting this workflow in taxonomy practice will help realise the vision of Wheeler et al. (2012), that “The resultant cyber-enabled taxonomy, or cybertaxonomy, would open access to biodiversity data to developing nations, assure access to reliable data about species, and change how scientists and citizens alike access, use and think about biological diversity information”.

Morphological analysis

Table 3 shows the morphological data matrix of 31 *Plectostoma* species and 11 general qualitative shell characters. Twenty-seven out of 31 *Plectostoma* species have a unique set of shell character states. The remaining four species share two unique sets of general characters states, namely, 1) *Plectostoma salpidomon* (van Benthem Jutting, 1952), and *Plectostoma laemodes* (van Benthem Jutting, 1961); and 2) *Plectostoma dindingensis* sp. n., and *Plectostoma mengaburensis* sp. n. However, each of these four species is distinguishable by other shell characters (see diagnosis and species description in the taxonomy section).

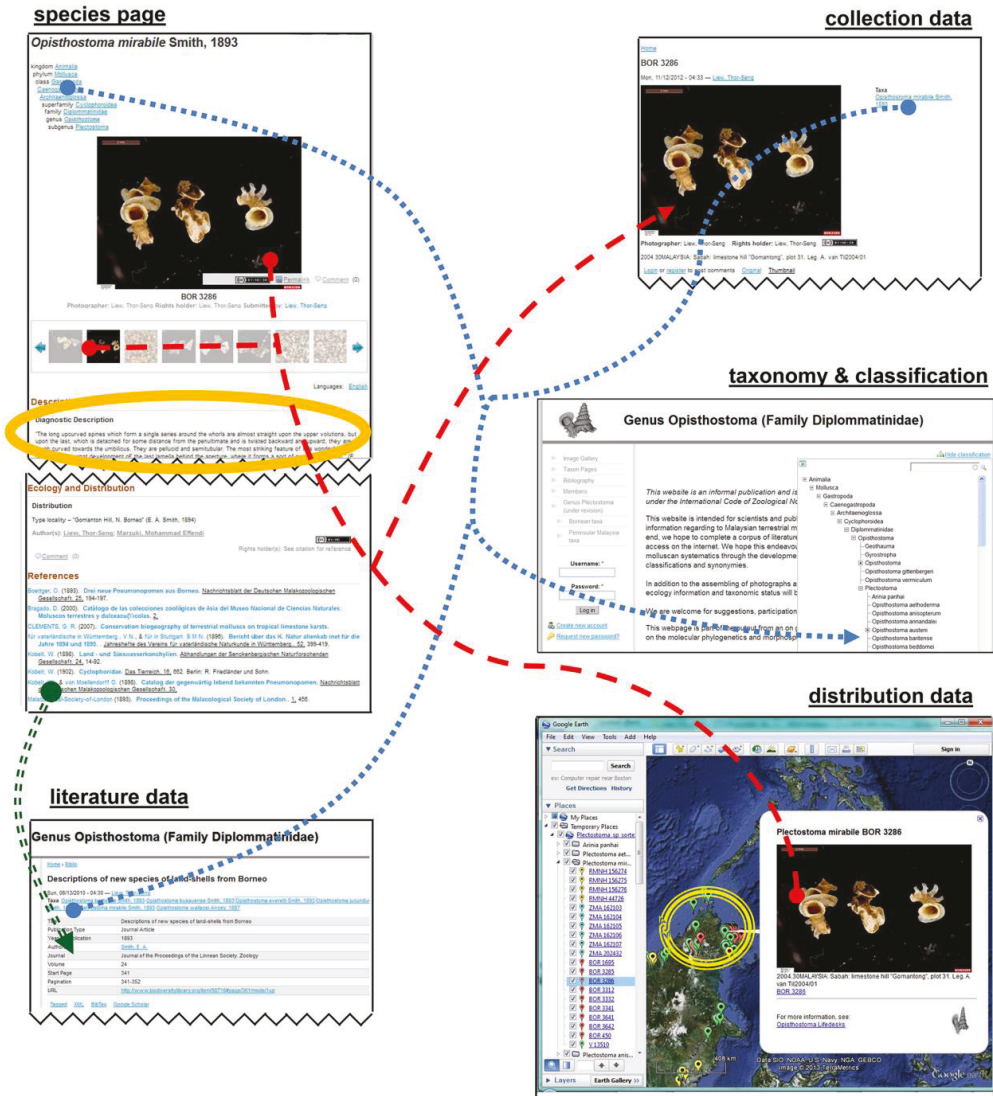


Figure 14. User interface of the Lifedesks online database and Google Earth. Lifedesks was used for data storage, management, and tagging; Google Earth was used for data sorting and exploration.

Our shell shape characterisation approach that views the shell as a petrified ontogeny provides a set of distinguishable general characters for species delimitation (Table 3). Most of the species in this study can be identified just by using these general shape characters. Furthermore, those species that are not distinguishable with these general shape characters, are distinguishable by using more specific shell shape and size characters (see Taxonomy Key).

However, it is important to note that the intra- and inter-specific variation in shell shape is more difficult to characterise than the variation in shell size. This is reflected in our species description, where the variation in shell size and countable shell characters, such as ribs, but not the variation in general shell shape are explicitly given. Nevertheless, the general qualitative shell shape characters do implicitly reflect the variation because many of these, such as spire shape, tuba, and spiral lines, are obtained by categorising the quantitative variation of these characters (e.g. Figures 4 and 5).

Conservation status assessment

Overall, we suggest that 10 of the non-Bornean *Plectostoma* species are threatened and *P. sciaphilum* is extinct. Specifically, *P. umbilicatum*, *P. senex*, *P. turriforme*, *P. retrovertens*, *P. charasense*, and *P. tenggekensis* are in the Critically Endangered category; *P. kubuensis* is in the Endangered category; and *P. dindingsis*, *P. palinhelix*, and *P. laidlawi* are in the Vulnerable category. All of these species, except *P. laidlawi*, occur in limestone hills in the State of Pahang, Malaysia, where many of these hills are being quarried or are at risk of being quarried. Our assessments would eventually be submitted to IUCN.

Molecular phylogeny and COI barcoding

As revealed by the Bayesian posterior probability (PP) and maximum likelihood analysis bootstrap (BS) values of the phylogenetic tree in Figure 16, *Plectostoma* is monophyletic (BI/ML/PA; 1.0/99/100) and is the sister taxon of the less well-supported clade of *Opisthostoma* + *Arinia* (0.5/<70/<70). Within the *Opisthostoma* + *Arinia* clade, all *Opisthostoma* except *Opisthostoma vermiculum* form a well-supported clade (0.98/88/71). The divergence between these clades is similar to the divergence between other genera in Diplommatinidae. Our phylogenetic analysis suggested that *Opisthostoma vermiculum* Clements & Vermeulen, 2008 in Clements et al. (2008) has been incorrectly assigned to the genus *Opisthostoma*.

Table 4 shows the Kimura 2-parameter distances for all sequence pairs within each group and the net average between groups of sequences (for sequence alignment see Appendix 16). This reveals that all species pairs exceed a divergence of 10 % (n = 169), with the exception of *Plectostoma crassipupa* vs. *Plectostoma christae* and *Plectostoma crassipupa* vs. *Plectostoma laidlawi*. Genetic divergence within each species is below 9% (n = 14, mean = 2.6%, SD = 0.1%), with the exception of *Plectostoma crassipupa*.

Table 3. Characters matrix for 31 *Plectostoma* species.

Species that share the same general character state	Species	Apex form	Apical spire form	Basal spire form	Parietal constriction teeth	Basal constriction teeth	Tuba form	Aperture view	Peristome types	Spiral lines	Rib shape	Rib thickness
‡	<i>Plectostoma salpidomon</i> (van Benthem Jutting, 1952)	1	2	2	2	2	2	2	2	2	2	2
‡‡	<i>Plectostoma laemodes</i> (van Benthem Jutting, 1961)	1	2	2	2	2	2	2	2	2	2	2
	<i>Plectostoma dindingsensis</i> sp. n.	2	2	2	4	2	1	3	2	1	3	2
	<i>Plectostoma mengaburensis</i> sp. n.	2	2	2	4	2	1	3	2	1	3	2
§	<i>Plectostoma ikanensis</i> sp. n. Form BOR 5504	2	2	1	4	2	2	1	2	1	3	2
§	<i>Plectostoma ikanensis</i> sp. n. Form BOR 5507	2	2	1	4	2	2	1	2	1	3	2
	<i>Plectostoma annandalei</i> (Sykes, 1903)	1	2	1	?	?	2	2	2	?	3	?
	<i>Plectostoma kayiani</i> sp. n.	2 or 3	2	1	4	2	2	1	2	2	1	2
	<i>Plectostoma charasense</i> (Tomlin, 1948)	1	1	1	2	1	2	2	2	2	2	1
	<i>Plectostoma christae</i> (Maassen, 2001)	2	2	2	2	2	1	4	2	2	3	2
	<i>Plectostoma crassipupa</i> (van Benthem Jutting, 1952)	2 or 3	2	2	4	2	3	4	2	1	3	2
	<i>Plectostoma davisoni</i> sp. n.	2 or 3	2	2	2	2	2	1	2	1	3	2
	<i>Plectostoma kaktense</i> (Tomlin, 1948)	2 or 3	2	2	2	2	2	2	2	2	3	2
	<i>Plectostoma kitteli</i> (Maassen, 2002)	1	1	1	2	2	2	2	2	2	2	2
	<i>Plectostoma klongsangensis</i> (Panha, 1997)	1	1	1	?	?	2	2	2	1	1	1
	<i>Plectostoma kubuensis</i> sp. n.	2 or 3	2	2	4	2	2	2	2	2	3	2
	<i>Plectostoma laidlawi</i> (Sykes, 1902)	1 or 2	2	1	2	2	2	2	2	1	3	2
	<i>Plectostoma palinhelix</i> (van Benthem Jutting, 1952)	3	2	2	2	2	2	3	2	1	3	2
	<i>Plectostoma panhai</i> (Maassen, 2001)	2	2	2	3	2	1	3	2	1	3	2
	<i>Plectostoma praeco</i> (van Benthem Jutting, 1961)	1	2	1	2	2	2	2	2	2	2	2

Table 3. (continued)

	<i>Plectostoma relauensis</i> sp. n.	2 or 3	2	2	3	2	2	2	1	2	1	2	1	3	2
	<i>Plectostoma retrovertens</i> (Tomlin, 1938)	2	2	2	2	2	2	2	3	2	1	3	1	3	2
	<i>Plectostoma sciaphilum</i> (van Benthem Jutting, 1952)	1	1	2	2	2	2	3	4	2	1	2	2	2	2
	<i>Plectostoma senex</i> (van Benthem Jutting, 1952)	1	1	2	2	2	1	3	4	2	2	2	2	2	2
	<i>Plectostoma sinyumensis</i> (Maassen, 2001)	2	2	3	4	2	1	3	2	2	3	2	2	3	2
	<i>Plectostoma siphonostomum</i> (van Benthem Jutting, 1952)	1	1	1	2	2	1	4	2	1	3	2	1	3	2
	<i>Plectostoma tenggekensis</i> sp. n.	2	2	1	2	2	2	2	2	2	2	2	2	1	2
	<i>Plectostoma tohchinyawi</i> sp. n.	1	1	1	2	2	2	2	2	2	2	1	1	1	1
	<i>Plectostoma tonkinianum</i> (Dautzenberg & Fischer, 1905)	1	2	2	1	2	3	1	1	2	2	2	2	2	2
	<i>Plectostoma turriforme</i> (van Benthem Jutting, 1952)	1	1	2	1	1	3	4	2	2	2	2	2	2	2
	<i>Plectostoma umbilicatum</i> (van Benthem Jutting, 1952)	2	1	2	4	2	1	3	2	1	3	2	1	3	2
	<i>Plectostoma whitteri</i> sp. n.	1	2	2	4	2	3	1	2	2	3	2	2	3	2

CharactersCharacter states

Apex form (Figure 4) 1 = distinctly convex; 2 = moderately convex; 3 = slightly convex.

Apical spire form (Figure 5)

1 = oblong; 2 = depressed.

Basal spire form (Figure 6)

1 = conical; 2 = ovoid; 3 = ellipsoid.

Parietal constriction teeth (Figure 7)

1 = two long lamella; 2 = two knob-shaped teeth; 3 = single knob-shaped tooth; 4 = no tooth.

Basal constriction teeth (Figure 8)

1 = two knob-shaped teeth; 2 = no tooth.

Tuba form (Figure 9)

1 = tuba type 1; 2 = tuba type 2; 3 = tuba type 3.

Aperture view

1 = frontal view; 2 = right lateral view; 3 = back view; and 4 = left lateral view.

Peristome types (Figure 11)

1 = simple peristome; 2 = double peristome.

Spiral lines (Figure 12)

1 = thick and thin; 2 = thin only.

Rib shape (Figure 13C)

1 = single-humped; 2 = slightly curved; 3 = straight.

Rib thickness (Figure 13B)

1 = thick; 2 = thin.

One key determinant for the success of DNA barcoding is prior knowledge of intra- and interspecific genetic distances for the barcoding marker in question. The optimum intra- and interspecific threshold in gastropods is higher than the conventional value (Hebert et al., 2003) of 3% (e.g. 4% in Davison et al. 2009, 6% in Köhler & Johnson 2012, 9.8%–25% in Parmakelis et al., 2013). In our study, we also found higher values of intraspecific variation and interspecific divergence' of COI for three well-defined species, namely, *Plectostoma salpidomon*, *Plectostoma christae*, and *Plectostoma siphonostomum* are larger and smaller than 10%, respectively.

A study on a pulmonate limestone-dwelling micro-landsnail in the same region also suggests intraspecific COI divergence not exceeding 10 % based on the Kimura 2-parameter model (Hoekstra & Schilthuizen, 2011), and similar values were obtained for *Everettia*, a Malaysian pulmonate not restricted to limestone (Liew et al., 2010). Hence, based on our results, together with the only other two studies on the COI variation of land snails in Sundaland, we advise caution in using a conventional threshold value in COI genetic variability for species delimitation, when the background genetic variability of COI is unknown for a particular taxon in a particular geographic region.

Figure 16. The phylogeny of Diplommatinidae genera with *Cochlostoma septemspirale* (Wagner, 1897) as outgroup. Bayesian inference 50% majority-rule consensus trees based on the concatenated dataset consisting of parts of 28S, 18S, COI, and 16S. Bayesian posterior probabilities, percent bootstrap support after 1000 maximum likelihood replicates, and percent bootstrap support after 1000 maximum parsimony replicates are shown for the major clades. Clade A consists of *Plectostoma* species, Clade B consists of *Opisthostoma* species. The shell forms are shown for representative taxa. Details of the taxa can be found in Table 1 (no. 1–28, 42, 48, 61, 69, 71, 73, and 78). Scale bar = 1 mm.

(See next page)

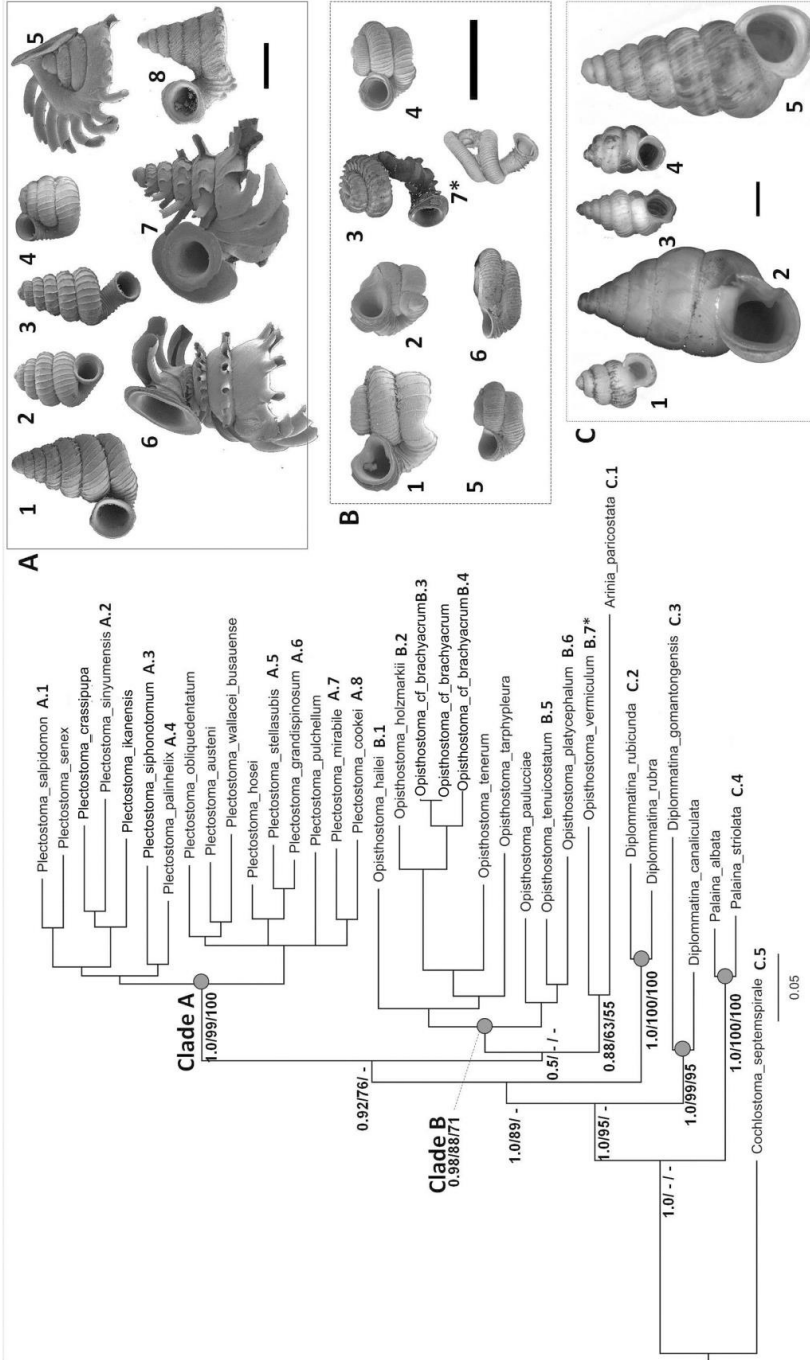


Table 4. COI sequence divergence† within and between 19 *Plectostoma* species.

		Divergence between Groups of Sequences §																					
Divergence within Groups ‡	number of specimens	<i>christae</i>	<i>crassipupa</i>	<i>davisoni</i>	<i>dindingensis</i>	<i>ikanensis</i>	<i>kakiense</i>	<i>kubuensis</i>	<i>laidlawi</i>	<i>mengaburensis</i>	<i>palinhelix</i>	<i>relanensis</i>	<i>retrovertens</i>	<i>salpidomon</i>	<i>senex</i>	<i>relauensis</i>	<i>retrovertens</i>	<i>salpidomon</i>	<i>umbilicatum</i>	<i>tohchinyawi</i>	<i>siphonostomum</i>	<i>sinyumensis</i>	
0.06	8																						
0.13	3		0.09*																				
0.00	2			0.12																			
n.a.	1			0.14	0.20																		
0.01	6			0.15	0.11	0.18	0.19																
n.a.	1			0.14	0.11	0.17	0.21	0.17															
0.00	2			0.16	0.14	0.20	0.18	0.19	0.16														
0.08	3			0.12	0.09 *	0.16	0.17	0.16	0.15	0.15													
0.01	2			0.14	0.10	0.18	0.20	0.16	0.21	0.14													
0.00	2			0.13	0.12	0.18	0.15	0.18	0.20	0.16	0.16	0.15	0.19	0.18	0.16								
n.a.	1			0.12	0.13	0.21	0.17	0.20	0.19	0.15	0.14	0.11	0.15	0.18	0.12								
n.a.	1			0.12	0.13	0.19	0.14	0.18	0.19	0.17	0.18	0.11	0.15	0.18	0.12								
0.04	5			0.11	0.11	0.15	0.14	0.16	0.19	0.14	0.15	0.12	0.15	0.15	0.12								
n.a.	1			0.15	0.14	0.19	0.18	0.19	0.21	0.15	0.22	0.14	0.19	0.14	0.12								

Table 4. (continued)

2	0.00	<i>sinyumensis</i>	0.17	0.12	0.19	0.21	0.20	0.18	0.20	0.15	0.19	0.20	0.20	0.20	0.18	0.21			
5	0.03	<i>siphonostomum</i>	0.10	0.12	0.17	0.15	0.17	0.17	0.17	0.15	0.17	0.14	0.14	0.12	0.12	0.18	0.19		
2	0.00	<i>tohchinyawi</i>	0.13	0.12	0.18	0.16	0.17	0.18	0.20	0.15	0.18	0.12	0.17	0.13	0.06	0.10	0.21	0.14	
2	0.00	<i>umbilicatum</i>	0.16	0.13	0.19	0.21	0.19	0.17	0.20	0.16	0.18	0.19	0.20	0.19	0.18	0.22	0.13	0.19	0.20
2	0.01	<i>whitteni</i>	0.15	0.14	0.18	0.16	0.21	0.21	0.23	0.18	0.20	0.15	0.18	0.14	0.11	0.11	0.21	0.15	0.10
																			0.21

†Analyses were conducted using the Kimura 2-parameter model (Kimura, 1980). The analysis involved 51 nucleotide sequences.

Codon positions included were 1st+2nd+3rd. All positions with less than 95% site coverage were eliminated. There were a total of 615 positions in the final dataset. These analyses were conducted in MEGA5 (Tamura et al. 2011).

‡The number of base substitutions per site from averaging over all sequence pairs within each group.

§The number of base substitutions per site from estimation of net average between groups of sequences. Genetic distances between two species smaller than 10% are shown in bold.

Key to non-Bornean *Plectostoma*

1	Oblong apical spire	2
-	Depressed apical spire	10
2	Tuba with type 1 coiling	3
-	Tuba with type 2 or 3 coiling	4
3	Constriction with 2 parietal teeth. Aperture visible when shell observed in left lateral view	<i>P. siphonostomum</i>
-	Constriction without parietal tooth. Aperture visible when shell observed in back view	<i>P. umbilicatum</i>
4	Tuba with type 2 coiling. Aperture visible when shell observed in right lateral view	5
-	Tuba with type 3 coiling. Aperture visible when shell observed in left lateral view	8
5	Spire with both thick and thin spiral lines	6
-	Spire with only thin spiral lines	7
6	Left lateral side of outer peristome projected not more than two times the width of the right lateral side	<i>P. tohchinyawi</i>
-	Left lateral side of outer peristome projected more than three times the width of the right lateral side	<i>P. klongsangensis</i>
7	Constriction with 2 basal teeth	<i>P. charasense</i>
-	Constriction without basal tooth	<i>P. kitteli</i>
8	Constriction without basal tooth	<i>P. sciaphilum</i>
-	Constriction with 2 basal teeth	9
9	Constriction with 2 long lamella-shaped parietal teeth	<i>P. turriforme</i>
-	Constriction with knob-shaped parietal teeth	<i>P. senex</i>
10	Tuba with type 1 coiling	11
-	Tuba with type 2 or 3 coiling	15
11	Constriction with 1 or 2 parietal teeth	12
-	Constriction without parietal teeth	13
12	Constriction with 1 parietal tooth	<i>P. panhai</i>
-	Constriction with 2 parietal teeth	<i>P. christae</i>
13	Ellipsoid basal spire	<i>P. sinyumensis</i>
-	Ovoid basal spire	14
14	More than 1/4 of the tuba visible in top view	<i>P. mengaburensis</i>
-	Less than 1/4 of the tuba visible in top view	<i>P. dindingensis</i>

Chapter 2

15	Tuba with type 3 coiling	16
-	Tuba with type 2 coiling	18
16	Simple peristome	<i>P. tonkinianum</i>
-	Double peristome	17
17	Aperture visible when shell observed in frontal view	<i>P. whitteni</i>
-	Aperture visible when shell observed in left lateral view	<i>P. crassipupa</i>
18	Aperture visible when shell observed in frontal or back views	19
-	Aperture visible when shell observed in right lateral view	24
19	Aperture visible when shell observed in back views	20
-	Aperture visible when shell observed in frontal views	21
20	Spire 1.6 – 1.9 mm high	<i>P. palinhelix</i>
-	Spire 2.3 – 2.6 mm high	<i>P. retrovertens</i>
21	Ovoid basal spire	22
-	Conical basal spire	23
22	Constriction with 1 parietal tooth	<i>P. relauensis</i>
-	Constriction with 2 parietal teeth	<i>P. davisoni</i>
23	Spire with both thick and thin spiral lines	<i>P. ikanensis</i>
-	Spire with only thin spiral lines	<i>P. kayiani</i>
24	Spire with straight radial ribs	25
-	Spire with slightly curved or single-humped radial ribs	28
25	Conical basal spire	26
-	Ovoid basal spire	27
26	Whorl periphery distinctly convex	<i>P. laidlawi</i>
-	Whorl periphery slightly convex	<i>P. annandalei</i>
27	Constriction without parietal teeth	<i>P. kubuensis</i>
-	Constriction with 2 parietal teeth	<i>P. kakiense</i>
28	Conical basal spire	29
-	Ovoid basal spire	30
29	Spire 1.6 – 1.7 mm high	<i>P. tenggekensis</i>
-	Spire 2.0 – 2.2 mm high	<i>P. praeco</i>
30	Whole tuba attaches to spire	<i>P. laemodes</i>
-	Less than 2/3 of the tuba attaches to spire	<i>P. salpidomon</i>

Taxonomy

Genus *Plectostoma*

Plectostoma Adam 1865: 177. Type species: *Plectostoma DeCrespignii* (by original designation)

Geothauma Crosse 1892: 282. Type species (by original designation): *Plectostoma grandispinosum* (Godwin-Austen, 1889).

Generic classification dispute. The genus *Opisthostoma* was described by Blanford and Blanford (1860) based on one species – *Opisthostoma nilgircum* from India. Adam (1865b) described a second species of *Opisthostoma*, namely, *Opisthostoma decrespignyi*, which he previously described under the new genus *Plectostoma* (Adam 1865a). Nevertheless, Blanford (1867) concluded that the conchological differences between these two taxa were not enough to create a different genus. Instead, he suggested these could be two different subgenera. Next, another two subgenera – *Gyrostropha* Ancey, 1887 and *Geothauma* Crosse, 1892, were proposed for different forms of *Opisthostoma* and *Plectostoma*. However, Smith (1893a) suggested that this subgeneric classification was not necessary until more data other than shell morphology were available. Since then, a classification into three subgenera within the genus *Opisthostoma*, namely, *Geothauma*, *Opisthostoma*, and *Plectostoma* has generally been accepted (e.g. von Martens & Thiele, 1908; van Benthem-Jutting; 1932, 1952), until, in a recent review of the genus *Opisthostoma*, Vermeulen (1991, 1994) followed a classification into only two subgenera, namely, *Opisthostoma* and *Plectostoma*.

Diagnosis. Despite the distinct ecological niche differences (see below–**Distribution and habitat**) between *Opisthostoma* and *Plectostoma*, it is not feasible to use this criterion in the genus identification, because information about the ecology is usually not available as most collections are made by soil sampling. After 150 years of work on *Opisthostoma*, it is still difficult to identify reliable apomorphic character states that can be used to distinguish between *Opisthostoma* and *Plectostoma* (Vermeulen, 1991, 1994). Both share the character state of the constriction, which is a slight shrinkage in the whorl towards the end of the spire. When the animal retracts into its shell, its operculum rests at the constriction (Vermeulen, 1991). It is, however, possible to make a morphological distinction between *Opisthostoma* and *Plectostoma* on the basis of the shell colouration in a fully grown adult, which is orange or pinkish in *Plectostoma* and white or pale yellowish in *Opisthostoma*. The colour differences between these two genera are very clear when comparing the living snails or freshly dead shell material (Figure 17, and Appendix 18). Some *Plectostoma* species have a regularly coiled tuba, and a shell form that is similar to *Arinia*. However, *Plectostoma* and *Arinia* can be easily distinguished by shell colour differences. The shell colour in *Arinia* is similar to that in *Opisthostoma*.

Description.

Apex. Protoconch is either slightly, moderately or distinctly convex (Figure 3).

Spire. Height: 1.0 mm – 3.7 mm. Width: 0.85 mm – 2.60 mm (Figure 11). Number of whorls between 2 3/4 – 7 1/4. Apical spire shape: oblong or depressed conical (Figure 4). Basal spire

shape: conical, ovoid or ellipsoid (Figure 5). Whorl periphery: flat, slightly, moderately or distinctly convex. Umbilicus: open, partially closed, or totally closed.

Constriction. Parietal teeth: parietal side of inner constriction whorl (Figure 2) with two long lamellae (Figure 6A), two ridges with a knob at each end (Figure 6B), one ridge with a knob at one end (Figure 6C), or no teeth (Figure 6D). Basal teeth: basal side of inner constriction whorl (Figure 2) with no teeth (Figure 7B), one ridge running parallel with the whorl growing direction, one ridge with a knob at one end running perpendicular to the whorl growing direction, or a combination of the latter two types (Figure 7A).

Tuba. Coiling direction: regular coiling (type 1, Figure 8A) or distorted (Type 2, or 3) (Figure 8B and C). Tuba whorl length in proportion to spire last whorl: *ca.* 3/8 – 1 1/2. Proportion of tuba that attaches to spire: whole to none.

Aperture and peristome. Peristome: simple aperture without outer peristome (Figure 10B), or double peristome (Figure 10C and 10D). Shape of outer peristome (Figure 10A): same as inner peristome and uniformly round, or highly projected or slightly projected at either a particular side or at a several sides of anterior, posterior, left and right lateral (Figure 9 and 10A).

Spiral lines. Either thick or thin, or only thin lines present (Figure 12).

Radial ribs. Rib density: 4 – 32 per mm on the spire's last whorl in right lateral view (Figure 13A). Intensity: thick or thin (Figure 13B). Shape: straight, slightly curved, distinctly curved, single humped, single looped or double looped and the shape remaining the same or changing between between the spire and the tuba (Figure 13C, but single-looped, and double-humped not shown). Inclination: from orthoclin to prosoclin.

Distribution and habitat. The distribution range of *Plectostoma* is about 4.6 million square kilometres within the extent limited by 11° N 97° E and 5° S 120°. However probably less than 5% of this large area is covered by limestone outcrops where suitable habitat may exist for obligate karst taxa like *Plectostoma*. The genus counts 79 species and occurs in Vietnam (1 species), Thailand (1), Peninsular Malaysia (28), Sumatra (1), and Borneo (48). Peninsular Malaysia, Sumatra and Borneo are part of the biogeographical region called Sundaland (Johnson, 1964). *Plectostoma* is found on most limestone hills. However, the genus is conspicuously absent on the limestone hills to the west of the central mountain ranges, such as the hills in the States of Perak and Kedah in Peninsular Malaysia, and in the northwestern half of Sumatra (Figure 18). No species have been recorded from the east coast of Sumatra, where hardly any limestone outcrops exist.

Based on collection data and our field experience, there is a distinct ecological divergence between *Plectostoma* and *Opisthostoma*. This was already observed in the 19th century (Blanford & Blanford, 1860; de Crespigny, 1865; Blanford, 1866), and also by Berry (1961). *Plectostoma* can only be found in limestone outcrops, where the rock face is its major habitat, although a few individuals can occasionally be found on vegetation debris below the limestone rock face. *Opisthostoma*, on the other hand, is a soil dweller, living in leaf litter on the forest floor. They are mostly but not exclusively found in forest over limestone bedrock (Schilthuizen et al., 2003b).



Figure 17. Photographs of 17 living *Plectostoma* species. **A** *Plectostoma salpidomon* (van Benthem Jutting, 1952), BOR 5569; **B** *Plectostoma umbilicatum* (van Benthem Jutting, 1952), BOR 5503; **C** *Plectostoma palinhelix* (van Benthem Jutting, 1952), BOR 5520; **D** *Plectostoma kakiense* (Tomlin, 1948), BOR 5516; **E** *Plectostoma mengaburensis* sp. n., BOR 5574; **F** *Plectostoma kubuensis* sp. n., BOR 5518; **G** *Plectostoma whitteni* sp. n., BOR 5536; **H** *Plectostoma senex* (van Benthem Jutting, 1952), BOR 5631; **I** *Plectostoma crassipupa* (van Benthem Jutting, 1952), BOR 5515; **J** *Plectostoma ikanensis* sp. n. Form BOR 5507, BOR 5507; **K** *Plectostoma ikanensis* sp. n. Form BOR 5504, BOR 5504; **L** *Plectostoma sinyumensis* (Maassen, 2001), BOR 5537; **M** *Plectostoma crassipupa* (van Benthem Jutting, 1952), BOR 5512; **N** *Plectostoma siphonostomum* (van Benthem Jutting, 1952), BOR 5557; **O** *Plectostoma laidlawi* (Sykes, 1902) Form BOR 5510, BOR 5510; **P** *Plectostoma relauensis* sp. n., BOR 5511; **Q** *Plectostoma christae* (Maassen, 2001), BOR 5505; **R** *Plectostoma retrovertens* (Tomlin, 1938), BOR 5559; **S** *Plectostoma tohchinyawi* sp. n., BOR 5533.

Phylogenetic relationships. Our molecular phylogenetic analysis reveals that *Plectostoma*, *Opisthostoma*, and *Arinia* are phylogenetically closely related (Figure 16). It is important to point out that the phylogenetic relationships among *Plectostoma*, *Opisthostoma* (except *O. vermiculum*), *O. vermiculum*, and *Arinia* are unresolved. Figure 16 shows representative shell morphologies of the taxa that were included in the phylogenetic analysis, and it is clear that it is rather difficult to find shared derived characteristics (synapomorphies) in size, spire shape, or tuba coiling regime, for either *Opisthostoma* or *Plectostoma*.

Nonetheless, we treat *Plectostoma* and *Opisthostoma* as two separate genera based on their ecological divergence and differences in adult shell colouration. Similarly, we propose that *O. vermiculum* and *Arinia* should be considered as two separate genera. However, this hypothesis needs further testing with more genetic data from *O. vermiculum* Clements & Vermeulen 2008 (in Clements et al., 2008), the conchologically similar *O. gittenbergeri* Vermeulen & Clements 2008 and further *Arinia* species.

***Plectostoma dindingensis* sp. n.**

Figure 19 and Appendix 7.

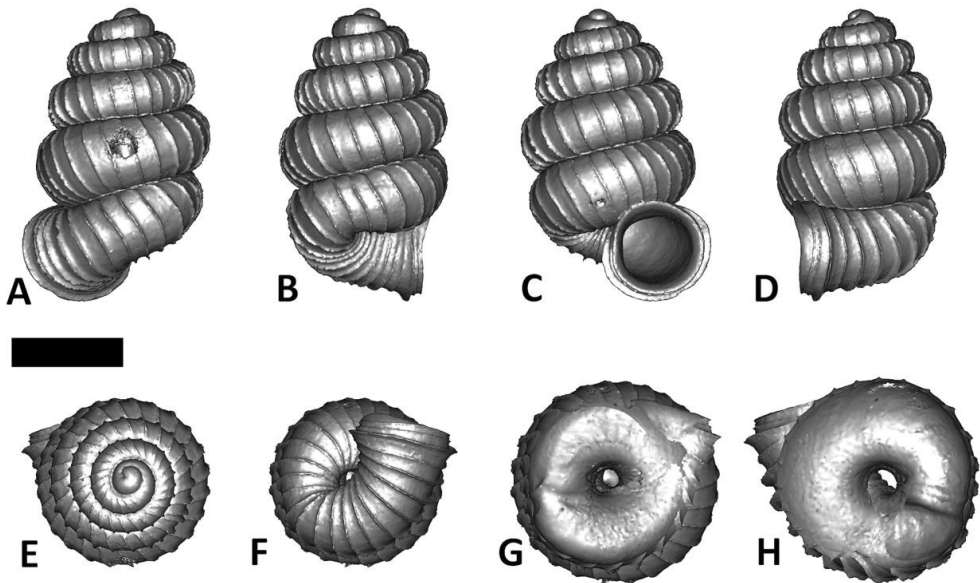


Figure 19. *Plectostoma dindingensis* sp. n. BOR 5642, Holotype. **A** frontal view; **B** left lateral view; **C** back view; **D** right lateral view; **E** top view; **F** bottom view; **G** parietal part of constriction inner whorl; **H** basal part of constriction inner whorl. Scale bar = 1 mm (for A – F).

Type material

Holotype: BOR 5642(1)

Paratypes: BOR 5612(3)

Diagnosis

Shares with *P. mengaburensis* and *P. panhai* the general shell form, in terms of apex, spire and tuba, but differs by lacking constriction teeth and having a more tightly coiled tuba (less than 1/4 of the tuba visible in top view).

Etymology

This species is named after its type locality – Dinding.

Description.

Apex. Shape: moderately convex.

Spire. Height: 1.8 – 1.9 mm. Width: 1.4 – 1.5 mm. Number of whorls: 3 7/8–4 5/8. Apical spire shape: depressed conical. Basal spire shape: ovoid. Whorl periphery: distinctly convex. Umbilicus: partially closed by tuba.

Constriction. Parietal teeth: none. Basal teeth: none.

Tuba. Coiling direction: type 1 and aperture visible from back view. Tuba whorl length in proportion to spire last whorl: *ca.* 5/8 – 3/4. Proportion of tuba that attaches to the spire: whole.

Aperture and peristome. Peristome: double peristomes. Outer peristome shape: same as inner peristome and uniformly projected all around, except the posterior part.

Spiral lines. Thick lines: present. Thin lines: present.

Radial ribs. Rib density: 6 – 8 ribs per mm. Rib intensity: thin. Shape: straight. Inclination: orthoclin.

Distribution

Type locality. The exact location is unknown. The specimens are labeled as collected from "dinding". It could be near Kampung Bukit Dinding, Pahang (3° 49' 41" N, 102° 22' 3" E).

Distribution range. This species has only been recorded from the type locality (Figure 18D).

Conservation status

Vulnerable (D2 ver. 10.1). The samples was collected from a living population in 1997. The population status remains unclear. The area around Kampung Bukit Dinding has been converted to plantation and no significant undisturbed forest coverage remains.

Discussion

See discussion under *P. christae*.

***Plectostoma mengaburensis* sp. n.**

Figures 17E and 20, and Appendix 7.

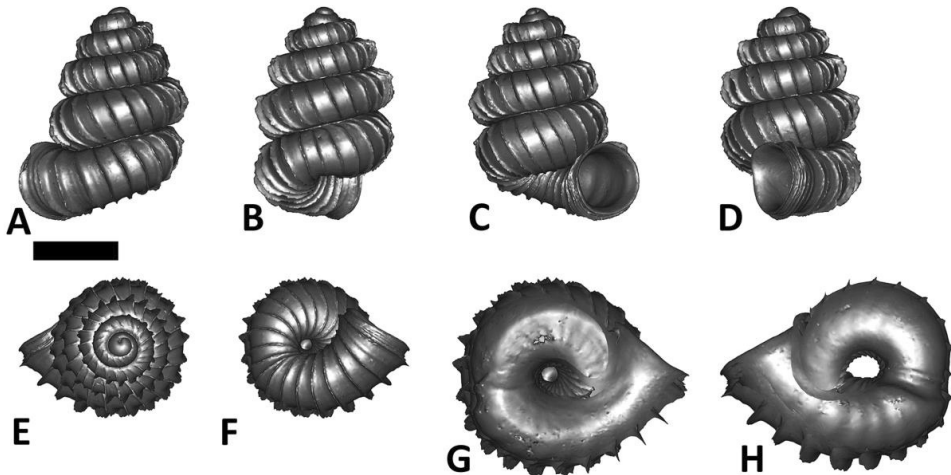


Figure 20. *Plectostoma mengaburensis* sp. n. BOR 5643. **A** frontal view; **B** left lateral view; **C** back view; **D** left lateral view; **E** top view; **F** bottom view; **G** parietal part of constriction inner whorl; **H** basal part of constriction inner whorl. Scale bar = 1 mm (for **A – F**).

Type material

Holotype: BOR 5643(1)

Paratypes: BOR 5574(>25), V8822 (6)

Diagnosis

Shares with *P. dindigenis* and *P. panhai* the general shell form, in the terms of apex, spire and tuba, but differs by lacking constriction teeth and having a less tightly coiled tuba (more than 1/4 of the tuba visible in top view).

Etymology

This species is named after its type locality – Mengabur.

Description.

Apex. Shape: moderately convex.

Spire. Height: 1.9 – 2.2 mm. Width: 1.4 – 1.6 mm. Number of whorls: 3 7/8–4 1/2. Apical spire shape: depressed conical. Basal spire shape: ovoid. Whorl periphery: distinctly convex. Umbilicus: open or half of the umbilicus closed by tuba.

Constriction. Parietal teeth: none. Basal teeth: none.

Tuba. Coiling direction: type 1 and aperture visible from back view. Tuba whorl length in proportion to spire last whorl: *ca.* 5/8. Proportion of tuba that attaches to spire: whole.

Aperture and peristome. Peristome: double peristomes. Outer peristome shape: same as inner peristome and uniformly projected all around, except the posterior part.

Spiral lines. Thick lines: present. Thin lines: present.

Radial ribs. Rib density: 7 ribs per mm. Rib intensity: thin. Shape: straight. Inclination: orthoclin.

Distribution

Type locality. An unnamed small limestone hill in the plantation near the large Bukit Mengabur quarry (3° 43' 50" N, 102° 49' 40" E).

Distribution range. This species only occurs in the Mengabur limestone cluster (Figure 18D).

Conservation status

Near Threatened. This species only occurs in the Mengabur limestone cluster, which is quite large (*ca.* 10 km², estimated from Google Earth), and its vegetation cover is largely undisturbed. However, quarrying activities have started at the eastern part of the cluster and the whole limestone cluster is surrounded by plantation.

Discussion

See discussion under *P. christae*.

***Plectostoma sinyumensis* (Maassen, 2001)**

Figures 17L and 21, and Appendix 7.

Opisthostoma sinyumensis Maassen, 2001: 52, figures 1, 6 & 7 (original description).

Opisthostoma sinyumensis Maassen, Clements (2007: 74).

Opisthostoma sinyumensis Maassen, Clements et al. (2008: 2760).

Opisthostoma sinyumensis Maassen, Webster et al. (2012: 628).

Type material

Holotype: ZMA 138439(1) (Seen).

Paratypes: ZMA 138440(>25) (Seen), RMNH 81804(2) (Seen).

Other examined materials

BOR 462(5), BOR 5537(>10), BOR 5623(>50).

Diagnosis

Shares with *P. dindigenis*, *P. mengaburensis*, *P. christae*, and *P. panhai* the general shell form, in terms of apex, apical spire and tuba, but differs by having an ellipsoid basal spire.

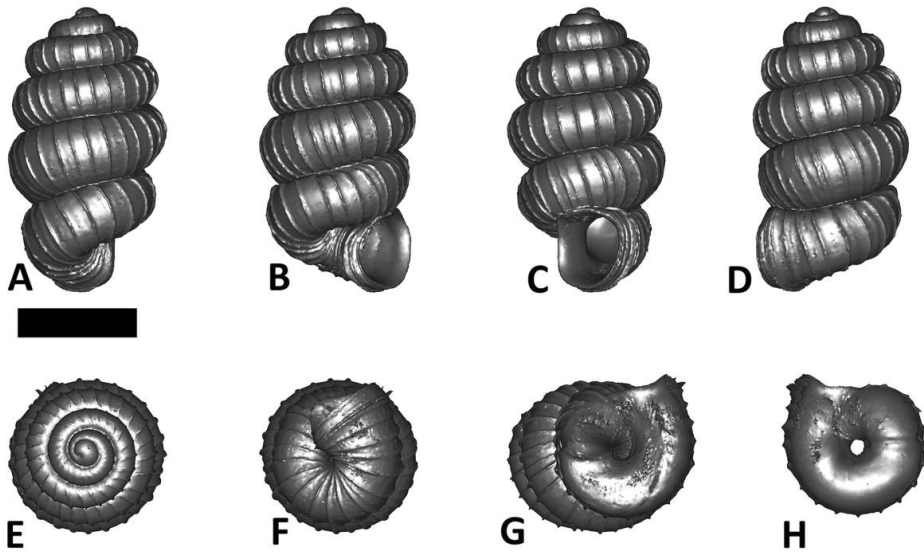


Figure 21. *Plectostoma sinyumensis* (Maassen, 2001) BOR5537. **A** frontal view; **B** left lateral view; **C** back view; **D** right lateral view; **E** top view; **F** bottom view; **G** parietal part of constriction inner whorl; **H** basal part of constriction inner whorl. Scale bar = 1 mm (for A – F).

Description.

Apex. Shape: moderately convex.

Spire. Height: 1.6 – 1.9 mm. Width: 1.2 – 1.3 mm. Number of whorls: 3 - 3 3/4. Apical spire shape: depressed conical. Basal spire shape: ellipsoid. Whorl periphery: distinctly convex. Umbilicus: almost completely closed by tuba.

Constriction. Parietal teeth: none. Basal teeth: none.

Tuba. Coiling direction: type 1 and aperture visible between right lateral and back view. Tuba whorl length in proportion to spire last whorl: *ca.* 5/8 – 3/4. Proportion of tuba that attaches to spire: whole.

Aperture and peristome. Peristome: double peristomes. Outer peristome shape: same as inner peristome and uniformly projected all around, except the posterior part.

Spiral lines. Thick lines: absent. Thin lines: present.

Radial ribs. Rib density: 9–10 ribs per mm. Rib intensity: thin. Shape: straight. Inclination: orthoclin.

Distribution

Type locality. Gunung Senyum, Pahang (3° 42' 35" N, 102° 26' 3" E).

Distribution range. In addition to the type locality, this species also was found at the Jebak Puyuh limestone outcrop, which lies about 1 km east of Gunung Senyum (Figure 18D). BOR 462 was collected in Pulau Singa Besar, which is located about 300 km from type locality. The reliability of the collection data is dubious (the same was found for BOR 463 of *P. relauensis*).

Conservation status

Near Threatened. There are four limestone hills in this cluster. Gunung Senyum and Jebak Puyuh are the larger among these four hills. The former is gazetted as recreation forest but the latter has been at risk of destruction. Jebak Puyuh had been earmarked for quarrying several years ago, but the plan has been abandoned. *P. sinyumensis* has been recorded from these two hills, but its status at the two smaller hills remains unknown. In a survey in July 2010, a living population was recorded at Jebak Puyuh, in an enclosed humid sinkhole. Intensive surveying on the limestone rock faces of Gunung Senyum and other parts of Jebak

Puyuh has failed to retrieve any additional living individuals, probably because most of the rock faces were very dry.

Discussion

See discussion under *P. christae*.

***Plectostoma umbilicatum* (van Benthem Jutting, 1952)**

Figure 17B and 22, and Appendix 8.

Opisthostoma umbilicatum van Benthem Jutting, 1952: 49, figure 25 (original description).

Opisthostoma umbilicatum van Benthem Jutting, van Benthem Jutting (1961: 39).

Opisthostoma umbilicatum van Benthem Jutting, Clements (2007: 74).

Opisthostoma umbilicatum van Benthem Jutting, Clements et al. (2008: 2760).

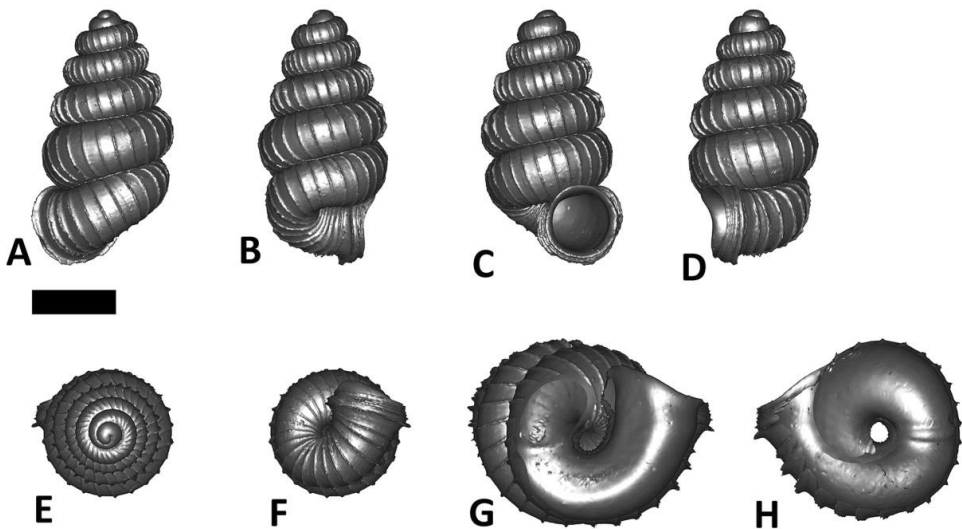


Figure 22. *Plectostoma umbilicatum* (van Benthem Jutting, 1952) BOR5503. **A** frontal view; **B** leftlateral view; **C** back view; **D** right lateral view; **E** top view; **F** bottom view; **G** parietal part of constriction inner whorl; **H** basal part of constriction inner whorl. Scale bar = 1 mm (for A – F).

Type material

Holotype: ZMA 136070(1) (Seen).

Paratypes: ZMA 136071(8) (Seen).

Other examined materials

BOR 5503(>10), BOR 5625(>25).

Diagnosis

Shares with *P. dindingenis*, *P. mengaburensis*, and *P. panhai* the tuba form, but differs by having an oblong conical apical spire.

Description.

Apex. Shape: moderately convex.

Spire. Height: 2.0 – 2.3 mm. Width: 1.3 – 1.5 mm. Number of whorls: 4 5/8–4 3/8. Apical spire shape: oblong conical. Basal spire shape: ovoid. Whorl periphery: distinctly convex. Umbilicus: completely open or partially closed by tuba.

Constriction. Parietal teeth: none. Basal teeth: none.

Tuba. Coiling direction: type 1 and aperture visible from back view. Tuba whorl length in proportion to spire last whorl: *ca.* 1/2 – 3/4. Proportion of tuba that attaches to spire: whole.

Aperture and peristome. Peristome: double peristomes. Outer peristome shape: same as inner peristome and uniformly projected all around, except the posterior part.

Spiral lines. Thick lines: present. Thin lines: present.

Radial ribs. Rib density: 6 – 9 ribs per mm. Rib intensity: thin. Shape: straight. Inclination: orthoclin.

Distribution

Type locality. Limestone hill cluster named Kota Tongkat (3° 53' 28" N, 102° 28' 23" E).

Distribution range. It is only known from the type locality. All other adjacent limestone outcrops have been sampled, but only other *Plectostoma* species were found (Figure 18D).

Conservation status

Critically Endangered (B2ab(iii)+C2a(i) ver. 10.1). The Kota Tongkat limestone cluster is surrounded by oil palm plantation and heavily degraded forest. This species is only known from this limestone cluster. Recent soil samplings have not revealed any recent dead shells (Clement et al., 2008). Nevertheless, we found a living population with fewer than 100 individuals at a wet stalagmite of the entrance of one the caves during an intensive survey in May 2011. During that survey, we noticed that all other rock surfaces of the limestone outcrops in Kota Tongkat were very dry. Thus, the recorded and other unknown living populations are at risk of extinction because a long drought might wipe them out.

Discussion

See discussion under *P. christae*.

Plectostoma siphonostomum (van Benthem Jutting, 1952)

Figure 17N and 23, and Appendix 8.

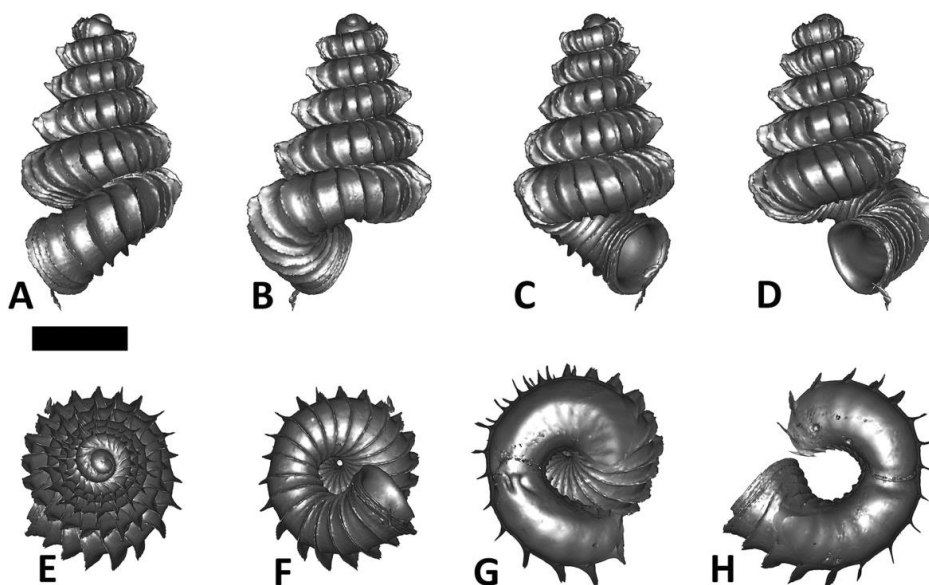


Figure 23. *Plectostoma siphonostomum* (van Benthem Jutting, 1952) BOR5539. **A** frontal view; **B** left lateral view; **C** back view; **D** right lateral view; **E** top view; **F** bottom view; **G** parietal part of constriction inner whorl; **H** basal part of constriction inner whorl. Scale bar = 1 mm (for A – F).

Opisthostoma siphonostomum van Benthem Jutting, 1952: 52, figure 27 (original description).

Opisthostoma siphonostomum van Benthem Jutting, van Benthem Jutting (1961: 39).

Opisthostoma siphonostomum van Benthem Jutting, Berry (1964: 203).

Type material

Holotype: ZMA 136054(1) (Seen).

Paratype: ZMA 136055(8) (Seen).

Other examined materials

ZMA 162138(>100), BOR 5513 (>25), BOR 5521(>10), BOR 5557(>10), V 8199(>50), V 8223(>25).

Diagnosis

Shares with *P. christae* the tuba form, but differs by having an oblong conical apical and conical basal spire.

Description.

Apex. Shape: distinctly convex.

Spire. Height: 1.9 – 2.1 mm. Width: 1.2 – 1.5 mm. Number of whorls: 4 3/4–5. Apical spire shape: oblong conical. Basal spire shape: conical. Whorl periphery: distinctly convex. Umbilicus: Open.

Constriction. Parietal teeth: two. Basal teeth: none.

Tuba. Coiling direction: type 1 and aperture visible between right lateral and back view. Tuba whorl length in proportion to spire last whorl: *ca.* 3/8 – 1/2. Proportion of tuba that attaches to spire: at least 1/2.

Aperture and peristome. Peristome: double peristomes. Outer peristome shape: same as inner peristome and uniformly projected all around, except the posterior part.

Spiral lines. Thick lines: present. Thin lines: present.

Radial ribs. Rib density: 7–8 ribs per mm. Rib intensity: thin. Shape: slightly curved. Inclination: orthoclin.

Distribution

Type locality. Gua Siput, Taman Negara, Pahang (4° 26' 47" N, 102° 14' 44" E).

Distribution range. *P. siphonostomum* has a similar distribution pattern as *P. salpidomon* and often occurs sympatrically with that species. It can be found in many limestone outcrops in the valley between the Titingwangsa Range, Tahan Range and Benom Range (Figure 18D).

Conservation status

Least Concern. Living populations of *P. siphonostomum* were recorded at several limestone hills during surveys between 2010 and 2011. Several of these are located within the National Park.

Discussion

See discussion under *P. christae*.

***Plectostoma panhai* (Maassen, 2001)**

Figure 24 and Appendix 7.

Arinia panhai Maassen, 2001: 55, figure 4, 12 & 13 (original description).

Type material

Holotype: RMNH 81809(1) (Seen).

Paratypes: RMNH 81810(2) (Seen).

Other examined materials

ZMA 138438(1).

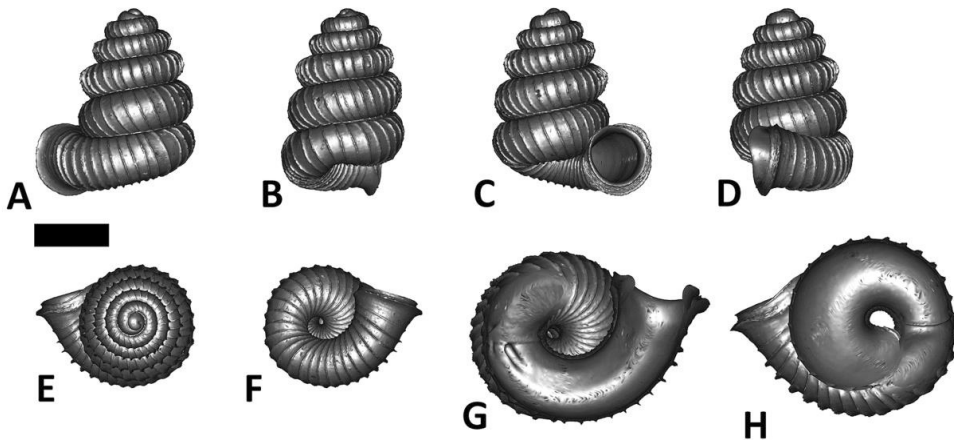


Figure 24. *Plectostoma panhai* (Maassen, 2001) ZMA 138438. **A** frontal view; **B** left lateral view; **C** back view; **D** right lateral view; **E** top view; **F** bottom view; **G** parietal part of constriction inner whorl; **H** basal part of constriction inner whorl. Scale bar = 1 mm (for A – F).

Diagnosis

Shares with *P. mengaburensis* and *P. dindingensis* the general shell form, in the terms of apex, spire and tuba, but differs by having a single parietal constriction tooth.

Description.

Apex. Shape: moderately convex.

Spire. Height: 2.1 – 2.2 mm. Width: 1.6 – 1.7 mm. Number of whorls: 4 1/2–4 5/8. Apical spire shape: depressed conical. Basal spire shape: ovoid. Whorl periphery: moderately convex. Umbilicus: open.

Constriction. Parietal teeth: one. Basal teeth: none.

Tuba. Coiling direction: type 1 and aperture visible from back view. Tuba whorl length in proportion to spire last whorl: *ca.* 3/4. Proportion of tuba that attaches to spire: whole.

Aperture and peristome. Peristome: double peristomes. Outer peristome shape: same as inner peristome and uniformly projected all around, except the posterior part.

Spiral lines. Thick lines: present. Thin lines: present.

Radial ribs. Rib density: 8 – 9 ribs per mm. Rib intensity: thin. Shape: straight. Inclination: orthoclin.

Distribution

Type locality. Tham Krachaeng, Thailand (6° 12' 50" N, 101° 12' 9" E). The location description in the original publication is not completely correct "(06° 55' 022" N, 101° 12' 160" E)" (Maassen 2001).

Distribution range. This species is only known from the type locality (Figure 18D).

Conservation status

Data Deficient.

Discussion

See discussion under *P. christae*.

Plectostoma christae (Maassen, 2001)

Figures 17Q and 25, and Appendix 6.

Opisthostoma christae Maassen, 2001: 52, figures 3, 10 & 11 (original description).

Opisthostoma jensi Maassen, 2001: 56, figures 5, 14 & 15 (original description), **syn. n.**

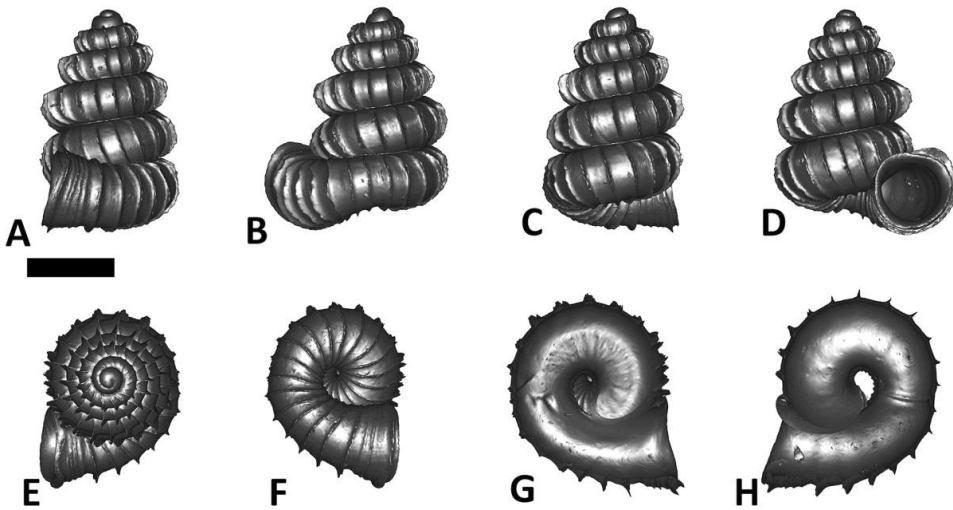


Figure 25. *Plectostoma christae* (Maassen, 2001) BOR 5572. **A** frontal view; **B** left lateral view; **C** back view; **D** right lateral view; **E** top view; **F** bottom view; **G** parietal part of constriction inner whorl; **H** basal part of constriction inner whorl. Scale bar = 1 mm (for A – F).

Type material

Holotype: RMNH 81805(1) (Seen).

Paratypes: RMNH 81806(1) (Seen).

Other examined materials

RMNH 81807(1), RMNH 81808(1), ZMA 138436(1), ZMA 138437(2), BOR 3496(1), BOR 5505(>25), BOR 5506(>50), BOR 5509(>25), BOR 5572(2), V 12702(1), V 8314(>25), V 8406(2), V 9153(2), V 9207(>100), V 9285(3).

Diagnosis

Shares with *P. dindingensis*, *P. mengaburensis*, and *P. panhai* the general shell spire form but differs by having two parietal constriction teeth and aperture visible when shell observed in left lateral view.

Description.

Apex. Shape: moderately convex.

Spire. Height: 1.9 – 2.6 mm. Width: 1.4 – 1.8 mm. Number of whorls: $3 \frac{5}{8}$ – $4 \frac{1}{2}$. Apical spire shape: depressed conical. Basal spire shape: ovoid. Whorl periphery: distinctly convex. Umbilicus: open.

Constriction. Parietal teeth: two. Basal teeth: none.

Tuba. Coiling direction: type 1 and aperture visible from left lateral view. Tuba whorl length in proportion to spire last whorl: *ca.* $\frac{3}{8}$ – $\frac{5}{8}$. Proportion of tuba that attaches to spire: whole.

Aperture and peristome. Peristome: double peristomes. Outer peristome shape: same as inner peristome and uniformly projected all around, except the posterior part.

Spiral lines. Thick lines: absent. Thin lines: present.

Radial ribs. Rib density: 5 – 6 ribs per mm. Rib intensity: thin. Shape: straight. Inclination: orthoclin.

Distribution

Type locality. Limestone hills, 16 km west of Gua Musang ($4^{\circ} 54' 46''$ N, $102^{\circ} 6' 22''$ E).

Distribution range. Limestone hills along the 50 km Northeast transect between $4^{\circ} 38' 51''$ N, $101^{\circ} 58' 58''$ E and $5^{\circ} 0' 13''$ N, $102^{\circ} 11' 59''$ E (Figure 18D).

Conservation status

Near Threatened. Until today, this species has been recorded from at least six limestone hills. In a field survey in 2011 and 2012, living populations of *P. christae* could be found on four of these hills. All of these are located near the road and are surrounded by oil palm plantation, although there is no immediate threat.

Discussion

P. christae, together with *P. dindingsensis*, *P. mengaburensis*, *P. sinyumensis*, *P. umbilicatum*, *P. siphonostomum*, and *P. panhai* represent a group of *Plectostoma* species that have a regulary coiled tuba (type 1 tuba). The species of this group occur only in Peninsular Malaysia and are genetically highly divergent (> 10 % differences in COI) from the others (Table 4). All of the seven species are distributed allopatrically (Figure 18D).

We synonymised *P. jensi* with *P. christae*, both of which were described from the same locality. Maassen (2001) distinguished between them by the slight difference in umbilicus opening and aperture tilting. In the material at our disposal, we recognised that these differences are intrapopulational variation. All individuals share the same diagnostic shell characters as mentioned above. In addition to the morphological evidence, the genetic variation between individuals with different shell forms is smaller than our species delimitation threshold of 10 %.

Two species of this group, namely *P. christae* and *P. siphonostomum*, have a wider distribution range than other species in this group. The two species occur parapatrically on the limestone hills in the centre of Peninsular Malaysia (Figure 18D). On the other hand, very little is known of the distribution range of *P. panhai*. Although this species was reported only once and only from the type locality, it might also occur at other limestone sites near the type locality. *P. panhai* is very similar to *P. christae*, but the two are separated by more than 150 km, and the limestone hills in between are occupied by three other *Plectostoma* species. The disjunct distribution and its single constriction tooth support the decision that *P. panhai* is a distinct species from *P. christae*.

The remaining four species of this group, namely, *P. sinyumensis*, *P. mengaburensis*, *P. dindingsensis*, and *P. umbilicatum*, are site endemics, occurring at each of the four small limestone clusters in the centre of Peninsular Malaysia (Figure 18D). These clusters are each quite isolated, with no other limestone hills within a 20 km radius.

Although these four species occur in adjacent limestone clusters, and they have similar shell shapes, their taxonomic status are clear. The COI sequence divergence between these species is larger than 13 % and each of them has a set of diagnostic shell characters (Tables 3 and 4). This may raise the question how each species evolved in each limestone cluster and how long these four species have been isolated. For example, a neighbouring species, *P. salpidomon*, has a similar distribution range as the former four species, but the morphological and genetic divergence is much smaller than in these four species. Presumably, the answer lies in the details of the geomorphological evolution of the limestone outcrops, which, however, remains largely unknown.

***Plectostoma crassipupa* (van Benthem Jutting, 1952)**

Figures 17I, 17M and 26, and Appendix 6.

Opisthostoma crassipupa van Benthem Jutting, 1952: 51, figure 26 (original description).

Opisthostoma crassipupa van Benthem Jutting, van Benthem Jutting (1961: 39).

Opisthostoma crassipupa van Benthem Jutting, Clements (2007: 74).

Opisthostoma crassipupa van Benthem Jutting, Clements et al (2008: 2760).

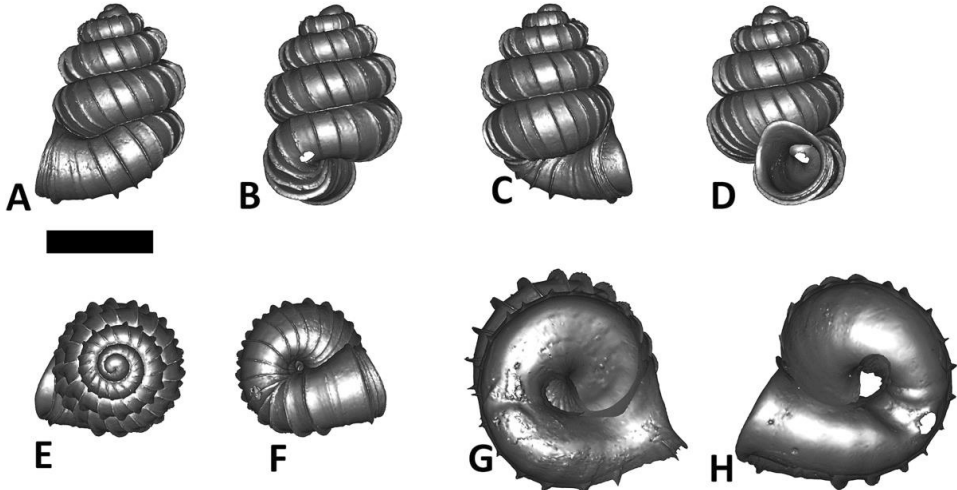


Figure 26. *Plectostoma crassipupa* (van Benthem Jutting, 1952) BOR 5512. **A** frontal view; **B** left lateral view; **C** back view; **D** left lateral view; **E** top view; **F** bottom view; **G** parietal part of constriction inner whorl; **H** basal part of constriction inner whorl. Scale bar = 1 mm (for A – F).

Type material

Holotype: ZMA 135994(1) (Seen).

Paratype: ZMA 135993(>50) (Seen).

Other examined materials

BOR 5512(>50), BOR 5515(2), BOR 5624(>10), BOR 5629(3), V 8392(>10), V 8407(10), V 8408(4), V 8437(>10), V 8898(7). V 8912(1), V 8956(1), V 9097(9), V 9157(>10), V 9326(>10), V 9353(3), V 9366(10).

Genetic distance between BOR 5512 and BOR 5515 is 14%.

Diagnosis

Shares with *P. sciaphilum*, *P. senex*, and *P. turriforme* the tuba form, but differs by having a slightly or moderately convex apex and depressed apical spire.

Description.

Apex. Shape: slightly or moderately convex.

Spire. Height: 1.3–3.0 mm. Width: 1.2–1.4 mm. Number of whorls: 3 1/2–4 1/2. Apical spire shape: depressed conical. Basal spire shape: ovoid. Whorl periphery: moderately or distinctly convex. Umbilicus: closed by tuba (common) or partially open (rare).

Constriction. Parietal teeth: none. Basal teeth: none.

Tuba. Coiling direction: type 3 and aperture visible from left lateral view. Tuba whorl length in proportion to spire last whorl: ca. 1/2–3/4 Proportion of tuba that attaches to spire: whole.

Aperture and peristome. Peristome: double peristomes. Outer peristome shape: same as inner peristome and uniformly projected all around, except the posterior part.

Spiral lines. Thick lines: present. Thin lines: present.

Radial ribs. Rib density: 6 – 8 ribs per mm. Rib intensity: thin. Shape: straight. Inclination: moderately prosoclin.

Distribution

Type locality. Gua Musang (4° 52' 59" N, 101° 58' 12" E).

Distribution range. This species mainly occurs in the limestone hills that are located between Gua Musang and as far as 30 km radius of Gua Musang. One populations exists at a limestone hill that is located about 90 km north of Gua Musang (Figure 18A).

Conservation status

Least Concern. Almost all the limestone hills are located along main roads and/or surrounded by oil palm plantation or cleared for urban development. However, several large limestone hills that hold the species are located in the well-protected National Park (Taman Negara), State of Pahang, Malaysia.

Discussion

The species is well-characterised, although it displays considerable variability in the shell shape (Appendix 6).

***Plectostoma tonkinianum* (Dautzenberg & Fischer, 1905)**

Figure 27 and Appendix 8.

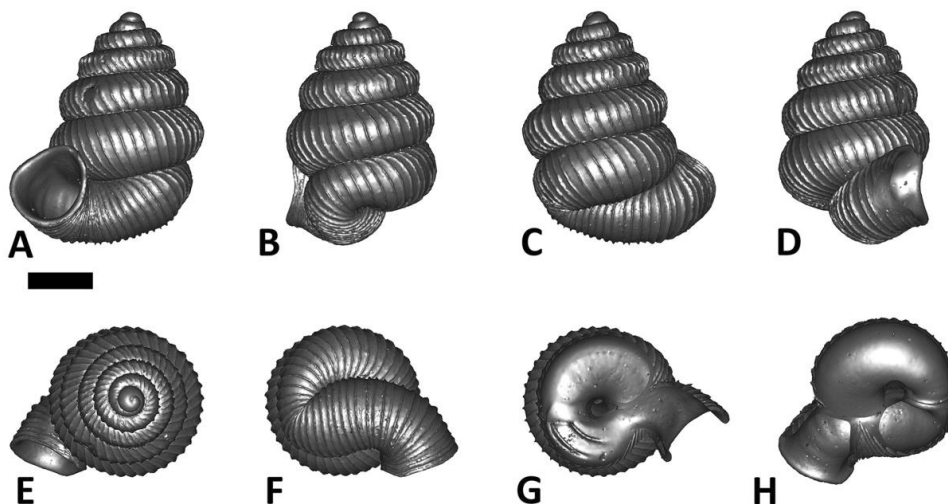


Figure 27. *Plectostoma tonkinianum* (Dautzenberg & Fischer, 1905) V 9940. **A** frontal view; **B** left lateral view; **C** back view; **D** right lateral view; **E** top view; **F** bottom view; **G** parietal part of constriction inner whorl; **H** basal part of constriction inner whorl. Scale bar = 1 mm (for A – F).

Opisthostoma tonkinianum Dautzenberg & Fischer, 1905: 444, plate 10 - figure 5, 6 & 7 (original description).

Opisthostoma tonkinianum Dautzenberg & Fischer, Saurin (1953: 134).

Opisthostoma tonkinianum Dautzenberg & Fischer, van Benthem-Jutting (1962: 12).

Opisthostoma tonkinianum Dautzenberg & Fischer, Fischer et al. (1963: 34).

Type material

Not seen.

Other examined materials

ZMA 162136(1), V 10000(>25), V 10010(>25), V 10022(>25), V 11243(>25), V 11270(>25), V 11432(3), V 11502(>50), V 7937(5), V 9940(>10), V 9957(>25).

Diagnosis

Shares with *P. whitteni* the general shell form, in terms of apex, spire and tuba, but differs by having two lamella-shaped constriction teeth and a higher spire (> 3 mm).

Description.

Apex. Shape: distinctly convex.

Spire. Height: 3.1 – 3.8 mm. Width: 2.4 – 2.6 mm. Number of whorls: 4 3/4 – 4 7/8. Apical spire shape: depressed conical. Basal spire shape: ovoid. Whorl periphery: distinctly convex.

Umbilicus: completely closed by tuba.

Constriction. Parietal teeth: two lamellae. Basal teeth: none.

Tuba. Coiling direction: type 3 and aperture visible in left lateral view. Tuba whorl length in proportion to spire last whorl: *ca.* 5/8. Proportion of tuba that attaches to spire: whole.

Aperture and peristome. Peristome: simple peristome.

Spiral lines. Thick lines: absent. Thin lines: present.

Radial ribs. Rib density: 6 – 7 ribs per mm. Rib intensity: thin. Shape: slightly curved to single-humped. Inclination: orthoclin.

Distribution

Type locality. "Tonkin" (Dautzenberg & Fischer, 1905). The exact locality should be the limestone hill near Chau Dao.

Distribution range. Limestone hills in the Province of Kien Giang (Figure 18A).

Conservation status

Data Deficient. Some recent dead shells have been collected but no information is available on the habitat and population status.

Discussion

In recent years, this species has been recorded at several limestone hills in the vicinity of Ha Tien, which is a popular tourism site. Although the type specimen cannot be located and the exact type locality cannot be determined, the shell morphology of the recent material fits well with the description in the original publication.

In the original publication, Dautzenberg and Fisher (1905) mentioned that this species was collected by M. Mansuy from Tonkin (French protectorate), which was a large area that included part of Southern China, and the Northern parts of Laos and Vietnam. Dautzenberg and Fisher (1905) further provided a list of locations where most of the snails were collected. One of these was, Chau Doc, which is located about 70 km from Ha Tien. Furthermore, a recent intensive land snail survey in the Northern Provinces of Laos, namely, Hua Phan and Luang Prabang, did not discover any *Plectostoma* species (Muratov & Abdou, 2006). Hence, *P. tonkinianum* probably occurs in the small limestone hill cluster in the coastal area of the Southern part of Vietnam and neighboring Cambodia.

***Plectostoma whitteni* sp. n.**

Figures 17G and 28, and Appendix 8.

Type material

Holotype: BOR 5644(1)

Paratypes: BOR 5536(>10), V 8802(1), V 8885(>10).

Diagnosis

Shares with *P. tonkinianum* the general shell form, in the terms of apex, spire and tuba, but differs by lacking constriction teeth and lower spire (< 2 mm).

Etymology

This species is named after Dr. Tony Whitten, who was senior biodiversity specialist of the World Bank between 1995 and 2010, and is currently the Regional Director for Asia-Pacific Fauna & Flora International. Dr. Whitten has been actively promoting the protection of the biodiversity that is associated with limestone and has been involved in conservation action to protect limestone habitats.

Description.

Apex. Shape: distinctly convex.

Spire. Height: 1.7 – 1.9 mm. Width: 1.4 – 1.6 mm. Number of whorls: 3 7/8 – 4 1/4. Apical spire shape: depressed conical. Basal spire shape: ovoid. Whorl periphery: distinctly convex. Umbilicus: completely closed by tuba.

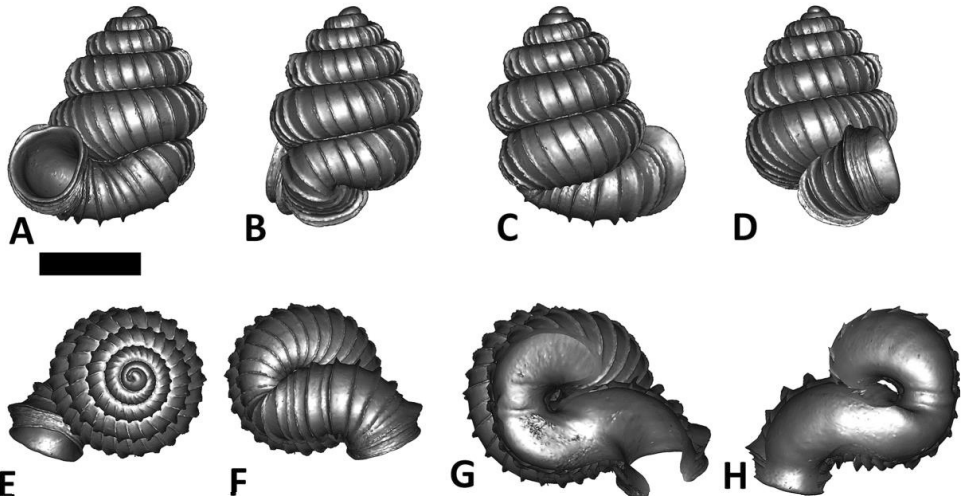


Figure 28. *Plectostoma whitteni* sp. n. BOR 5644. **A** frontal view; **B** left lateral view; **C** back view; **D** right lateral view; **E** top view; **F** bottom view; **G** parietal part of constriction inner whorl; **H** basal part of constriction inner whorl. Scale bar = 1 mm (for A – F).

Constriction. Parietal teeth: none. Basal teeth: none.

Tuba. Coiling direction: type 3 and aperture visible in left lateral view. Tuba whorl length in proportion to spire last whorl: *ca.* 1/2–5/8. Proportion of tuba that attaches to spire: whole.

Aperture and peristome. Peristome: double peristomes. Outer peristome shape: same as inner peristome and uniformly projected all around, except the posterior part.

Spiral lines. Thick lines: absent. Thin lines: present.

Radial ribs. Rib density: 6 – 7 ribs per mm. Rib intensity: thin. Shape: straight. Inclination: orthoclin.

Distribution

Type locality. Gua Taat, Tasik Kenyir (4° 51' 3" N, 102° 43' 21" E).

Distribution range. This species only occurs in Gua Taat, Tasik Kenyir (Figure 18A).

Conservation status

Least Concern. Gua Taat is located in a prioritised protected National Park with good forest cover.

Discussion

The general shell form of *P. whitteni* is similar to *P. tonkinianum*. There is no genetic information for *P. tonkinianum*, but *P. whitteni* is genetically closer to *P. tohchinyawi* than to any of the other 18 species. Nevertheless, *P. whitteni* is considered a distinct species as compared to *P. tonkinianum* and *P. tohchinyawi* because of the lack of constriction teeth.

***Plectostoma sciaphilum* (van Benthem Jutting, 1952)**

Figure 29 and Appendix 7.

Opisthostoma sciaphilum van Benthem Jutting, 1952: 45, figure 23 (original description).

Type material

Holotype: ZMA 136049(1) (Seen).

Paratypes: ZMA 136050(>10) (Seen).

Diagnosis

Shares with *P. senex* and *P. turriforme* the tuba form, but differs by lacking basal constriction teeth.

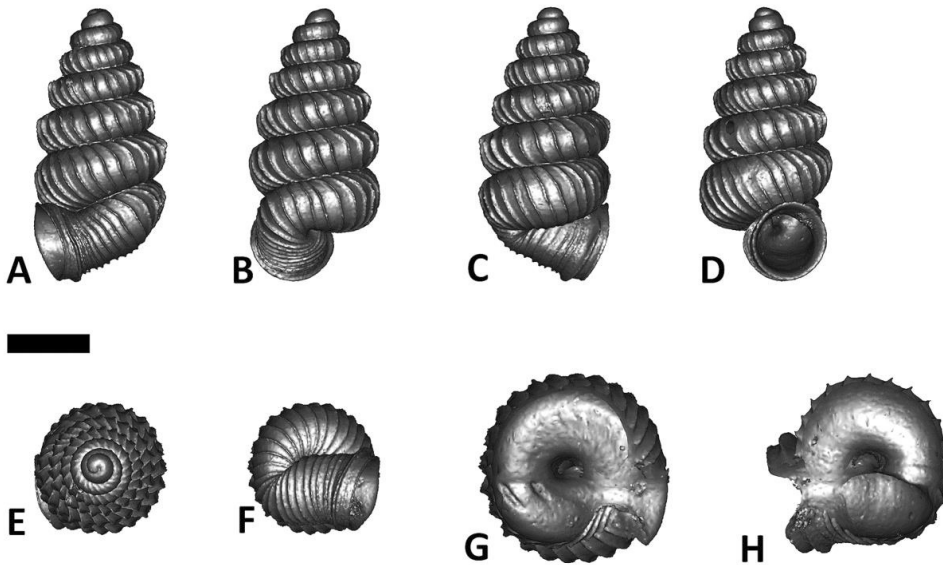


Figure 29. *Plectostoma sciaphilum* (van Benthem Jutting, 1952) ZMA 136050. **A** frontal view; **B** left lateral view; **C** back view; **D** right lateral view; **E** top view; **F** bottom view; **G** parietal part of constriction inner whorl; **H** basal part of constriction inner whorl. Scale bar = 1 mm (for A – F).

Description.

Apex. Shape: distinctly convex.

Spire. Height: 2.6 – 2.9 mm. Width: 1.5 – 1.6 mm. Number of whorls: 4 1/4 – 5 1/2. Apical spire shape: oblong conical. Basal spire shape: ovoid. Whorl periphery: distinctly convex. Umbilicus: completely closed by tuba.

Constriction. Parietal teeth: two. Basal teeth: none.

Tuba. Coiling direction: type 3 and aperture visible in left lateral view. Tuba whorl length in proportion to spire last whorl: *ca.* 3/8. Proportion of tuba that attaches to spire: whole.

Aperture and peristome. Peristome: double peristomes. Outer peristome shape: same as inner peristome and uniformly projected all around, except the posterior part.

Spiral lines. Thick lines: present. Thin lines: present.

Radial ribs. Rib density: 6 – 8 ribs per mm. Rib intensity: thin. Shape: slightly curved.

Distribution

Type locality. Bukit Panching, Pahang (3° 53' 28" N, 103° 8' 26" E).

Distribution range. Endemic to Bukit Panching (not seen in Figure 18A because its symbol overlaps with *P. senex*).

Conservation status

Extinct. Its only habitat—Bukit Panching, has been completely quarried away (see also Schilthuizen & Clements 2008). The ruin is now inundated. The status of this species in a previous assessment (IUCN redlist) was: Critically Endangered B2ab(ii,iii) ver. 3.1 (Clements, 2009a).

Discussion

See under *P. turriforme*.

Plectostoma senex (van Benthem Jutting, 1952)

Figures 17H and 30, and Appendix 7.

Opisthostoma senex van Benthem Jutting, 1952: 47, figure 24 (original description).

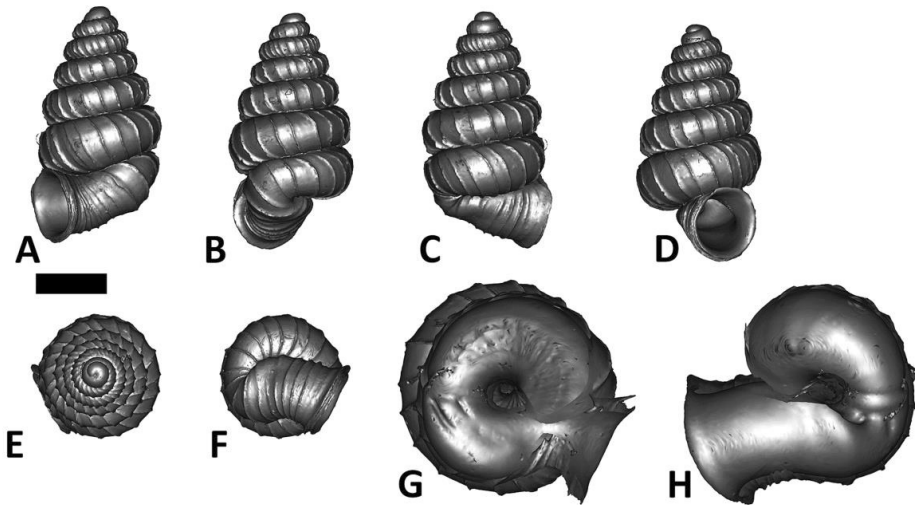


Figure 30. *Plectostoma senex* (van Benthem Jutting, 1952) BOR 5603. **A** frontal view; **B** left lateral view; **C** back view; **D** right lateral view; **E** top view; **F** bottom view; **G** parietal part of constriction inner whorl; **H** basal part of constriction inner whorl. Scale bar = 1 mm (for A – F).

Type material

Holotype: ZMA 136052(1) (Seen).

Paratypes: ZMA 136053(>10) (Seen).

Other examined materials

RMNH 44723(5), BOR 460(1), BOR 5575(3), BOR 5603(2), BOR 5628(>100), BOR 5631(>10), V 5117(9).

Diagnosis

Shares with *P. sciaphilum* and *P. turriforme* the tuba form, but differs by having two knob-shaped constriction teeth and fewer than 6 whorls.

Description.

Apex. Shape: distinctly convex.

Spire. Height: 2.6 – 3.1 mm. Width: 1.6 – 1.7 mm. Number of whorls: 5 1/8 – 5 5/8. Apical spire shape: oblong conical. Basal spire shape: ovoid. Whorl periphery: moderately to distinctly convex. Umbilicus: completely closed by tuba.

Constriction. Parietal teeth: two. Basal teeth: one transverse tooth.

Tuba. Coiling direction: type 3 and aperture visible in left lateral view. Tuba whorl length in proportion to spire last whorl: ca. 3/8. Proportion of tuba that attaches to spire: whole.

Aperture and peristome. Peristome: double peristomes. Outer peristome shape: same as inner peristome and uniformly projected all around, except the posterior part.

Spiral lines. Thick lines: absent. Thin lines: present.

Radial ribs. Rib density: 4 ribs per mm. Rib intensity: thin. Shape: slightly curved. Inclination: orthoclin.

Distribution

Type locality. Gua Charas, limestone hill near Sungai Lembing in the state of Pahang, Malaysia (3° 54' 27" N, 103° 8' 47" E).

Distribution range. In addition to the type locality, this species had been recorded from Bukit Panching (Figure 18A).

Conservation status

Critically Endangered (B2ab(iii)+C2a(i) ver. 10.1). This species is known from two locations.

One of these, Bukit Panching, does not exist anymore. Two intensive surveys at the other location, Bukit Charas, were conducted in Feb. 2010 and May 2011. Two living populations with fewer than 50 individuals were found at wet staglamites near the cave. No other living population was found elsewhere on Bukit Charas. The status of this species in a previous assessment (IUCN redlist) was: vulnerable D2 ver. 3.1 (Clements, 2009b).

Discussion

See discussion under *P. turriforme*.

***Plectostoma turriforme* (van Benthem Jutting, 1952)**

Figure 31 and Appendix 8.

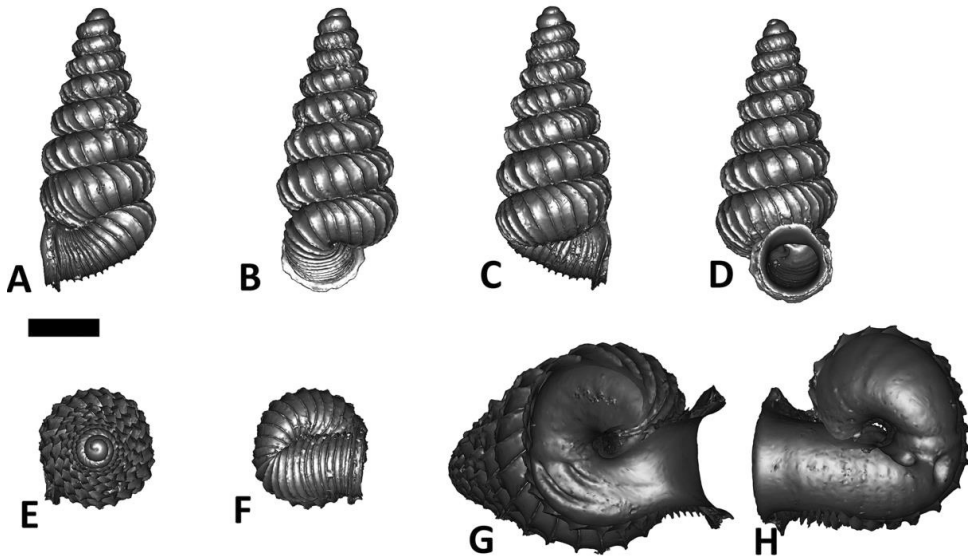


Figure 31. *Plectostoma turriforme* (van Benthem Jutting, 1952) BOR 5609. **A** frontal view; **B** leftlateral view; **C** back view; **D** right lateral view; **E** top view; **F** bottom view; **G** parietal part of constriction inner whorl; **H** basal part of constriction inner whorl. Scale bar = 1 mm (for A – F).

Opisthostoma turriforme van Benthem Jutting, 1952: 43, figure 22 (original description).

Type material

Holotype: ZMA 136068(1) (Seen).

Paratypes: ZMA 136069(>10) (Seen).

Other examined materials

BOR 461(2), BOR 5609(2).

Diagnosis

Shares with *P. sciaphilum* and *P. senex* the tuba form, but differs by having two lamella-shaped constriction teeth and having more than 6 whorls.

Description.

Apex. Shape: distinctly convex.

Spire. Height: 3.2 mm. Width: 1.6 mm. Number of whorls: 7. Apical spire shape: oblong conical. Basal spire shape: conical. Whorl periphery: distinctly convex. Umbilicus: completely closed by tuba.

Constriction. Parietal teeth: two. Basal teeth: two.

Tuba. Coiling direction: type 3 and aperture visible in left lateral view. Tuba whorl length in proportion to spire last whorl: *ca.* 3/8. Proportion of tuba that attaches to spire: whole.

Aperture and peristome. Peristome: double peristomes. Outer peristome shape: same as inner peristome and uniformly projected all around, except the posterior part.

Spiral lines. Thick lines: absent. Thin lines: present.

Radial ribs. Rib density: 5 ribs per mm. Rib intensity: thin. Shape: slightly curved. Inclination: orthoclin.

Distribution

Type locality. Bukit Tenggek, Pahang (4° 0' 51" N, 103° 9' 34" E).

Distribution range. In addition to the type locality, this species can be found at nearby Bukit Sagu (Figure 18A).

Conservation status

Critically Endangered (B2ab(iii)+C2a(i) ver. 10.1). The whole Bukit Tenggek will disappear by 2014 because of quarrying activity. Moreover, more than half of Bukit Sagu has already been quarried away (see also Schilthuizen & Clements 2008). Although living individuals had been recorded from Bukit Sagu in 1997 (BOR 5609), neither living nor recently dead individuals were found in a recent survey conducted in 2010 and 2011.

Discussion

P. turriforme, *P. sciaphilum*, and *P. senex* are three very similar species than occur in the four lenticular easternmost limestone hills in Peninsular Malaysia (Figure 18A). These four hills, namely, Bukit Panching, Bukit Charas, Bukit Sagu, and Bukit Tenggek are located along a 15 km longitudinal transect. *P. turriforme* occurs at the two former sites and *P. senex* at the two latter sites. *P. sciaphilum* occurs sympatrically with *P. turriforme* in Bukit Panching. These four hills (and thus the three species) are among the most isolated limestone outcrops in Peninsular Malaysia.

***Plectostoma palinhelix* (van Benthem Jutting, 1952)**

Figures 17C and 32, and Appendix 12.

Opisthostoma palinhelix van Benthem Jutting, 1952: 40, figure 20 (original description).

Type material

Holotype: ZMA 136030(1) (Seen).

Paratype: ZMA 136031(>10) (Seen).

Other examined materials

BOR 466(1), BOR 5520(5), V 5104(5).

Diagnosis

Shares with *P. retrovertens* the spire and tuba form, but differs by having spire height between 1.6 – 1.9 mm.

Description.

Apex. Shape: slightly convex.

Spire. Height: 1.6 – 1.9 mm. Width: 1.1 – 1.3 mm. Number of whorls: 3 3/4 - 4 1/4. Apical spire shape: depressed conical. Basal spire shape: ovoid. Whorl periphery: moderately to distinctly convex. Umbilicus: partially or completely closed by tuba.

Constriction. Parietal teeth: two. Basal teeth: none.

Tuba. Coiling direction: type 2 and aperture visible between right lateral and back view; the tuba coils upward until the first teleconch whorl of the spire. Tuba whorl length similar to that of the last whorl of the spire. Proportion of tuba that attaches to spire: whole.

Aperture and peristome. Peristome: double peristomes. Outer peristome shape: similar to inner peristome, projected all around, except the posterior part, where the two lateral sides are slightly more projected than the anterior side.

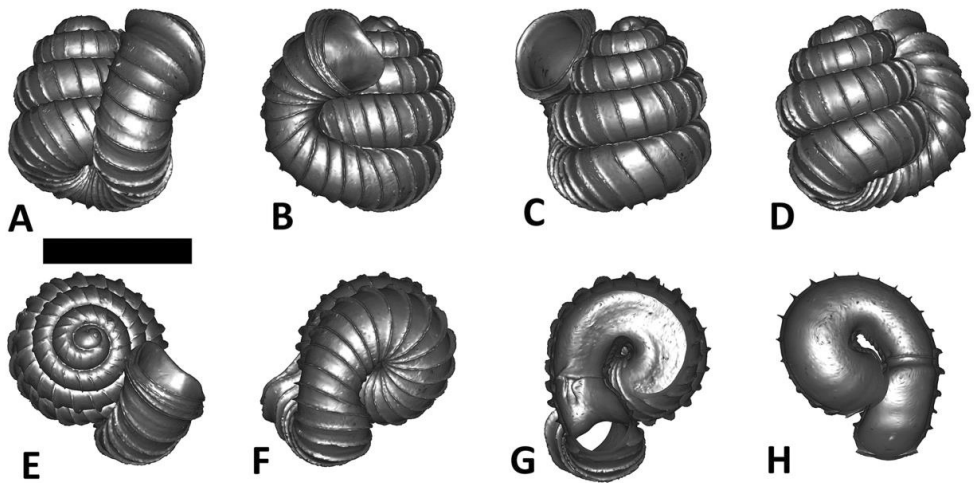


Figure 32. *Plectostoma palinhelix* (van Benthem Jutting, 1952) BOR 5520. **A** frontal view; **B** left lateral view; **C** back view; **D** right lateral view; **E** top view; **F** bottom view; **G** parietal part of constriction inner whorl; **H** basal part of constriction inner whorl. Scale bar = 1 mm (for A – F).

Spiral lines. Thick lines: present. Thin lines: present.

Radial ribs. Rib density: 7 – 8 ribs per mm. Rib intensity: thin. Shape: straight. Inclination: orthoclin.

Distribution

Type locality. Bukit Serdam, Pahang (3° 49' 47" N, 101° 55' 36" E).

Distribution range. To date, this species has been recorded from three limestone hills, namely Bukit Serdam, Gua Kechil and a small hill nearby (Figure 18C).

Conservation status

Vulnerable (B2ab(iii) ver. 10.1). There are four limestone hills in this area, of which Bukit Serdam and its next unnamed hill support populations (assessment done in 2010 and 2011). Two of the hills, namely, Bukit Serdam and Gunung Panas, are now being quarried. The smallest unnamed hill is highly degraded and Gua Kechil is surrounded by oil palm plantation.

Discussion

See discussion under *P. retrovertens*.

***Plectostoma retrovertens* (Tomlin, 1938)**

Figures 17R and 33, and Appendix 13.

Opisthostoma retrovertens Tomlin, 1938: 73, Plate 2- figure 3 (original description).

Opisthostoma retrovertens Tomlin, van Benthem-Jutting (1952: 39).

Opisthostoma retrovertens Tomlin, Berry (1961).

Opisthostoma retrovertens Tomlin, Berry (1962).

Opisthostoma retrovertens Tomlin, Berry (1963).

Opisthostoma retrovertens Tomlin, Berry (1964).

Opisthostoma retrovertens Tomlin, Berry (1966).

Opisthostoma retrovertens Tomlin, Solem (1966).

Opisthostoma retrovertens Tomlin, Illert (1987: 800, figure 2a).

Opisthostoma retrovertens Tomlin, Solem and Solem (1976: 31).

Opisthostoma retrovertens Tomlin, Heller (2001: 426).

Opisthostoma retrovertens Tomlin, Clements (2007: 74).

Opisthostoma retrovertens Tomlin, Clements et al. (2008: 2760).

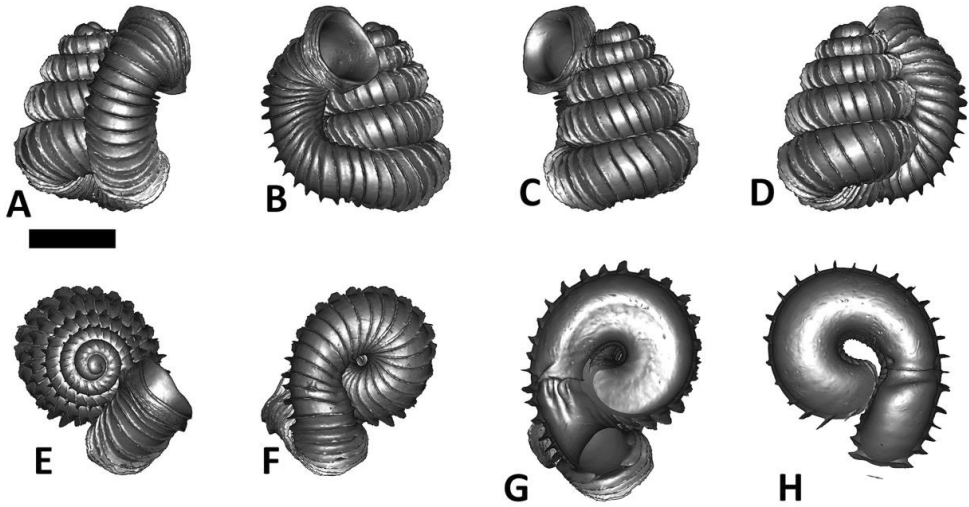


Figure 33. *Plectostoma retrovertens* (Tomlin, 1938) BOR 5559. **A** frontal view; **B** left lateral view; **C** back view; **D** right lateral view; **E** top view; **F** bottom view; **G** parietal part of constriction inner whorl; **H** basal part of constriction inner whorl. Scale bar = 1 mm (for A – F).

Type material

Holotype: BMNH 1938.10.25.2(1) (Seen)

Paratype: ZMA 136044(>10) (Seen)

Other examined materials

RMNH 244699(1), RMNH 44725(8), ZMA 162133(>10), ZMA 162148(8), BOR 5559(3), BOR 5621(9), V 5124(9).

Diagnosis

Shares with *P. palinhelix* the spire and tuba form, but differs by having spire height between 2.3 – 2.6 mm.

Description.

Apex. Shape: moderately convex.

Spire. Height: 2.3 – 2.6 mm. Width: 1.5 – 1.7 mm. Number of whorls: 4 5/8–5. Apical spire shape: depressed conical. Basal spire shape: ovoid. Whorl periphery: distinctly convex. Umbilicus: partially or completely closed by tuba.

Constriction. Parietal teeth: two. Basal teeth: none.

Tuba. Coiling direction: type 2 and aperture visible between right lateral and back view; the tuba coils upward until the first teleconch whorl of the spire. Tuba whorl length similar to the length of the last whorl of the spire. Proportion of tuba that attaches to spire: whole.

Aperture and peristome. Peristome: double peristomes. Outer peristome shape: similar to inner peristome, projected all around, except the posterior part, where two lateral sides are slightly more projected than the anterior side.

Spiral lines. Thick lines: present. Thin lines: present.

Radial ribs. Rib density: 7 – 9 ribs per mm. Rib intensity: thin. Shape: straight. Inclination: orthoclin.

Distribution

Type locality. Bukit Chintamanis, Pahang (3° 26' 45" N, 102° 0' 51" E).

Distribution range. Endemic to the type locality (Figure 18C).

Conservation status

Critically Endangered (B2ab(iii)+C2a(i) ver. 10.1). This species is endemic to a single limestone hill - Bukit Chintamanis. Most of the western part of this hill is gone due to the quarry activity in the past and this part is now covered by secondary vegetation. The rest of the outcrop is surrounded by plantation, which is subjected to periodic clearing and replanting. According to Berry (1961), live individuals can only be found at the rock surface (Site A in Berry, 1961). Berry (1962) reports finding several thousand individuals at Site A.

A recent intensive survey for *P. retrovertens* was done at the type locality in August 2010 and May 2011. Site A is a rock surface smaller than 20 m². It appears that the vegetation cover and habitat structure of Site A has not changed as compared to the assessment done by Berry (1962, 1964). However, only three live individuals were found during the survey in Aug. 2010. Furthermore, the surrounding of Bukit Chintamanis has been cleared in 2011. Judging by the population trends and habitat conditions together, this species is at the brink of extinction. The status of this species in a previous assessment (IUCN redlist) was: vulnerable D2 ver. 3.1 (Clements, 2009c).

Discussion

P. retrovertens and *P. palinhelix* are very distinct from other *Plectostoma* by having a very long tuba in relation to their spire. In fact, a preliminary phylogenetic analysis suggests that these two are basal species for all Peninsular Malaysia's *Plectostoma*. These two species are located more 40 km apart on outcrops that belong to the same limestone facies (Figure 18C). The two species are very similar in their shell shape, but *P. retrovertens* is about one-third larger than *P. palinhelix*. Furthermore, the genetic divergence between the two species is 10%.

Plectostoma ikanensis sp. n.

Figures 17J, 17K, 34 and 35, and Appendix 11 and 14.

Type material

Holotype: BOR 5645(1)

Paratypes: BOR 5507(6), BOR 5622(>50), BOR 5504(>10), V 9446(>100), V 9320(6).

Etymology

This species is named after its type locality – Gua Ikan.

Diagnosis

Shares with *P. kayiani* the general shell form, in terms of spire and tuba shape, but differs by having both thick and thin spiral lines.

Description for shell form 5504 (Figs. 17K and 34, and Appendix 14).

Apex. Shape: moderately convex.

Spire. Height: 1.7 mm. Width: 1.3 mm. Number of whorls: 4 1/8–4 1/4. Apical spire shape: depressed conical. Basal spire shape: conical. Whorl periphery: distinctly convex. Umbilicus: open.

Constriction. Parietal teeth: none. Basal teeth: none

Tuba. Coiling direction: type 2 and aperture visible in right lateral view. Tuba whorl length in proportion to spire last whorl: ca.3/4–7/8. Proportion of tuba that attaches to spire: whole.

Aperture and peristome. Peristome: double peristomes. Outer peristome shape: similar to inner peristome, projected all around, except the posterior part, where left lateral sides are slightly more projected than the anterior and right lateral side.

Spiral lines. Thick lines: present. Thin lines: present.

Radial ribs. Rib density: 5 ribs per mm. Rib intensity: thin. Shape: straight. Inclination: orthoclin.

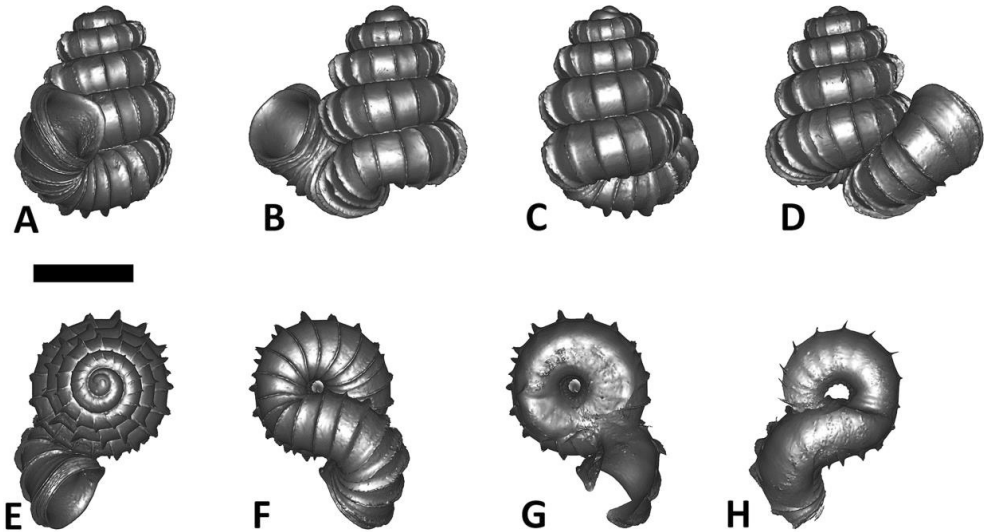


Figure 34. *Plectostoma ikanensis* sp. n. (Form BOR 5504) BOR 5504. **A** frontal view; **B** left lateral view; **C** back view; **D** right lateral view; **E** top view; **F** bottom view; **G** parietal part of constriction inner whorl; **H** basal part of constriction inner whorl. Scale bar = 1 mm (for A – F).

Description for shell form 5507 (Figs. 17J and 35, and Appendix 11).

Apex. Shape: moderately convex.

Spire. Height: 1.8 – 1.9 mm. Width: 1.3 mm. Number of whorls: 3 7/8–4. Apical spire shape: depressed conical. Basal spire shape: conical. Whorl periphery: distinctly convex. Umbilicus: open.

Constriction. Parietal teeth: none. Basal teeth: none.

Tuba. Coiling direction: type 2 and aperture visible in left lateral view. Tuba whorl length in proportion to spire last whorl: *ca.* 5/8. Proportion of tuba that attaches to spire: whole.

Aperture and peristome. Aperture with double peristome. Peristome: double peristomes.

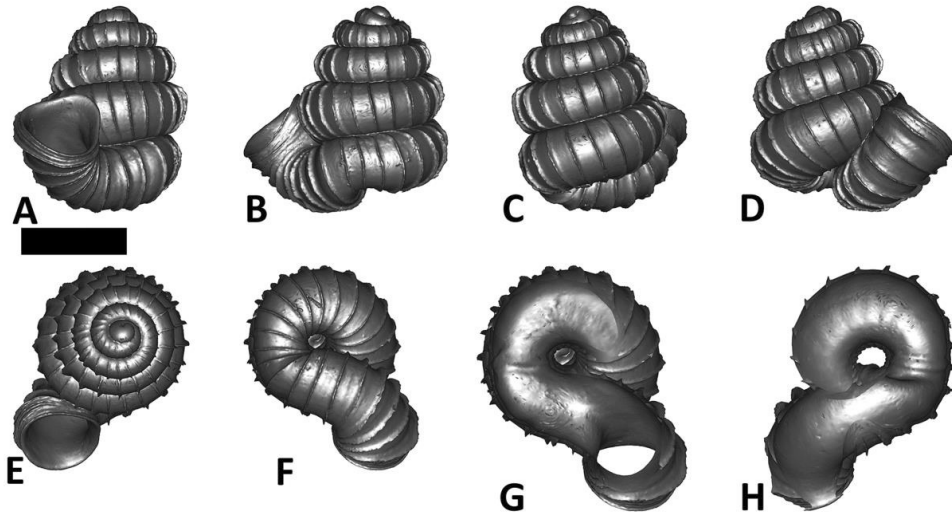


Figure 35. *Plectostoma ikanensis* sp. n. (Form BOR 5507) BOR 5645. **A** frontal view; **B** left lateral view; **C** back view; **D** right lateral view; **E** top view; **F** bottom view; **G** parietal part of constriction inner whorl; **H** basal part of constriction inner whorl. Scale bar = 1 mm (for A – F).

Outer peristome shape: similar to inner peristome, projected all around, except the posterior part, where left lateral sides are slightly more projected than the anterior and right lateral side.

Spiral lines. Thick lines: present. Thin lines: present.

Radial ribs. Rib density: 7 ribs per mm. Rib intensity: thin. Shape: straight. Inclination: orthoclin.

Distribution

Type locality. Gua Ikan in the State of Kelantan (5° 21' 9" N, 102° 1' 34" E).

Distribution range. In addition to the type location, this species also occurs at nearby limestone hills as far as 30 km away (Figure 18C).

Conservation status

Least Concern. Living populations of *P. ikanensis* were recorded at the type locality in 2011. The type locality is gazetted as recreation forest.

Discussion

The two forms of *Plectostoma ikanensis* were found in the type locality at two different parts of the hill that within a distance of 100 m. The overall shell appearances of these two forms are very different, especially in terms of tuba coiling direction and spire shape. Interestingly, one of the *P. ikanensis* forms (i.e. BOR 5507) is very similar to *P. davisoni* on the basis of these two shell characters. In most of the other *Plectostoma* species examined in this study, tuba coiling direction and spire shape are rather stable characters within a species. Nevertheless, both *P. ikanensis* forms lack a constriction which unite them and distinguish them from other similar species (see Diagnosis). In addition to the morphological evidence, we found that the genetic divergence of these two forms is smaller than 1 % (Table 4), and our preliminary phylogenetic analysis shows that the two forms are reciprocally monophyletic. We therefore conclude that they be classified as the same species.

***Plectostoma kayiani* sp. n.**

Figure 36 and Appendix 11.

Type material

Holotype: RMNH 330803 (1)

Paratypes: V 8883(6), V 14243(1).

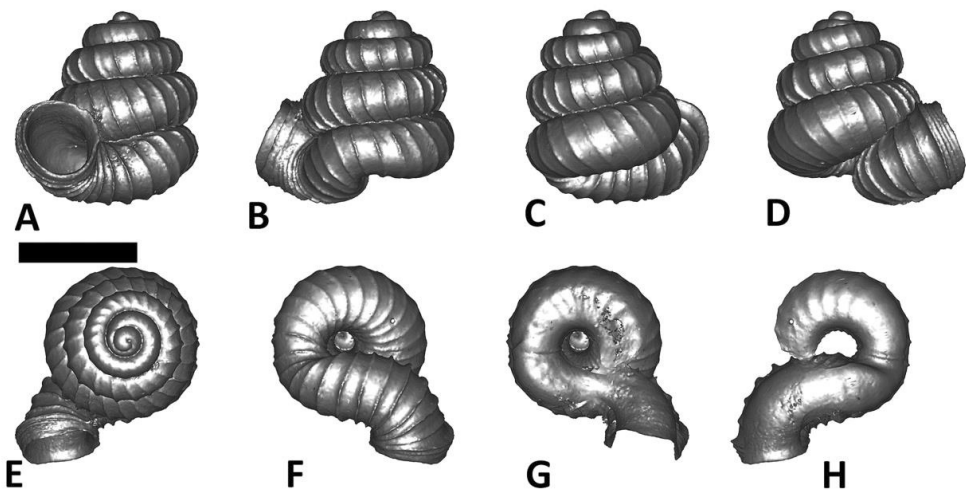


Figure 36. *Plectostoma kayiani* sp. n. RMNH 330803. **A** frontal view; **B** left lateral view; **C** back view; **D** right lateral view; **E** top view; **F** bottom view; **G** parietal part of constriction inner whorl; **H** basal part of constriction inner whorl. Scale bar = 1 mm (for **A – F**).

Etymology

This species is named after Kay Arnold and Ian Mellsop from New Zealand, who have generously supported wildlife conservation work in many parts of Peninsular Malaysia, including the forests around Lake Kenyir where this species was discovered.

Diagnosis

Shares with *P. ikanensis* the general shell form, in terms of spire and tuba shape, but differs by lacking thick spiral lines.

Description.

Apex. Shape: slightly to moderately convex.

Spire. Height: 1.4 – 1.6 mm. Width: 1.2 – 1.4 mm. Number of whorls: 3 1/2–3 3/4. Apical spire shape: depressed conical. Basal spire shape: conical. Whorl periphery: distinctly convex. Umbilicus: open.

Constriction. Parietal teeth: none. Basal teeth: none.

Tuba. Coiling direction: type 2 and aperture visible from front view. Tuba whorl length in proportion to spire last whorl: *ca.* 5/8 – 3/4. Proportion of tuba that attaches to spire: almost whole except the part near the aperture.

Aperture and peristome. Peristome: double peristomes. Outer peristome shape: similar to inner peristome, projected all around, except the posterior part, where left lateral sides are slightly more projected than the anterior and right lateral side.

Spiral lines. Thick lines: absent. Thin lines: present.

Radial ribs. Rib density: 8–10 ribs per mm. Rib intensity: thin. Shape: slightly curved. Inclination: orthoclin.

Distribution

Type locality. Gua Bewah, Tasik Kenyir (4° 51' 3" N, 102° 43' 21" E).

Distribution range. To date, this species is only known to occur at two neighbouring limestone outcrops, namely, Gua Bewah and Gua Taat at the southern part of Tasik Kenyir (Figure 18C).

Conservation status

Least Concern. The outcrops where this species is found, are partially submerged in Southeast-Asia's largest man-made lake, Tasik Kenyir. Despite this, there is a good forest cover around and on the limestone outcrops. Furthermore, these two hills are located in a protected National Park.

Discussion

This species occurs sympatrically with *P. tohchinyawi* and *P. whitteni*.

***Plectostoma davisoni* sp. n.**

Figure 37, and Appendix 9 and 10.

Type material

Holotype: BOR 5646(1)

Paratypes: ZMA 162069(>25), ZMA 162070(3), ZMA 162071(>50), ZMA 162146(7), ZMA 162147(8), BOR 5508(>25), BOR 5626(>25), BOR 5641(9), V 8652(6), V 8929(>25), V 9206(6), V 8265(>10), V 8301(>25), V 9243(>50), V 9340(7), V 9417(7), V 14242(5).

Diagnosis

Shares with *P. relauensis* the general shell form, in terms of apex, spire, and tuba shape, but differs by having two parietal constriction teeth.

Etymology

This species is named after Dr. Geoffrey Davison, who has been involved in the conservation of limestone hills in Malaysia, and has collected a lot of snail specimens, many of which are included in this revision of *Plectostoma* from Malaysia.

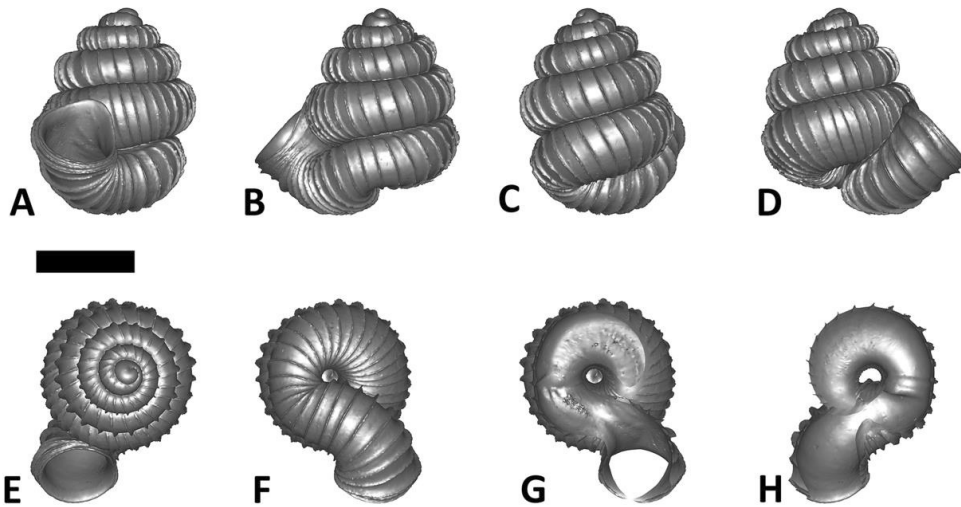


Figure 37. *Plectostoma davisoni* sp. n. BOR 5646. **A** frontal view; **B** left lateral view; **C** back view; **D** right lateral view; **E** top view; **F** bottom view; **G** parietal part of constriction inner whorl; **H** basal part of constriction inner whorl. Scale bar = 1 mm (for **A – F**).

Description.

Apex. Shape: slightly to moderately convex.

Spire. Height: 1.6 – 2.0 mm. Width: 1.4 – 1.5 mm. Number of whorls: 3 5/8–4 7/8. Apical spire shape: depressed conical. Basal spire shape: ovoid. Whorl periphery: moderately to distinctly convex. Umbilicus: open.

Constriction. Parietal teeth: two. Basal teeth: none.

Tuba. Coiling direction: type 2 and aperture visible in frontal view. Tuba whorl length in proportion to spire last whorl: ca. 5/8 – 3/4. Proportion of tuba that attaches to spire: whole.

Aperture and peristome. Peristome: double peristomes. Outer peristome shape: similar to inner peristome, projected all around, except the posterior part, where the two lateral sides are slightly more projected than the anterior side.

Spiral lines. Thick lines: present. Thin lines: present.

Radial ribs. Rib density: 6 - 7 ribs per mm. Rib intensity: thin. Shape: straight. Inclination: orthoclin.

Distribution

Type locality. Limestone hill on the right hand side of the road D29, at km 17 when travelling from Jelawang to Gua Musang (4° 59' 4" N, 101° 57' 53" E).

Distribution range. This species has a very large distribution range, ca. 80 km diameter. It can be found in many limestone outcrops in the central part of Peninsular Malaysia, mainly in the State of Kelantan (Figure 17D). In addition, it can also be found in a cluster of limestone hills located at upper Sungai Keniyam Kecil in Taman Negara (ca. 60 km from Gua Musang).

Conservation status

Least Concern. This is a widespread species. Although many hills in Kelantan are being degraded and surrounded by oil palm plantations, there are a few well protected hills in Taman Negara in Pahang, where this species occurs.

Discussion

This species is highly variable in the shell form (Appendix 9 and Appendix 10), and has a very wide distribution range which partly overlaps with many other *Plectostoma* species (Figure 18). It is very densely distributed in the State of Kelantan, parapatric with *P. christae*. The species becomes more sparse toward the limestone hills in Taman Negara,

Pahang (Figure 18C). In view of this, it is possible that the species actually consists of two or more cryptic species, and thus more genetic data are needed.

***Plectostoma relauensis* sp. n.**

Figures 17P and 38, and Appendix 13.

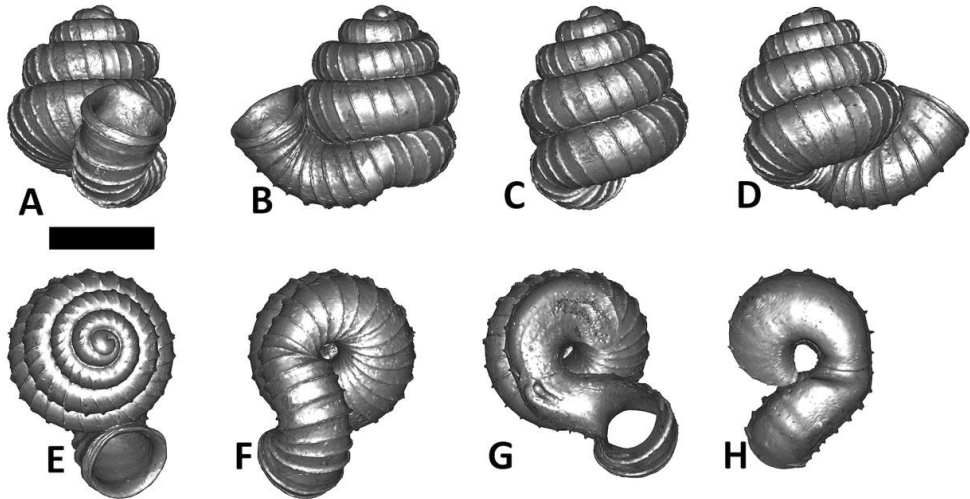


Figure 38. *Plectostoma relauensis* sp. n. BOR 5511. **A** frontal view; **B** left lateral view; **C** back view; **D** right lateral view; **E** top view; **F** bottom view; **G** parietal part of constriction inner whorl; **H** basal part of constriction inner whorl. Scale bar = 1 mm (for A – F).

Type material

Holotype: BOR 5647(1)

Paratypes: BOR 463(2), BOR 5511(>25), V 8169(9).

Etymology

This species is named after its type locality – Relau substation of Taman Negara, where Gua Gajah is located.

Diagnosis

Shares with *P. davisoni* the general shell form, in terms of apex, spire, and tuba shape, but differs by having a single parietal constriction tooth.

Description.

Apex. Shape: slightly to moderately convex.

Spire. Height: 1.5 – 1.9 mm. Width: 1.5 – 1.6 mm. Number of whorls: $3 \frac{3}{8}$ – $3 \frac{5}{8}$. Apical spire shape: depressed conical. Basal spire shape: ovoid. Whorl periphery: moderately to distinctly convex. Umbilicus: open.

Constriction. Parietal teeth: one. Basal teeth: none.

Tuba. Coiling direction: type 2 and aperture visible in frontal view. Tuba whorl length in proportion to spire last whorl: ca. $\frac{1}{2}$ – $\frac{5}{8}$. Proportion of tuba that attaches to spire: whole.

Aperture and peristome. Peristome: double peristomes. Outer peristome shape: same as inner peristome and uniformly projected all around, except the posterior part.

Spiral lines. Thick lines: present. Thin lines: present.

Radial ribs. Rib density: 4 - 7 ribs per mm. Rib intensity: thin. Shape: straight to slightly curved. Inclination: orthoclin.

Distribution

Type locality. Gua Gajah in the Relau substation, Taman Negara. (4° 38' 15" N, 102° 3' 50" E).

Distribution range. This species also occurs at a limestone hill located about 20 km north of the type locality. BOR 463 was collection in Pulau Singa Besar, which is located about 300 km from type locality. The reliability of the collection data is dubious (see also BOR 462 of *P. sinyumensis*).

Conservation status

Least Concern. A large living population of *P. relauensis* was found at Gua Gajah, which is located in the National Park.

Discussion

This species occurs sympatrically with *P. siphonostomum* on the same limestone hills. Despite the high density of limestone hills in the area, where many other *Plectostoma* species occur, *P. relauensis* is only found in two of these (Figure 18).

***Plectostoma kakiense* (Tomlin, 1948)**

Figures 17D and 39, and Appendix 11.

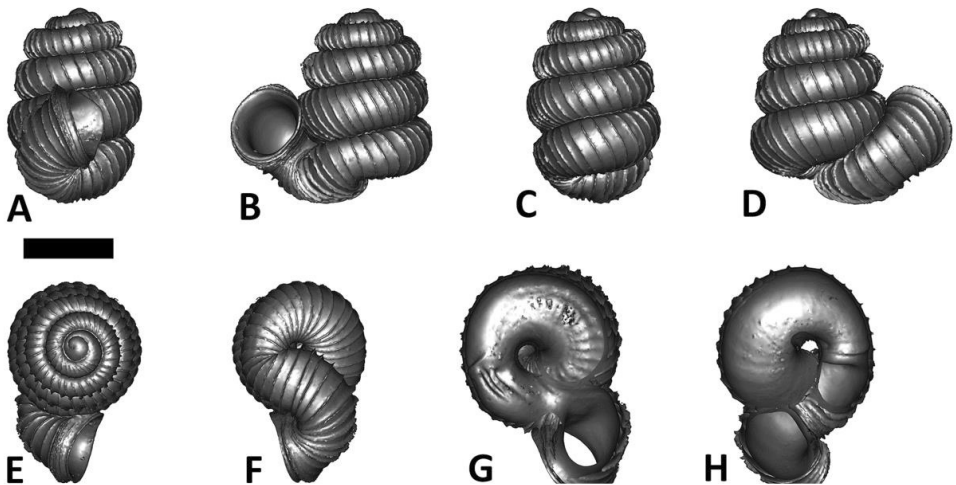


Figure 39. *Plectostoma kakiense* (Tomlin, 1948) BOR 5516. **A** frontal view; **B** left lateral view; **C** back view; **D** right lateral view; **E** top view; **F** bottom view; **G** parietal part of constriction inner whorl; **H** basal part of constriction inner whorl. Scale bar = 1 mm (for A – F).

Opisthostoma kakiense Tomlin, 1948: 225, Plate 2 - figure 5 (original description).

Opisthostoma kakiense Tomlin, van Benthem-Jutting (1952: 39).

Opisthostoma kakiense Tomlin, Ali and Taakob (2001: 145).

Opisthostoma sp., Razalli et al. (2010: figure 2C).

Type material

Holotype: BMNH 1948.10.2.3(1) (seen)

Other examined materials

ZMA 136009(1), ZMA 162094(5), BOR 445(1), BOR 5516(>25), BOR 5517(>10), BOR 5598(3), V 8789(2).

Diagnosis

Shares with *P. kubuensis* the general shell form, in terms of apex, spire, and tuba shape, but

differs by having two parietal constriction teeth.

Description.

Apex. Shape: slightly to moderately convex.

Spire. Height: 1.7 – 2.1 mm. Width: 1.5 – 1.6 mm. Number of whorls: 3 3/4 – 4 1/4. Apical spire shape: depressed conical. Basal spire shape: ovoid. Whorl periphery: moderately to distinctly convex. Umbilicus: partially closed by tuba.

Constriction. Parietal teeth: two. Basal teeth: none.

Tuba. Coiling direction: type 2 and aperture visible in right lateral view. Tuba whorl length in proportion to spire last whorl: ca. 5/8 – 3/4. Proportion of tuba that attaches to spire: whole.

Aperture and peristome. Peristome: double peristomes. Outer peristome shape: similar to inner peristome, projected all around, except the posterior part, where the two lateral sides are slightly more projected than the anterior side.

Spiral lines. Thick lines: absent. Thin lines: present.

Radial ribs. Rib density: 8 - 10 ribs per mm. Rib intensity: thin. Shape: straight to slightly curved. Inclination: moderately prosoclin.

Distribution

Type locality. Kaki Bukit (6° 38' 42" N, 100° 12' 6" E) (Figure 18C).

Distribution range. Wang Kelian limestone outcrops.

Conservation status

Near Threatened. To date, only two populations are known for two large limestone outcrops in the vast limestone formation in Perlis. These two locations are Kaki Bukit and Wang Kelian, both located in the protected Wang Kelian State Park.

Although Kaki Bukit is a large limestone outcrop with good forest cover, the population density of *P. kakiense* is very low. During a survey in May 2011, this species was only found near the top of Kaki Bukit where several hundred individuals were found at one location (limestone wall) within an area of ca. 10 m². There were several small populations (fewer than 10 individuals) in small pockets of suitable habitat. The population in Wang Kelian was recorded by Ali and Yaakob (2001), but its status is not known. No live or dead individuals were collected at the dozen isolated limestone hills located within 5 km around Wang Kelian State Park.

Discussion

See discussion under *Plectostoma kubuensis*.

***Plectostoma kubuensis* sp. n.**

Figures 17F and 40, and Appendix 12.

Type material

Holotype: BOR 5648(1).

Paratypes: BOR 5518(>25), BOR 5519(>10).

Diagnosis

Shares with *P. kakiense* the general shell form, in terms of apex, spire, and tuba shape, but differs by lacking constriction teeth.

Etymology

This species is named after its type locality – Bukit Kubu, Perlis.

Description.

Apex. Shape: slightly to moderately convex.

Spire. Height: 1.6 – 2.0 mm. Width: 1.3 – 1.5 mm. Number of whorls: 3 5/8 – 4 1/4. Apical spire shape: depressed conical. Basal spire shape: ovoid. Whorl periphery: moderately to distinctly convex. Umbilicus: open or partially closed by tuba.

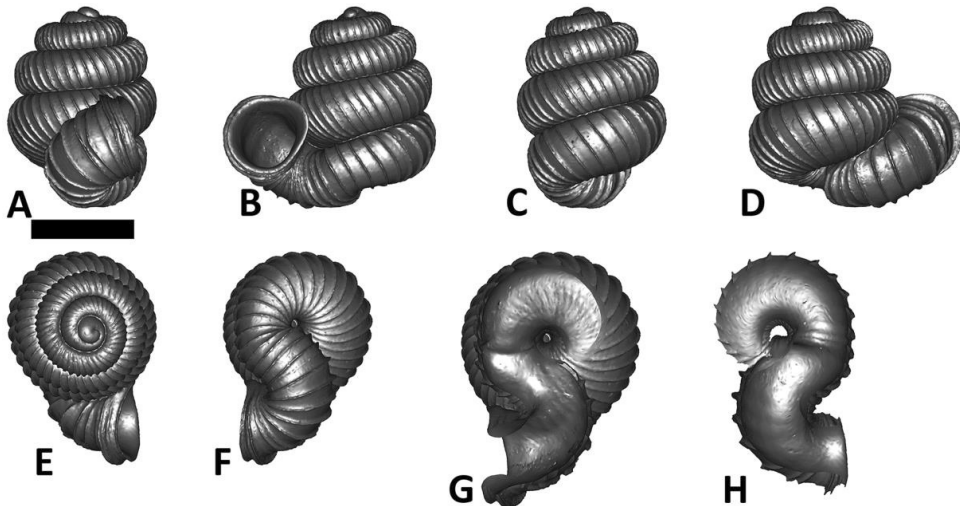


Figure 40. *Plectostoma kubuensis* sp. n. BOR 5648. **A** frontal view; **B** left lateral view; **C** back view; **D** right lateral view; **E** top view; **F** bottom view; **G** parietal part of constriction inner whorl; **H** basal part of constriction inner whorl. Scale bar = 1 mm (for A – F).

Constriction. Parietal teeth: none. Basal teeth: none.

Tuba. Coiling direction: type 3 and aperture visible in right lateral view. Tuba whorl length in proportion to spire last whorl: *ca.* 5/8 – 3/4. Proportion of tuba that attaches to spire: whole.

Aperture and peristome. Peristome: double peristomes. Outer peristome shape: similar to inner peristome, projected all around, except the posterior part, where the left lateral sides are slightly more projected than the anterior and right lateral side.

Spiral lines. Thick lines: absent. Thin lines: present.

Radial ribs. Rib density: 10 - 11 ribs per mm. Rib intensity: thin. Shape: straight to slightly curved. Inclination: moderately prosoclin.

Distribution

Type locality. Bukit Kubu (6° 24' 15" N, 100° 8' 37" E) (Figure 18C).

Distribution range. Endemic to the type locality.

Conservation status

Endangered (B2ab(iii)+C2a(i) ver. 10.1). During a survey of a dozen isolated limestone hills of the State of Perlis in May 2011, only Bukit Kubu was found to support a living population of *P. kubuensis*, consisting of several hundred individuals at the top of Bukit Kubu. Several very small populations (< 50 individuals) live at the other part of Bukit Kubu where the habitat is relatively more exposed and dry. Bukit Kubu is gazetted by Perlis State government as a recreation forest, and its surroundings consist of urban development and paddy fields.

Discussion

From the conchological point of view, the overall shape and size of *P. kubuensis* and *P. kakiense* is almost the same. Nevertheless, two inconspicuous but significant shell characters, namely, basal and parietal constriction teeth, mark the difference between these two species. Despite the similarity in shell form, there is a great genetic distance between the two species (16%). The species occur at two limestone hills that lie about 30 km apart. During our survey, we could not find either species at the six limestone hills that are located between these two hills. A single *Plectostoma* shell was recorded by Norhanis et al. (2010) from Pulau Dayang Bunting, Langkawi, and might belong to this species.

***Plectostoma laemodes* (van Benthem Jutting, 1961)**

Figure 41 and Appendix 12.

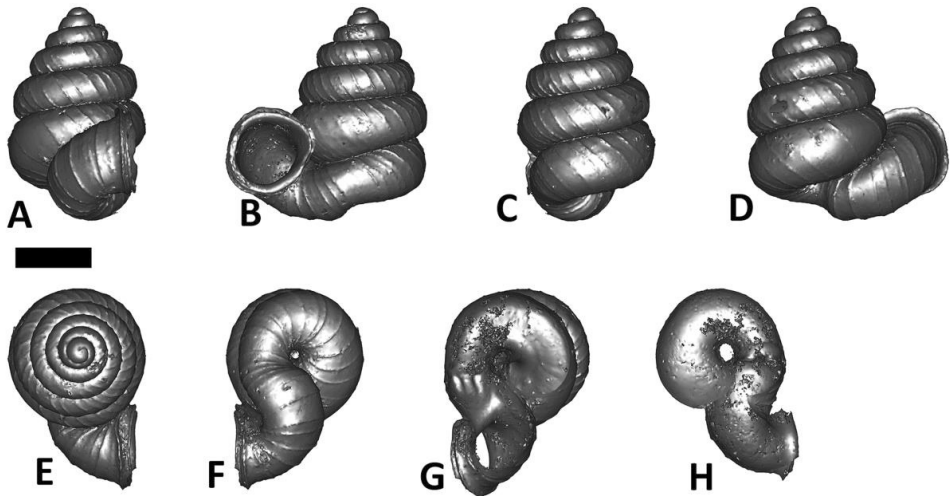


Figure 41. *Plectostoma laemodes* (van Benthem Jutting, 1961) ZMA 136011. **A** frontal view; **B** left lateral view; **C** back view; **D** right lateral view; **E** top view; **F** bottom view; **G** parietal part of constriction inner whorl; **H** basal part of constriction inner whorl. Scale bar = 1 mm (for **A – F**).

Opisthostoma laemodes van Benthem Jutting, 1961: 40, plate 11 - figure 6 (original description).

Type material

Holotype: ZMA 136010(1) (Seen).

Paratypes: ZMA 136011(3) (Seen), ZMA 136012(3) (Seen), ZMA 136013(4) (Seen).

Other examined materials

RMNH 156267(7), V 8490(>25).

Diagnosis

Shares with *P. salpidomon* the general shell form, in terms of apex, spire, and tuba shape, but differs by having the whole tuba attached to the spire.

Description.

Apex. Shape: distinctly convex.

Spire. Height: 2.3 – 2.7 mm. Width: 1.6 – 1.8 mm. Number of whorls: 3 1/8 – 4 5/8. Apical spire shape: depressed conical. Basal spire shape: ovoid. Whorl periphery: moderately to distinctly convex. Umbilicus: open or partially closed by tuba.

Constriction. Parietal teeth: two. Basal teeth: none.

Tuba. Coiling direction: type 3 and aperture visible in right lateral view. Tuba whorl length in proportion to spire last whorl: ca. 1/2 – 5/8. Proportion of tuba that attaches to spire: whole.

Aperture and peristome. Peristome: double peristomes. Outer peristome shape: similar to inner peristome, projected all around, except the posterior part, where the left lateral sides are slightly more projected than the anterior and right lateral side.

Spiral lines. Thick lines: absent. Thin lines: present.

Radial ribs. Rib density: 6–7 ribs per mm. Rib intensity: thin. Shape: straight to slightly curved. Inclination: prosoclin.

Distribution

Type locality. Batu Tai Gajah, Ulu Keniyam Kechil, Taman Negara, Pahang Malaysia (4° 37' 0" N, 102° 25' 14" E) (Figure 18B).

Distribution range. This species mainly occurs in a cluster of limestone hills that are located at upper Sungai Keniyam Kecil in Taman Negara (Figure 18B). In addition, this species has been recorded from Bukit Jereng, Blau, Kelantan, which is about 80 km west from Sungai Keniyam Kecil.

Conservation status

Least Concern. Although no living population has been recorded so far, several large and well protected limestone hills in the Taman Negara probably support a viable population.

Discussion

From a conchological point of view, this species is similar to *P. salpidomon*; the two may be closely related. In view of biogeography, this species occurs parapatrically with *P. salpidomon*, which occurs in the limestone hills in between Bukit Jereng and the limestone cluster at Sungai Keniyam Kecil (Figure 18B). Further genetic data are needed to verify the taxonomic status of *P. laemodes*.

***Plectostoma salpidomon* (van Benthem Jutting, 1952)**

Figures 17A and 42, and Appendix 13.

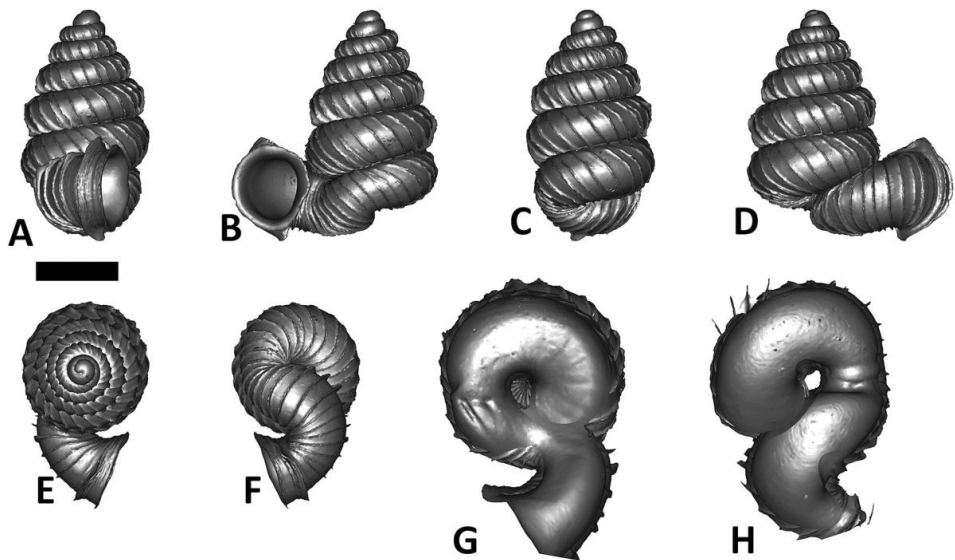


Figure 42. *Plectostoma salpidomon* (van Benthem Jutting, 1952) BOR 5539. **A** frontal view; **B** left lateral view; **C** back view; **D** right lateral view; **E** top view; **F** bottom view; **G** parietal part of constriction inner whorl; **H** basal part of constriction inner whorl. Scale bar = 1 mm (for A – F).

Opisthostoma salpidomon van Benthem Jutting, 1952: 42, figure 21 (original description).

Opisthostoma salpidomon van Benthem Jutting, van Benthem Jutting (1961: 39).

Type material

Holotype: ZMA 136045(1) (Seen).

Paratypes: ZMA 136046(>25) (Seen), ZMA 136047(2) (Seen), ZMA 136048(>10) (Seen).

Other examined materials

ZMA 162137(>25), BOR 459(1), BOR 5539(>10), BOR 5540(>10), BOR 5541(5), BOR

5542(>25), BOR 5569(>25), BOR 5611(1), V 8171(4), V 8658(>25), V 8706(6), V 9116(7), V 9292(3).

Diagnosis

Shares with *P. laemodes* the general shell form, in terms of apex, spire, and tuba shape, but differs by having a tuba that attaches partly to the spire.

Description.

Apex. Shape: distinctly convex.

Spire. Height: 2.5 – 2.8 mm. Width: 1.5 – 1.7 mm. Number of whorls: 4 5/8 – 5 1/4. Apical spire shape: depressed conical. Basal spire shape: ovoid. Whorl periphery: moderately to distinctly convex. Umbilicus: completely or partially closed by tuba.

Constriction. Parietal teeth: two. Basal teeth: none.

Tuba. Coiling direction: type 2 and aperture visible in right lateral view. Tuba whorl length in proportion to spire last whorl: ca. 3/4 – 7/8. Proportion of tuba that attaches to spire: less than 2/3.

Aperture and peristome. Peristome: double peristomes. Outer peristome shape: similar to inner peristome, projected all around, except the posterior part, where the two lateral sides are slightly more projected than the anterior side.

Spiral lines. Thick lines: absent. Thin lines: present.

Radial ribs. Rib density: 5–6 ribs per mm. Rib intensity: thin. Shape: slightly curved. Inclination: prosoclin.

Distribution

Type locality. Gua Bama, Pahang (4° 11' 37" N, 101° 58' 2" E) (Figure 18B).

Distribution range. *P. salpidomon* can be found in many limestone hills in the valley in between the Titiwangsa, Tahan and Benom mountain ranges (Figure 18B).

Conservation status

Least Concern. *P. salpidomon* has a wide distribution range. Living populations have been recorded in many limestone hills and some of these are in protected areas.

Discussion

See discussion under *P. laemodes*.

***Plectostoma kitteli* (Maassen, 2002)**

Figure 43 and Appendix 11.

Opisthostoma kitteli Maassen, 2002: 176, figures 35 & 36 (original description).

Type material

Holotype: RMNH 92942(1) (seen)

Paratypes: RMNH 92956(>25) (Seen), V 12697(9) (Seen).

Other examined materials

BOR 1697(>10). YSC.

Diagnosis

Shares with *P. charasense*, *P. tohchinyawi*, and *P. klongsangensis* the general shell form, in terms of apex, spire, and tuba shape, but differs by lacking thick spiral lines and basal constriction teeth.

Description.

Apex. Shape: distinctly convex.

Spire. Height: 2.9 – 3.0 mm. Width: 1.7 – 1.8 mm. Number of whorls: 5 5/8 – 5 3/4. Apical spire shape: oblong conical. Basal spire shape: conical. Whorl periphery: distinctly convex. Umbilicus: partially closed by tuba.

Constriction. Parietal teeth: two. Basal teeth: none.

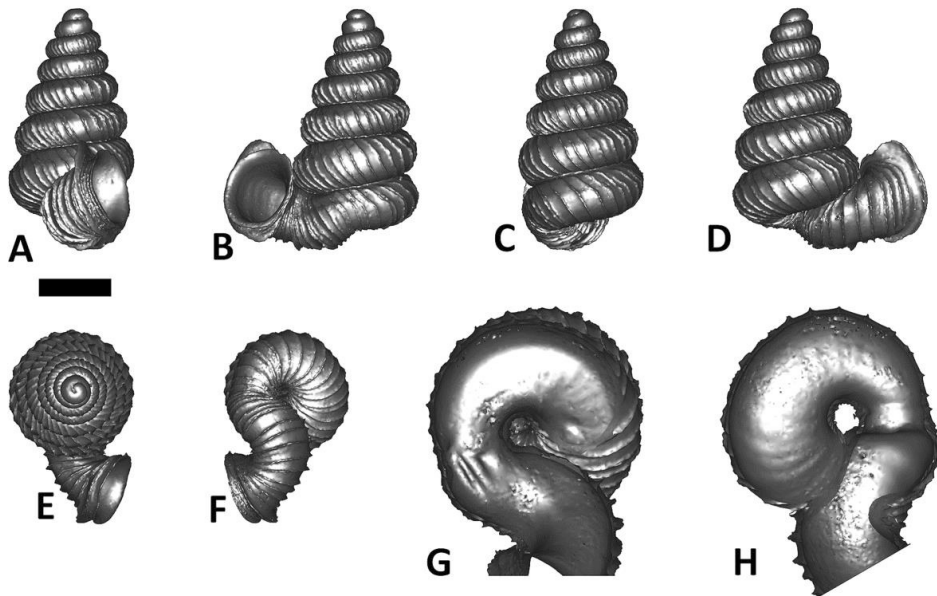


Figure 43. *Plectostoma kitteli* (Maassen, 2002) V 12697. **A** frontal view; **B** left lateral view; **C** back view; **D** right lateral view; **E** top view; **F** bottom view; **G** parietal part of constriction inner whorl; **H** basal part of constriction inner whorl. Scale bar = 1 mm (for A – F).

Tuba. Coiling direction: type 2 and aperture visible in right lateral view. Tuba whorl length in proportion to spire last whorl: ca. 3/4 – 7/8. Proportion of tuba that attaches to spire: less than 2/3.

Aperture and peristome. Peristome: double peristomes. Outer peristome shape: similar to inner peristome, projected all around, except the posterior part, where the two lateral sides are slightly more projected than the anterior side.

Spiral lines. Thick lines: absent. Thin lines: present.

Radial ribs. Rib density: 5–6 ribs per mm. Rib intensity: thin. Shape: slightly curved. Inclination: orthoclin.

Distribution

Type locality. Cave Pangian (local name Ngalau Pangian - 0° 27' 45" S, 100° 45' 8" E)

Distribution range - This species was also found at a limestone hill near Kampung Desa Gadut, West Sumatra (0° 15' 36" S, 100° 44' 16" E). This hill is located about 20 km from the type locality. In addition, a private collector (Yansen Chen, pers. comm.) also collected the same species at Tiangko cave, about 230 km from the type locality (Figure 18B). It therefore appears to have a wide distribution range in Sumatra. It may thus be expected that the limestone outcrops around the three hills mentioned, might support the same species.

Conservation status

Data Deficient. This species has only been recorded from three limestone hills in West Sumatra. The population status and actual distribution range of this species remain unknown. Nevertheless, concern is warranted, as the surroundings of the type locality and several other limestone outcrops in the same area are highly degraded.

Discussion

There are large areas in the Northern and Western provinces of Sumatra that are covered by limestone hills (Verstappen & Genootschap, 1973). Despite intensive malacological surveys in some of these areas (van Benthem Jutting, 1959), no *Plectostoma*

species was found until 1997. To date, *Plectostoma kitteli* is the only *Plectostoma* species found in Sumatra (Maassen, 2002).

***Plectostoma klongsangensis* (Panha, 1997)**

Opisthostoma klongsangensis Panha, 1997: 133, figure 1 (original description).

Opisthostoma klongsangensis Panha, Hemmen and Hemmen (2001: 39).

Opisthostoma klongsangensis Panha, Nabhitabhata (2009: 50).

Type material

Holotype: CUIZMD 0001 (not seen).

Paratypes: CUIZMDM 0002 (Not seen), CUIZMDM 0003 in ZMA (Not seen, specimen could not be located in ZMA).

Diagnosis

Shares with *P. charasense*, *P. tohchinyawi*, and *P. kitteli* the general shell form, in terms of apex, spire, and tuba, but differs by having both thin and thick spiral lines, and the left lateral side of outer peristome projected more than three times the distance of the right lateral side of outer peristome.

Description (estimated from figure in Panha 1997).

Apex. Shape: distinctly convex.

Spire. Height: 2.3 mm. Width: 1.7 mm. Number of whorls: 5 1/2. Apical spire shape: oblong conical. Basal spire shape: conical. Whorl periphery: distinctly convex. Umbilicus: open.

Constriction. Unknown.

Tuba. Coiling direction: type 2 and aperture visible in right lateral view. Tuba whorl length in proportion to spire last whorl: ca. 7/8. Proportion of tuba that attaches to spire: less than 2/3.

Aperture and peristome. Peristome: double peristomes. Outer peristome shape: different from inner peristome, the left lateral side of outer peristome is projected from inner peristome about 0.7 mm, and the right side of outer peristome about 0.1 mm, but narrowed toward the anterior part of outer peristome.

Spiral lines. Thick lines: present. Thin lines: present.

Radial ribs. Rib density: 3 ribs per mm. Rib intensity: thick. Shape: single-looped. Inclination: prosoclin.

Distribution

Type locality. Khlong Saeng Wildlife Sanctuary Surat Thani Province, Thailand (8° 31' 13" N, 98° 25' 17" E) (Figure 18B).

Distribution range - Unknown.

Conservation status

Data Deficient. This species has been collected once in Khlong Saeng Wildlife Sanctuary.

Discussion

From a conchological point of view, this species appears not to be related to *Plectostoma* species from the Malay Peninsula and Sumatra. Instead, it is almost identical to *Plectostoma mirabile*, an endemic species from Gomantong Cave, Sabah, Borneo. These two species are separated by the South China Sea and located more than 2000 km apart. It remains to be determined whether this similarity is due to a disjunct distribution of closely related forms, or rather convergent shell evolution.

The taxonomic status of the species remains doubtful. In the original publication, Panha (1997) compared it with *P. heteropleuron* (Vermeulen, 1994) and *P. perspectivum* (Vermeulen, 1994) from Northern Borneo, but not with *P. mirabile* (Smith, 1893), which has an almost identical shell as *P. klongsangensis*. This is all the more remarkable, as *P. mirabile*

(Smith, 1893) was treated in Vermeulen (1994), where both *P. heteropleuron* and *P. perspectivum* were originally described.

In conclusion, more data are needed to verify the taxonomic status and the interesting biogeography of this species.

***Plectostoma charasense* (Tomlin, 1948)**

Figure 44 and Appendix 14.

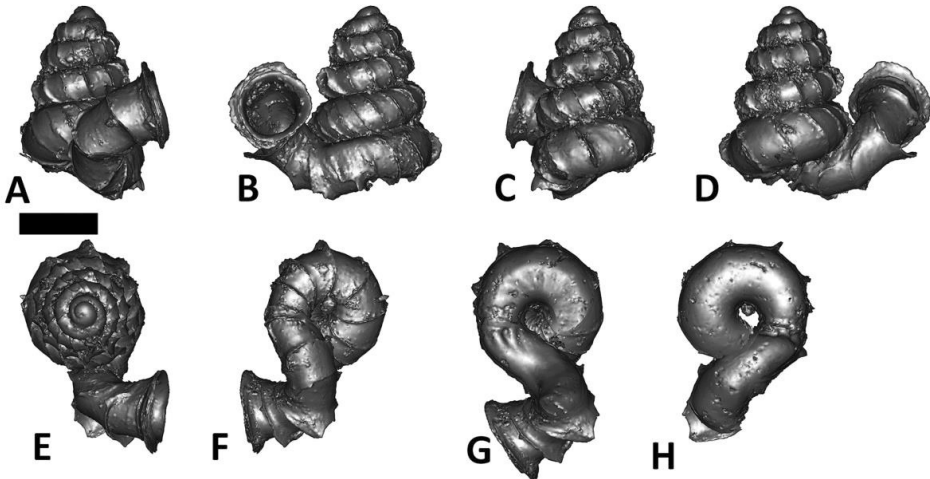


Figure 44. *Plectostoma charasense* (Tomlin, 1948) ZMA 162063. **A** frontal view; **B** left lateral view; **C** back view; **D** right lateral view; **E** top view; **F** bottom view; **G** parietal part of constriction inner whorl; **H** basal part of constriction inner whorl. Scale bar = 1 mm (for A – F).

Opisthostoma charasense Tomlin, 1948: 225, Plate 2 - figure 4 (original description).

Opisthostoma charasense Tomlin, van Benthem-Jutting (1952: 42).

Type material

Holotype: BNHM 1948.10.2.2(1) (Seen).

Other examined materials

ZMA 162063(>10), ZMA 162064(>10).

Diagnosis

Shares with *P. kitteli*, *P. tohchinyawi*, and *P. klongsangensis* the general shell form, in terms of apex, spire, and tuba shape, but differs by lacking thick spiral lines and by having two basal constriction teeth.

Description.

Apex. Shape: distinctly convex.

Spire. Height: 1.9 - 2.0 mm. Width: 1.3 – 1.4 mm. Number of whorls: 4 1/8. Apical spire shape: oblong conical. Basal spire shape: conical. Whorl periphery: distinctly convex. Umbilicus: open.

Constriction. Parietal teeth: two. Basal teeth: two.

Tuba. Coiling direction: type 2 and aperture visible from right lateral view. Tuba whorl length in proportion to spire last whorl: ca. 7/8. Proportion of tuba that attaches to spire: less than 1/2.

Aperture and peristome. Peristome: double peristomes. Outer peristome shape: same as inner peristome and uniformly projected all around, except the posterior part.

Spiral lines. Thick lines: absent. Thin lines: present.

Radial ribs. Rib density: 4 ribs per mm. Rib intensity: thick. Shape: slightly curved to single-humped. Inclination: moderately prosoclin.

Distribution

Type locality. Gua Charas, limestone hill near Sungai Lembing in the state of Pahang, Malaysia (3° 54' 27" N, 103° 8' 47" E).

Distribution range. Until now, this species has been recorded from two neighbouring limestone hills, namely, Gua Charas and Bukit Panching. However, the whole hill of Bukit Panching has been lost to quarrying (Figure 18B).

Conservation status

Critically Endangered (B2ab(iii)+C2a(i) ver. 10.1). Gua Charas might support a viable population. However, the hill is currently surrounded by oil palm plantation with a very narrow forested buffer zone. No living individuals or fresh dead shells were found at Gua Charas after exhaustive search during several sampling trips in 2010 and 2011.

Discussion

The taxonomic status of this species is stable. Although the two neighbouring species, *P. tohchinyawi* and *P. praeco*, are similar to *P. charansense*, there are a few key shell characters that separate *P. charansense* from the others. See discussion under *P. tohchinyawi* for more discussion about the biogeography of this species.

***Plectostoma tohchinyawi* sp. n.**

Figure 17S and 45, and Appendix 14.

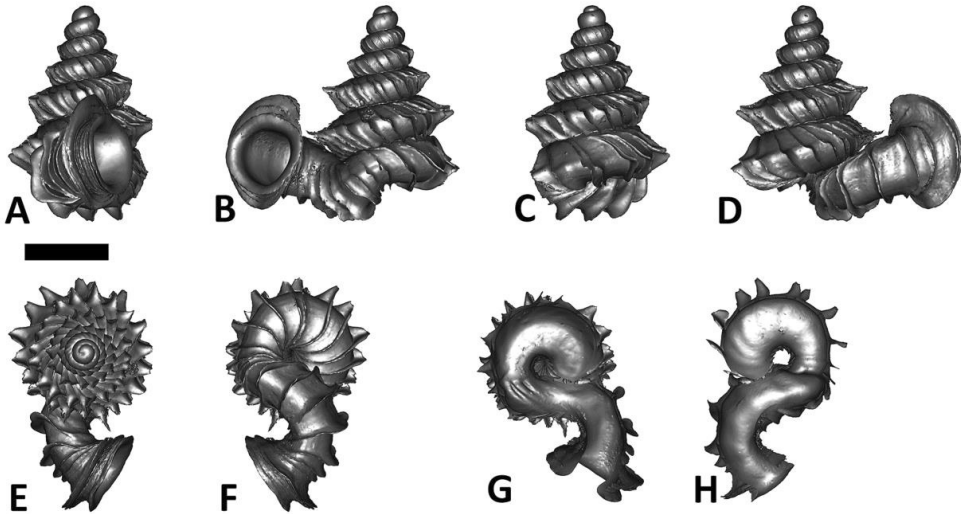


Figure 45. *Plectostoma tohchinyawi* sp. n. BOR 5649. **A** frontal view; **B** left lateral view; **C** back view; **D** right lateral view; **E** top view; **F** bottom view; **G** parietal part of constriction inner whorl; **H** basal part of constriction inner whorl. Scale bar = 1 mm (for A – F).

Type material

Holotype - BOR 5649(1).

Paratypes - BOR 5533(>10), BOR 5534(>10), BOR 5535(>10), V 8811(>25).

Diagnosis

Shares with *P. charansense*, *P. kitteli*, and *P. klongsangensis* the general shell form, in terms of apex, spire, and tuba shape, but differs by having both thin and thick spiral lines, and the

left lateral side of outer peristome projected not more than twice the width of the right lateral side of outer peristome.

Etymology

This species is named after Dato' Toh Chin Yaw, who was the Chairman of Industry, Trade and Environment Committee in the Terengganu State Government between 2008 and 2013. It is rare to find politicians working closely with the public for wildlife conservation. During his time in office, Dato' Toh was tireless in his efforts to promote and preserve Terengganu's natural heritage. One of his most influential decisions was getting the State to ban the hunting of threatened flying foxes (*Pteropus vampyrus*). Before he left office, he was working with scientists to gazette the Kenyir Wildlife Corridor as a protected area and was helping to secure funds to improve anti-poaching efforts in that area.

Description.

Apex. Shape: distinctly convex.

Spire. Height: 2.1 - 2.4 mm. Width: 1.3 – 1.5 mm. Number of whorls: 4 7/8 – 5 3/8. Apical spire shape: oblong conical. Basal spire shape: conical. Whorl periphery: distinctly convex. Umbilicus: open.

Constriction. Parietal teeth: two. Basal teeth: none.

Tuba. Coiling direction: type 2 and aperture visible in right lateral view. Tuba whorl length in proportion to spire last whorl: ca. 7/8 – 8/8. Proportion of tuba that attaches to spire: less than 1/2.

Aperture and peristome. Peristome: double peristomes. Outer peristome shape: similar to inner peristome, projected all around, except the posterior part, where the two lateral sides are distinctly more projected than the anterior side.

Spiral lines. Thick lines: present. Thin lines: present.

Radial ribs. Rib density: 4–6 ribs per mm. Rib intensity: thick. Shape: slightly curved to single-humped. Inclination: prosoclin.

Distribution

Type locality. Gua Bewah, Tasik Kenyir (4° 51' 3" N, 102° 43' 21" E).

Distribution range. To date, this species is only known to occur at two neighbouring limestone outcrops, namely, Gua Bewah and Gua Taat at the Southern part of Tasik Kenyir (Figure 18B).

Conservation status

Least Concern. The only two limestone outcrops where this species was found are partially submerged in Southeast Asia's largest man-made lake, Tasik Kenyir. Nonetheless, there is good forest cover around and on the limestone outcrops. Furthermore, these two hills are located in the Taman Negara Pahang, which is a prioritised protected area.

Discussion

From a conchological point of view, this species is related to *P. charasense*. Both are thought to be affiliated with the *Plectostoma* species from North Borneo. *P. tohchinyawi* has a high conical spire, thick and projected radial ribs, and a long detached tuba. These are the typical characteristics for dozens of *Plectostoma* species in North Borneo. In addition, *P. tohchinyawi* and *P. charasense* live on the five lenticular limestone outcrops that are the easternmost outcrops of the Malay Peninsula, thus closest geographically to Borneo (Figure 18B).

***Plectostoma annandalei* (Sykes, 1903)**

Opisthostoma annandalei Sykes, 1903: 198, Plate 20 - figures 4 & 5 (original description).

Opisthostoma annandalei Sykes, Laidlaw (1928: 36).

Opisthostoma annandalei Sykes, van Benthem-Jutting (1952: 41).

Type material

Not seen.

Diagnosis

Shares with *P. laidlawi*, *P. tenggekensis*, and *P. praeco* the general shell form, in terms of spire and tuba shape, but differs by having slightly convex whorl periphery and straight ribs.

Description (estimated from figure in Sykes 1903).

Apex. Shape: moderately convex.

Spire. Height: 2 mm. Width: 1.3 mm. Number of whorls: 4 1/2. Apical spire shape: depressed conical. Basal spire shape: conical. Whorl periphery: moderately convex. Umbilicus: Open.

Constriction. Unknown.

Tuba. Coiling direction: type 2 and aperture visible in right lateral view. Tuba whorl length in proportion to spire last whorl: approximately the same as the spire's last whorl length. Proportion of tuba that attaches to spire: less than 1/2.

Aperture and peristome. Peristome: double peristomes. Outer peristome shape: same as inner peristome and uniformly projected all around, except the posterior part.

Spiral lines. Unknown

Radial ribs. Rib density: 5 ribs per mm. Rib intensity: unknown. Shape: straight. Inclination: orthoclin.

Distribution

Type locality. This species is only known from its type locality, Jalor (Biserat). The exact location was not described in the original publication of this species. From the collectors' report (Annandale & Robinson, 1913), we estimated the location and name of the limestone hill from a map in the report. This hill was named Bukit Bayu. Later, we estimated its coordinates from Google Earth (6° 16' 48" N, 101° 13' 35" E) (Figure 18B).

Distribution range. Unknown.

Conservation status

Data Deficient.

Discussion

This species has not been seen or collected after the original description. The type specimens cannot be located. Sykes (1903) mentioned that it is similar to *Plectostoma laidlawi* but he did not explain explicitly in what way. This is not unexpected, as *P. laidlawi* was the only one *Plectostoma* known from Peninsular Malaysia at the time, although more than 20 *Plectostoma* species had already been described from Borneo. Thus, one can assume that the statement made by Sykes was based on the geographical proximity.

Interestingly, *P. panhai* was described from a limestone hill located just 8 km from the location where *P. annandalei* was found. In addition to the geographical proximity, the two neighbouring species are similar in several shell characteristics. The shell spires are very similar in terms of number of whorls, overall shape and size. On the other hand, the main difference between these two species is the tuba coiling direction (type 1 vs. type 2).

***Plectostoma praeco* (van Benthem Jutting, 1961)**

Figure 46 and Appendix 14.

Opisthostoma praeco van Benthem Jutting, 1961: 39, Plate 2 - figure 5 (original description).

Type material

Holotype: ZMA 136034(1) (Seen).

Paratypes: ZMA 136041(>50) (Seen), ZMA 136042(>25) (Seen).

Other examined materials

ZMA 162150(>100), ZMA 162151(>100), ZMA 162152(>100), ZMA 162153(>10).

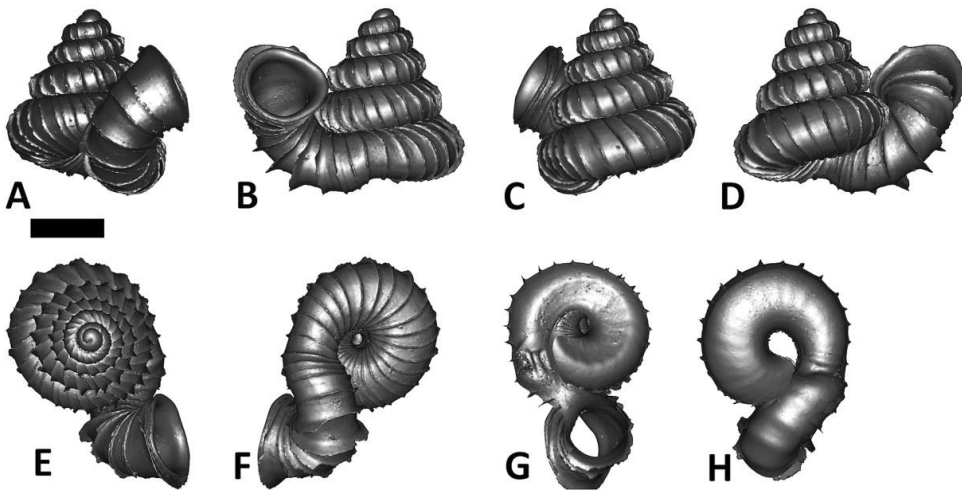


Figure 46. *Plectostoma praeco* (van Benthem Jutting, 1961) ZMA 162150. **A** frontal view; **B** left lateral view; **C** back view; **D** right lateral view; **E** top view; **F** bottom view; **G** parietal part of constriction inner whorl; **H** basal part of constriction inner whorl. Scale bar = 1 mm (for A – F).

Diagnosis

Shares with *P. laidlawi*, *P. tenggekensis*, and *P. annandalei* the general shell form, in terms of spire and tuba shape, but differs by having slightly curved ribs.

Description.

Apex. Shape: distinctly convex.

Spire. Height: 2.0 – 2.2 mm. Width: 1.8 – 2.0 mm. Number of whorls: 4 $\frac{1}{4}$ –4 $\frac{5}{8}$. Apical spire shape: depressed conical. Basal spire shape: conical. Whorl periphery: moderately to distinctly convex. Umbilicus: open.

Constriction. Parietal teeth: two. Basal teeth: none.

Tuba. Coiling direction: type 2 and aperture visible in right lateral view. Tuba whorl length in proportion to spire last whorl: ca. $\frac{5}{8}$ – $\frac{7}{8}$. Proportion of tuba that attaches to spire: more than $\frac{1}{3}$ but less than $\frac{1}{2}$.

Aperture and peristome. Peristome: double peristomes. Outer peristome shape: similar to inner peristome, projected all around, except the posterior part, where the left lateral sides are slightly more projected than the anterior and right lateral side.

Spiral lines. Thick lines: absent. Thin lines: present.

Radial ribs. Rib density: 6 – 7 ribs per mm. Rib intensity: thin. Shape: slightly curved. Inclination: moderately prosoclin.

Distribution

Type locality. Batu Che Derani, Taman Negara Pahang (4° 35' 57" N, 102° 25' 57" E).

Distribution range. *P. praeco* has been recorded from four other hills at upper Sungai Keniyam Kecil, which is in the vicinity of the type locality (Figure 18B).

Conservation status

Least Concern. All the limestone hills where *P. praeco* occurs, are located in the National Park.

Discussion

There is no genetic information for *P. praeco*. Morphological similarity suggests that *P. praeco* and *P. tenggekensis* are closely related. Each of the two species has a narrow distribution range and they are separated from each other by at least 50 km.

***Plectostoma tenggekensis* sp. n.**

Figure 47 and Appendix 14.

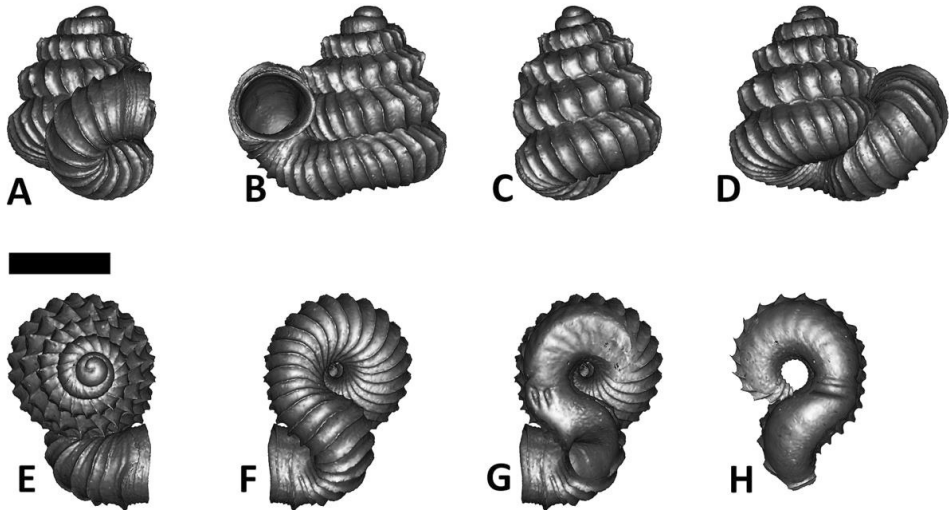


Figure 47. *Plectostoma tenggekensis* sp. n. BOR 5650. **A** frontal view; **B** left lateral view; **C** back view; **D** right lateral view; **E** top view; **F** bottom view; **G** parietal part of constriction inner whorl; **H** basal part of constriction inner whorl. Scale bar = 1 mm (for A – F).

Type material

Holotype: BOR 5650(1)

Paratypes: V 13554(5), BOR 444(4), BOR 5596(>10).

Diagnosis

Shares with *P. laidlawi*, *P. annandalei*, and *P. praeco* the general shell form, in terms of spire and tuba shape, but differs by having single-humped shaped ribs.

Etymology

This species is named after its type locality – Bukit Tenggek, Kuantan, Pahang.

Description.

Apex. Shape: moderately convex.

Spire. Height: 1.6 – 1.7mm. Width: 1.3 – 1.4 mm. Number of whorls: 4–4 1/4. Apical spire shape: depressed. Basal spire shape: conical. Whorl periphery: moderately convex. Umbilicus: open.

Constriction. Parietal teeth: two. Basal teeth: none.

Tuba. Coiling direction: type 2 and aperture visible in right lateral view. Tuba whorl length in proportion to spire last whorl: *ca.* 5/8 of the spire last whorl length. Proportion of tuba that attaches to spire: less than 1/3.

Aperture and peristome. Peristome: double peristomes. Outer peristome shape: similar to inner peristome, projected all around, except the posterior part, where the left lateral sides are slightly more projected than the anterior and right lateral side.

Spiral lines. Thick lines: absent. Thin lines: present.

Radial ribs. Rib density: 6–7 ribs per mm. Rib intensity: thin. Shape: slightly curved. Inclination: moderately prosoclin.

Distribution

Type locality. Bukit Tenggek, Pahang (4° 0' 51" N, 103° 9' 34" E).

Distribution range. Endemic to type locality (Figure 18B).

Conservation status

Critically Endangered (B2ab(iii)+C2a(i) ver. 10.1). The entire Bukit Tenggek will be gone by 2014 because of quarrying activity.

Discussion

See discussion under *P. praeco*.

***Plectostoma laidlawi* (Sykes, 1902)**

Figures 17O, 48 and 49, and Appendix 15.

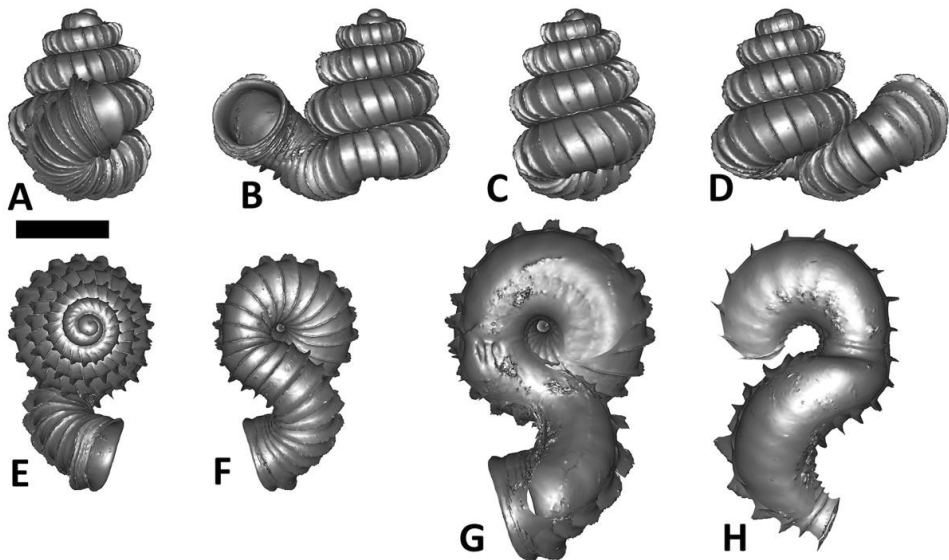


Figure 48. *Plectostoma laidlawi* (Sykes, 1902) (Form BOR 5510). **A** frontal view; **B** left lateral view; **C** back view; **D** right lateral view; **E** top view; **F** bottom view; **G** parietal part of constriction inner whorl; **H** basal part of constriction inner whorl. Scale bar = 1 mm (for A – F).

Opisthostoma laidlawi Sykes, 1902a: 22 (original description).

Opisthostoma laidlawi Sykes, Sykes (1902b: Plate 3 - figures 13 & 14).

Opisthostoma laidlawi Sykes, von Moellendorff (1902: 143).

Opisthostoma laidlawi Sykes, Laidlawi (1928: 36).

Opisthostoma laidlawi Sykes, van Benthem-Jutting (1952: 41).

Opisthostoma laidlawi Sykes, Ito et al. (2009: 58).

Opisthostoma laidlawi Sykes, Sasaki (2010: 126, figure 2.7B).

Type material

Holotype: Not Seen

Paratype: ZMA 136014(1) (Seen).

Other examined materials

BMNH C_ACC1825(1), BOR 5510(>25), BOR 5571(2), RMNH 156268(1), ZMA 162095(2), ZMA 162097(>25), ZMA 162099(>10), ZMA 162100(>25), ZMA 162096(1), V5558(1), V 7878(3), V 8345(>100), V 8476(>25), V 8670(>25), V 8693(>50), V 8950(>50), V 9044(>25), V 9109(>25), V 9125(>25), V 9359(6).

Diagnosis

Shares with *P. annandalei*, *P. tenggekensis*, and *P. praeco* the general shell form in terms of

spire and tuba shape, but differs by having a distinctly convex whorl periphery and straight ribs.

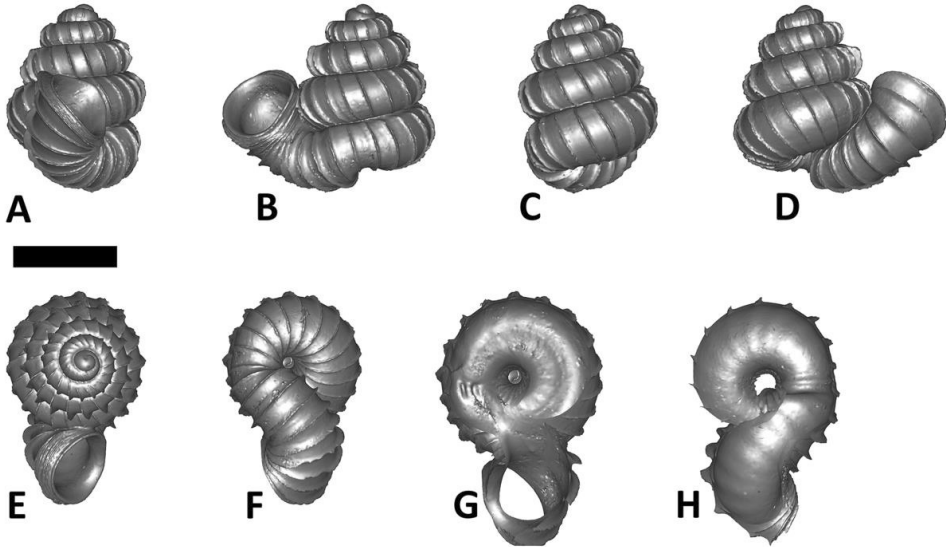


Figure 49. *Plectostoma laidlawi* (Sykes, 1902) (Form BOR 5571). **A** frontal view; **B** leftlateral view; **C** back view; **D** right lateral view; **E** top view; **F** bottom view; **G** parietal part of constriction inner whorl; **H** basal part of constriction inner whorl. Scale bar = 1 mm (for A – F).

Description.

Apex. Shape: moderately to distinctly convex.

Spire. Height: 1.6 – 2.3 mm. Width: 1.3 – 1.8 mm. Number of whorls: 3 5/8 – 4. Apical spire shape: depressed conical. Basal spire shape: conical to ovoid. Whorl periphery: distinctly convex. Umbilicus: open.

Constriction. Parietal teeth: two. Basal teeth: none.

Tuba. Coiling direction: type 2 and aperture visible in right lateral view. Tuba whorl length in proportion to spire last whorl: ca. 5/8 – 7/8. Proportion of tuba that attaches to spire: varies from completely attached to as much as half of the tuba detached from spire.

Aperture and peristome. Peristome: double peristomes. Outer peristome shape: similar to inner peristome, projected all around, except the posterior part, where the two lateral sides are slightly more projected than the anterior side or left lateral sides slightly more projected than the anterior and right lateral side.

Spiral lines. Thick lines: present. Thin lines: present.

Radial ribs. Rib density: 5 - 6 ribs per mm. Rib intensity: thin. Shape: straight to slightly curved. Inclination: moderately prosoclin.

Distribution

Type locality. “Kelantan, Malay Peninsula”, collected by J. Waterstradt (Sykes, 1902). According to Waterstradt’s (1902) itinerary, he visited one of the limestone hills at Kampung Pulau. The Pulau Princess cave (4° 47' 38" N, 101° 56' 31" E) fits perfectly with Waterstradt's descriptions on the local population, temples and hill's topography; he also described that he and his collectors sampled shells here (Waterstradt, 1902: 9–10). We conclude that Pulau Princess Cave must be the type locality of *Plectostoma laidlawi*. However, a recent survey at the highly degraded Bukit Pulau Princess cave failed to retrieve any shells of *Plectostoma*.

Distribution range. This species occurs on the limestone hills along Berok River and Nenggiri River (Figure 18B).

Conservation status

Vulnerable (D2 ver. 10.1). Living populations were present on only two limestone hills during a survey in May 2011. All the limestone hills for which this species is known are surrounded by degraded forest and oil palm plantation.

Discussion

The morphology of this species is quite variable in shell size and degree of attachment of the tuba to the spire. The distribution range partially overlaps with that of *P. davisoni*. It is possible that the species actually consists of two or more cryptic species, and thus more genetic data are needed.

Acknowledgements

We thank Geoffrey Davison, Reuben Clements, Yansen Chen, Wim Maassen, and A.J. de Winter for help and fruitful discussion. Petherine Jimbau (BOR), Jonathan Ablett and Fred Naggs (BMNH), and Jeroen Goud, Rob Moolenbeek, and Bram van der Bijl (Naturalis) made the museum collections accessible for TSL. TSL thanks Universiti Malaysia Sabah and the Ministry of Higher Education (Malaysia) for support. TSL thanks Economic Planning Unit, Prime Minister's Department (UPE: 40/200/19/2524), State Planning Unit, Chief Minister's Department, Sarawak ((47) UPN/S/G1/I/10.1 Vol.27), Forest Department Sarawak (Research Permit NPW.907.4.4(V)-19; Park Permit No. 07/2010; Export Permit No. 09003), and Department of Wildlife and National Parks (Mr. Burhanuddin Mohd Nor). This project is supported by ALW-NWO (819.01.012) and EOL Rubenstein Fellowship (2010) to TSL. We thank Frank Koehler, Zoltán Fehér and an anonymous reviewer for useful comments which improved this paper.

Appendix (<http://dx.doi.org/10.6084/m9.figshare.830412>)

Appendix 1 Video tutorials of cybertaxonomy procedures.

Appendix 2 Details for collection data.

Appendix 3 Spiral striation profile on the shell spire of 29 *Plectostoma* species.

Appendix 4 Radial rib spacing profile on the shell spire of 29 *Plectostoma* species.

Appendix 5 A KML file consisting of collection data, image links and distribution data.

Appendix 6 A Blender file consisting of 17 shell 3D models of 2 species, Part 1 of 10.

Plectostoma christae (Maassen, 2001)

- V 12702 (1), BOR 5505 (1), BOR 5506 (2), BOR 5572(1), V 9285 (2).

Plectostoma crassipupa (van Benthem Jutting, 1952)

- BOR 5512 (1), V 8392 (2), V 9097 (3), V 9326 (2), V 9353 (2).

Appendix 7 A Blender file consisting of 18 shell 3D models of 6 species, Part 2 of 10.

Plectostoma dindingensis sp. n.

- BOR 5612 (3), BOR 5642 (1).

Plectostoma mengaburensis sp. n.

- BOR 5643 (1), V 8822 (1).

Plectostoma panhai (Maassen, 2001)

- ZMA 138438 (1), RMNH 81810 (2).

Plectostoma sciaphilum (van Benthem Jutting, 1952)

- ZMA 136050 (3).

Plectostoma senex (van Benthem Jutting, 1952)

- BOR 5628 (2), BOR 5603 (1).

Plectostoma sinyumensis (Maassen, 2001)

- BOR 5623 (2), BOR 5537 (1).

Appendix 8 A Blender file consisting of 14 shell 3D models of 5 species, Part 3 of 10.

Plectostoma siphonostomum (van Benthem Jutting, 1952)

- BOR 5521 (1), BOR 5557 (1).

Plectostoma whitteni sp. n.

- BOR 5644 (1), V 8885 (2).

Plectostoma tonkinianum (Dautzenberg & Fischer, 1905)

- V 11502 (1), V 9940 (1).

Plectostoma turriforme (van Benthem Jutting, 1952)

- BOR 5509 (1), ZMA 136069 (2).

Plectostoma umbilicatum (van Benthem Jutting, 1952)

- BOR 5503 (2), BOR 5625 (2).

Appendix 9 A Blender file consisting of 19 shell 3D models of 1 species, Part 4 of 10.

Plectostoma davisoni sp. n.

- BOR 5626 (2), BOR 5641 (2), BOR 5646 (1), V 14242 (1), V 8265 (3), V 8652 (3), V 9206 (1), V 9243 (2), ZMA 162071 (4).

Appendix 10 A Blender file consisting of 19 shell 3D models of 1 species, Part 5 of 10.

Plectostoma davisoni sp. n.

- V 9340 (2), ZMA 162069 (5), ZMA 162070 (3), ZMA 162146 (3), ZMA 162147 (6).

Appendix 11 A Blender file consisting of 18 shell 3D models of 4 species, Part 6 of 10.

Plectostoma kayiani sp. n.

- RMNH 330803 (1), V 8883 (2)

Plectostoma ikanensis sp. n. Form BOR 5507

- BOR 5645 (1), V 9320 (4), V9446 (4).

Plectostoma kakiense (Tomlin, 1948)

- BOR 5516 (1), BOR 5517 (2).

Plectostoma kitteli (Maassen, 2002)

Chapter 2

- RMNH 92956 (2), V 12697 (1).

Appendix 12 A Blender file consisting of 14 shell 3D models of 3 species, Part 7 of 10.

Plectostoma kubuensis sp. n.

- BOR 5518 (1), BOR 5519 (3), BOR 5648 (1).

Plectostoma laemodes (van Benthem Jutting, 1961)

- RMNH 156267 (3), V 8490 (2), ZMA 136011 (1).

Plectostoma palinhelix (van Benthem Jutting, 1952)

- BOR 5520 (1), V 5104 (2).

Appendix 13 A Blender file consisting of 11 shell 3D models of 3 species, Part 8 of 10.

Plectostoma relauensis sp. n.

- BOR 5511 (2), BOR 5647 (1), V 8196 (2).

Plectostoma retrovertens (Tomlin, 1938)

- V 5142 (2), BOR 5559 (1).

Plectostoma salpidomon (van Benthem Jutting, 1952)

- BOR 5539 (1), V 8658 (2).

Appendix 14 A Blender file consisting of 13 shell 3D models of 5 species, Part 9 of 10.

Plectostoma tohchinyawi sp. n.

- BOR 5533 (2), BOR 5649 (1), V 8811 (2).

Plectostoma charasense (Tomlin, 1948)

- ZMA 162063 (1), ZMA 162064 (2).

Plectostoma praeco van Benthem Jutting, 1961

- ZMA 162150 (1), ZMA 162151 (1), ZMA 162152 (1).

Plectostoma ikanensis sp. n. Form BOR 5504

- BOR 5504 (1).

Plectostoma tenggekensis sp. n.

- BOR 5596 (1), BOR 5649 (1).

Appendix 15 A Blender file consisting of 10 shell 3D models of 1 species, Part 10 of 10.

Plectostoma laidlawi (Sykes, 1902) Form BOR 5510

- BOR 5510 (1), V 5558 (1), ZMA 136014 (1).

Plectostoma laidlawi (Sykes, 1902) Form BOR 5571

- BOR 5571 (1), V 7878 (2), ZMA 162099 (4).

Appendix 16 51 COI sequences for 19 *Plectostoma* species in FASTA format. Each sequence is labeled with BOLD process ID, GenBank accession no, sample ID and species name.

Appendix 17 DNA sequence alignment for phylogenetic analysis.

Appendix 18 Shell colouration of *Opisthostoma* species.

Chapter 3

On growth and form of a heteromorphic terrestrial snail: *Plectostoma concinnum* (Fulton, 1901) (Mollusca: Caenogastropoda: Diplommatinidae)

(Submitted to *PeerJ*, and
published as preprint at <http://dx.doi.org/10.7287/peerj.preprints.289v1>)

Thor-Seng Liew^{1,2,3}, Annebelle CM Kok^{1,2}, Menno Schilthuizen^{1,2,3}, and Severine Urdy^{2,4,5}

1 Institute Biology Leiden, Leiden University, P.O. Box 9516, 2300 RA Leiden, the Netherlands.

2 Naturalis Biodiversity Center, P.O. Box 9517, 2300 RA Leiden, the Netherlands.

3 Institute for Tropical Biology and Conservation, Universiti Malaysia Sabah, Jalan UMS, 88400, Kota Kinabalu, Sabah, Malaysia.

4 Centrum Wiskunde & Informatica, Science Park 123, 1098 XG Amsterdam, the Netherlands.

5 University of California San Francisco (UCSF), Anatomy Department, Genentech Hall, 600 6th Street, San Francisco, CA 94158-2517.

Email: T-S L: thorsengliew@gmail.com

ACMK: annebelle.kok@gmail.com

MS: Menno.Schilthuizen@naturalis.nl

SU: severine.urdy@ucsf.edu

Author Contributions

LTS, ACMK, MS, and SU conceived and designed the experiments. LTS, ACMK collected data. LTS, ACMK, SU analysed the data. LTS, ACMK, MS, and SU contributed reagents/materials/analysis tools. LTS, SU wrote the paper. MS, ACMK commented on earlier versions of the manuscript.

Supplemental Information

(<http://dx.doi.org/10.6084/m9.figshare.960018>)

Abstract

The molluscan shell can be viewed as a petrified representation of the organism's ontogeny and thus can be used as a record of changes in form during growth. However, little empirical data is available on the actual growth and form of shells, as these are hard to quantify and examine simultaneously. To address these issues, we studied the growth and form of a heteromorphic and heavily ornamented land snail – *Plectostoma concinnum*. The growth data were collected in a natural growth experiment and the actual form changes of the aperture during shell ontogeny were quantified. We used an ontogeny axis that allows data of growth and form to be analysed simultaneously. Then, we examined the association between the growth and the form during three different whorl growing phases, namely, the regular coiled spire phase, the transitional constriction phase, and the distortedly-coiled tuba phase. In addition, we also explored the association between growth rate and the switching between whorl growing mode and rib growing mode. As a result, we show how the changes in the aperture ontogeny profiles in terms of aperture shape, size and growth trajectory, and the changes in growth rates, are associated with the different shell forms at different parts of the shell ontogeny. These associations suggest plausible constraints that underlie the three different shell ontogeny phases and the two different growth modes. We found that the mechanism behind the heteromorphy is the rotational changes of the animal's body and mantle edge with respect to the previously secreted shell. Overall, we propose that future study should focus on the role of the mantle and the columellar muscular system in the determination of shell form.

Introduction

The physical form of organisms is central to different fields of biology, such as taxonomy, evolutionary biology, ecology and functional biology. Two major themes are the way the organism's form changes as it grows and the way the organism's form changes as it evolves. The formal investigation of growth and form was established by Thompson (1917) in his monumental *On Growth and Form*. In his book, Thompson studied the way organisms achieve their body form during growth, from the viewpoint of the mathematical and physical aspects of the ontogenetic processes. An extensively discussed example of these body forms are molluscan shells.

The molluscan shell, with the exception of those of bivalves, is a single structure that accommodates the animal's soft body. The shell is secreted by the mantle edge, a soft elastic sheet of connective tissue covered by an epithelium. Accretionary growth occurs when the mantle lying inside the shell slightly extends beyond the current aperture and adds a shell increment to the margin. Thus, a shell is essentially a petrified ontogeny of the aperture (i.e. the mantle edge). A large amount of preserved ontogenetic information that can be used for Evo-Devo studies is available from both fossilized and extant shell-bearing species (Urdu et al., 2013). In addition, the molluscan shell's geometrically simple structure, resulting from a straightforward accretionary growth mode makes it more popular than the body forms of other taxa in the study of theoretical morphospace (Dera et al., 2008). However, it remains

challenging to empirically study the actual growth and form of a shell because of differences in the approaches of growth-orientated versus form-orientated studies.

There have been few changes in the study of shell growth rate since Wilbur & Owen (1964). The most commonly used method deals with the quantification of a shell's linear dimensions such as shell length, shell width or number of whorls increment, which are then plotted against time (e.g. Kobayashi & Hadfield, 1996; Sulikowska-Drozd, 2011). Although these measurements are good estimators of the overall growth of the animal's soft body (measured in weight; Oosterhoff, 1977; Chow, 1987; Elkarmi & Ismail, 2007; Silva, Molozzi & Callisto, 2010), they can hardly be linked with the accretionary growth process and spiral geometry of the shell. In addition, shell growth may be episodic because of different seasons, diurnal rhythms, or periods of activity and inactivity (Linsley & Javidpour 1980). Thus, it is not easy to determine the temporal axis for shell ontogeny from a shell alone.

Similarly, studies of the changes in shell form throughout ontogeny tend to be based on the same morphometrics as in growth studies. These morphometrics are measured from the overall shell and are plotted against whorl or rib count, or rotation angle along the shell columella (Kohn & Riggs, 1975; Johnston, Tabachnick & Bookstein, 1991; Checa, 1991). However, these measurements do not provide an accurate record of shell form changes during ontogeny because the overall shell form is an accumulation of previous growth. Moreover, whorl count depends on a single imaginary coiling axis, which is missing in irregularly shaped (heteromorphic) shells.

As a consequence, seldom are growth and form of a shell analysed simultaneously because the reference axes are usually not the same. For instance, a time axis may be used for shell growth, and a whorl count axis for shell form. Furthermore, these shell morphometrics do not closely approach the actual accretionary growth of the aperture in terms of form changes and growth trajectory changes (e.g. Stone 1996; Stone 1997).

Apart from the limitations in methodology, shell growth studies have initially been biased towards aquatic gastropods, and have mostly been conducted in the laboratory. For example, the chapter on molluscan growth in Wilbur and Owen (1964) mentions only a single shelled terrestrial gastropod species was. Although the form and structure of aquatic and terrestrial gastropod shells are very similar, there are fundamental differences in the physiological and physical aspects of shell growth between them (Wagge, 1951; Kado, 1960; Fournié & Chétail, 1984). In recent decades, more studies on terrestrial gastropods have been conducted (e.g. Berry, 1962; Umiński, 1975; Oosterhoff, 1977; Baur, 1984; Ahmed & Raut, 1991; Johnson & Black, 1991; Kobayashi & Hadfield, 1996; Kramarenko & Popov, 1999; de Almeida & de Almeida, 2001a; de Almeida & de Almeida, 2001b; D'Avila & de Almeida, 2005; Bloch & Willig, 2009; Silva et al., 2009; Sulikowska-Drozd, 2011; Kuźnik-Kowalska et al., 2013; Silva et al., 2013). It is worth mentioning that most of these growth experiments used traditional morphometric methods and were conducted in the laboratory (but see Oosterhoff, 1977; Johnson & Black, 1991). Because discrepancies in growth patterns exist

between field and laboratory experiments (Chow, 1987), further growth studies are needed from the natural habitat.

All the species investigated in the above-mentioned studies have shells that grow according to a regular coiling regime and with only simple calcareous sculptures on the shell surface, if any (but see Berry, 1962). For shells with irregular coiling, that is, those that pass through several dissociated growth stages, very little information is available as to how the growth and form changes during those different shell ontogeny phases. To alleviate all these limitations, we investigate the growth and form of a heteromorphic and heavily ornamented tropical land snail species, *Plectostoma concinnum*, in its natural habitat.

We examined two aspects of shell growth and form: 1) the growth and form at three different whorl growing phases of the *Plectostoma concinnum* shell; 2) the switching between whorl growing mode and rib growing mode. First, we obtained a unified accretionary growth reference axis (hereafter termed “ontogeny axis”), namely the total arc length of the shell whorl (see “Definition of ontogeny axis” in Materials and Methods for more details), so that both shell growth and form data can be analysed together. Second, we obtained shell growth rate information that was measured as arc length of ontogeny axis (i.e. whorl length) added per day for live snails of different growth stages. Third, we quantified both the aperture form (size and shape), and the aperture growth trajectory (rotation, curvature and torsion) from a series of apertures (hereafter termed “aperture ontogeny profile”) that could be identified from the shells, by using 3D technology. Fourth, we explored the pattern of switching between whorl growing mode and rib growing mode that determined the number of ribs on the shell (see “organisms” in Materials and Methods). Finally, we examined the associations between the growth and the form of the *Plectostoma concinnum* shell in all three whorl growing phases and both growing modes, from developmental-biological and a theoretical-morphological points of view.

Materials and Methods

Ethics Statement

The permissions for the work in the study sites were given by the Wildlife Department of Sabah (JHL.600-6/1 JLD.6, JHL.6000.6/1/2 JLD.8) and the Economic Planning Unit, Malaysia (UPE: 40/200/19/2524).

Organisms

The tropical terrestrial micromollusc subgenus *Plectostoma* consists of 69 species that are only known from limestone hills of Southeast Asia (Vermeulen, 1994; **Chapter 2**). It is one of the most diverse subgenera in the Gastropoda in terms of shell form. In this study, we selected *Plectostoma concinnum* (Fulton, 1901), an endemic species in northern Borneo. This species is exclusively found in limestone habitat and thus presumably not limited by calcium availability. It occurs in high population densities with several millions of individuals estimated to live on limestone hills of less than 0.5 km² (Schilthuizen et al., 2003).

In this study, we followed the terminology of Vermeulen (1994) in the discussion of the shell form of this species, and we used the term whorl growing mode and rib growing mode in the discussion of two different growth modes. At least in the case of this particular species, we think these two terms are more precise than generic terms such as spiral and radial growth (e.g. Spight & Lyons, 1974; Vermeij, 1980). For the whorl growing mode, three growth phases can be distinguished, namely, spire, constriction and tuba.

As an adult, the species has about 5.5 – 6.5 shell whorls and is about 3 mm in height and 3.5 mm in width. The protoconch is smooth (Fig. 1A). The first 5 or 6 whorls of the teleoconch are regularly coiled (hereafter termed “spire”) while the last half whorl (hereafter termed “tuba”) is detached from the spire (Fig. 1A). The transition from the spire to the tuba is marked by a narrowing of the whorl (hereafter termed “constriction”), where calcareous lamellae are formed inside the aperture (hereafter termed “constriction teeth”) (Figs. 1A, 3E and 3F). The three parts are formed during the whorl growing mode. It has an operculum which rests behind the constriction teeth when the animal’s soft parts withdraw into the shell (hereafter “the animal” refers to the foot, the columellar muscle, and the mantle). Such an extreme morphological transition between spire and tuba is also known in several other extant and fossil mollusk species (e.g. Okamoto, 1988; Savazzi, 1996; Vermeulen, 1994; Clements et al., 2008; Frýda & Ferrová, 2011). The shell growth of this species is definite and the whorl growing mode ends with a "differentiated" peristome.

The shell exhibits regularly spaced projected commarginal ribs. As there is no standardisation in the rib morphology terminology, to avoid confusion, we use the term commarginal ribs (*sensu* Seilacher, 1991) for the type of ribs of *Plectostoma concinnum* because it describes the ribs with reference to ontogeny and form and thus is more accurate than other terminologies (such as “radial ribs” or “growth halt” *sensu* Laxton, 1970). These commarginal ribs are the product of a rib growing mode, which is entered when the animal’s mantle edge expands dramatically and forms an aperture that is much larger than the previous aperture produced in whorl growing mode. After shell deposition stops at this rib growing mode, the subsequent whorl growing mode continues from the aperture that was produced in the previous whorl growing mode. The switching between these two growing modes produces the projected commarginal ribs.

Definition of ontogeny axis

To analyse the growth rate in terms of ontogeny axis growth per day and the form changes in terms of aperture ontogeny profile over time, one needs to extract a set of homologous points in an ontogenetic series that reflect the accretionary spiral growth. These points have to be homologous in a biological sense meaning that the different growth stages of the same individual as well as those of several different individuals are comparable. These landmarks can correspond to the localisation of a specific structure (geometrical homology), to the temporal repetition of the same structure (serial homology) or to the occurrence of a developmental event such as the onset of metamorphosis or senescence (developmental homology) (Johnston, Tabachnick & Bookstein, 1991).

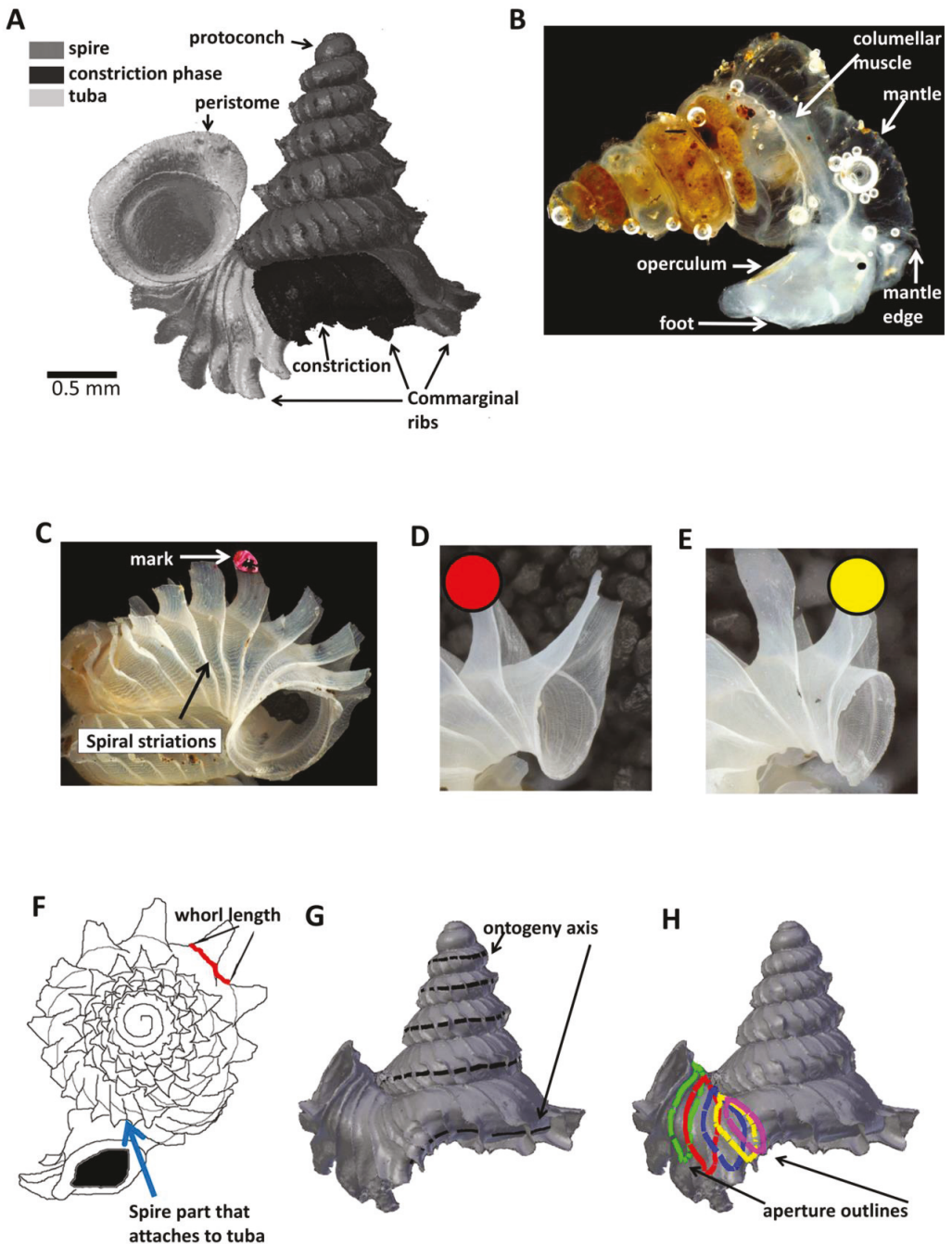


Figure 1. Terminology used for *Plectostoma concinnum* in this study. (A) Terminology used in the descriptions of shell, (B) Terminology used in the descriptions of animal, (C) An example of a shell with a nail polish mark and with the spiral striation on the shell indicated, (D) marking scheme for a shell at rib growing mode, (E) marking scheme for a shell at whorl growing mode, (F) Whorl length measured from a specimen and the spire part that attaches to tuba, (G) Ontogeny axis consists of a concatenation of whorl lengths of a shell, and (H) Tracing aperture outlines from a shell.

In *P. concinnum*, the spiral line at the anterior point of the aperture (Figs. 1C, 1G and 2A) fulfils the conditions for geometrical homology since such striations are produced by particular cells at the mantle edge (Salas et al., 2012). It corresponds to the point of the aperture with maximum growth rate and the curvature is maximal at this point (Figs. 1F, 1G and 2A). The successive protruded radial ribs fulfil the conditions for serial homology, while the protoconch-teleoconch boundary and the spire-tuba constriction define developmentally homologous events. Thus, we used an ontogeny axis, starting from the protoconch-teleoconch boundary (Figs. 1F and G), and obtained by concatenating the arc lengths measured from the points of maximum growth rate between successive protruded radial ribs. Our ontogeny axis is similar to those used by Gould (1969), Vermeij (1980), Savazzi (1985), Savazzi (1990), Checa (1991) and Johnston, Tabachnick & Bookstein (1991). The ontogeny axis of each shell was obtained and the growth and form variables derived below were then plotted and analysed along this ontogeny axis. Different positions along the ontogeny axis represent different growth stages of a shell.

Experimental design and sampling

The growth experiments were carried out at two limestone outcrops in the vicinity of Kampung (Village) Sukau, Lower Kinabatangan Valley in the state of Sabah, Malaysia, between 20th April and 10th May, 2011. These two isolated limestone outcrops, Batu Kampung (5°32'11"N 118°12'47"E) and Batu Pangi (5°31'59"N 118°18'44"E), are located 10 km apart, and thus are under the same climate. Thanks to the rainy season, the microclimates were constant throughout the three weeks of the experiment (Supplemental Information File S1). Six rock surfaces (*ca.* 10 m² each, hereafter referred to as “plots”) with high densities of *Plectostoma concinnum* and similar ecological conditions were selected. The numbers of replicated plots, growth experiment durations and specimens examined are shown in Table 1.

Table 1. Experimental setups and number of specimens used in this study.

Dataset	Hill	Plots	Duration and date of experiment	Number of specimens
1	Kampung	1	2 days (7th May - 9th May 2011)	18
2	Kampung	2	3 days (7th May - 10th May 2011)	11
3	Pangi	1	13 days (20th April - 3th May 2011)	6
4	Pangi	2	13 days (20th April - 3th May 2011)	3
5	Pangi	3	11 days (22th April - 3th May 2011)	12
6	Pangi	4	4days (4th May- 8th May 2011)	15

We used a capture-mark-recapture method (CMR) in the plots. In each one-hour session, we collected between 100 and 200 juveniles of *Plectostoma* at different growth stages. Then, in a field lab, using a dissecting microscope, we marked each shell with a nail polish mark located on either the second most recently grown rib (if the snail was at rib growing mode) (Fig. 1D) or the most recently grown rib (if the snail was at whorl growing mode) (Fig. 1E). We used this marking scheme instead of one in which a mark was placed on the aperture edge, to prevent the nail polish to come in direct contact with the animal mantle. Our nail polish marking technique fulfilled the general requirements for CMR approach (*sensu* Henry & Jarne, 2007). The marks were clearly visible, persisted for at least two months under field

conditions and had no noticeable effect on the mantle edge. All marked individuals were released at their exact point of capture within 24 hours and were recaptured between 2 and 13 days later (see table 1). All recaptured individuals were killed by drying and retained. A total of 97 shells were thus obtained from both study sites, of which 15 had suffered aperture damage and were discarded. All specimens were deposited as voucher samples in the BORNEENSIS collection, Universiti Malaysia Sabah – BOR).

The remaining 82 shells (65 juveniles and 17 fully grown at the time of recapture) were used for the following analyses. For shell growth rate analysis (Part 1), we used the 65 juvenile shells (36 from Batu Pangi; collection sample BOR 5653 and 29 from Batu Kampung; collection sample BOR 5654). For the aperture profile analysis (Part 2), we quantified (a) aperture shape and size for five representative shells (out of the 65 juvenile shells) at different growth stages; and (b) growth trajectory of a fully grown shell (out of the 17 adult shells). For the analysis of whorl and rib growing mode (Part 3), we examined (a) the number of switches between the two growing modes in the 17 fully grown shells that collected from the same location (collection sample BOR 5652); and (b) the pattern of whorl spacings between two rib growing modes of the 35 shells (out of the 65 juvenile shells) that had grown beyond the constriction.

Part 1 – Shell whorl arc length growth rate along the shell ontogeny.

Each of the 65 juvenile shells was photographed (with a Leica DFC495 attached to a Leica M205C microscope). Photographs were taken in apical view (Fig. 1F and Supplemental Information File S2). For those specimens that grew up to the tuba stage, we aligned the tuba with a plane and we took additional photographs (Supplemental Information File S2). The arc length at the point of maximum growth rate was calculated using the program Leica Application Suite V3.7.0. Although the arc length is measured from two-dimensional images (Fig. 1F), it is a good proxy for the three-dimensional arc length (Fig. 1G and Supplemental Information File S3: $r = 0.82$, $n = 251$ (3 shells), $p = 0.000$). We thus obtained 5,475 arc lengths measured between successive ribs and pooled these data (Supplemental Information File S4). The arc length of the ontogeny axis for each of the 65 shells was calculated as the sum of all the arc lengths between successive ribs of each shell.

Based on the nail polish mark on the shell, we measured the arc length before and after the growth experiment. Then, we calculated growth rate as the whorl arc length (i.e. ontogeny axis) added over the duration of the experiment (i.e., mm day^{-1}). We tested for the correlation between the measured growth rates and the position of the specimen on the ontogeny axis prior to the growth experiment. The analyses were done separately on the two growth phases of *Plectostoma concinnum*, namely, spire and tuba. Spearman correlation was used since the data were not normally distributed.

Part 2 – Aperture ontogeny profile changes between spire growth phase and tuba growth phase.

In this part, we examined the animal's orientation and aperture form changes along the ontogeny axis. First (Part 2a), we obtained aperture forms by quantifying the traced aperture

on 3D shell models. Second (Part 2b), we quantified aperture growth trajectory changes by examining the animal orientation with respect to its shell and by quantifying the spiral geometry of the ontogeny axis in terms of curvature and torsion estimators.

We used microcomputed X-ray tomography to obtain 3D models of the various growth stages of *P. concinnum* (n=6). Five of these 3D models (immature shells) were used for aperture outline analysis while one 3D model of an adult shell was used for animal rotation analysis (see below). The microcomputed tomography used a high-resolution micro-CT scanner (SkyScan, model 1172, Aartselaar, Belgium). The scan conditions were as follows: voltage – 100kV; pixel – 1336 rows X 2000 columns; camera binning – 2 X 2; image pixel size – 3.42 μ m; rotation step – 0.4°; and rotation – 360°. Next, the volume reconstruction on the acquired images was performed with the manufacturer’s software NRecon ver. 1.6.6.0 (SkyScan). The images were aligned to the reference scan and reconstruction was done with the following settings: beam hardening correction – 100%; reconstruction angular range – 360°; image conversion (dynamic range) – ca. 0.12 and ca. 20.0; and result file type – BMP. Finally, 3D models were created from the reconstruction images with the manufacturer’s software CT Analyser ver. 1.12.0.0 (SkyScan) with the following settings: binary image index – 1 to 255; and saved as digital polygon mesh objects (*.ply format). The 3D models were then simplified by quadric edge collapse decimation to ca. 30,000 faces, with a method implemented in MeshLab v1.3.0 (Cignoni, Corsini & Ranzuglia, 2008). The subsequent analyses for the digital 3D shell models were done in 3D modelling open source software – Blender ver. 2.63 (Blender Foundation, www.blender.org).

Part 2 (a) Aperture form changes between spire growth phase and tuba growth phase.

The acquisition of aperture outlines and their trajectories was done in Blender software with its embedded object-oriented programming language Python. We wrote custom Python scripts to extract the outline points’ coordinates for shape analysis (Supplemental Information File S5). We used the “grease Pencil” tool of Blender to trace the aperture and ontogeny axis outlines on the five immature shell 3D models (Figs. 1G and H). Then, we converted these traced outlines into Bezier curves, where the outlines were represented by a series of points with three-dimensional Cartesian coordinates. We obtained outline data of five 3D shell models with a total of 33 apertures (Supplemental Information File S6), which were then analysed together with their homologous ontogeny axis.

We obtained the aperture outline perimeter by summing the distances between the successive points of each aperture outline. Before that, we smoothed each of the Bezier curve outlines by a three-dimensional Elliptic Fourier Analysis (hereafter termed “3D EFA”; Kuhl & Giardina, 1982; Godefroy et al., 2012) to minimize the possible noise coming from the digitalization process. We ran the 3D EFA with the following parameterization: number of harmonics = 5, starting point = anterior point, and outline orientation = clockwise. We used five harmonics because they were sufficient to reliably describe the aperture outlines (Supplemental information File S7). Next, we reverted 3D EFA function so that each outline was reconstructed from the same set of five harmonics and by using 100 sample points along the outline. Finally, we extracted the aperture perimeters from the 100 points of each outline.

We obtained principal component analysis (PCA) scores from normalized coefficients of 3D EFA for each of the 33 aperture outlines (hereafter termed “shape scores”). The coefficients of the 3D EFA harmonics were normalized according to Godefroy et al. (2012) so that they were invariant to size and rotation. After normalization, all of the 30 normalized Fourier coefficients for each of the 33 aperture outlines were analysed by PCA in R statistical package 2.15.1 (R Core Team, 2012). R scripts are in Supplemental Information File S4.

The aperture perimeter and shape scores of each aperture were examined together along the ontogeny axis. In addition, a linear regression was performed on the spire aperture perimeter changes along the ontogeny axis in R statistical package 2.15.1 (R Core Team, 2012).

Part 2 (b) Aperture growth trajectory changes between spire growth phase and tuba growth phase.

In the plots at Batu Kampung, we collected additional specimens at different growth stages to examine the growth trajectory of the aperture and the orientation of the living animal with respect to its shell. The living individuals were carefully picked up with a pair of soft forceps while active, were immediately frozen with Freeze spray (KÄLTE, Art. Nr. 20.844.6.09.12.01) and preserved in 70% ethanol. The body rotation of the animals of different shell growth stages was examined with scanning electron microscopy (SEM).

We found that the highest projected point of the commarginal rib corresponds to the anteroposterior axis of the animal. In addition, the changes in the orientation of successive segments correspond to the changes in orientation of the animal as evidenced by the homologous anterior landmark of the aperture (Figs. 2B, 3A, 3B and 3C). Hence, the growth trajectory changes in terms of animal rotation can be inferred directly from the shell. We therefore quantified the orientation changes of the animal along the shell ontogeny from a 3D model of an adult shell with Blender. We restrict this analysis to the ontogeny corresponding to the 1.5 whorls before the constriction up to maturity where the most drastic changes in shell coiling direction occur (Supplemental Information File S8).

We obtained the ontogeny axis for the shell and then separated the digital 3D shell into segments corresponding to successive commarginal ribs (Figs. 2A and 2B, Supplemental Information File S8). We obtained changes in the rotation between two consecutive segments (hereafter termed: “NEW” and “OLD” segments). The changes in animal orientations were inferred from these two segments with respect to the anatomical directions of the animal. First, we aligned the anteroposterior axis of the NEW shell segment with the x-axis of the global 3D Cartesian system (Fig. 2B). Second, we aligned the anterior point of the OLD segment to the anterior point of the NEW segment (Fig. 2C). Third, we rotated the OLD segment along the x, y and z axes until it was aligned with the NEW segment (Figs. 2D, 2E and 2F). Finally, the rotation changes (in angles) were plotted along the ontogeny axis.

The rotations around the three animal anatomical directions were interpreted as following. First, rotation around x-axis corresponds to the aperture “inclination” with respect to the

previous aperture (Fig. 2D). It corresponds to the direction where the animal tilts to right or left. Second, the rotation around y-axis corresponds to the rotation of the dorsoventral axis (i.e. shell growth direction). Third, the rotation around z-axis corresponds to the rotation of the anteroposterior axis (rotation of the aperture plane around its centroid). When the animal is viewed in dorsal view, we describe this rotation as either clockwise or anticlockwise. From our observation (see above), it seems the most important changes in animal orientation at different growth phases are the rotations around the x-axis and the z-axis (Fig. 2B, 3A, 3B and 3C)

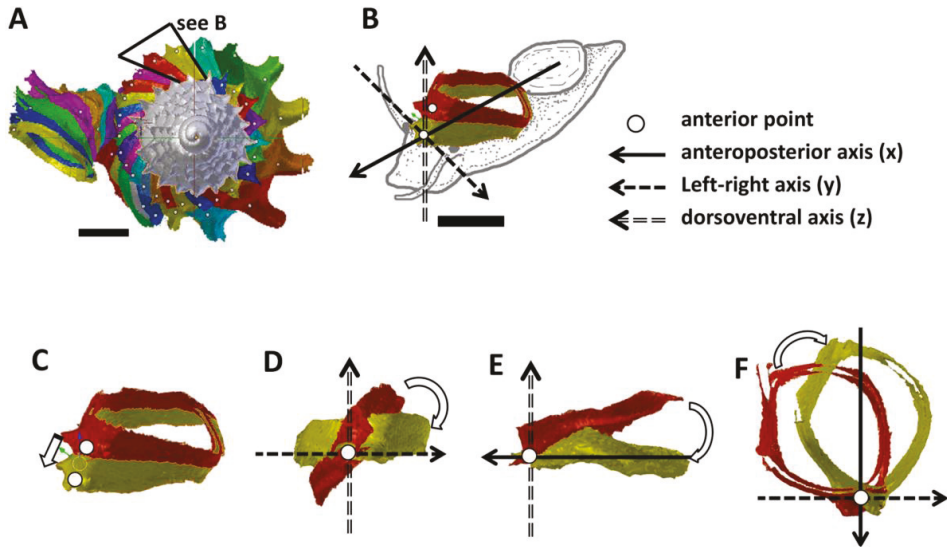


Figure 2. Steps in the analysis of aperture (i.e. animal) orientation changes. A) Segmentation: each segment consists of whorl and rib part. For each analysis, two segments were included which represent the two animal orientations, namely, the newly formed segment (NEW – in yellow) and the previously formed segment (OLD – in red segment), (B) Reset the NEW segment orientation according to the animal axes, (C) Translation: move the OLD segment to NEW segment, so that the anterior points of the two segments were aligned, (D) Rotation of OLD segment around x-axis corresponding animal left or right tilting from animal's anterior view, (E) Rotation of OLD segment around y-axis corresponding to rotation of the dorsoventral axis (shell growth direction), and (F) Rotation of OLD segment around z-axis corresponding to rotation of the animal clockwise or anticlockwise rotation from animal's dorsal view. Scale bar = 0.5 mm.

We are aware that the discrete rotation analysis between shell segments may not realistically reflect the continuous changes of the growth trajectory. Thus, we estimated curvature and torsion, two parameters that are convenient to describe a 3D spiral (Okamoto, 1988; Harary and Tal, 2011). These were estimated from the same adult shell as above (Supplemental Information File S9). The curvature (κ) and torsion (τ) were estimated from each sample point along the ontogeny axis by a weighted least-squares fitting and local arc length approximation (Lewiner et al., 2005). The calculation was done by custom written Python scripts, which were run in the Blender environment (Supplemental Information File S5). The estimation was done with 100 points on the left and right

sides for each sample point. The value of curvature is a positive value; the ontogeny axis is a straight line (i.e. shell is an orthocone) when $\text{Kappa} = 0$; and the larger the curvature, the smaller the radius of curvature ($1/\text{Kappa}$). The torsion Tau estimates the deviation of the curve from a plane - the zero value meaning that the shell is planispiral. In addition, a negative/positive torsion value corresponds to a left-handed/right-handed coiling respectively.

Part 3 – Switching between whorl growing mode and rib growing mode; frequency and trend.

We examined the variation of the number of ribs, which indicates the number of switches between the two growing modes. Then we compared the switching patterns among shells varying in rib number.

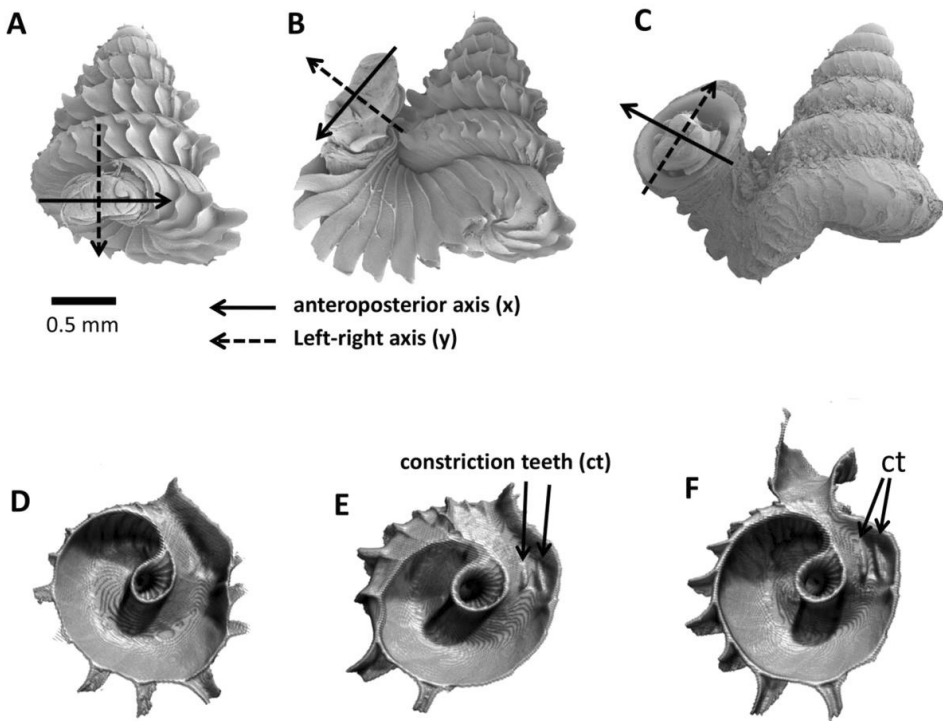


Figure 3. Animal orientations and formation of constriction teeth of *Plectostoma concinnum* at different growth phases. (A) – (C) Orientation of animal with respect to shell at spire phase, tuba phase, and adult, (D) Constriction teeth begin to form inside the shell at the end of spire growth, (E) – (F) Constriction teeth become more prominent during the tuba growth.

Part 3 (a) Variation of total number of ribs between shells.

The numbers of ribs were counted on the spire and tuba parts of each of the 17 adult shells which had completed their shell growth under similar ecological conditions in our field experiment. Because the number of ribs on the spire correlated with the number of ribs on the tuba (see Results), in a subsequent analysis, we counted the number of ribs and arc length of the ontogeny axis on the fully grown spire of 35 juvenile shells. We tested if there is a

correlation between the total number of ribs and the total ontogeny axis length. As all data were normally distributed, we used Pearson correlation in R 2.15.1 (R Core Team, 2012); R scripts may be found in Supplemental Information File S4.

Part 3 (b) Switching trends between the whorl growing mode and the rib growing mode.

We plotted 3,263 arc lengths (both spire and tuba) between successive ribs of the 35 shells along the same ontogeny axis.

Results

Part 1 – Shell whorl arc length growth rate along the shell ontogeny.

The growth rates are measured in mm/day along the arc length travelled by the point of maximal growth rate during ontogeny (n=65, Supporting Information File S4). The absolute shell whorl arc lengths added to the shells during the growth experiments are found in Supporting Information S10.

Figure 4 shows the growth rate variations along the ontogeny axis for the spire and tuba growth phases of 65 shells. For the growth patterns of the spire, the growth rate is positively correlated with the ontogeny axis ($r = 0.45$, $n=30$, $p=0.01$). On the other hand, after the constriction, the growth rate is negatively correlated the ontogeny axis ($r = -0.38$, $n=35$, $p=0.02$). These data demonstrate that *O. concinnum* follows a S-shaped growth curve (with regard to time), with the maximum growth rate occurring during the transitional phase (inflexion point).

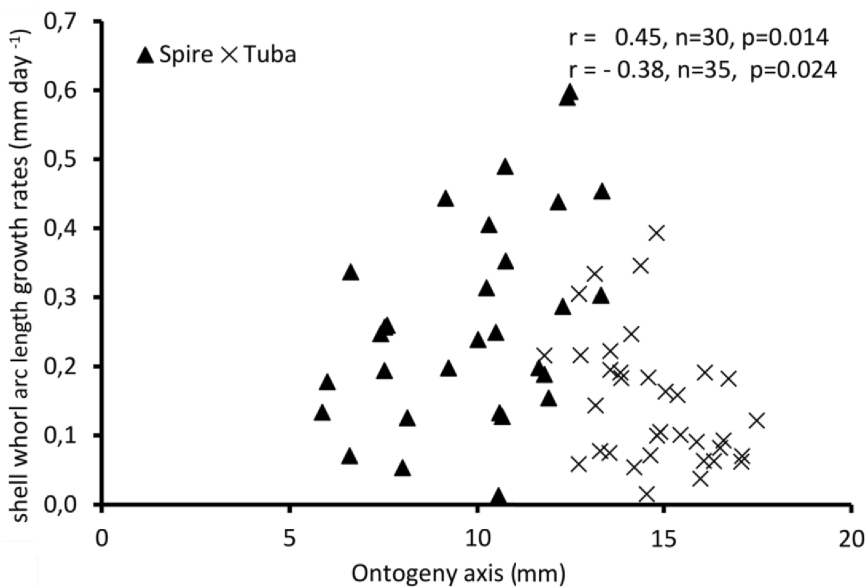


Figure 4. Growth of shell whorl arc length along the shell ontogeny for 65 specimens. Growth rate increases along the shell ontogeny for the spire part but decreases in the tuba part of the shell.

Part 2 – Aperture ontogeny profile changes between spire growth phase and tuba growth phase.

Part 2 (a) Aperture form changes between spire growth phase and tuba growth phase.

Figure 5A shows the changes of aperture perimeter from around 5 mm until the end of the ontogeny axis. The aperture perimeter changes along the ontogeny of the five different specimens share a common trend. The perimeter of the aperture increases linearly, in a constant rate ($\beta = 0.166$), between 5 mm and *ca.* 11 mm at the ontogeny axis (linear regression model: (aperture perimeter) = 0.166 (position of ontogeny axis) + 0.457, $R^2 = 0.97$, $F = 591.4$, $df = 1, 20$, $p=0.000$). Then, the aperture size decreases during the constriction part of the ontogeny before the size increases again during the tuba part of the ontogeny.

For the aperture shape analysis, the PCA reveals that the first three components accounted for 53.8%, 14.2%, and 9.7% of the total shape variation of all five sets of harmonics (Supplemental information File S11). The correlation analysis reveals that the first component is significantly correlated with 15 out of the 30 normalized Fourier coefficients, especially the Fourier coefficients of the first harmonics (Supplemental information File S11). Thus, we retained the PCA first component's scores as shape descriptor of aperture (due to the nature of the EFA, the first harmonic contains a large part of the variation and most of the shape information ; Kuhl and Giardina, 1982).

Figure 5B shows the changes of aperture shape along the ontogeny axis. During the spire part of the ontogeny, the aperture has a diamond shape with a round corner. Its perimeter is slightly convex at the right anterior, left anterior and posterior sides, but slightly concave at the right posterior side. Approaching the constriction part of the ontogeny, the diamond-shaped aperture becomes elongated along the anteroposterior axis with slightly rounded corners. At the tuba part of the ontogeny, the aperture has an ovate shape that is symmetrical along the anteroposterior axis, acute at the anterior and wide at the posterior.

Part 2 (b) – Aperture growth trajectory changes between spire growth phase and tuba growth phase.

Figure 6 shows the rotational changes of each new segment with respect to the previous segment. Rotation around the x-axis at the constriction and part of the last whorl shows that the changes in the animal's orientation are in the opposite direction compared to most of the spire and tuba parts of the ontogeny. There is no change of rotation direction around the y-axis as the shell follows a spiral growth. The magnitude of rotation in the y-axis is related to the whorl length between two ribs (*confer* Fig. 8). Rotations around the z-axis reveal that the rotational changes between two ribs for the spire and the tuba part of the ontogeny are in opposite direction.

Figure 7 shows how the curvature and torsion values change along the ontogeny axis. The curvature value decreases rather constantly from *ca.* 3 to *ca.* 1 with small fluctuations along the spire part of the ontogeny. However, for the constriction to the tuba part of the ontogeny, the curvature value fluctuates between 0.9 and 1.3. Torsion values along the spire decrease

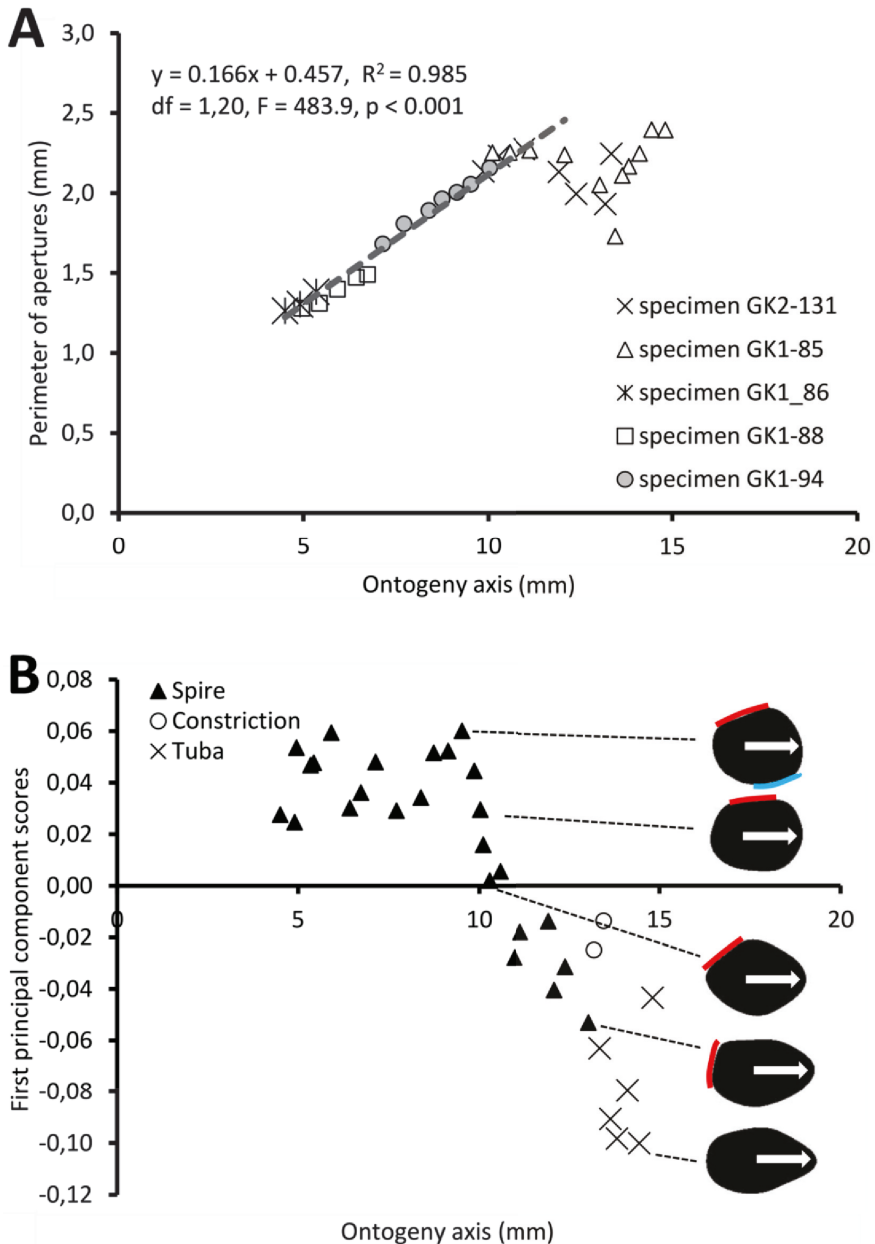


Figure 5. Aperture form changes along shell ontogeny axis. (A) The apertures perimeter changes in the five specimens show unified patterns along ontogeny axis, (B) Changes of aperture shape (summarized in PC 1 scores, as measured from five specimens) along the ontogeny axis. Arrow points to the anterior direction of apertures. The part of the aperture that attaches to previous whorl (red line) and to subsequent whorl (blue line).

gradually from 0.9 to 0.1. From the constriction onwards, however, torsion fluctuates wildly, becoming strongly negative before returning to positive values.

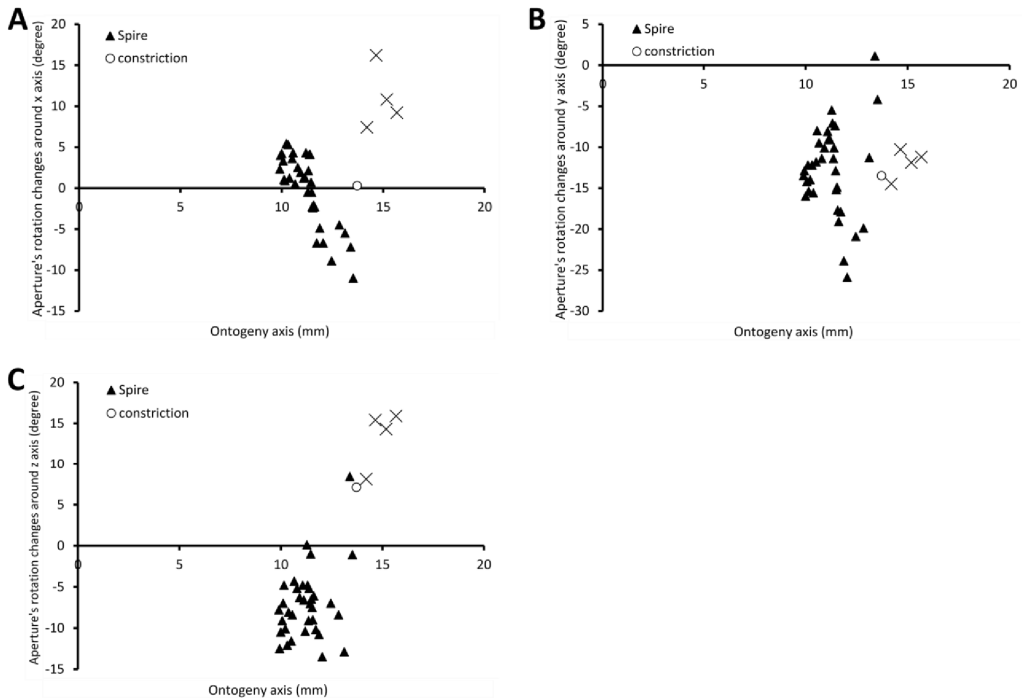


Figure 6. Changes of an animal's orientation in terms of standardised rotation in angle during the growth between two consecutive segments along the ontogeny axis. (A) Rotational changes around x-axis—animal tilts to either left (negative angles) or right (positive angles), (B) Rotational changes around y-axis—shell growth direction, and (C) Rotational changes around z-axis—animal rotates either clockwise (negative angles) or anticlockwise (positive angles).

Part 3 – Switching between whorl growing mode and rib growing mode; frequency and trend.

Part 3 (a) Variation of total number of ribs between shells.

The arc lengths measured between two consecutive spines in 35 individuals of *Plectostoma concinnum* were pooled together (3263 arc lengths in total, raw data in Supporting Information). There is no significant correlation between the number of spines and the total arc length (Pearson correlation, $r = -0.22$, $n = 35$, $p = 0.2$), highlighting that the number of spines varies extensively among individuals exhibiting a similar total arc length. However, there is a significant correlation between the number of spines before the constriction and the number of spines after the constriction (Pearson correlation, $r = 0.55$, $n = 17$, $p = 0.02$). This means that there is still a consistent ontogenetic pattern in this set of pooled data: the individual ontogenies do not vary to the extent that the spiral and tuba phase are mixed together in the pooled data.

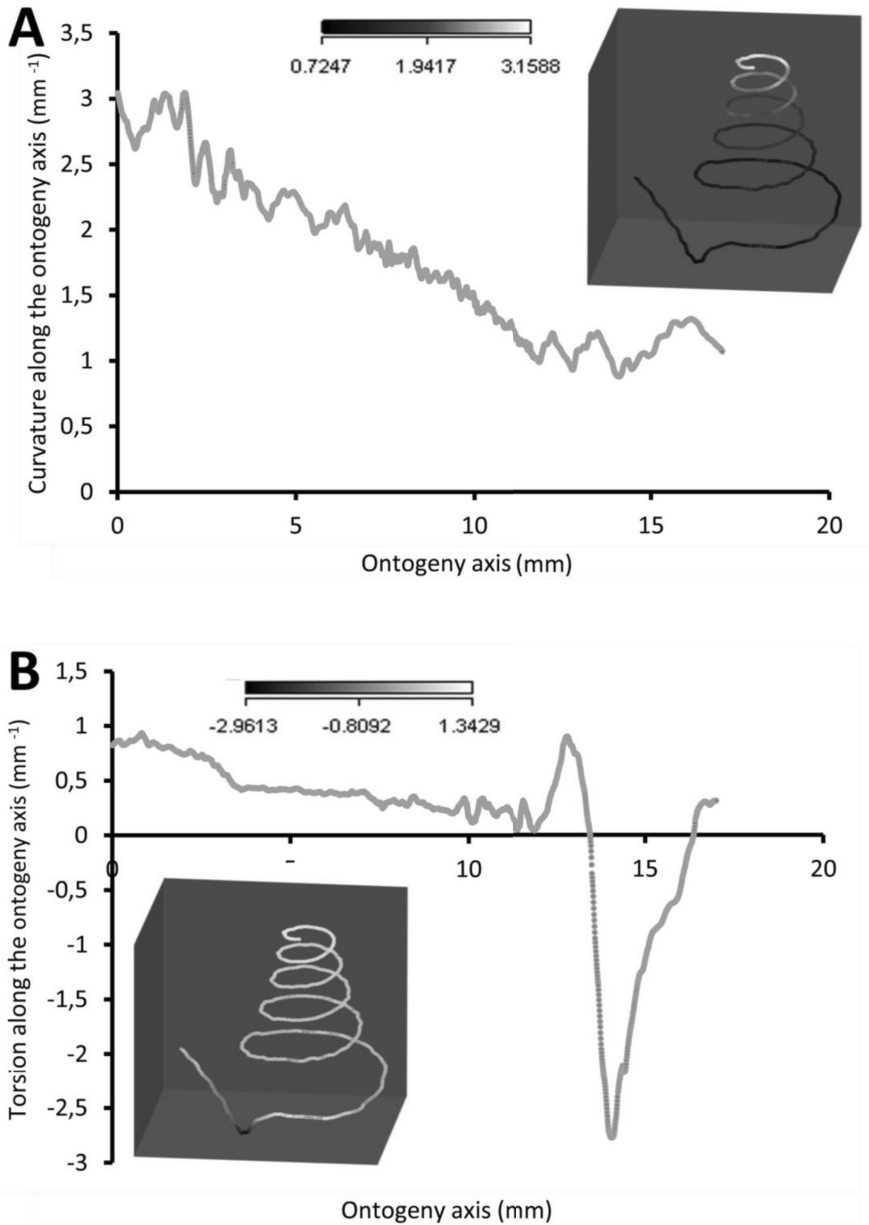


Figure 7. Curvature and torsion of a shell along the ontogeny axis. (A) curvature, inset shows curvature changes along the growth trajectory, (B) torsion, inset shows torsion changes along growth trajectory.

Part 3 (b) Switching trends between the whorl growing mode and the rib growing mode.

Figure 8 shows that the spacing between successive ribs increases constantly from right after the protoconch (i.e. at position 0) to *ca.* 8 millimetres along the ontogeny axis. The spacing between ribs then decreases until *ca.* 10 millimetres on the ontogeny axis (Figs. 1F and 8). Then, this spacing increases from *ca.* 10 to *ca.* 13 millimetres on the ontogeny axis, when the

shell is about to form the constriction part. The spacing then decreases during the transitional constriction phase (from *ca.* 13 to *ca.* 14 mm on the ontogeny axis) and remains approximately constant during the tuba phase (from *ca.* 14 mm to the end of the ontogeny axis). Shells with different numbers of ribs show the same trend but of a different magnitude – the average rib spacing of densely ribbed shells being shorter than that of sparsely ribbed shells at the same growth stage.

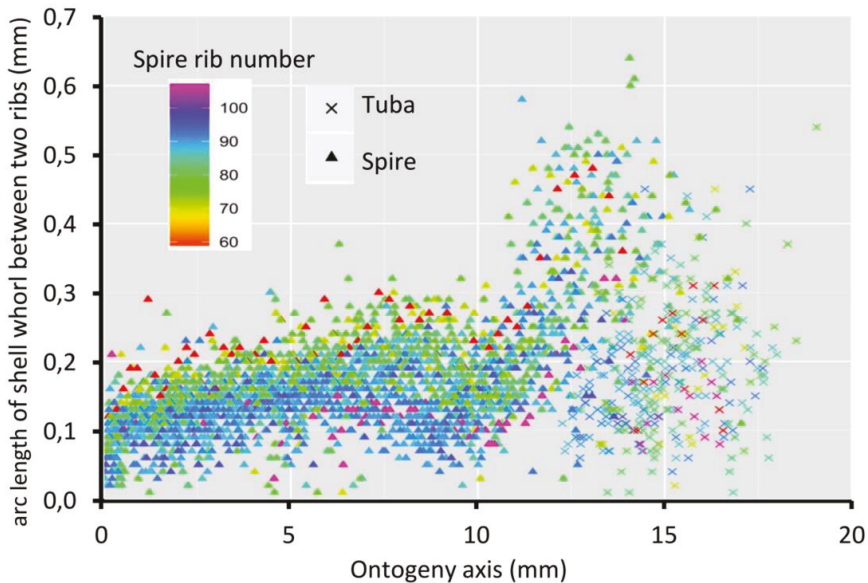


Figure 8. Trends in whorl arc length between two commarginal ribs in 35 shells which vary in the number of ribs on the spire along the ontogeny axis.

Discussion

Growth and form of whorl growing mode in terms of aperture form and growth rate.

The overall shell ontogeny of *Plectostoma concinnum* does not comply at all with the ideal shell growth model in which the growth parameters remain constant throughout the ontogeny. Although such ideal shell growth has been an essential part in the development of gastropod theoretical morphology (Moseley, 1838; Thompson, 1917; Raup, 1966), the shells of most gastropods do deviate to some extent (Raup, 1966; Gould, 1968; Vermeij, 1980; Urdy et al., 2010). The shell ontogeny of *P. concinnum* begins with a regular growth phase that approximates a dextral isometric logarithmic spiral (spire phase, between 0 and *ca.* 13 mm on the ontogeny axis), followed by a more variable transitional growth phase (constriction phase, *ca.* 13-*ca.* 14 mm of ontogeny axis), which gives way to an open-coiling growth phase (tuba phase, from *ca.* 14 mm to the end of the ontogeny axis). Thus, it provides a unique opportunity for us to investigate how shell form changes in relation to the growth rate.

Spire – The spire is dextral, has a regular growth trajectory and form, and thus its curvature and torsion estimators obey the 3D logarithmic spiral geometry with minor deviation (Fig. 7). During the growth of the spire, the aperture ontogeny profiles either remain the same or change in a constant manner. The aperture remains of almost the same shape (Fig. 5B), the aperture perimeter increases linearly and constantly, the animal (i.e. the mantle) always rotates clockwise (Fig. 6C) from the animal's dorsal view (e.g. Fig. 2B and 2F), and the aperture inclination declines (Fig. 6A). These variables alter when the spire phase changes over to the constriction phase.

Constriction – The constriction part of the ontogeny breaks the simple logarithmic spiral growth rule. Every aspect of the aperture ontogeny profiles changes: the aperture shape differs from the spire aperture (Fig. 5B); the aperture perimeter drops, the animal (and its mantle edge) begin to rotate anticlockwise (Fig. 6C) from animal's dorsal view (e.g. Fig. 2B and 2F), and the aperture inclination increases (Fig. 6A).

Our data show that changes in the animal's orientation are responsible for the break in the preceding growth rule (Figs. 6A, C and 7). It has been shown theoretically that the rotation of the animal within the shell – which is equivalent to changing the pattern of growth rates around the aperture – is the cause behind the drastic changes in the coiling pattern that are observed in heteromorph ammonites (Okamoto, 1988) and cemented gastropods exhibiting distorted coiling (Vermeij, 1993; Rice, 1998). Our data support this hypothesis, and suggest that the deviation is caused by the continuous rotation of the mantle edge in opposite direction to that of the spire part, during the accretionary growth process at the aperture.

Several studies have pointed out a general correspondence between the life position and the shell morphology in recent gastropods (Linsley, 1977; Linsley et al., 1978; Morita, 1991a; Morita, 1991b; Morita, 1993; Morita, 2003; Checa, Jiménez- Jiménez, & Rivas, 1998; Vermeij, 2002), indicating that the life position of gastropods is almost equal to the gravitationally stable position of their empty shells. These studies argued that the direction and degree of coiling, as well as aperture shape are at least partly determined by the columellar muscle, the animal's living position (at the time of shell secretion), and the previous whorl ('road-holding', Hutchinson, 1989; Checa, Jiménez- Jiménez, & Rivas, 1998). Although some details are available regarding the structure and retraction function of the columellar muscle (Brown & Trueman, 1982; Kier, 1988; Frescura & Hodson, 1992; Thompson, Lowe & Kier, 1998; Suvorov, 2002), how the columellar muscle may act to affect shell morphogenesis is unknown.

In addition to the aperture shape and growth trajectory changes at the constriction phase, the aperture size also decreases along the shell ontogeny before increasing again when approaching the tuba phase. This process produces a narrower shell whorl, and is unlikely to be directly involved in the aperture rotation. Yet the constricted whorl might play a key role in the ontogeny of the tuba part of shell. At the beginning of the tuba phase, several constriction teeth are formed inside the constricted whorl. These constriction teeth are associated with the columellar muscle and thus could play a role in controlling the animal's

orientation with respect to the shell (Figs. 1B, 3D, 3E and 3F). For example, the columellar muscle could coil around the shell columella during the spire phase whereas the columellar muscle has to extend far from the shell columella during tuba phase. Hence, the constriction teeth could serve as a holdfast for the columellar muscle and prevent it from shifting position while under tension (e.g. Signor & Kat, 1984; Price, 2003). This kind of internal structure is also common in other heteromorphic gastropods (Savazzi, 1996). So, we support Suvorov's view that the constriction teeth could be important for an effective management of shell orientation (Suvorov, 1993; Suvorov, 1999a; Suvorov, 1999b; Suvorov, 2002). The constriction phase might therefore pave the way for the later tuba phase in forming a detached whorl.

Tuba – Two significant aspects of the tuba part of the shell ontogeny are its anticlockwise rotation on the growth trajectory (Fig. 6C) and its detachment from the spire of the shell. At this phase, the aperture shape changes rapidly (Fig. 5B) and the aperture perimeter increases again with a trend similar to the spire (Fig. 5A). Here, we can show that the transition from a tightly-coiled and almost isometric dextral shell to an open-coiled tube only requires a relatively small and continuous change in the main growth direction. This is achieved by the continuous rotation of the animal within the shell, in opposite direction as compared to the spire phase, possibly controlled by the columellar muscle as discussed above.

The continuous rotation of the aperture causes the later part of the tuba to detach from the spire. In the spire part, only a thin layer of shell is deposited at the right lateral part of the aperture along the surface of the previous whorl, causing fusion with the previous whorl. In contrast, during the tuba part of the ontogeny where the whorls are detached, thicker shell layers are deposited all around the aperture.

The shell whorl overlapping at the spire part is a more economical growth strategy than detached whorls (Heath, 1985; Stone, 1999; Stone, 2004). We suggest that the differences in growth rate between spire and tuba might result from the detached growth of the tuba. As the aperture size of the tuba and the later part of the spire is similar, and calcium is not a limiting resource for this limestone-dwelling species, the formation of the detached whorl may slow down because more time is required for its formation compared to the spire. However, as growth is determinate in this species, we expect growth to slow anyway at the onset of maturity with the development of the reproductive organs (e.g. Terhivuo, 1978; Lazaridou-Dimitriadou, 1995).

Finally, the change from tight to open coiling in *Plectostoma concinnum* could provide an opportunity to revisit theoretical models on whorl overlap – the road-holding model (Hutchinson, 1989) and its mechanical effect on aperture shape (Morita, 1991a, b, 1993, 2003). In his morphogenetic model, Morita (1991a) defines the mantle as a whole as a hydroskeleton which is usually in a state of expansion resulting from internal haemolymph pressure. Consequently, the mantle is simulated as a double elastic membrane connected by internal springs. Its physical state is supposed to be in balance between its internal stress and

the forces acting on it, such as the pressure of the haemolymph, the pressure induced by the foot/columnar muscle and the boundary of the shell. The deformation of the mantle is then deduced from its stress field using a finite element analysis. Morita investigates the effect of a zone where the mantle cannot deform - presumably because of the foot/muscle/soft parts pressing on the mantle edge. He shows that initially circular walls change into elliptically elongated ones with pressure rising. In other words, the existence of a fixed zone - whether that zone is large or small in size - breaks initial symmetry in the specific manner: the direction of elongation is perpendicular to the fixed zone. On the contrary, all tube shapes tend to converge to circular outlines when no fixed zone exists. Morita (1991b, 1993, 2003) argues that this fixed zone represents whorl overlap and may explain why most open coiling or minimally overlapping gastropods have circular apertures. On the other hand, outer apertural lips accompanied by a distinct whorl overlap zone are either extended perpendicularly to the overlap zone or are abapically inflated.

In *Plectostoma concinnum*, there are extensive shape differences between the spire and the tuba apertures- notably the part of the aperture which was previously in contact with the previous whorl exhibits smoothed corners in the open-coiling phase and is more symmetrical than before (Fig. 5B). However, the aperture shape of the tuba is not tending towards a circle but has an ovate shape that is elongated along the anteroposterior axis where the ribs are forming. Morita did not address the case of ornamented specimens, so our data is not well suited to test the predictions of this model in its current state.

Number of times and trend in the switching between whorl growing mode and rib growing mode.

The total number of ribs (i.e. number of switches between whorl growing and rib growing mode) can vary substantially between individuals even if they are of similar shell size (i.e. similar ontogeny axis length). The number of switches between these two growing modes also does not affect the final ontogeny axis length. However, we could not determine whether a shell with dense ribs would need more time to become fully grown.

Despite differences in rib number, the trends in rib spacing patterns are similar. At the spire part, the spacing between ribs initially increases and then decreases towards where the tuba starts to detach from the spire (ca. 9 – 10 mm along the ontogeny axis, Fig. 1G). After that, the rib spacing increases again and reaches its maximum at the constriction (ca. 13 – 14 mm along the ontogeny axis).

A previous growth study on *Plectostoma retrovertens* showed that each rib represents a day of growth (Berry, 1962). However, *Plectostoma concinnum* ribs are heavier than those of *Plectostoma retrovertens*, and its commarginal ribs do not represent daily growth stages. Furthermore, our specimens were in a cohort and collected over the same period (i.e. under similar weather condition), thus the rib spacing pattern is unlikely to be caused by environmental factors.

When the trend between rib spacing (Fig. 8), aperture perimeters (Fig. 5A) and growth rates (Fig. 4) are examined closely, interesting relationships among these shell parameters emerge. First, the spacing between ribs is the largest, the aperture perimeter is the smallest, and the growth rate is the highest at the constriction phase. Second, the rib spacing increases together with the increase of the growth rate along the spire ontogeny, while rib spacing decreases with decreasing growth rates in the tuba part. This suggests there might be a possible positive association between growth rate and rib spacing, and hence rib density. Further studies are needed to investigate whether this association is incidental or not. With limited data, we cannot decipher the ontogenetic mechanisms that produce the ribs. Although several theoretical mechanisms have been proposed (e.g. Hammer, 2000; Moulton, Goriely & Chirat, 2012; Chirat, Moulton & Goriely, 2013), the actual biological processes responsible for the growth of commarginal ribs remain poorly understood. Hence, we suggest that future studies examine the growth rates (shell deposition rate) in relation to ornamental patterns to improve our understanding of the possible relationship between rib frequency and growth rates.

Conclusion

In this study, we have developed an approach which can be used to extract aperture morphological changes along the ontogeny from a shell and we have found a way to analyse the growth and form parameters simultaneously. By analysing growth and form in this heteromorphic shell, we have shown the associations between aperture ontogeny profiles and growth rate in the determination of final shell form. Our aperture ontogeny profile analysis of the shell and observations on living specimens provide for the first time direct evidence for the mechanism behind the heteromorphy: the rotational changes of animal and mantle edge during the shell ontogeny. Overall, we have also highlighted that there is a need to improve our understanding of the developmental biology of snails, especially with reference to the mantle and columellar muscular systems and their potential relationship to shell morphogenesis.

Although our study provides little direct information on the developmental and genetic factors that govern the shell growth and form, it already highlights some plausible constraints – related to the columellar muscle and living position - underlying the three shell ontogeny phases and two different growth modes of this species. As these three phases are known to occur in all of the species in this genus, including those with more regularly coiled shells, our results may be generalised further in the future. Our study sets the stage for future studies using mollusc species in general to address issues concerning the ecology, the evolution and the development of mollusc using a mixture of insights coming from aperture ontogeny profiles obtained by a 3D morphometric approach.

Acknowledgement

We wish to thank Asni and Harizah's family from Kampung Sukau for logistic support in the field. We are indebted to Willem Renema (Naturalis) for help in CT-scanning. We are also grateful to Reuben Clements and Heike Kappes for comments on the early version of this paper. This work was carried out under the research permit from Economic Planning Unit, Malaysia (UPE: 40/200/19/2524) and permission from the Wildlife Department and the Forestry Department of Sabah, both to LTS. LTS received support from Ministry of Higher Education, Malaysia and Universiti Malaysia Sabah. ACMK received Outbound Study Grant, LUSTRA, and Leids Internationaal Studie Fonds, all from Leiden University. SU was supported by the Swiss National Science Foundation (200021_124784/1 and PA00P3-136478). This project is funded by Netherlands Organisation for Scientific Research (NWO, ALW 819.01.012).

Supplemental Information

(<http://dx.doi.org/10.6084/m9.figshare.960018>)

Supplemental Information File S1. Microclimatic variation for Pangli plots.

Supplemental Information File S2. Raw image of 65 measured shells for Part 1 and Part 3(b).

Supplemental Information File S3. Correlation between 2D and 3D arc length measurement of three specimens.

Supplemental Information File S4. Raw data for analysis in Parts 1, 2 and 3, and the R scripts.

Supplemental Information File S5. Python scripts for 3D aperture morphometrics and growth trajectory analysis.

Supplemental Information File S6. Digitalised aperture outlines (n=33) of 5 specimens used in Part 2(a).

Supplemental information File S7. Comparison between raw digitised and Elliptical Fourier reconstructed aperture outlines.

Supplemental Information File S8. Data of rotation analysis in Blender format for Part 2(b).

Supplemental information File S9. Digitalised 3D ontogeny axis of a shell for torsion and curvature analysis in Blender.

Supplemental Information File S10. Absolute shell whorl arc length added during the growth experiments.

Supplemental information File S11. PCA results of Elliptical Fourier coefficient for aperture shape analysis in Part 2(a).

Chapter 4

A method for quantifying, visualising, and analysing gastropod shell form

(Submitted to *PeerJ*, and
published as preprint at <http://dx.doi.org/10.7287/peerj.preprints.157v2>)

Thor-Seng Liew and Menno Schilthuizen

1 Institute Biology Leiden, Leiden University, P.O. Box 9516, 2300 RA Leiden, The Netherlands.

2 Naturalis Biodiversity Center, P.O. Box 9517, 2300 RA Leiden, The Netherlands.

3 Institute for Tropical Biology and Conservation, Universiti Malaysia Sabah, Jalan UMS, 88400, Kota Kinabalu, Sabah, Malaysia.

Email: T-S L: thorsengliew@gmail.com

MS: Menno.Schilthuizen@naturalis.nl

Author Contributions

Conceived and designed the experiments: LTS. Performed the experiments: LTS. Analyzed the data: LTS. Contributed reagents/materials/analysis tools: LTS MS. Wrote the paper: LTS MS.

Supplementary Information

(<http://dx.doi.org/10.6084/m9.figshare.877061>)

Abstract

Quantitative analysis of organismal form is an important component for almost every branch of biology. Although generally considered an easily-measurable structure, the quantification of gastropod shell form is still a challenge because shells lack homologous structures and have a spiral form that is difficult to capture with linear measurements. In view of this, we adopt the idea of theoretical modelling of shell form, in which the shell form is the product of aperture ontogeny profiles in terms of aperture growth trajectory that is quantified as curvature and torsion, and of aperture form that is represented by size and shape. We develop a workflow for the analysis of shell forms based on the aperture ontogeny profile, starting from the procedure of data preparation (retopologising the shell model), via data acquisition (calculation of aperture growth trajectory, aperture form and ontogeny axis), and data presentation (qualitative comparison between shell forms) and ending with data analysis (quantitative comparison between shell forms). We evaluate our methods on representative shells of the genus *Opisthostoma* and *Plectostoma*, which exhibit great variability in shell form. The outcome suggests that our method is robust, reproducible, and versatile for the analysis of shell form. Finally, we propose several potential applications of our methods in functional morphology, theoretical modelling, taxonomy, and evolutionary biology.

Introduction

Empirical and theoretical approaches in the study of shell form

The external form diversity of organisms is the most obvious evidence for their evolution, and thus is a key element in most branches of biology. The Molluscan shell has been a popular example in morphological evolution studies because it is geometrically simple, yet diverse in form. The shell form is controlled by the shell ontogenetic process, which follows a simple accretionary growth mode where new shell material is accumulatively deposited to the existing aperture. The evolution of shell forms has been studied either by using empirical approaches that focus on the quantification of actual shell forms or by using theoretical approaches that focus on the simulation of shell ontogenetic processes and geometric forms.

Notwithstanding the active development in both empirical and theoretical approaches to the study of shell form, there has been very little integration between both schools. For the empirical approach, the quantification methods of shell form have evolved from traditional linear measurement to landmark-based geometric morphometrics and outline analyses (for an overview see Van Bocxlaer & Schultheiß, 2010). At the same time, for the theoretical approach, the simulations of shell form have evolved from simple geometry models that aimed to reproduce the form, to more comprehensive models that simulate shell ontogenetic processes (for an overview see Urdy et al., 2010). Hence, each of the two approaches has been moving forward but away from each other, where synthesis between the two schools of shell morphologists has become more challenging.

In empirical morphological studies, shell form, either in terms of heights and widths in traditional morphometrics or in terms of geometry of procrustes distances in geometric

morphometrics, is quantified by a set of homologous reference points or landmarks on the shell, which can be easily obtained from the fixed dimensions of the shell. Thus, both methods could abstract the shell form in terms of size and shape of the particular shell dimensions, and the between-sample variation of shell size and shape can be assessed (in most cases only within one study). On the other hand, it is not possible to reconstruct the actual shell form from these quantitative measurements, because the shell's accretionary growth model and spiral geometry cannot be quantified on the basis of arbitrary reference points or fixed dimensions (Stone, 1997). Nevertheless, the traditional and geometric morphometric methods have been accepted widely as standard quantification methods for shell form in many different fields of research.

In contrast to empirical morphometrics in which the aim is to quantify the actual shell, theoretical morphologists focus on the simulation of an accretionary growth process which produces a shell form that is similar to actual shells. This field was established with the theoretical shell model of D.M. Raup (Raup, 1961; Raup & Michelson, 1965). Within the first two decades after these publications, only a few different versions of shell models were proposed (e.g. Løvtrup & von Sydow, 1974; Bayer, 1978; McGhee, 1978; Kawaguchi, 1982; Illert, 1983). The subsequent two decades, thanks to the popularity and power of desktop computing, many more theoretical shell models were published (e.g., Savazzi, 1985; Okamoto, 1988; Cortie, 1989; Ackerly, 1989a; Savazzi, 1990; Checa, 1991; Fowler et al., 1992; Illert & Pickover, 1992; Checa & Aguado, 1992; Cortie, 1993; Savazzi, 1993; Rice, 1998; Ubukata, 2001; Galbraith, Prusinkiewicz & Wyvill, 2002). Finally, we saw further improvements in the published theoretical models in recent years. These recent models simulate shell forms that more accurately resemble actual shells because of improved programming software, better algorithms, and 3D technology (e.g. Picado, 2009; Stępień, 2009; Meinhardt, 2009; Urdy et al., 2010; Harary & Tal, 2011; Moulton & Goriely, 2012; Moulton, Goriely & Chirat, 2012; Faghih Shojaei et al., 2012; Chacon, 2012). Here, we will not further discuss the details of the at least 29 published shell models, but refer to the comprehensive overviews and descriptions of these models in Dera et al. (2009) and Urdy et al. (2010).

In brief, the latest theoretical shell models are able to simulate irregularly-coiled shell forms and ornamentations that resemble actual shells, whereas the earlier models could only simulate the regular and general shape of shells. The major refinements that have been made during the almost five decades' development of theoretical shell models are the following modifications of the algorithm: 1) from a fixed reference frame to a moving reference frame system; 2) from modelling based on numerical geometry parameters to growth-parameter-based modelling (e.g. growth rates); 3) from three parameters to more than three parameters, which has made fine-tuning of the shell simulation (e.g. aperture shape) possible. The key element of the theoretical modelling of shells is the generation of shell form by simulating the aperture ontogeny in terms of growth trajectory and form along the shell ontogeny. Hence, this has an advantage over the empirical approach in the numerical representation of the shell geometry form in terms of the 3D quantification and the actual shell ontogenetic processes.

Since the empirical and theoretical researchers studying shell form with two totally different quantification methods, our understanding of shell evolution cannot progress solely by using either empirical morphometrics or theoretical models. Ideally, theoretical models need to be evaluated by empirical data of shell morphometrics, and, vice-versa, empirical morphometric methods need to be improved to obtain data that better reflect the actual shell form and morphogenesis which can then be used to improve the theoretical models. In this dilemma lies the central problem of shell form quantification and it urgently needs to be addressed in order to integrate and generalise studies of shell form evolution.

Why empirical morphologists rarely use theoretical shell models

Despite the fact that, since the 1980s, many shell models have been published that are more complex and versatile, the first theoretical shell model of Raup still remains the most popular. There were many attempts by empirical morphologists to use the original or a modified version of Raup's parameters to quantify natural shell forms (e.g. Raup, 1967; Vermeij, 1971; Davoli & Rosso, 1974; Graus, 1974; Kohn & Riggs, 1975; Newkirk & Doyle, 1975; Warburton, 1979; Cameron, 1981; Verduin, 1982; Ekaratne & Crisp, 1983; Saunders & Shapiro, 1986; Tissot, 1988; Foote & Cowie, 1988; Johnston, Tabachnick & Bookstein, 1991; Emberton, 1994; Clarke, Grahame & Mill, 1999; Samadi, David & Jarne, 2000). Surprisingly, all the other shell models, many of which produce more realistic forms, have received very little attention as compared to Raup's model (see e.g. Savazzi, 1992; Okajima & Chiba, 2011; Okajima & Chiba, 2012, for exceptions). This ironic situation might be explained by the elegance of Raup's model that is intuitively and mathematically simple to be used by empirical morphologists (mostly biologists), with limited mathematical and programming experience.

As discussed above, most of the theoretical models can simulate a shell that has a form resembling the actual shell in a realistic 3D geometry, based on shell ontogeny processes. In contrast, empirical morphometrics can only quantify and compare certain dimensions of actual shells. Clearly, the theoretical approach is better than the empirical approach in its accuracy of shell form quantification, because accurate morphological quantification is essential for functional, ecological and evolutionary studies of shell form. Below, we identify and discuss a few impediments that currently prevent empirical morphologists from adopting the theoretical approach in shell form quantification.

First, the requirement of a computation resource was an impediment in the past. These theoretical models may only be implemented in a computation environment. As mentioned above, the advances of computation hardware in speed and 3D graphic technology have promoted the development of more complex theoretical shell models. For example, the current speed and storage of a desktop computer is at least four orders of magnitude greater than those used by Cortie (1993) only two decades ago. Clearly, the computation hardware is no longer an impediment (e.g. Savazzi, 1995) for the application and development of theoretical shell models.

Notwithstanding the hardware development, programming skills are still a prerequisite for the implementation of theoretical models. Many of the early models that were published between the 1960s and 1990s, used third-generation programming languages such as Fortran and C++, which essentially lack a graphic user interface. This situation has improved now that the simulation of theoretical shell models can be done in fourth-generation programming languages such as Mathematica (e.g. Meinhardt, 2009; Noshita, 2010; Okajima & Chiba, 2011; Okajima & Chiba, 2012) and MATLAB (e.g. Boettiger, Ermentrout & Oster, 2009; Urdy et al. 2010, Faghieh Shojaei et al., 2012). Most of these shell models were described with intensive mathematical notation, at least from a biologist's point of view, in the publication; and some of these were published together with the information on algorithm implementation. However, the actual programming codes are rarely published together with the paper though they may be available from the authors upon request (but see Meinhardt, 2009; Noshita, 2010; Okajima & Chiba, 2011). Only one theoretical modelling software package based on Raup's model has a graphic user interface that is comparable to contemporary geometric morphometric software (Noshita, 2010). Thus, the rest of the modern theoretical models are far less approachable than the morphometric software for empirical morphologists. This is because those advanced theoretical models have not been delivered in a form that allowed empirical morphologists to have "hands-on experience" with them, without extensive mathematical literacy (Savazzi, 1995; McGhee, 2007).

Second, theoretical shell models simulate the shell form based on the input of a set of parameters, which could be non-biological or/and biologically meaningful. Non-biological meaningful parameters are counter-intuitive for empirical morphologists because these parameters are not extrinsic shell traits. Nevertheless, many of these non-biological parameters are required for the model to fit the shell form schematically (Hutchinson, 1999). When the biological parameters do represent shell traits, they are often difficult to obtain accurately and directly from the actual shell because of the three-dimensional spiral geometry (Cain, 1977; Ackerly, 1989a; Ackerly, 1989b; Okamoto, 1988; Schindel, 1990; Checa & Aguado, 1992, Hutchinson, 1999; McGhee, 1999). Since the development of theoretical shell models, almost all simulated shell models have been made by an ad hoc approach, where the parameters are chosen for the model and then the simulated shells are compared with the actual shells. In almost all cases, the correct parameters are chosen after a series of trial-and-error, and the parameters are selected when the form of the simulated shell matches the actual shell. Okamoto (1988) suggested that this ad hoc approach based on pattern matching was easier than obtaining the parameters empirically from the shell.

Third, although the overall forms of the simulated shells resemble the actual shells, the simulated shell is not exactly the same as the actual shell (Kohn & Riggs, 1975; Goodfriend, 1983). For many models, its original parameters are not sufficient to simulate the shell form exactly (Schindel, 1990; Fowler, Meinhardt & Prusinkiewicz, 1992). These simulated general shell forms are adequate for theoretical morphologist interests in their exploration of general shell forms. However, the subtle features on a real shell or the subtle differences among different shell forms of real species that cannot be simulated by theoretical models may have significant functional implications that are important for empirical morphologists.

In brief, it is clear that the implementation of current theoretical shell models is less accessible to empirical shell morphologists. Yet, empirical morphologists are using traditional and geometric morphometrics as a routine method for shell quantification.

Why empirical morphologists use traditional and geometric morphometrics

In addition to the impediments arising from the theoretical shell model itself that are limiting its popularity among empirical morphologists, the theoretical approach faces competition from geometric morphometric methodology. The popularisation of desktop computing that led to the flourishing of theoretical shell models in the late 1980s, also promoted the development of morphometric methods, such as Elliptical Fourier Analysis (EFA) and geometric morphometrics (GM). Rohlf and Archie (1984) set a benchmark for the quantification of an organism's form by EFA, which was improved from Kaesler and Waters (1972) and Kuhl and Giardina (1982). Rohlf and Slice (1990) and Bookstein (1991) developed a complete standard protocol for GM. Soon after these pioneer papers, various software with Graphic User Interface (GUI) were developed for the application of EFA and GM (Cardini & Loy, 2013, see <http://life.bio.sunysb.edu/morph/>). In contrast to the application of theoretical shell models, an understanding of mathematics and programming languages is not a prerequisite for the user of these morphometric tools. Thus, EFA and GM have been well received by biologists, and have been adopted in the morphometric study of shell form.

These geometric morphometric software packages have standard and interactive workflows that help empirical morphologists in every step of: obtaining morphometric data (e.g. placing landmark coordinates), analysing data (e.g. procrustes superimposition), statistical analysis (e.g. ANOVA, PCA), and visualising shape and shape changes (e.g. thin-plate spline, PCA plots). This has made geometric morphometrics approachable and attractive to empirical morphologists, who want to examine the similarities and differences among shell forms.

Geometric morphometrics is actually a statistic of shape that is calculated from Cartesian coordinate data from a sample of objects (Cardini & Loy, 2013). However, it is not an exact quantification of form and is not particularly suitable for comparison and quantification of shell form, for the following two reasons.

First, GM analysis is based on homologous landmarks on the form, but shell has only arbitrary landmarks because it has a low degree of morphological complexity (Van Bocxlaer & Schultheiß 2010). There are no evolutionary homologies that can be defined as landmarks on a shell, since the helical coiled tube offers no points that can be fixed across different individuals. In most cases, 2D landmarks are chosen at the shell apex, suture, and aperture or whorl outline that can be identified from a 2D image that is taken in standard apertural view of a shell. These landmarks are chosen to be analysed by GM but these points have little biological meaning. Furthermore, as opposed to the form of many other organisms, 3D

landmarks are even more difficult to be obtained from a shell (3D model) as compared to 2D landmarks because many of these landmarks, such as suture points, that are obtained from a 2D image are just artefacts of the fixed 2D view of the shell.

Second, the results of separate, independent studies of shell forms cannot be integrated, even though these studies use the same GM method. Statistical analysis of the Cartesian coordinate data that abstractly represent the shell form is adequate in quantifying the variation of a shell within a context of other shells that are included in a single study or within similar taxa where similar landmarks are obtained. However, the raw coordinate data and analysed shape variation from a study are incomparable and incompatible with the data from other studies (Klingenberg, 2013). For example, the raw data (coordinates) from two studies cannot be combined if they use different landmarks and the shape variables (e.g. PCA scores) from a study cannot be compared and analysed together with other studies.

Despite the fact that geometric morphometrics has been widely used by empirical morphologists, it is not an ideal tool in the quantification of shell form for the reasons given above. The increasing availability of the software and application in the literature might cause morphologists to stray away from their initial aims of studying shell form. Hence, it is important to return to the core of the question: what do biologists want to learn from the study of shell form? Clearly, in addition to quantitatively compare shell forms, biologists want to know more about the general characteristics and physical properties of the shell form that are key elements in gaining insight into functional and ecological aspects of the shell (Evans, 2013). However, functional and ecological aspects of shell form can only be determined if the shell form can be exactly quantified.

Using 3D technology to quantify shell form based on aperture ontogeny profiles

In this paper, we propose an interactive approach to the quantification and analysis of shell forms based on state of the art 3D technology and by integrating the theoretical principles of shell modelling and the empirical principles of morphometric data handling. There are no theoretical models that can simulate all existing shell forms. However, the theoretical background of the theoretical models is biologically sound – simulating the shell form by simulating the shell ontogenetic process. On the basis of this shell-ontogenesis principle, we used state-of-the-art X-ray microtomography (micro-CT scan) and 3D modelling software to obtain a series of shell aperture changes from the shell in an interactive workflow that is similar to empirical morphometric analysis.

First, a series of shell aperture outlines were digitised directly from the reconstructed 3D shell model obtained from micro-CT scanning by using open-source 3D-modelling software – Blender ver. 2.63 (www.blender.org). Then, the growth trajectory and form of the shell aperture outline were quantified and extracted with our custom scripts that run in Blender through its embedded open-source Python interpreter (<http://www.python.org/>). The changes of aperture size and shape, and aperture growth trajectory in terms of curvature and torsion

along the shell ontogeny axis length were obtained (hereafter “aperture ontogeny profiles”). The final aperture ontogeny profiles are in a form of multivariate time series data, which consist of a number of instances (i.e. number of quantified apertures that depends on the length of the whorled shell tube) and attributes that represent the growth trajectories, aperture form, and size.

These aperture ontogeny profiles can be plotted when each shell is examined individually. On the other hand, the aperture ontogeny profiles can be visually compared between different shells by plotting the data as radar chart (i.e. spider and star plots). In addition, the differences between shells can be assessed quantitatively by calculating the dissimilarity of aperture ontogeny profiles among shells. Furthermore, the dissimilarity matrix can be used to plot the dendrogram and NMDS plots, which resemble a shell morphospace. All our procedures were implemented by using open source and free software.

Finally, we discuss some possible applications and implications of these shell form quantification methods in theoretical morphology, functional morphology, taxonomy and shell shape evolutionary studies.

Materials and Methods

Ethics Statement

Specimens were collected in Malaysia with permissions from the Economic Planning Unit, Malaysia (UPE: 40/200/19/2524).

Scanning instrumentation

A micro-CT scanner (SkyScan, model 1172, Aartselaar, Belgium) and its accompanying software, NRecon ver. 1.6.6.0 (Skyscan©) and CT Analyser ver. 1.12.0.0 (Skyscan©), were used to generate digital shell 3D models from the actual shell specimens.

Computation software and hardware

Various commercial 3D modelling and statistical software exist for visualising, manipulating, and understanding morphology, such as Amira[®] (Visage Imaging Inc., San Diego, CA) and Autodesk Maya (San Rafael, CA) (reviewed by Abel, Laurini & Richter, 2012). However, in this study, we used only two open-source 3D data modelling and processing software packages, namely Blender ver. 2.63 (www.blender.org) and Meshlab ver. 1.3.2 (Cignoni, Corsini & Ranzuglia, 2008, <http://meshlab.sourceforge.net/>). Both have been used in biology to visualise and model morphology (for Meshlab: Im et al., 2012; Chaplin, Yu & Ros, 2013; Atwood & Sumrall, 2012; for Blender: Pyka et al., 2010: 22); Haug, Maas & Waloszek, 2009; Cassola et al., 2010; Haug et al., 2010; Andrei et al., 2012; Haug et al., 2012; Lv et al., 2013; Mayer et al., 2012). However, these programs have not been used to their full extent in morphological quantification and analysis of 3D data for organisms. For quantification of morphology, we used the open-source Python interpreter ver. 3.2 that is embedded in Blender

2.63. In addition, we also used an extension to the Python programming language – NumPy (Oliphant, 2007) which consists of high-level mathematical functions.

All the morphological data were explored and analysed with the statistical open source programming language R version 3.0.1 (R Core Team, 2013) in the environment of RStudio (RStudio, 2012). We installed three additional packages in R, namely, "lattice": Lattice Graphics (Sarkar, 2008), "pdc": Permutation Distribution Clustering (Brandmaier, 2012a; Brandmaier, 2012b), and "fmsb" (Nakazawa, 2010).

All the computation analyses were carried out with a regular laptop computer with the following specifications: Intel®Core™i7-3612QM @ 2.1GHz, 8 GB memory (RAM), NVIDIA® GeForce GT 630M with 2GB memory.

Procedures

1. Obtaining digital 3D models from actual shells

The scan conditions were as follows: voltage – 80kV or 100kV; pixel – 1336 rows × 2000 columns; camera binning – 2 × 2; image pixel size – 3–6 μm; rotation step – 0.4° or 0.5°; and rotation – 360°. Next, the volume reconstruction on the acquired images was done in NRecon. The images were aligned to the reference scan and reconstruction was done on the following settings: beam hardening correction – 100%; reconstruction angular range – 360 degree; minimum and maximum for CS to image conversion (dynamic range) – ca. 0.12 and ca. 20.0; and result file type – BMP. Finally, 3D models were created from the reconstruction images in CT Analyser with the following setting: binary image index – 1 to 255 or 70 to 255; and were saved as digital polygon mesh object (*.PLY format).

2. Pre-processing digital shell models

The 3D models were then simplified by quadric edge collapse decimation implemented in MeshLab (Cignoni, Corsini & Ranzuglia, 2008) to reduce computation requirements. The raw polygon mesh shells in PLY format have millions of faces and a file size between 20 to 80 Mbytes. Thus, we reduced the number of faces for all model to 200,000 – 300,000 faces, which range between 3 and 6 Mbytes in file size. In addition, for the sake of convenience during the retopology processes, all 3D models were repositioned so that the shell protoconch columella was parallel with the z-axis. This was done by using manipulator tools in MeshLab.

3. Creating reference: Tracing aperture outlines and ontogeny axis from shell models (Supplementary Information File 1)

The digital shell 3D model in PLY format consists of 3D Cartesian coordinate vertices in which each of the three vertices constitutes a triangular face, and all faces are connected through a complex network. In other words, these vertices and faces are not biologically meaningful structures, and it is not possible to extract aperture outlines data directly from a raw PLY digital shell model. Monnet et al. (2009), for example, attempted to extract aperture outline automatically from a digital 3D model by making a plane cross-sectioning of the shell

model, but its outlines do not reflect the form of the actual aperture outlines. Hence, we retopologised the raw 3D mesh models according to the aperture ontogeny for later data extraction.

We used Blender, which is more flexible than the commercial software used by Monnet et al. (2009). For the sake of convenience, we describe the following workflow, including the tools or the function (e.g. “Import PLY”) which can be called after hitting the SPACE bar while in the Blender environment. However, this workflow may be modified by the user.

To begin, we imported a PLY shell model into the Blender environment (“Import PLY”). Then, we resized the model $1000 \times$ (“Resize”) so that the scale of 1 Blender unit was equal to 1 mm. After that, we examined the traces of aperture outlines (i.e. growth lines, ribs, spines) (Figure 1A) and ontogeny axis (i.e. spiral striation, ridges, colour lines) (Figure 1B) of the actual shells. However, it is not possible to trace apertures from the shell protoconch because the protoconch is an embryonic shell that may not grow accretionarily and usually has no growth lines. In many cases, the aperture of the overlapping whorls cannot be traced from the outer shell wall. One of the ways to deal with this situation is to trace the aperture at the inner shell wall and the obscured aperture outline can then be inferred by studying conspecific juvenile specimens (see video tutorial 05:00–08:00 of Supplementary Information File 1).

After these aperture traits were identified, we selected the 3D model (by clicking “right mouse button”), and traced all these traits on the surface of the raw 3D mesh model in Blender by using the “Grease Pen Draw” tool. After that, the grease pen traced aperture traits were converted to Bezier curves with “Convert Grease Pencil” (Figure 1C). We would like to emphasise that this is the most critical step that determines the efficiency of this shell quantification method. Thus, the key lies in the good understanding of the way the aperture is structured, which is essential to trace the aperture outlines accurately. However, the orientation of the shell when the aperture is digitalised would not influence the aperture ontogeny data.

4. Retopologising aperture outlines from the reference and generating retopologised shell models (Supplementary Information File 1 and File 4)

For each shell, we created a set of new Non Uniform Rational B-Splines (NURBS) surface circles (“Add Surface Circle”) and modified these (“Toggle Editmode”) according to the aperture outlines. We created a 16 points NURBS surface circle and aligned the circle to the aperture outline by translation (“Translate”), rotation (“Rotate”), and resizing (“Resize”) (Figure 1D). After the NURBS surface circle was generally aligned, each of the 16 points of the NURBS surface circle were selected and adjusted by translation (“G”) one by one, so that the outline of the NURBS surface circle was exactly the same as the aperture outline. At the same time, the second point of the NURBS surface circle was aligned to the ontogeny axis (Figures 1B and 1C).

After the first aperture outline was retopologised as a NURBS surface circle, the NURBS surface circle was duplicated (“Duplicate Objects”) and aligned to the next aperture outline as

the previous one. This step was repeated until all the aperture outlines were retopologised into NURBS surface circles (Figures 1D and 1E). Then the shell surface was created in the form of a NURBS surface based on the digitised aperture NURBS surface circle (“(De)select All” and “Make Segment” in “Toggle Editmode”) (Figures 1F and 1G). Lastly, we made the surface meet the end points in U direction and increased the surface subdivision per segment (resolution $U = 8$) through the properties menu of the object (Properties (Editor types)>Object Data>Active Spline).

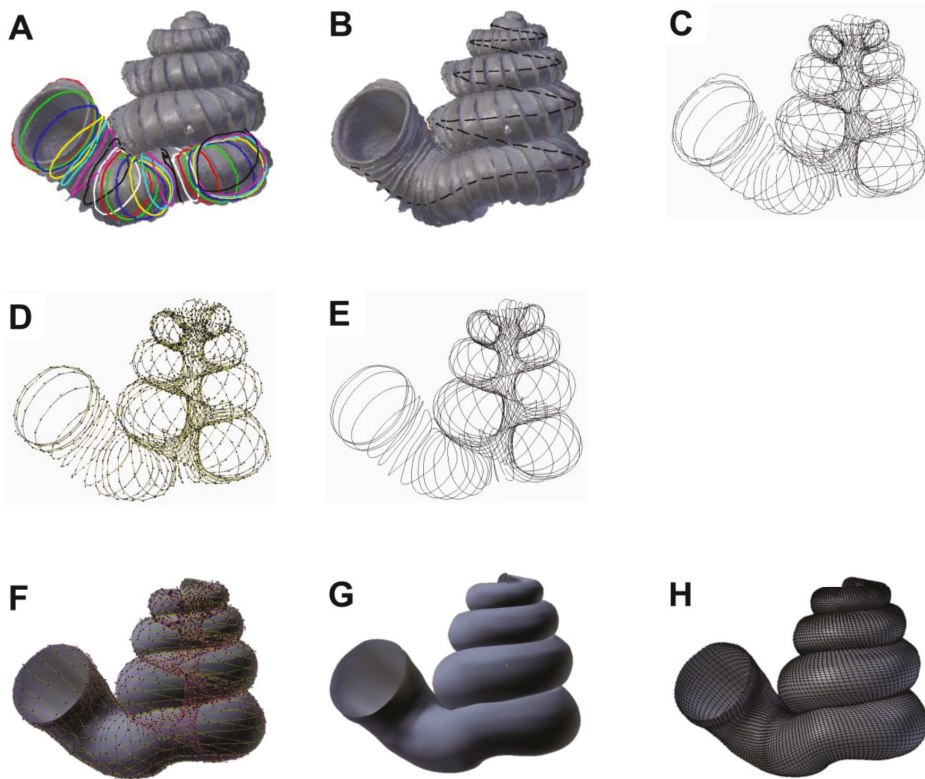


Figure 1. Procedures to generate a retopologised shell based on the aperture ontogeny from a shell by using Blender software. (A) Procedure 3 - Creating reference: Tracing aperture from shell model. (B) Procedure 3 - Creating reference: Tracing ontogeny axis. (C) Procedure 3 – both traced aperture outline and ontogeny axis were converted to Bezier curves. (D) Procedure 4 – Retopologising aperture outlines from the reference by using NURBS circles in EDIT mode. (E) Retopologised aperture outlines. (F) Procedure 4 – Generating retopologised shell surface models from NURBS circles in EDIT mode. (G) Final retopologised NURBS surface shell model. (H) Retopologised 3D shell mesh converted from retopologised NURBS surface shell model.

After that, we converted the NURBS surface 3D model into a 3D Mesh model that consists of vertices, edges, and faces (“Convert to” - “Mesh from Curve/Meta/Surf/Text”). The final retopologised 3D shell Mesh consists of X number of apertures outlines and each aperture outline has Y number of vertices and then a total of $X*Y$ vertices. Each of the vertices is

connected to four other nearest vertices with edges to form a wireframe shell and face (Figure 1H).

It is important to note that the NURBS surface circle is defined by a mathematic formula which does not imply any biology perspective of the shell. We choose NURBS surface circle because the 3D aperture outline form can be digitalised by a small number of control points and shell surface can be recreated by NURBS surface based on the digitised aperture NURBS surface circle. The final 3D polygon mesh model is more simplified than the raw PLY 3D model and each of its vertex data resemble the actual accretionary process of the shell (Figures 1A and 1H).

5. Quantifying aperture growth trajectory

The aperture ontogeny profiles were quantified as described in **Chapter 3** with slight modifications where both aperture growth trajectory and aperture form were quantified directly from the retopologised 3D shell model. This aperture growth trajectory was quantified as a spatial curve, which is the ontogeny axis as represented by a series of first points of the aperture outlines. We estimated two differential geometry parameters, namely, curvature (κ) torsion (τ), and ontogeny axis length for all apertures (Okamoto, 1988; Harary & Tal, 2011). The local curvature and torsion, and accumulative ontogeny axis length were estimated from the aperture points along the growth trajectory by using weighted least-squares fitting and local arc length approximation (Lewiner et al., 2005). All the calculations were done with a custom-written Python script which can be implemented in Python interpreter in the Blender ver. 2.63 environment. The whole workflow was: (1) selecting the retopologised 3D shell Mesh (by clicking “right mouse button”), (2) input parameters for number of sample points “q = ##” in the python script, and (3) paste the script into the Python interpreter (Supplementary Information File 2). The final outputs with torsion, curvature and ontogeny axis reference for each aperture were saved as CSV files.

We found a convergence issue in curvature and torsion estimators. The accuracy of the curvature and torsion estimates depends on the number and density of the vertices in the ontogeny axis (i.e. number of aperture outlines), and the number of sample points. Nevertheless, different numbers of sample points can be adjusted until good (i.e. converged) curvature and torsion estimates are obtained. We used 10% of the total points as number of sample points of the ontogeny axis, which gave reasonably good estimates for curvature and torsion.

Notwithstanding the algorithm issue, the curvature and torsion estimators are informative in describing the shell spiral geometry growth trajectory. Curvature is always larger or equal to zero ($\kappa \geq 0$). When $\kappa = 0$, the spatial curve is a straight line; the larger the curvature, the smaller the radius of curvature ($1/\kappa$), and thus the more tightly coiled the spatial curve. On the other hand, the torsion estimator can be zero or take either negative or positive values ($-\infty \leq \tau \leq \infty$). When $\tau = 0$, the spatial curve lies completely in one plane (e.g. a flat planispiral shell), negative torsion values correspond to left-handed coiling and to right-handed coiling

for positive torsion values; the larger the torsion, the smaller the radius of torsion ($1/\tau$), and thus the taller the spiral.

6. Quantifying aperture form

We quantified the aperture outline sizes as perimeter and form as normalised Elliptic Fourier coefficients (normalised EFA) by using a custom-written Python script which can be implemented Python interpreter embedded in the Blender environment. The workflow was (1) selecting the retopologised 3D shell mesh (by clicking “right mouse button”), (2) input parameters for “number_of_points_for_each_aperture = ##” in the python script, and (3) paste the script into the Python interpreter of Blender (Supplementary Information File 2). The final outputs were saved as CSV files.

Aperture outline perimeter was estimated from the sum of lengths (mm) for all the edges that are connecting the vertices (hereafter “aperture size”). For aperture form analysis, we used 3D normalised EFA algorithms (Godefroy et al., 2012) and implemented these in the custom python script. Although many algorithms exist for describing and quantifying the form of a closed outline (Claude, 2008), we used EFA because it is robust to unequally spaced points, can be normalised for size and orientation, and can capture complex outline form with a small number of harmonics (Rohlf & Archie, 1984; Godefroy et al., 2012). In this study, we used five harmonics, each with six coefficients which were sufficient to capture the diverse aperture shapes of our shells. For quantification of apertures shape that are invariant to size and rotation, we normalised EFA of aperture outlines for orientation and size. If needed for comparison with other studies, the normalised EFA can be repeated for the same dataset with higher or lower numbers of harmonics.

After normalisation, we ran principal components analysis (PCA) to summarise the 30 normalised Fourier coefficients as principal components scores (hereafter “aperture shape scores”). After that, we selected the major principal components (explaining > 90 % of the variance) for further analysis. The aperture shape scores of each selected principal component were plotted and analysed against the ontogeny axis.

7. Visualising aperture form and trajectory changes along the shell ontogeny

For exploration of data, we used two graphical techniques for representing aperture ontogeny profile changes along the shell ontogeny. For each shell, we made a vertical four-panels scatter plot in which each of the four variables (namely, curvature, torsion, aperture size, and the first principal component aperture shape score) were plotted against the ontogeny axis. When necessary, the second and third principal component aperture shape scores were also included. In addition, the axis of each variable was rescaled so that it was the same for the same variable of all shells. After standardisation of the axis, the aperture ontogeny profiles of several shells could be quantitatively compared side by side.

However, comparison of between plots would become less effective with a larger number of shells. Alternatively, therefore, all aperture ontogeny profile variables of each shell can also be represented in a radar chart, instead of scatter plots. This chart is effective in showing the

variable outliers within a chart and the overall similarity between charts. Before plotting the data in a radar chart, the datasets of all shells need to be restructured because the dataset of different shells could differ in the number of data points (i.e. quantified aperture), which depends on the ontogeny axis length of each shell.

We did this by dividing the ontogeny axis of each shell into 20 equal length intervals, and then by sampling the variable values at the end of every interval. In the restructured dataset, the trend of the aperture ontogeny profile of each variable is retained and all radar charts have the same number of data points. Thus, the changes of aperture variables between each subsequent 1/20 of the ontogeny axis can be examined within a shell and be compared among different shells in a synchronistic manner. We suggest to use 20 points to summarise hundreds variable points of the aperture ontogeny profile variables along ontogeny axis because the radar would be overwhelming with too many points and hard to interpret. Similar to the scatter plot, we standardised the axis scales of each variable of all radar charts.

In addition, we added a new variable which represents the ontogeny axis interval length in order to compensate for the loss of shell size information during the standardisation of ontogeny axis length. Finally, we plotted the variables, namely, curvature, torsion, aperture size, and ontogeny axis length, and aperture shape scores in a radar chart for each shell by using the “fmsb” library (Nakazawa, 2010) with R version 3.0.1 (R Core Team, 2013) (Supplementary Information File 5).

8. Quantitative comparison between shell forms

In addition to the qualitative comparison between shells forms as described above, the dissimilarity between different shells can be analysed quantitatively. We used Permutation Distribution Clustering (PDC) which finds similarities in a time series dataset (Brandmaier, 2012a; Brandmaier, 2012b). PDC can be used for the analysis of the changes in a variable along shell ontogeny between different shells (i.e. two-dimensional dataset: number of shells × number of apertures) and multiple variable changes between shells (i.e. three-dimensional dataset: number of shells × number of variables × number of apertures). We applied the most recent analysis developed by Brandmaier (2012a & b) because it has an R package that can be applied and can calculate the trend similarity. That said, the same data can always be analysed by other “better” algorithms in the future.

Although PDC is robust to the length differences between datasets, our preliminary analysis showed that the PDC output would be biased when there was a great (around two-fold) length difference in the total ontogeny axis length. Hence, we standardised the data as in procedure 7, but dividing the ontogeny axis of each shell into 50, instead of 20, equal length intervals. This standardisation procedure allows comparison of trends in variable changes along the shell ontogeny without the influences of size. In other words, the dissimilarity is zero between two shells that have exactly the same shape, but differ only in size. In addition to the shape comparison, we obtained the shell size in terms of volume by using “Volume” function in Blender after the 3D shell model was closed at both ends by creating faces “Make edge/Face”) on selected apertures at both end (“Loop Select”) in EDIT mode.

The aperture ontogeny profiles of all shells were combined into a three-dimensional data matrix consisting of n shells \times four variables \times 50 aperture data points. We ran four PDCs, each for the five data matrices with: 1) all four variables, 2) torsion, 3) curvature, 4) aperture size, and 5) aperture shape scores. The parameter settings for the PDC analysis were as follows: embedding dimension = 5; time-delay of the embedding = 1; divergence measure between discrete distributions = symmetric alpha divergence; and hierarchical clustering linkage method = single. The dissimilarity distances between shells were used to produce the dendrogram. PDC analysis was performed with the “pdc” library (Brandmaier, 2012b) in R version 3.0.1 (R Core Team, 2013) (Supplementary Information File 5).

In addition to the dendrogram representation of the output from PDC, we plotted the dissimilarity as a non-metric multidimensional scaling (NMDS) plot which resembles a morphospace. NMDS was performed by using “MASS” library (Venables & Ripley, 2002) in R version 3.0.1 (R Core Team, 2013) (Supplementary Information File 5).

Worked example: Comparative analysis of *Opisthostoma* and *Plectostoma* species shell form and simulated shell form

We evaluated the above-described shell form quantification method by using the shells of *Opisthostoma* and *Plectostoma*, which exhibit a great variability in shell form. Some of the species follow a regular coiling regime whereas others deviate from regular coiling in various degrees. It remains a challenging task to quantify and compare these shell forms among species, either by using traditional or geometric morphometrics, because a standard aperture view for the irregular and open coiled shells cannot be determined.

We selected four species, namely, *Plectostoma laidlawi* Skyes 1902 (Figure 2A), *Plectostoma crassipupa* van Benthem Jutting, 1952 (Figure 2B), *Plectostoma christae* Maassen 2001 (Figure 2C), and *Opisthostoma vermiculum* Clements and Vermeulen, 2008 (in Clements et al., 2008) (Figure 2D), for which the shell forms are, respectively: regularly coiled, slight distortion of the last whorl, strong distortion of the last whorl, and complete distortion of most of the whorls. Despite the narrow taxonomic range of the selected species, the range of shell forms of these four species do cover a very large diversity of shell form. We retopologised these four shells by following the procedures 1 to 4 (Supplementary Information Files 6).

In addition to the four retopologised 3D shell models, we manually created another four shell models by transforming three out of the four retopologised NURBS surface 3D shell models by using the “Transform” function in Blender. These models are: 1) *Plectostoma laidlawi* that was resized to half the original size and given slight modification of the aperture size (Figure 2E); 2) *Plectostoma christae* that was reshaped into an elongated form by reducing the model size (linear dimension) to one-half along the x and y axes, and by doubling the size along the z axis (Figure 2F); 3) *Plectostoma christae* that was reshaped into a depressed form by multiplying by 1.5 the model size along the x and y axes, and by reducing to one-half along the z axis (Figure 2G); and 4) *Opisthostoma vermiculum* that consists of one *Opisthostoma*

vermiculum original 3D model of which we connected the aperture to another, enlarged, *Opisthostoma vermiculum* (Figure 2H). Finally, we analysed all these eight shell models by following the procedures 5 to 8.

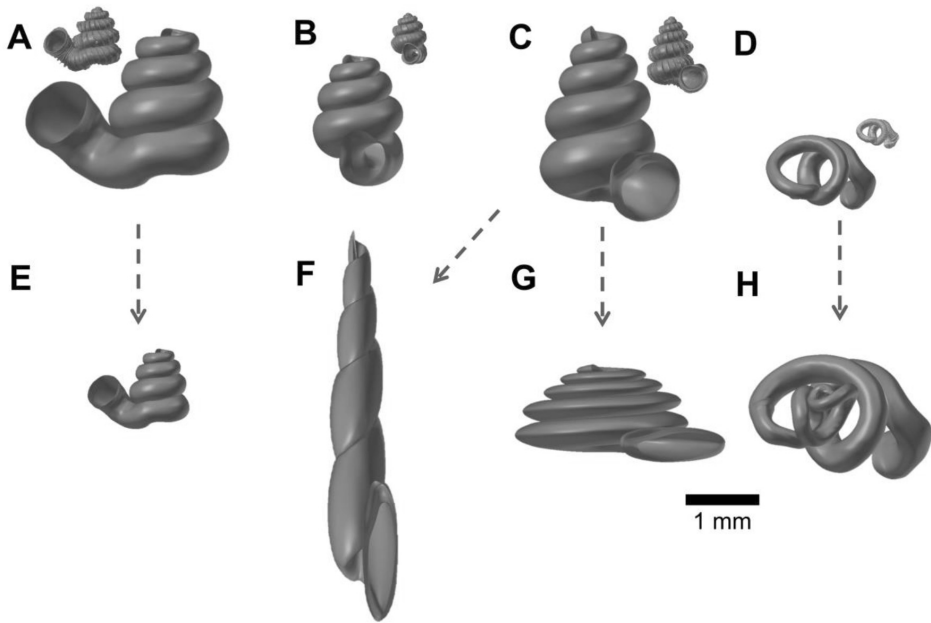


Figure 2. Retopologised shell 3D models obtained by repotologising real shells (A – D) and by transformation of retopologised shells (E – H). (A) Shell of *Plectostoma laidlawi* (Sykes 1902). (B) Shell of *Plectostoma crassipupa* (van Benthem Jutting), 1952. (C) Shell of *Plectostoma christae* (Maassen 2001). (D) Shell of *Opisthostoma vermiculum* Clements and Vermeulen, 2008. (E) *Plectostoma laidlawi* shell that was resized by one-half and with slight modification of the last aperture size. (F) *Plectostoma christae* shell that was reshaped into an elongated form by reducing the model size (linear dimension) by one-half along the x and y axes, and by doubling the size along the z axis. (G) *Plectostoma christae* shell that was reshaped into a depressed form by increasing by 1.5 the model size along the x and y axes, and by reducing the size by one-half along the z axis. (H) *Opisthostoma vermiculum* shell that consists of one *Opisthostoma vermiculum* original 3D model of which the aperture was connected to a second, enlarged, *Opisthostoma vermiculum*.

Results and Discussion

Retopologied 3D shell models

All the final retopologised 3D shell models can be found in Supplementary Information (Files 7 to 14) in PLY ASCII mesh format, with the raw data as a list of vertices, followed by a list of polygons, which can be accessed directly without the need of any 3D software. Each vertex is represented by x, y, z coordinates. Each polygon face consists of four vertices. This simplified yet biologically informative 3D mesh shell model allows the quantification of aperture form and growth trajectory. Moreover, the 3D shell models and their raw vertices

data could potentially be used in studies of functional morphology and theoretical modelling of shell form, respectively.

Malacologists have been focusing on empirical shell morphological data, from which the functional, ecological and evolutionary aspects were then extracted. The physical properties were then determined by its form (e.g. Okajima & Chiba 2011; Okajima & Chiba, 2012). By using the 3D models, the shell properties and function can be analysed *in silico*. For example, the thickness of the shell can be added to the 3D shell model (Figure 3E and Figure 3F) in order to obtain the shell material's volume, the shell's inner volume, its inner and outer surface area, and centre of gravity. We used the “build” function of the software, which can only “solidify” the model by uniform thickness. However, if necessary, it is possible to write a custom Python script to add the desired thickness to the shell. Quantification of shell properties may then be done by using the geometry approach in Meshlab or Blender, as compared to the pre-3D era where mathematical descriptions of the shell form were required (e.g. Moseley, 1838; Raup & Graus, 1972; Stone, 1997). Furthermore, it is possible to convert the 3D models to a 3D finite element (FE) model, of which the physical properties (e.g. strength) can be tested (e.g. Faghieh Shojaei et al., 2012).

In addition to the potential use of 3D shell models in functional morphology, the coordinate data of the vertices of 3D shell models could be used directly by theoretical morphologists (see Figure 1 in Urdy et al., 2010). For example, these data can be extracted in different formats that fit the data requirement of different types of theoretical shell models, namely, generating curve models using a fixed reference frame or moving reference frame (Figure 3C), helicospiral or multivector helicospiral models using a fixed reference frame (Figure 3A, Figure 3B and Figure 3D) or growth vector models using a moving reference frame (Figure 3A and Figure 3B).

The retopologising of the aperture ontogeny from a raw 3D shell model (procedures 1 to 4) is a time-consuming and tedious process compared with traditional and geometric morphometrics. There are no differences in the time required for data analysis between GM and our method. The only time differences are in the data acquisition. In our experience, two to three days are needed to collect the aperture data from the shell. For example, the four shell models were created by retopologising between 73 and 96 separate apertures (ca. 1500 points for 90 apertures). From the viewpoint of short-term cost-benefit balance, this may be seen as a waste of time, because GM requires not more than a few dozen points for each shell, which can generate the shape variables for a study, even though these points are not comparable to other points of other shells or other studies. However, in the long run, it is a good time investment, since it will allow the understanding of shell function, growth, and evolution, as the same set of data is obtained from different shell forms and can be accumulated and analysed together. Moreover, as with all newly-developed techniques, improvements in efficiency and automation are possible and may remove these impediments in the future.

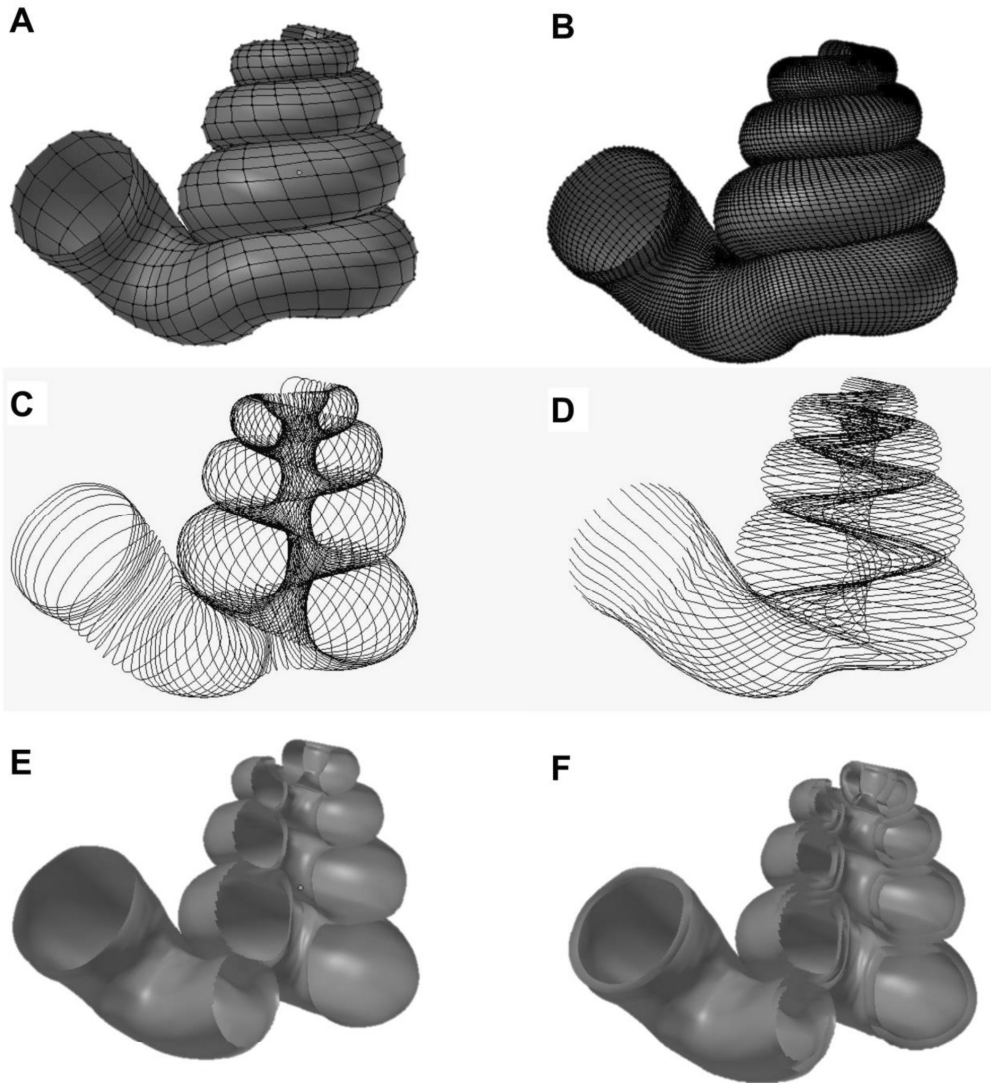


Figure 3. Different data types that could be obtained directly from a 3D shell model that was retopologised on the basis of the aperture ontogeny. (A) Aperture maps (*sensu* Rice, 1998) or growth vector maps (*sensu* Urdy et al., 2010). (B) same as (A), but the data can be obtained in a greater resolution. (C) Aperture outlines data for generating curve models. (D) Multiple ontogeny axes for helicospiral models. (E) Simple 3D surface shell model with no thickness. (F) 3D surface shell model with added thickness.

Comparing shell form from the view of shell ontogeny

Figure 4 gives an overview of the aperture ontogeny profile and shell volume for each species. The curvature, torsion perimeter, and ontogeny axis are represented by true numerical values with the unit of mm^{-1} and mm , and thus can be interpreted directly. In contrast, the aperture shape scores are just statistics of Fourier coefficients and are not the absolute quantification of aperture shape. The PCA score of an aperture shape depends on the

shape of other aperture outlines and thus it might change whenever other aperture outlines are added into the analysis. Nevertheless, the aperture scores will stabilise as data of more shells become available and when most of the extreme aperture forms are included. In this study, the first principal component explained 92% of the total variance; the second and third principal component explained only 3% or 1% of the total variance. We showed that the shell form can be represented by the ontogeny changes of the aperture growth trajectory in terms of curvature and torsion, and aperture form, in terms of perimeter and shape.

Our first example evaluates this method in illustrating the differences between two shells that have the same shape but differ in shell size – the half-size *Plectostoma laidlawi* (Figure 4E) shell and the original *Plectostoma laidlawi* shell (Figure 4C). As revealed by their aperture ontogeny profiles, the size difference between the two shells has had an effect on the curvature, torsion, ontogeny axis length and aperture size. For the resized *Plectostoma laidlawi* shell, the values of curvature and torsion are twice as large as for the original, whereas the ontogeny axis length and aperture size are only half those of the original shell. However, there is no discrepancy in the aperture shape statistics. Despite this scalar effect, the overall trends in the changes of these variables along the ontogeny axis are comparable between these two shells (Figure 6B).

Another example shows the ontogeny profiles of three shells, namely, the elongated (Figure 4G), depressed (Figure 4H), and original (Figure 4A) versions of the *Plectostoma christae* shell. Comparison of aperture profiles among these show the most obvious discrepancies in greater torsion values for the elongated shell, which change in a more dramatic trend along the shell ontogeny. In addition, each of the three shells has its unique aperture shape scores, though there are no big discrepancies in the aperture size. The differences in ontogeny axis length, curvature and torsion are related to the differences of the aperture shape statistics among the three shells. However, our small dataset with only three shells is not sufficient for thorough disentangling of the interplay between aperture size, shape, and growth trajectory in relation to the shell form.

Our last example is the comparison between the original (Figure 4D) and the composite (Figure 4F) *Opisthostoma vermiculum* shell. It is clear that our method has high sensitivity and robustness in the analysis of such bizarre shell forms. As shown in Figure 4F, the start of the aperture ontogeny profile of the composite shell was the same as for the original shell (Figure 4D). In addition, the later parts of the ontogeny profile trends are still comparable to the first part, but different in value because of the scalar effect.

As an alternative visualisation, Figure 5 shows the radar charts that summarise the same aperture ontogeny profiles of each species. The polygon edges in each chart show how dramatically the aperture form (size and shape), and growth trajectory (curvature and torsion) are changing at each of the subsequent 5% intervals of the shell ontogeny. The aperture size (mm) and the ontogeny segment length (mm) variables indicate the shell size (i.e. volume). To illustrate this, aperture size and ontogeny axis length can be seen as the circle size and

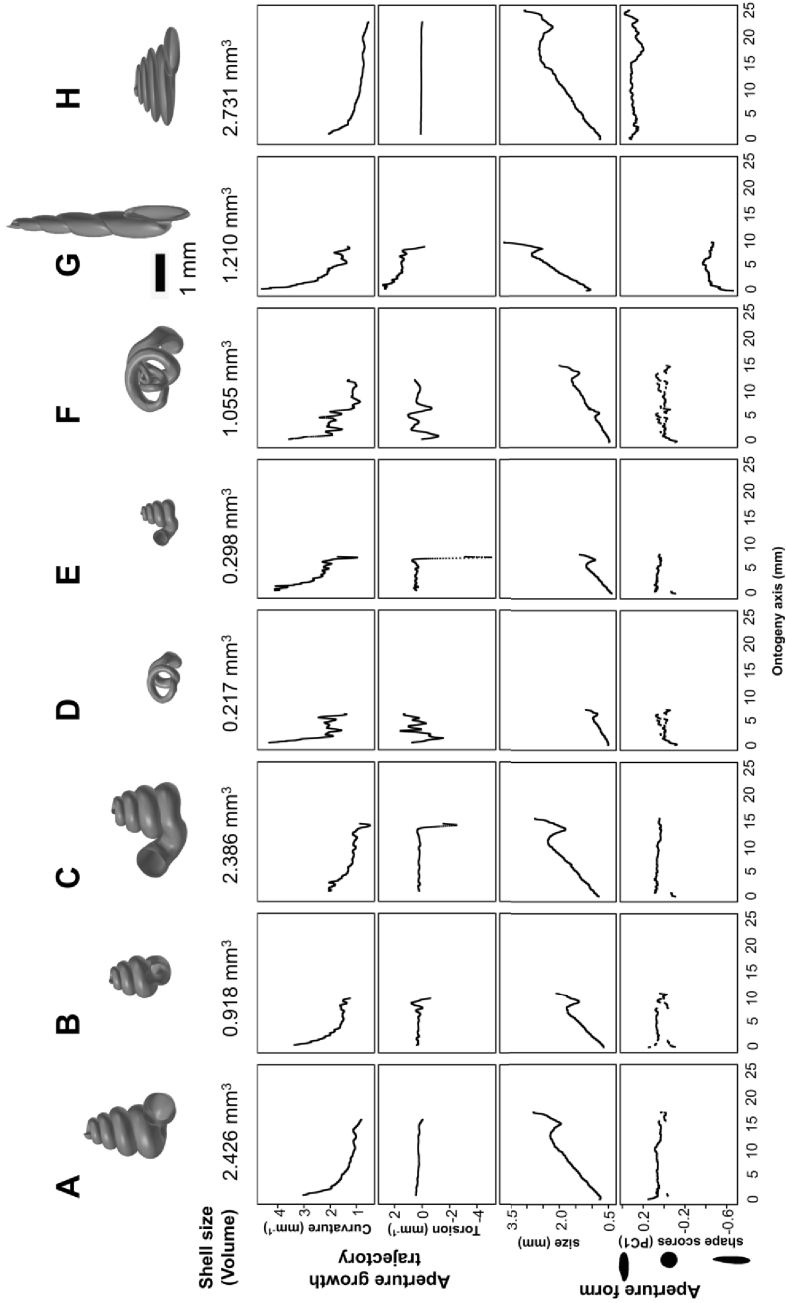


Figure 4. Shell size (volume) and aperture ontogeny profiles in terms of aperture growth trajectory (curvature and torsion) and aperture form (size and shape) of eight shells. (A) Shell of *Plectostoma laidlawi* (Sykes 1902). (B) Shell of *Plectostoma crassipupa* (van Benthem Jutting, 1952). (C) Shell of *Plectostoma christae* (Maassen 2001). (D) Shell of *Opisthostoma vermiculum* Clements and Vermeulen, 2008. (E) *Plectostoma laidlawi* shell that was resized by one-half and with slight modification of the last aperture size. (F) *Plectostoma christae* shell that was elongated form by reducing the model size (linear dimension) by one-half along the x and y axes, and by doubling the size along the z axis. (G) *Plectostoma christae* shell that was reshaped into a depressed form by increasing the x and y axes, and by doubling the size along the x and y axes, and by reducing the size by one-half along the z axis. (H) *Opisthostoma vermiculum* shell that consists of one *Opisthostoma vermiculum* original 3D model of which the aperture was connected to a second enlarged *Opisthostoma vermiculum*.

height of a cylinder. This chart is useful for the visual comparison between shells that are similar in size, for example, *Plectostoma christae* (2.43 mm³), *Plectostoma laidlawi* (2.39 mm³), and the depressed *Plectostoma christae* (2.73 mm³). The radar chart shows that (1) the depressed *Plectostoma christae* is the largest and has a very different aperture shape as compared to the other two shells; (2) most of the shell whorls' form of *Plectostoma christae* is very similar to *Plectostoma laidlawi* (i.e. most of the polygons in the chart were similar), but the *Plectostoma laidlawi* shell differs from *Plectostoma christae* shell by having distorted whorls at the last part of the shell ontogeny (magenta lines at torsion) and a more open umbilicus at the beginning of the shell ontogeny (red lines at curvature and aperture size).

However, comparison of radar charts between shells that differ greatly in size would be less informative. For example, the radar charts between the resized *Plectostoma laidlawi* shell and the original *Plectostoma laidlawi* shell are very different, though the resized one has the same shell shape as the original. The difference in radar charts between the two shells was therefore mainly caused by the size difference.

As we have shown in both graphical techniques (Figures 4 and 5), the shell forms can be explored and compared qualitatively on the basis of aperture ontogeny profiles. Users might need some training in the interpretation of the plots because they are different from both linear dimension measurement plots and geometric morphometric shape coordinate plots. Our evaluation suggested that both data visualisation methods are sensitive and robust in capturing the aperture ontogeny profile for any shell form and thus make the qualitative comparison across gastropod taxa and studies possible.

This method could be applied in malacological taxonomy because its core business is the description of shell form. Despite hundreds of years of taxonomic history of shells, there has been little change in the way shell form is being described. For example, shell form is usually described in terms of linear dimensions: shell width and height; number of whorls; shell shape – flat, depressed, globose, conical, or elongated; whorls shape – from flat to convex. Here, we suggest that the aperture ontogeny profiles would be a great supplement to the classical approach to shell description. For example: (1) the size of the shell (its volume) depends on the ontogeny axis length and aperture size; (2) the shell shape depends on the growth trajectory in terms of curvature and torsion; (3) the shape of the whorls depends on the shape of the aperture (Figure 4). In our case of the four shells (Figures 2A – 2D), it is clear that aperture size of each shell is constricted at roughly the same part of the respective shell ontogeny, namely between 70% and 85%, regardless of the dissimilar shell sizes and shapes (Figures 4A – 4D, and aperture size profiles in Figure 5B). In fact, these aperture size decreases during ontogeny are in accordance with the shell constriction, one of the shell characters that have been used in the taxonomy of *Opisthostoma* and *Plectostoma* (Vermeulen, 1994; **Chapter 2**). However, the shell constriction has not been quantified previously, and we show that it could also be an important developmental homology for the two genera. This preliminary results suggest that these aperture ontogeny profiles could aid the taxonomist in decision-making for grouping taxa based on homologous characters.

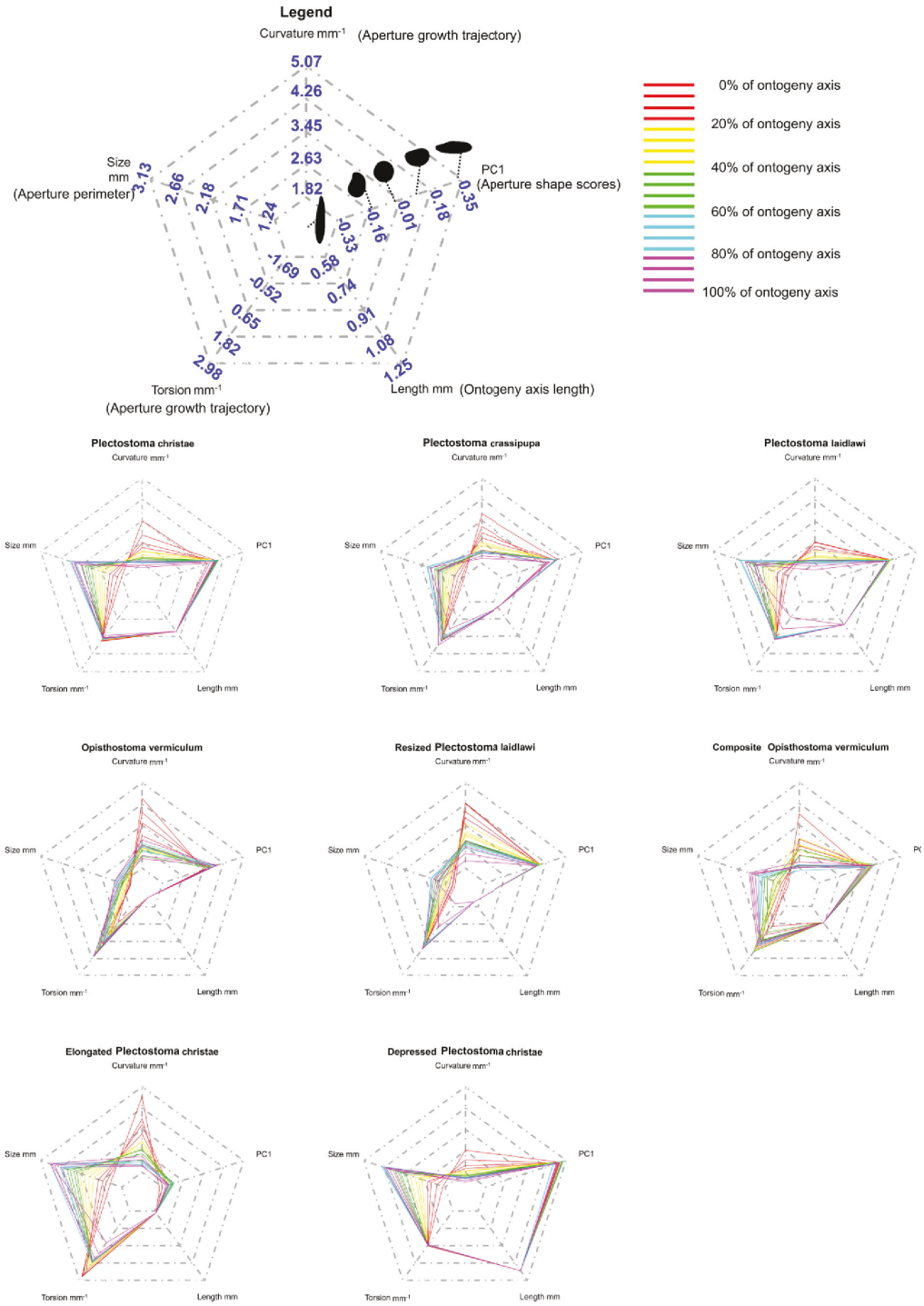


Figure 5. Radar charts of the aperture ontogeny profiles of eight shells. Each radar chart shows the value and trends of the curvature, torsion, aperture size, aperture shape scores, and ontogeny axis length of each shell.

Quantitative comparison between different shell forms

Figure 6 shows dendrograms resulting from a permutation distribution clustering analysis of the eight shells in terms of their aperture ontogeny profiles. Figure 6A shows the hierarchical clustering of the eight shells based on all four aperture ontogeny profiles. From this dendrogram, the composite *Opisthostoma vermiculum* is completely separate from the other shells. The remaining seven shells are clustered into two groups. One consists of the more regularly coiled shells, namely, *Plectostoma christae* and its two transformed shells, and *Plectostoma crassipupa*; the other group consists of the shells that deviate from regular coiling, namely *Plectostoma laidlawi* and its transformed shell, and *Opisthostoma vermiculum*. Nevertheless, there were high dissimilarities between shells within each group

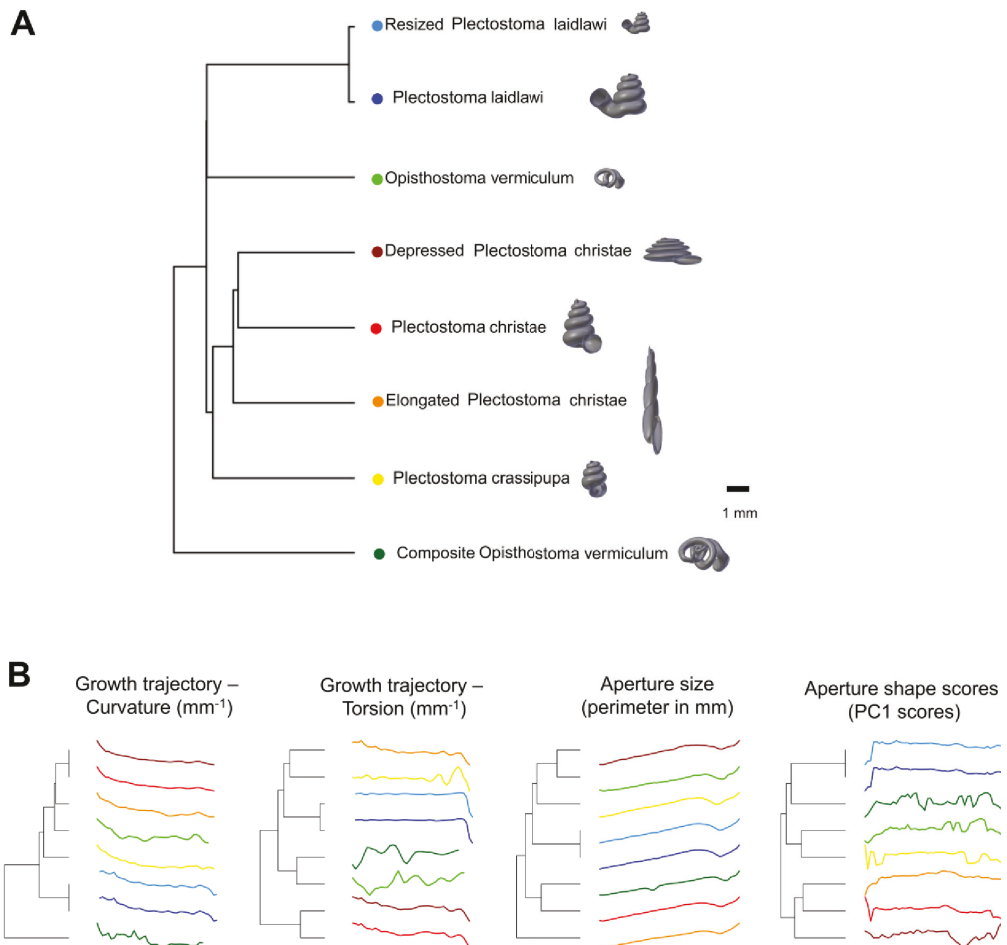


Figure 6. Dendrogram from permutation distribution clustering of the aperture ontogeny profiles of eight shells. (A) Dendrogram from permutation distribution clustering of the four aperture ontogeny profiles, namely, curvature, torsion, aperture size, and aperture shape scores, of eight shells. (B) Four dendrograms from permutation distribution clustering of eight shells, which each for the four aperture ontogeny profiles, namely, curvature, torsion, aperture size, and aperture shape scores.

as revealed by the long branch lengths in Figure 6A, except for the two *Plectostoma laidlawi* shells (Table 1). The aperture ontogeny profiles for the *Plectostoma laidlawi* shell and its reduced version are almost the same. The high dissimilarity among the other six shells can be explained when each of the variables in the aperture ontogeny profile is analysed separately as shown in Figure 6B.

Table 1. Dissimilarity matrix of aperture ontogeny profiles of eight shells obtained from Permutation Distribution Clustering.

Shell	(1)	(2)	(3)	(4)	(5)	(6)	(7)	(8)
(1) <i>Plectostoma laidlawi</i>	0.00							
(2) <i>Plectostoma crassipupa</i>	2.44	0.00						
(3) <i>Plectostoma christae</i>	2.65	2.83	0.00					
(4) <i>Opisthostoma vermiculum</i>	2.63	2.56	2.59	0.00				
(5) half-sized <i>P. laidlawi</i>	2.69	2.80	0.09	2.55	0.00			
(6) composite <i>O. vermiculum</i>	3.12	3.48	3.40	3.39	3.34	0.00		
(7) elongated <i>P. christae</i>	2.09	2.55	3.03	2.79	3.03	3.36	0.00	
(8) depressed <i>P. christae</i>	2.01	2.73	3.16	2.94	3.21	3.84	2.62	0.00

Figure 6B shows the dendrograms of aperture ontogeny profiles for each of the four variables. All four dendrograms have a different topology than the one in Figure 6A. Among the variables, the aperture ontogeny profile of the curvature has the smallest discrepancies among shells. The two *Plectostoma laidlawi* shells are the only pair that clusters together in all the dendrograms of Figures 6A and 6B because they are identical in every aspect of aperture ontogeny profile except torsion. Hence, the independent analysis of aperture ontogeny profile variables corresponds well to the overall analysis of aperture ontogeny profiles.

Figure 7 shows a three-dimensional NMDS plot of the distance matrix (Table 1) that was generated from PDC analysis on all four aperture ontogeny profiles. The very low stress level (0.000) indicates that this 3D plot is sufficient to represent the distance matrix of the aperture ontogeny profiles. This NMDS plot can therefore be regarded as a morphospace of the shell shape, as derived from aperture ontogeny profiles. However, neither the dendrogram nor the NMDS plot contains information about the shell size because the analysis of PDC is based on the standardised ontogeny profiles and their trends. Thus, both plots are useful for the comparative analysis of shell shape, but not shell size. Nevertheless, the size comparison between shells is rather straightforward.

The conventional quantification of shell size is based on the linear measurement of two or three dimensions of a shell, for example, shell height and shell width. These measurements are extremely effective for size comparisons between similarly-shaped shells. However, the linear measurements have limitations when comparison is made between shells that are different in shape. For example, shell height comparison between a discoidal shell and a

fusiform shell tells very little about size differences because the dimensional measurements are tied to a shell shape that results from a different coiling strategy.

Thus, shell size may be more appropriately given as shell volume, which can be estimated easily from retopologised 3D shell models (Figure 4). This quantification of shell size in terms of volume is more meaningful from the functional and developmental point of view because a snail should grow a shell in which its entire soft body can fit when the snail withdraws into the shell. In addition to the exact volume, a shorthand to qualitatively comparing size between two shells is by examining the ontogeny axis length and aperture size in the radar chart (Figure 5). We can then compare the form between shells when the

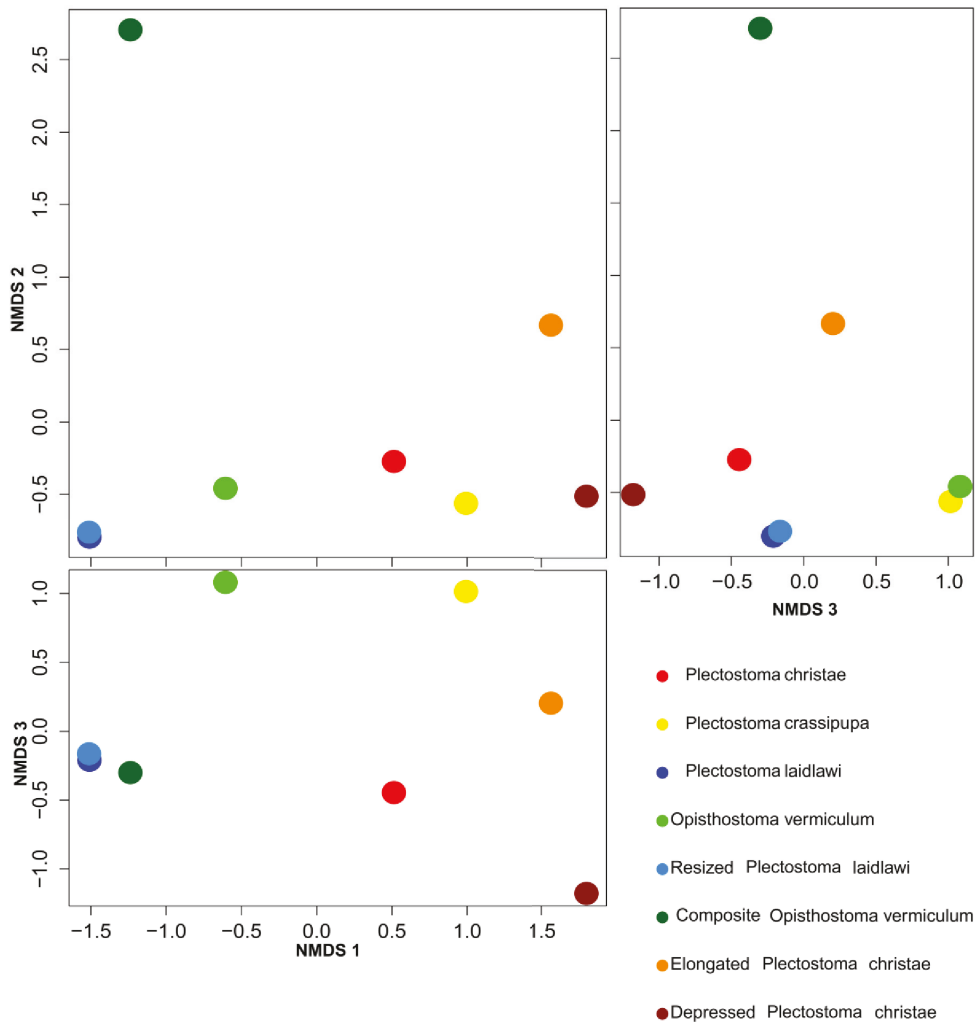


Figure 7. Non-metric multidimensional scaling (NMDS) 3D plots as shell morphospace. The NMDS plots were generated from a dissimilarity matrix of eight shells aperture ontogeny profiles, which were analysed by permutation distribution clustering.

dendrograms or NMDS plot are interpreted together with shell size (volume) data. For example, the *Plectostoma laidlawi* shell has the same shape as, but is eight times larger than, the resized *Plectostoma laidlawi*.

In addition to the construction of morphospace, the dissimilarity matrix can be used in phylogenetic signal tests (Hardy & Pavoine, 2012). Furthermore, it can also be analysed together with other distance matrices, such as for geographical or ecological distance, to improve our understanding of the evolutionary biology of shell forms.

Conclusions, limitations and future directions

We demonstrated an alternative workflow for data acquisition, exploration and quantitative analysis of shell form. This method has several advantages: (1) robustness – this method can be used to compare any shell form: The same aperture profiles can be obtained from any form of shell. Then, these profiles from different shells and/or different studies can be analysed together. These parameters can be obtained from the aperture as long as the shell grows accretionarily at the aperture; (2) scalability and reproducibility – the data obtained from different studies and different gastropod taxa can be integrated: Aperture ontogeny profiles were obtained from the aperture outlines. This is a trait that exists in every gastropod shell. We believe that the aperture outline that is obtained by multiple experienced malacologists, on different shells, would be highly similar; (3) versatility – the raw 3D shell mesh models, coordinates data of the vertices, aperture ontogeny profiles, and dissimilarity matrix between shell forms comply with the data standard that is required in taxonomy, functional morphology, theoretical modelling, and evolutionary studies.

Yet, our method has its limitations. Firstly, our retopology procedures rely on a 3D shell model that requires CT-scan technology. In fact, although a CT-scan 3D shell model can certainly facilitate the retopology process of a shell, it is not indispensable. The key of the retopology processes is to digitise the aperture along the shell ontogeny, and thus a shell can be retopologised fully in Blender with a good understanding of the aperture ontogeny profiles by studying the real specimens even without a reference shell model. Secondly, the retopology procedure which is essential for our data acquisition is more time-consuming than traditional and geometric morphometric where data can be obtained from an image taken from a shell. Thirdly, our method is effective in the analysis of overall shell form, but not of the shell ornamentation.

In the future, our method can be improved to accommodate the shell ornamentation analysis. Parts of our method (i.e. procedures 1 – 6) can be used to obtain shell ornamentation data, such as radial ribs (i.e., commarginal ribs), but these data cannot be analysed with our qualitative and quantitative approaches that focus on longitudinal growth (i.e. procedures 7 – 8). Finally, we hope this shell form quantification method will simulate more collaboration within malacologists that work in different research fields, and between empirical and theoretical morphologists.

Acknowledgments

We are thankful to Heike Kappes, Ton de Winter, Jaap Vermeulen, and Severine Urdu for fruitful discussion. We are grateful to Willem Renema for introducing LTS to CT-Scan instrumentation. Finally, we would like to acknowledge Robert Toonen, Ronald Allan Cruz, and an anonymous reviewer for providing useful comments that improved the manuscript.

Supplementary Information (<http://dx.doi.org/10.6084/m9.figshare.877061>)

File 1 – Video tutorial for procedure 3 and 4.

File 2– A python script for procedures 5 and 6 – Aperture form and growth trajectory analysis on retopologised 3D shell mesh in Blender.

File 3– A python script to convert normalised elliptical Fourier coefficients to polygon mesh in Blender.

File 4 – Python script for retopologising procedure.

File 5 – An R script for data analysis as described in procedures 7 and 8.

File 6 – A Blender file consisting of raw data of 8 shells of procedures 1 – 4.

File 7 – PLY ASCII mesh 3D model of *Plectostoma laidlawi* Sykes 1902.

File 8 – PLY ASCII mesh 3D model of *Plectostoma crassipupa* van Benthem Jutting, 1952.

File 9 – PLY ASCII mesh 3D model of *Plectostoma christae* Maassen 2001.

File 10 – PLY ASCII mesh 3D model of *Opisthostoma vermiculum* Clements and Vermeulen, 2008.

File 11 – PLY ASCII mesh 3D model of *Plectostoma laidlawi* that was reduced in size by one-half and with slight modification of the last aperture size.

File 12 – PLY ASCII mesh 3D model of *Plectostoma christae* that was reshaped into an elongated form by reducing the model size (linear dimension) by one-half along the x and y axes, and by doubling the size along the z axis.

File 13 – PLY ASCII mesh 3D model of *Plectostoma christae* that was reshaped into a depressed form by doubling the model size along the x and y axes, and by reducing the size by one-half along the z axis.

File 14 – PLY ASCII mesh 3D model of *Opisthostoma vermiculum* that consists of one *Opisthostoma vermiculum* original 3D model of which the aperture was connected to a second enlarged *Opisthostoma vermiculum*.

Chapter 5

Association between shell morphology of micro-land snails (genus *Plectostoma*) and their predator's predatory behaviour

(*PeerJ* 2:e329, <http://dx.doi.org/10.7717/peerj.329>)

Thor-Seng Liew and Menno Schilthuizen

1 Institute Biology Leiden, Leiden University, P.O. Box 9516, 2300 RA Leiden, The Netherlands.

2 Naturalis Biodiversity Center, P.O. Box 9517, 2300 RA Leiden, The Netherlands.

3 Institute for Tropical Biology and Conservation, Universiti Malaysia Sabah, Jalan UMS, 88400, Kota Kinabalu, Sabah, Malaysia.

Email: T-S L: thorsengliew@gmail.com

MS: Menno.Schilthuizen@naturalis.nl

Author Contributions

Conceived and designed the experiments: LTS. Performed the experiments: LTS. Analyzed the data: LTS. Contributed reagents/materials/analysis tools: LTS MS. Wrote the paper: LTS MS.

Supplementary Information

(<http://dx.doi.org/10.6084/m9.figshare.830399>)

Abstract

Predator-prey interactions are among the main ecological interactions that shape the diversity of biological form. In many cases, the evolution of the mollusc shell form is presumably driven by predation. However, the adaptive significance of several uncommon, yet striking, shell traits of land snails are still poorly known. These include the distorted coiled “tuba” and the protruded radial ribs that can be found in micro-landsnails of the genus *Plectostoma*. Here, we experimentally tested whether these shell traits may act as defensive adaptations against predators. We characterised and quantified the possible anti-predation behaviour and shell traits of *Plectostoma* snails both in terms of their properties and efficiencies in defending against the *Atopos* slug predatory strategies, namely, shell-apertural entry and shell-drilling. The results showed that *Atopos* slugs would first attack the snail by shell-apertural entry, and, should this fail, shift to the energetically more costly shell-drilling strategy. We found that the shell tuba of *Plectostoma* snails is an effective defensive trait against shell-apertural entry attack. None of the snail traits, such as resting behaviour, shell thickness, shell tuba shape, shell rib density and intensity can fully protect the snail from the slug’s shell-drilling attack. However, these traits could increase the predation costs to the slug. Further analysis on the shell traits revealed that the lack of effectiveness in these anti-predation shell traits may be caused by a functional trade-off between shell traits under selection of two different predatory strategies.

Introduction

Predator-prey interactions are among the key ecological interactions that shape the diversity of biological form (Vermeij, 1987). Predation may drive the evolution of prey morphology, as prey forms that possess anti-predator characteristics increase survival and are selected under predation selection pressure. Among the studied prey traits, those of snail shells have been popular examples in demonstrating anti-predation adaptation (Vermeij, 1993). Among the reasons for this popularity are the fact that the shell is a conspicuous external structure, and the fact that its anti-predation properties may be observed directly as compared to other non-morphological anti-predation traits. Also, the interaction between predator and snail and the effectiveness of the anti-predation traits of the shell can be studied indirectly by examining traces and marks of both successful and unsuccessful predation on the shells (Vermeij, 1982; Vermeij, 1993). More importantly, the predator-prey interaction and evolution can be traced over time because shells with those predation marks are preserved in the fossil record (Alexander & Dietl, 2003; Kelley & Hansen, 2003).

The adaptive significance of shell anti-predation traits is better known for marine snails than for land snails (Goodfriend, 1986; Vermeij, 1993). This does not mean that land snails are less likely to be preyed upon in terrestrial ecosystems as compared to the marine ecosystems. In fact, the terrestrial ecosystem is a hostile environment to land snails, who face a taxonomically wide range of predators (Barker, 2004 and reference therein). The fact that molluscs have diversified to become the second largest phylum on land after the arthropods (Bieler, 1992; Brusca & Brusca, 2003), suggests that land snails have evolved successful

adaptations to deal with predation, and the evolution of shell morphology is likely to have played an important part.

The land snail shell is a single piece of coiled exoskeleton that consists of several layers of calcium carbonate. Its basic ontogeny follows a straightforward accretionary growth. Shell material is secreted by the mantle, which is located around the shell aperture, and is added to the existing aperture margin. Despite this general shell ontogeny that produces the basic coiled shell of all land snails, there is a great diversity of shell forms.

Many of the shell traits of land snails (e.g., whorl number and size, shell periphery form, umbilicus, shell coiling direction, aperture shape and size, and shell shape, thickness and size) are adaptive responses to abiotic ecological factors; by contrast, very few traits, viz. aperture shape and size, shell size, and shell wall thickness, are known to offer a selective advantage when faced with predation (Goodfriend, 1986). Since Goodfriend's (1986) review, few additional studies have shown the adaptive significance of land snail shell traits under predation pressure, namely, aperture form (Gittenberger, 1996; Quensen & Woodruff, 1997; Konumu & Chiba, 2007; Hosono & Hori, 2008; Hosono, 2012; Wada & Chiba, 2013); shell form (Quensen & Woodruff, 1997; Schilthuizen et al., 2006; Moreno-Rueda, 2009; Olson & Hearty, 2010); shell ribs (Quensen & Woodruff, 1997); and shell coiling direction (Hosono et al., 2010).

Conspicuously lacking from this list are protruding radial ribs and distorted-coiling of the last whorl. These traits have been shown to have anti-predation function in marine snails (Vermeij, 1993; Allmon, 2011), but it remains unclear whether the same is true for land snails, where such traits are less common (Vermeij & Covich, 1978). Probably the only land snail taxon that possesses both of these traits is the genus *Plectostoma* (Figure 1E). Some *Plectostoma* species have a regularly-coiled, dextral shell throughout their ontogeny, similar to most of the other gastropods. However, many *Plectostoma* species are unusual in having a shell that coils dextrally at the beginning of shell ontogeny (hereafter termed 'spire'), then changes direction at the transitional shell part (hereafter termed 'constriction'), and finally forms a last whorl that is detached from the spire and coils in an opposite direction (hereafter termed 'tuba'; van Benthem Jutting, 1952; Vermeulen, 1994; **Chapter 2**). Similar morphological transitions during shell ontogeny are known for other extant and fossil molluscs (e.g. Okamoto, 1988; Clements et al., 2008). In addition to this irregular coiling, there is great diversity in the shell radial ribs of *Plectostoma* in terms of density, shape, and intensity (i.e. amount of shell material in the ribs) (van Benthem Jutting, 1952; Vermeulen, 1994). Clearly, *Plectostoma* is a good model taxon to improve our understanding of the ecological function of both of these unusual shell traits.

So far, the only known predator of *Plectostoma* snails is the slug *Atopos* (Rathoussiidae) that uses a shell-apertural entry strategy to attack juvenile snails or uses a shell-drilling strategy to attack adult snails (Schilthuizen et al., 2006; Schilthuizen & Liew, 2008). In addition, we have also observed *Pteropyyx* beetle larvae (Lampyridae) attacking *Plectostoma* snails using a shell-apertural entry strategy (Figures 1A and 1B; Supplementary materials File S1, Page 1:

Table S1). It has been suggested that predatory behaviour within a taxon would be quite conserved (Barker, 2004 and reference therein).

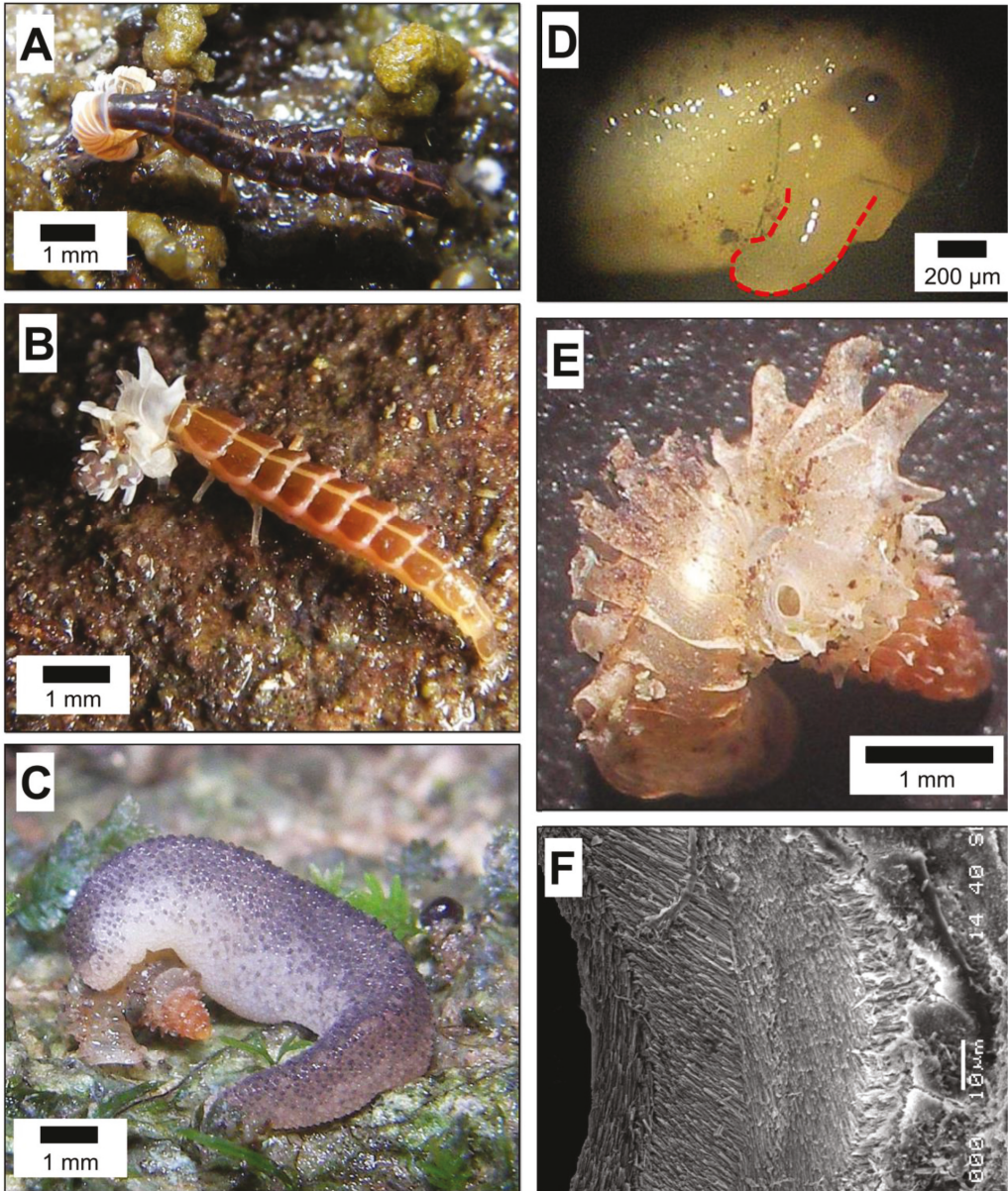


Figure 1. Predatory strategies that are used by *Atopos* slugs and Lampyridae beetle larvae to attack micro-land snails – *Plectostoma* species. (A) *Pteroptyx* cf. *valida* (Olivier, 1883) larva, which was probably at its fifth instar, attacking *Plectostoma laidlawi* (Sykes, 1902) by shell-apertural entry. (B) *Pteroptyx tener* (Olivier, 1907) larva, which was probably at its fifth instar, attacking *Plectostoma fraternum* (Smith, 1905) by shell-apertural entry. (C) *Atopos* slug attacking *Plectostoma concinnum* (Fulton, 1901) by shell-drilling. (D) *Atopos* slug proboscis (marked with red outline) that was used for shell-drilling (the proboscis was not fully extended). (E) A drill hole on the shell of *Plectostoma concinnum* (Fulton, 1901) made by *Atopos*. (F) The appearance of the margin around the drill hole.

Indeed, the predatory behaviour of these two predator taxa are generally concordant with that recorded from previous studies. Lampyridae beetle larvae use shell-apertural entry to attack and consume the snail (Clench and Jacobson, 1968; Thornton, 1997:65; Archangelsky and Branham, 1998; Wang et al., 2007; Madruga Rios and Hernández Quinta, 2010, for details see Supplementary materials File S1, Page 3: Table S2). Rathousiidae slugs are known to have two strategies to attack and to consume the snail. Primarily, it uses shell-apertural entry (Heude, 1882-1890; Kurozumi, 1985; Wu et al., 2006; Tan & Chan, 2009) and secondarily, it uses shell-drilling when the opening of the prey is not available or accessible (Kurozumi, 1985; Wu et al., 2006; for details see Supplementary materials File S1, Page 4: Table S3).

Although some of the *Plectostoma* shell traits have been shown to have some association with the shell drilling behaviour of the rathousiid slug *Atopos* (Schilthuizen et al., 2006), it is unclear how exactly the shell traits help *Plectostoma* defend against attacks from the *Atopos* slug and *Pteroptyx* larva. Direct observations and experiments on the interaction between the *Plectostoma* snails and their predators are prohibited by the predators' ecology. Both are nocturnal predators and they probably hide in the cracks of limestone rocks during the day. Hence, they appear to be very sensitive to light and manipulation.

Here, we attempt to reconstruct the predatory strategies of one of the predators, the *Atopos* slug, against the *Plectostoma* snail and try to empirically unravel any anti-predation function of the unusual *Plectostoma* shell traits through a series of experiments, and direct and indirect observations (hereafter known as "Tests"). We examined the effectiveness of several *Plectostoma* shell traits, namely, 1) ribs on shell surface ; 2) shell whorl thickness; 3) shell tuba; and 4) snail resting behaviour. These three shell traits and one behavioural trait were selected because these are known in other snail taxa for having antipredation properties against shell-apertural entry and shell-drilling behaviour by other predators (see overview in Goodfriend, 1986; Vermeij, 1993). We examined the effectiveness of the first three shell traits of *Plectostoma* against *Atopos* slug shell-drilling (Test 1); and the effectiveness of the last two traits of *Plectostoma* against *Atopos* slug shell-apertural entry (Test 2). Additionally, we investigate possible constraints in the development of anti-predation shell traits. Finally, we discuss the results of this study in the context of predator-prey interactions and shell-trait evolution in general.

Materials and Methods

Ethics Statement

The permissions for the work in the study sites were given by the Wildlife Department of Sabah (JHL.600-6/1 JLD.6, JHL.6000.6/1/2 JLD.8) and the Economic Planning Unit, Malaysia (UPE: 40/200/19/2524).

Predation tests

Test 1: *Plectostoma* snails' anti-predation traits against *Atopos* slug shell-drilling behaviour.

Study on predatory drill holes on the shell provide information about the predator's drilling behaviour (Kowalewski, Dulai & Fürsich, 1998). *Atopos* and other Rathousiidae slugs drill a distinctive hole in the prey shells (Schilthuizen et al., 2006; Figure 1E and 1F; Supplementary materials File S1, Page 2; Kurozumi, 1985; Wu et al., 2006). Thus, the location and the size of the drill hole provide important information about the drilling behaviour of the slugs. In test 1, we tested the effectiveness of the tuba and shell ribs by examining whether *Atopos* drill holes on the tuba of the prey shell (Test 1 a) and whether *Atopos* have a tendency for drilling holes between two ribs (Test 1 a). In addition, we also examined the correlation between the rib density and other shell traits, such as rib intensity (i.e. amount of shell material in the ribs) (Test 1 b), shell whorl thickness (Test 1 c), and shell size (Test 1 c) (Figure 2).

Test 1 (a) – Association between slug shell-drilling, and adult snail shell tuba and rib density.

Like in marine predator-snail interactions, where predators tend to drill a hole at less-ornamented positions of the prey shell (Kelley & Hansen, 2003) we may expect *Atopos* to drill its holes preferentially between shell ribs, rather than through them. Conversely, if snail shell ribs are adaptive traits in the context of the slug's shell-drilling behaviour, we would expect the snail shell to have evolved more densely-placed, thicker, and more protruded ribs to defend themselves against shell drilling predators.

To examine the association between shell rib density and drill hole position, we studied *Plectostoma* shell specimens from museum collections collected from two limestone outcrop, namely, Batu Kampung (5°32'11"N 118°12'47"E), and Batu Tomanggong Besar (5°32'3"N 118°23'1"E). These two limestone outcrops support dense *Plectostoma* populations, which show high variability in shell rib density. We selected museum specimens that belongs to two samples (i.e. populations) from Batu Kampung (*P. concinnum*, collection numbers BOR 1690, BOR 2196), and 9 samples (i.e. populations) from Batu Tomanggong Besar (collection numbers RMNH.MOL 330506; *P. cf. inornatum*: Samples T29, T33, T34, and T45; *P. fraternum*: Samples T7, T21, T22, and T42; and *P. cf. fraternum*: Sample T 44). All were collected between April 2002 and January 2004.

Each of the samples consisted of *Plectostoma* empty shells collected beneath the rock face where living *Plectostoma* individuals were also found. For each sample, shells with a characteristic *Atopos* drill hole were selected for analysis. We divided the shells into two groups based on the drill hole position: 1) hole directly through the shell wall and located between two ribs (hereafter BETWEEN RIBS), and 2) hole drilled through one or two ribs as well as the shell wall (hereafter ON RIBS). The two groups were used as the dependent variable, and were binary scored as (1) for BETWEEN RIBS and (0) for ON RIBS. In addition, we identified three predictor variables that may influence the slug drilling behaviour. First, the slug proboscis size, which was measured as the greatest diameter (mm) for circular and slightly oval drill holes (hereafter HOLE SIZE). Second, the rib density of

the shell which was quantified as the total number of ribs on the shell (hereafter RIB DENSITY) because all shells have a similar number of whorls (mean: 5.15, SD: 0.35; Supplementary materials File S2, Page 22: Table S2). Lastly, the random chance – the probability that a hole was made in between ribs, which is related to the HOLE SIZE and RIB DENSITY. For example, by random chance, a slug with a narrow proboscis (i.e., low HOLE SIZE) has a greater probability to drill a hole in between the ribs on a shell that has fewer ribs (low RIBS DENSITY) because more rib spacings that are larger than the slug proboscis size are available. Thus, we counted total number of rib spacings larger than HOLE SIZE (hereafter CHANCES).

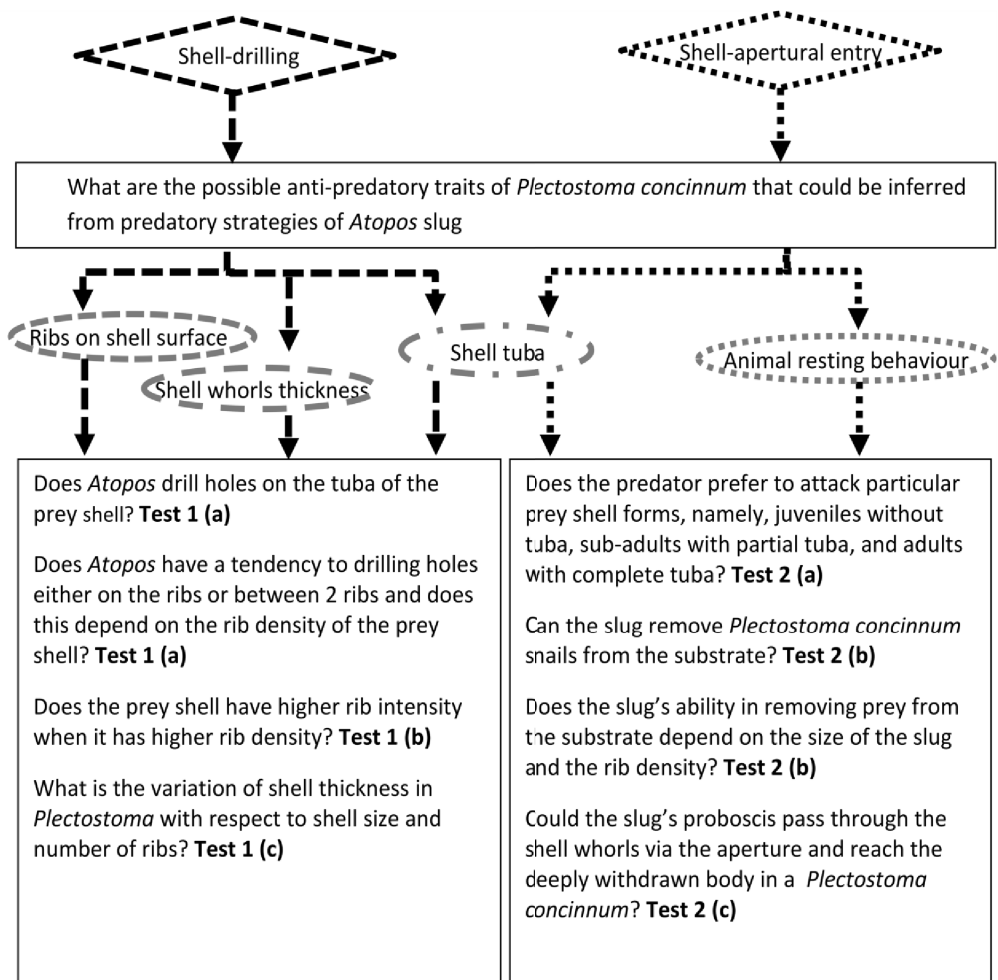


Figure 2. Flowchart shows experimental design for 8 research questions of this study. Bold text represents the respective tests for each research question; text bounded in each diamond shape represents the predatory behaviour of *Atopos*; text bounded in each oval shape represents the *Plectostoma* shell trait that was tested for their anti-predation property.

We used a logistic regression to model the likelihood that the slug drills a hole either BETWEEN RIBS or ON RIBS as a function of HOLE SIZE, RIB DENSITY, and CHANCES (i.e., Predicted logit of (BETWEEN RIBS) = $\beta_0 + \beta_1*(\text{HOLE SIZE}) + \beta_2*(\text{RIB DENSITY}) + \beta_3*(\text{CHANCES})$). Our objective was to investigate the amounts of variance attributable to each predictor variable. The analysis was done in R statistical package 2.15.1 (R Core Team, 2012) and the R scripts can be found in Supplementary materials File S3.

Test 1 (b) – Correlation between *Plectostoma* shell rib density and rib intensity.

In addition to rib density, it is essential to quantify the amount of shell material that *Plectostoma* snails invest to grow thick and protruded ribs (hereafter we call this rib intensity). However, we cannot quantify this from the same shell remains that we had used in test 1(a) because the shell ribs of these specimens were heavily eroded. Thus, we analysed rib intensity from 14 preserved *Plectostoma* individuals that were collected alive from the same rock face at Batu Kampung and Tomanggong Besar, where the shell remains were collected (collection number RMNH 330508; T 21 (n = 3), T 22 (n = 1), T 42 (n = 2), T 7 (n = 1), T 44 (n = 1), BOR 2991 (n = 3), T 33 (n = 3)). These 14 shells have different rib densities (47 – 138 ribs per shell), which spans the broadest possible range of rib density, and have the most intact ribs on the shell.

We used X-ray microtomography (μ CT) to estimate the amount of shell material that *Plectostoma* invests in rib growth (Figure 3). First, we obtained a series of X-ray tomographies of each shell with a high-resolution SkyScan 1172 (Aartselaar, Belgium). The scan conditions were: 60 kV; pixels: 668 rows X 1000 columns; camera binning 4 X 4; image pixel size 7 – 9 μ m; rotation step 0.5°; rotation 360° (Step 1 in Figure 3).

Then, we reconstructed 2D grey scale images (i.e. cross-sections) from X-ray tomography series with NRecon 1.66 (©SkyScan). The settings were: beam-hardening correction 100% and ring artifacts reduction 20. Next, these 2D images were transformed to the final half-tone binary images for each shell in CTAnalyser 1.12 (©SkyScan). This was done by filtering out grayscale index <70. At this stage, each shell was represented by hundreds of 2D cross-section binary images (Step 2 in Figure 3).

Each of these 2D images consisted of white and black pixels, where the white pixels represent the solid shell material (shell together with ribs) and the black pixels are background or lumen. When the series of cross-section images was analysed, the total voxels which represent the shell material volume could be determined. Hence, we analysed the volume of shell material from two datasets of each shell. The first was the original 2D cross-section binary images which represent the total volume of shell material contained in whorls and ribs (Step 3 in Figure 3). The second was the volume of shell material contained in the shell whorls only, after removal of the shell ribs from each cross-section image. The latter was done manually by changing white rib-pixels into black ones in Paint (©Microsoft Windows 7) (Step 4 in Figure 3). After that, the volume of shell material was calculated for both datasets with Individual 3D object analysis, as implemented in CT Analyser 1.12 (©SkyScan) (Step 5 in Figure 3). Finally, the rib intensity (i.e. amount of shell material in the

ribs) was calculated by subtracting the volume after rib removal from the total volume with ribs included (Step 6 Figure 3).

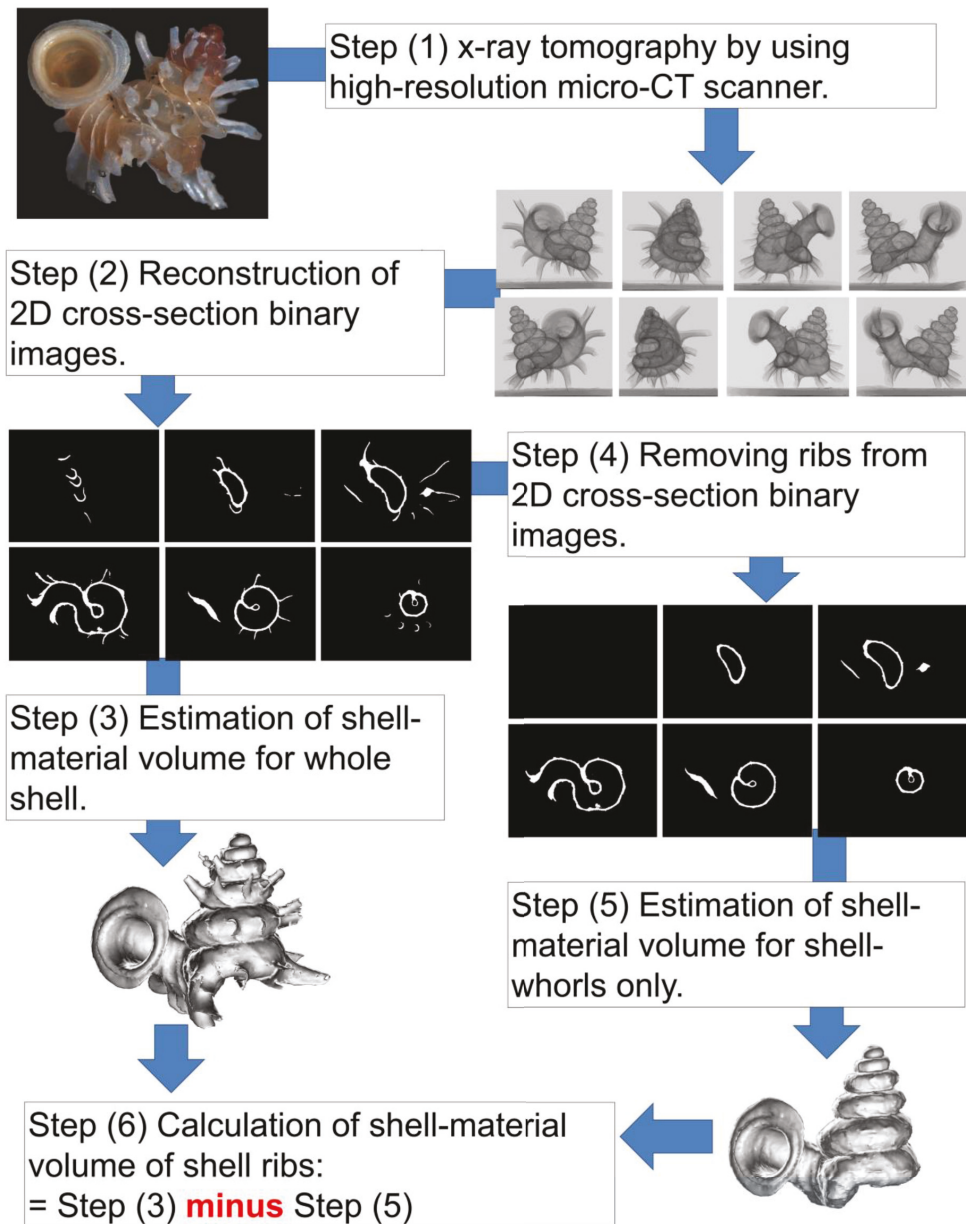


Figure 3. Procedures used to quantify the shell volume of material of the ribs and shell whorls (Test 1b).

We wished to test if there is a significant correlation between rib intensity and number of ribs. However, as there is variability in the shell size for the shells that vary in rib density, we quantified a set of size variables of the shell (number of whorls, height, width, and volume of shell material of the shell whorls after rib removal) and then checked for confounding effects of shell size variables with the anti-predation shell traits. The results showed that only one of the shell size variables, i.e. the volume of shell material after rib removal, is significantly correlated with the anti-predation shell traits (Supplementary materials File S2, Page 23: Table S3).

So, we also ran an additional partial correlation test between the same two variables (rib intensity vs. number of ribs) after controlling for total volume of shell material after rib removal, to account for confounding effects of the shell size difference. Pearson correlations were performed in the two tests as all variables were normally distributed (Shapiro-Wilk normality test, $p > 0.05$) with R statistical package 2.15.1 (R Core Team, 2012) and R scripts can be found in Supplementary materials File S3.

Test 1 (c) – Relationships between shell thickness, rib number, and shell size.

We obtained 3D models (PLY format) of each of the 14 shells by using the original 2D cross-section binary images that were obtained from experiment 1(b). After that, we measured the shell thickness of the last spire whorl by making a cross-section of the digital 3D models with Blender 2.63 (Blender Foundation, www.blender.org). We obtained the shell thickness data from the digital 3D models instead of the actual specimens because it is difficult to make a clean cross-section on this tiny shell.

In order to assess if the prey invests more shell material in increasing the shell thickness when it invests less in the ribs, we tested the correlation between shell thickness and number of ribs. Similar to test 1(b), we also ran an additional partial correlation test between the same two variables after controlling for the volume of shell material after rib removal, to account for the variability in shell size differences. In addition, the relationships between shell thickness, rib number, and shell size were explored. Pearson correlations were performed in these tests as all variables were normally distributed (Shapiro-Wilk normality test, $p > 0.05$) in R statistical package 2.15.1 (R Core Team, 2012) and R scripts can be found in Supplementary materials File S3.

Test 2: *Plectostoma* snails' anti-predation traits against the apertural-entry behaviour of the *Atopos* slug

Unlike test 1, testing the associations between the prey shell traits and slug apertural-entry behaviours is more challenging because this type does not leave a distinctive trace on the prey shell after successful predation. One of the ways to assess the interaction between the prey shell and predator behaviour is with a manipulative experiment. However, this slug is very sensitive and hard to manipulated and thus sufficient replicates cannot be achieved. Hence, we used observations (Test 2 a), indirect data (Test 2 b), and a simulative model (Test 2 c) to unravel the effectiveness of the shell traits against the predator shell-apertural entry behaviour (Figure 2).

Test 2 (a) – Observation of predator preferences for three different prey shell forms.

So far, we have not observed drill holes in *Plectostoma* shells with no tuba (Schilthuizen et al., 2006; Liew TS, unpublished data), and only once the slug was seen attacking a juvenile prey without a tuba by shell-apertural entry (Schilthuizen & Liew, 2008). However, we do not know if the slug has a preference for juvenile or adult prey. Thus, we conducted a small experiment to check prey age preference.

Two *Atopos* slugs, with body lengths of 7 and 15 mm, were collected from Site A (No. 7 & 8 in Supplementary materials File S1, Page 1: Table S1). Each of the slugs was kept in a plastic box (12 cm × 8 cm × 7.5 cm), which contained a piece of limestone rock and its temperature and humidity were controlled. The boxes were kept under the table in a room with opened window to simulate the natural habitat for the slugs that are active nocturnally and rest in a shaded place during the daytime.

Live *P. concinnum* individuals were collected from Batu Kampung for this test. For each experiment, three individuals were placed on the rock in the plastic boxes. The three preys represented three different shell forms (i.e. growth stages): 1) shell with no tuba and peristome lip (juvenile, e.g. Figure 4A: shells e – g), 2) shell with partial tuba but no peristome lip (sub-adult, e.g. Figure 4A: shells h – j), and 3) shell with fully grown tuba and peristome lip (adult, e.g. Figure 4A: shell l). During the experiment, the interactions between predator and prey were checked every 3 hours to minimise the disturbance to the organisms. Each experiment ended after the slug was observed inactive (i.e. hiding under the rock) and at least one of the prey was consumed. After that, the three prey shells were removed for further analysis, and replaced with another three living snails to start a new experiment.

We ran nine such experiments, one with slug No.7 and eight with slug No. 8. After each experiment, each of the three shell forms was scored as having either survived or died (Specimens deposited in BOR 5657). Also, the shell of each dead prey was examined for possible traces left by slug predation. In addition, we also estimated the predator's attack and consuming time from the time intervals between the moments when all prey were last seen alive and the moment the experiment was ended. After each experiment, we checked if all three shell forms were equally likely to be killed by the predator.

Test 2 (b) – Effectiveness of resting behaviour of *Plectostoma* snails against *Atopos* shell-apertural entry predatory behaviour.

When a *Plectostoma* snail is resting or is disturbed, it withdraws its soft body into the shell and adheres its shell aperture to the substrate. Thus, when the snail is in this position, its aperture is not accessible to the slug, and for the slug to access the shell aperture, it would need to remove the shell from the substrate. In this test, the ability of the slug to manipulate the adherent prey shell was inferred by examining the drill hole location of the specimens used in Test 1(b). We predict that the sector of the shell facing the substrate is less susceptible to drilling by the slug if it is unable remove the adherent prey shell from the substrate.

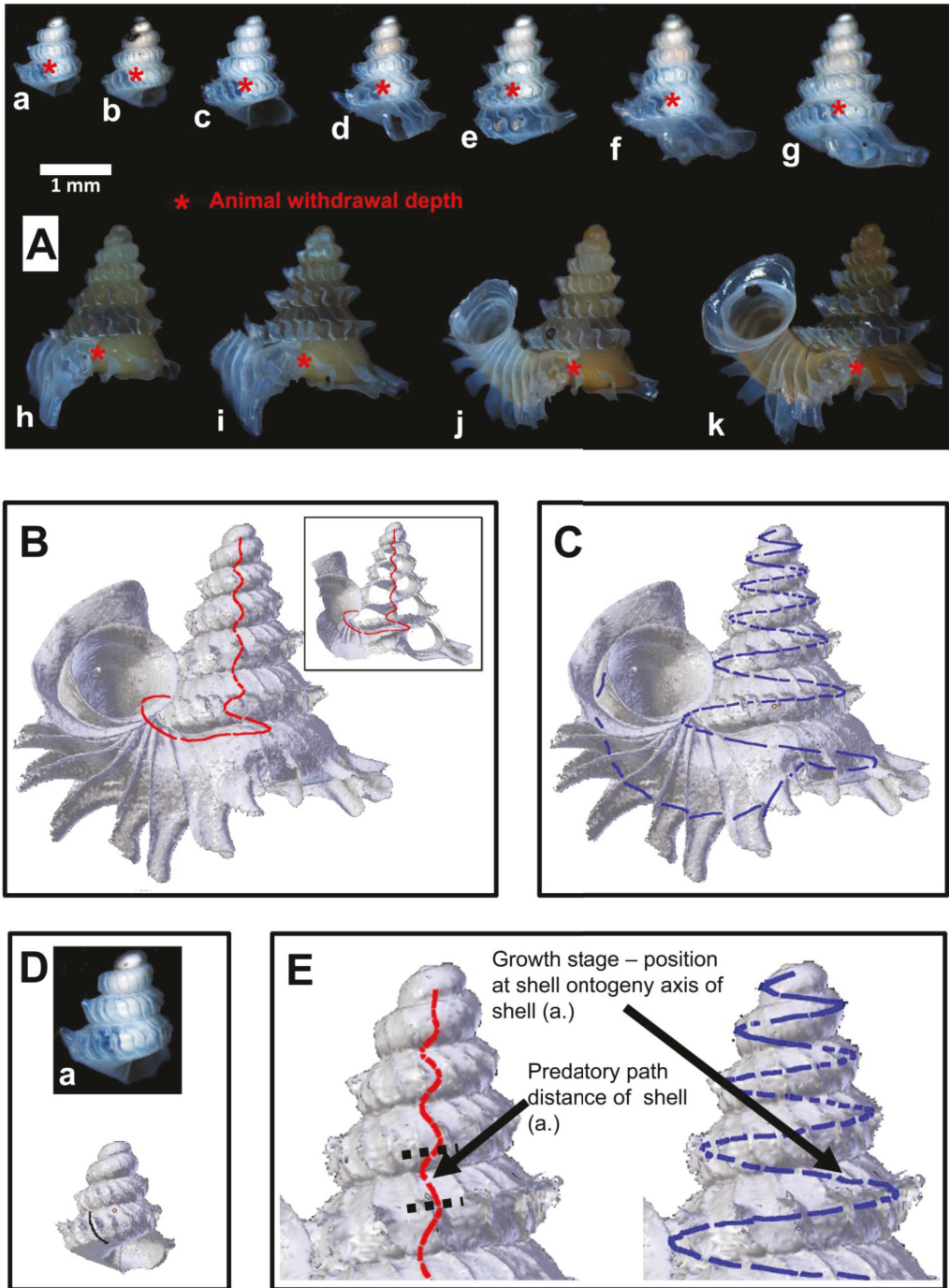


Figure 4. Shell withdrawal path analysis of *Plectostoma concinnum* (Fulton, 1901). (A) Animal withdrawal depth at different growth stages of the shell. (B) Predatory path in the shell (red line). (C) Shell ontogeny axis (blue line). (D) Determination of animal withdrawal depth and growth stage by using photograph and 3D shell model. (E) Transferring information of predatory path and growth stage from each shell to an adult reference shell.

For each of 133 shells, we recorded the location of the drill hole. We divided drill-hole locations of these shells into four categories, which represent different sectors, namely: A) shell whorls that face the substrate; B) shell whorls that face the tuba; C) shell whorls opposite (A); and D) shell whorls opposite (B) (Figure 5A). Then, we tested if all four sectors of shell whorls are equally susceptible to slug drilling by using chi-squared test (goodness-of-fit). We also tested if the rib density (indicating prey defence), differ among these four categories with Kruskal-Wallis rank sum test (`kruskal.test`). All statistical analyses were done in R 2.15.1 (R Core Team, 2012) and R scripts can be found in Supplementary materials File S3.

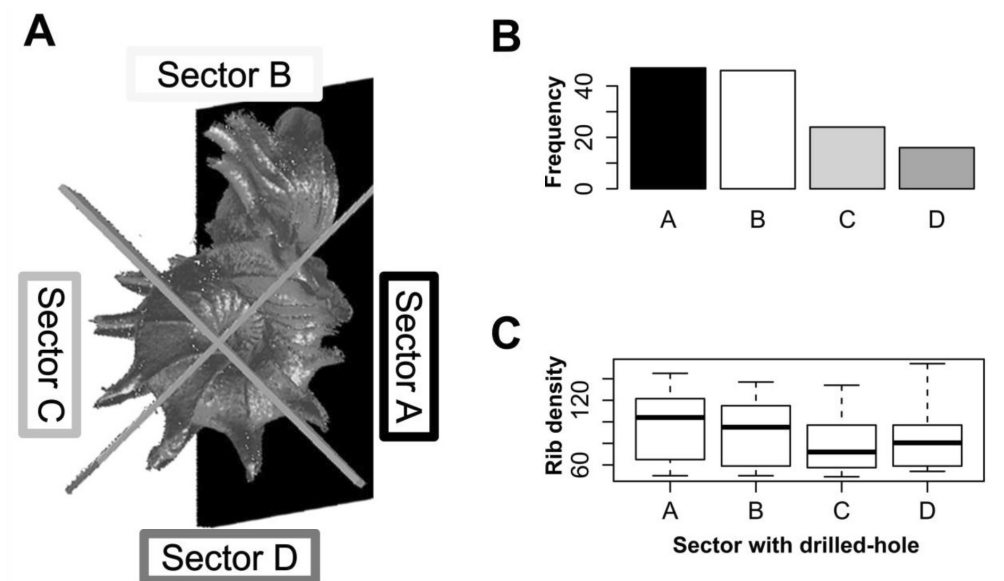


Figure 5. Analysis of the drill hole location on the shells. (A) four different sectors of the shell whorls divided with reference to the snail's position when adhering to the substrate: Sector A – shell whorls facing the substrate; Sector B – shell whorls facing the tuba; Sector C – shell whorls at the back of Sector A; and Sector D – shell whorls at the back of Sector B. (B) Frequencies of drill holes found in each of four shell whorl sectors are significantly different ($\chi^2 = 22.1$, $df = 3$, $p < 0.0001$). (C) The χ^2 rib density of the shells does not significantly differ among these four shell sectors (Kruskal-Wallis $\chi^2 = 3.71$, $df = 3$, $p = 0.29$).

Test 2 (c) – Effectiveness of prey's shell whorl morphometrics against shell-apertural entry by *Atopos proboscis*.

When a *Plectostoma* snail withdraws into its shell, part of the lower shell whorls are left vacant. We named this vacant part the 'predatory path', located between shell aperture and soft-body withdrawal terminal point (i.e. between the endpoint of the shell whorls and the withdrawn snail's operculum). In shell-apertural entry predation events, the predator's

feeding apparatus would need to pass through the predatory path to reach the snail that is withdrawn deeply into the shell. Hence, success of a predation event would depend on the interplay between the morphometrics of both the prey's predatory path and the predator's feeding apparatus. In this section, we quantified these morphometrics. Because both prey and predator traits vary throughout their growth, we assessed variability of these morphometrics at several different growth stages.

For the predatory path analysis, we selected from site A, 11 living snails representing a range of shell developmental stages (Figure 4A, Specimens deposited in BOR 5656). Then, in the field, we disturbed each snail with a forceps so that the animal withdrew into the shell. Immediately after that, the snail was killed with and preserved in 70% ethanol. After arriving in the laboratory, we photographed each specimen to record the withdrawal position of the animal in its translucent shell. Then, we obtained 3D models (PLY format) of these shells, based on the X-ray microtomography (μ CT) technique as described in Test 1(b), using CT Analyser 1.12 ($^{\circ}$ SkyScan).

After the 3D models were obtained, we extracted the whole predatory path from the 3D model of an adult shell (hereafter "reference shell"). This is the shortest possible path when traveling inside the shell whorls from the aperture in the direction of the apex of the adult shell (Figure 4B). We also extracted from the reference shell the whole shell ontogeny axis (**Chapter 4**), which represents the entire shell's growth (Figure 4C). Next, we determined the terminal withdrawal point for each corresponding growth stage from the photographs and 3D models of the 11 shells (Figure 4D). After that, we calculated the distance of the portion of the whole predatory path which corresponded to the predatory path for each the 11 growth stages, and plotted these predatory path distances on the ontogeny axis (Figure 4E). Then, we described the geometry of the shell whorls as a 3D spiral, in terms of torsion and radius of curvature (Harary & Tal, 2011), which were used to explore the geometry of the whorls along the predatory path.

Then, we performed the morphometrics of the slug's proboscis. However, we could not obtain an accurate measurement for the length of a fully extended proboscis because we were limited by the small number of *Atopos* specimens and the fact that the proboscis was not fully extended in most preserved specimens. Nevertheless, we attempted to estimate the length of the proboscis based on the following facts and assumptions: (1) we know that the drill hole size corresponds to proboscis diameter (Kurozumi, 1985; Wu et al. 2006); (2) we know the maximum and minimum sizes of the drill holes from Test 1(a) are 0.13 mm and 0.33 mm, which represent the range of proboscis diameters of *Atopos* in Site A and Tomanggong Besar; and (3) we assume that the dimension (i.e. diameter \times length) of our slug proboscis is similar to those published for *Atopos kempii* (Ghosh, 1913: Plate X) (Figures 6A and 6B). Based on this information, we estimated that the minimum and maximum dimensions of the proboscis are 0.13×0.8 mm and 0.33×1.7 mm.

Finally, we overlaid the shell predatory path with the slug proboscis morphometrics across the ontogenetic trajectory. We evaluated the growth stages for which the prey shells are not

susceptible to the predator's shell-apertural entry, by comparing the morphometrics for the prey predatory path with the predator proboscis. To do this, we considered that the prey is safe from the predator when the distance of the predatory path is longer than the predator's proboscis length and when the prey's radius of curvature is smaller than predator's proboscis diameter, so that the predator's proboscis is too large to enter the shell. However, we do not know to what extent the possible exhalation or desanguination would change the proboscis diameter during the sucking.

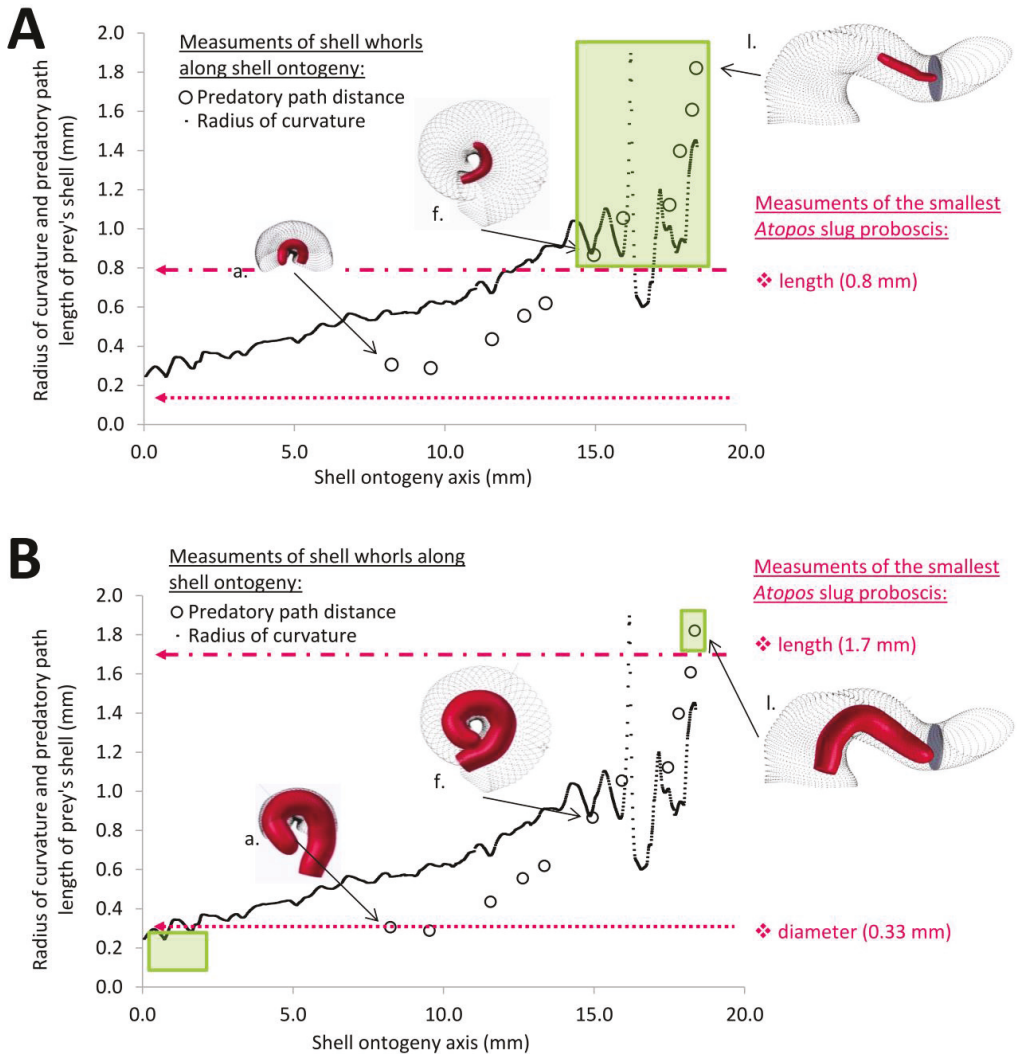


Figure 6. Association between the predator proboscis morphometrics (pink symbols) and the prey shell whorls morphometrics (black symbols). Green boxes represent the section of shell ontogeny (i.e. prey growth stages) that are not susceptible to *Atopos* attack by shell-apertural entry (i.e. predatory path distance > proboscis length & whorl radius of curvature < proboscis diameter). The insets show the simulation of interaction between slug proboscis and snail predatory path at three growth stages, namely, a, f and l (see figure 3A). (A) Smallest predator scenario. (B) Largest predator scenario.

Results

First set of tests: (1) *Plectostoma* anti-predatory traits against *Atopos* shell-drilling behaviour.

Test 1 (a) – Association between slug shell-drilling behaviour and adult snail shell tuba and rib density.

The drill hole diameters of the 133 prey shells varied between 0.13 mm and 0.33 mm (mean = 0.230 mm, SD = 0.045, n = 133; Supplementary materials File S2, Page 2 – 19: Figure S2 - S12). Four of these (3%) had two drill holes, one on the tuba and another on the spire (Supplementary materials File S2, page 20 – 21: Figure S13). The drill hole of 70 shells (53%) was made through the ribs (ON RIBS), whereas the drill hole of the other 63 shells (47%) was made in between the ribs (BETWEEN RIBS). The result showed a logistic model that was more effective than the null model as follows: Predicted logit of (BETWEEN RIBS) = 10.448 - 11.316*(HOLE SIZE) - 0.095*(RIBS DENSITY) + 0.033*(CHANCES), (AIC = 83.382; $\chi^2 = 109.63$, df = 3, p = 0; Figure 7). According to the model, the statistically significant coefficients were for intercept ($\beta_0 = 10.448$, Z = 2.867, p = 0.001) and RIB

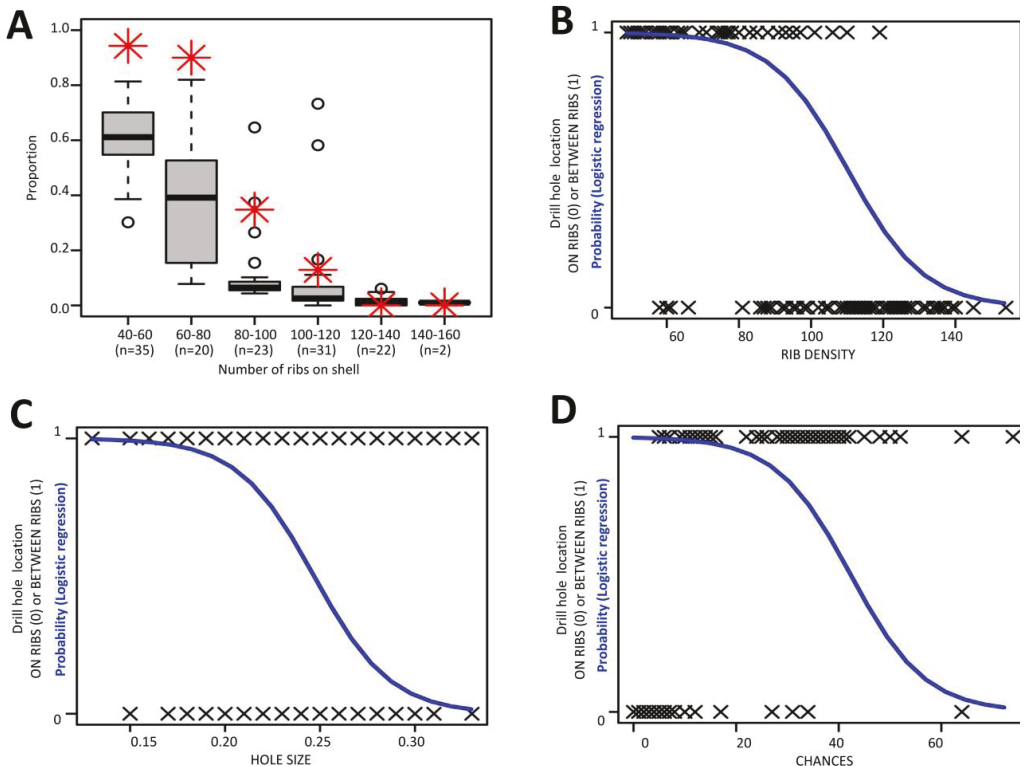


Figure 7. Analysis of the relationship between the likelihood of the slug drill hole BETWEEN RIBS and the three predictor variables. (A) Proportion of the ribs spacings larger than HOLE SIZE for the shells (boxplot) and the proportion of shells having holes in between ribs (red asterisk) for each RIB DENSITY category. (B) – (D) Logistic curve showing the probability of the slug drill hole in between the ribs based on (B) RIB DENSITY (i.e., total number of ribs on shell), (C) HOLE SIZE (i.e., drill hole size, which represents the slug proboscis size), and (D) CHANCES (i.e., number of the ribs spacings that are larger than HOLE SIZE).

DENSITY ($\beta_2 = -0.0916$, $p < 0.0005$; Odds Ratio = 0.91, CI = 0.87-0.95). The number of available space for drilling in between ribs (CHANCES) and the slug size (HOLE SIZE) were not significant ($p > 0.1$). In other words, the slug is less likely to drill a hole through the ribs on a densely ribbed shell, and this tendency is independent of hole size and chance.

Test 1 (b) - Correlation between rib density and rib intensity of *Plectostoma*.

Different *Plectostoma* species and populations exhibit high variability in the rib density, ranging from 49 ribs to 154 ribs per shell. There is a significant negative correlation between the rib intensity (i.e. amount of shell material in the ribs) and the number of ribs of the shell (Figure 8A; $r = -0.95$, $t = -10.74$, $df = 12$, $p < 0.001$; Supplementary materials File S2, Page 22 and 24: Table S2, Figure S14). Both rib intensity and number of ribs are strongly correlated with the amount of shell materials after removal of the ribs (= shell size) (Supplementary materials File S2, Page 25: Figure S15 and S16). Nevertheless, after controlling for this, there is still a significant negative correlation between rib intensity and number of ribs on the shell (Figure 8B; $r = -0.63$, $t = -2.71$, $n = 14$, $p < 0.001$). These results indicate that there is a statistically significant trade-off between rib density and rib intensity, irrespective of shell size.

Test 1 (c) – Variation of shell thickness of *Plectostoma* with varying shell size and number of ribs.

Different *Plectostoma* populations and species have different shell thicknesses, ranging between 0.29 mm and 0.46 mm. There is a significant negative correlation between shell thickness and number of ribs (Figure 9A; $r = -0.73$, $t = -3.70$, $df = 12$, $p < 0.005$; Supplementary materials File S2, Page 22: Table S2). Shell thickness is strongly correlated with the amount of shell materials after removal of the ribs (= shell size) (Supplementary materials File S2, Page 26: Figure S17). After controlling for this, there is no significant correlation between the shell thickness and the number of ribs on the shell (Figure 9B; $r = 0.06$, $t = -0.192$, $n = 14$, $p = 0.85$). Thus, larger *Plectostoma* shells simply are thicker.

Second set of tests: (2) Anti-predation traits in *Plectostoma* against shell-apertural entry behaviour of *Atopos*.

Test 2 (a) – Observations on predator preference for different prey shell growth stages.

Table 1 shows the snails of three ontogenetic categories that did and did not survive. It indicates that the slugs prefer to attack and consume prey with an incomplete tuba or no tuba at all (Table 1; Supplementary materials File S2, Page 27 – 29: Table S4, Figure S18). In all observations, adults with a complete tuba and peristome survived shell-apertural entry. The predatory behaviour of the slug could not be observed directly because the slug proved very sensitive to disturbance and light. Shells of consumed prey did not show any drill-holes, which confirms Schilthuis and Liew (2008)'s single observation that the slug attacked the juvenile prey via the shell aperture. Furthermore, 11 out of the 15 predated shells still had an intact operculum attached to the posterior side of the shell aperture (Figure 10). It is likely that it took the slug at least seven hours to attack and consume the entire soft body of juvenile and sub-adult prey (Test no. 12 in Table 1).

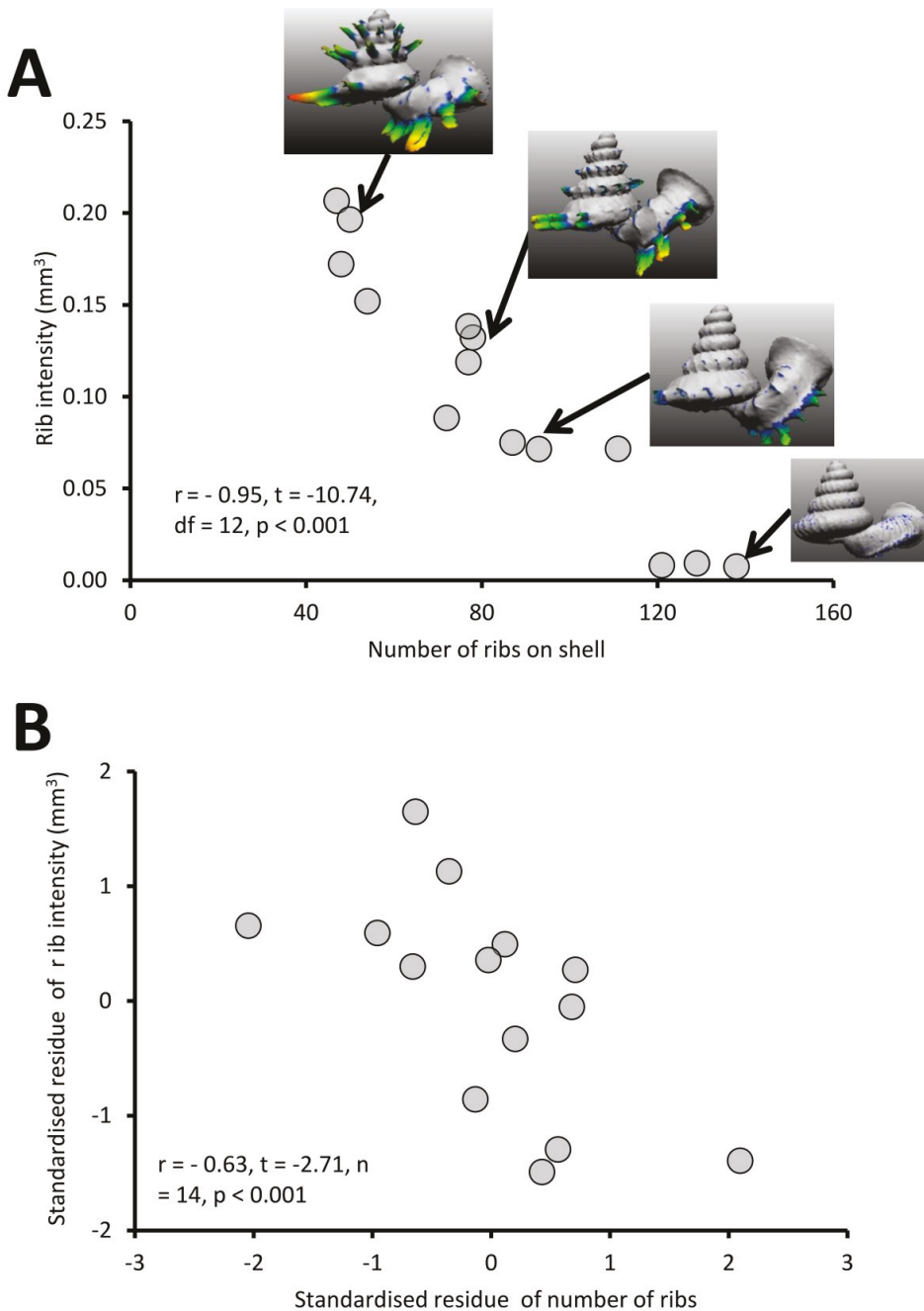


Figure 8. The graphs show the correlation between the number of ribs on the shell and rib intensity before and after controlling for shell size. (A) Correlation between number of ribs on the shell and rib intensity ($r = -0.95, t = -10.74, df = 12, p < 0.001$). The rib intensity (i.e. total shell material of all shell ribs in mm^3) and the number of ribs were measured from 14 shells, which belong to several *Plectostoma* species and populations that vary in rib number. The inset of four examples of shells. (B) The graph shows the partial correlation of number of ribs on the shell and rib intensity after correcting for total shell material volume ($r = -0.63, t = -2.71, df = 14, p < 0.001$). The group mean values are represented by “0” on both axes.

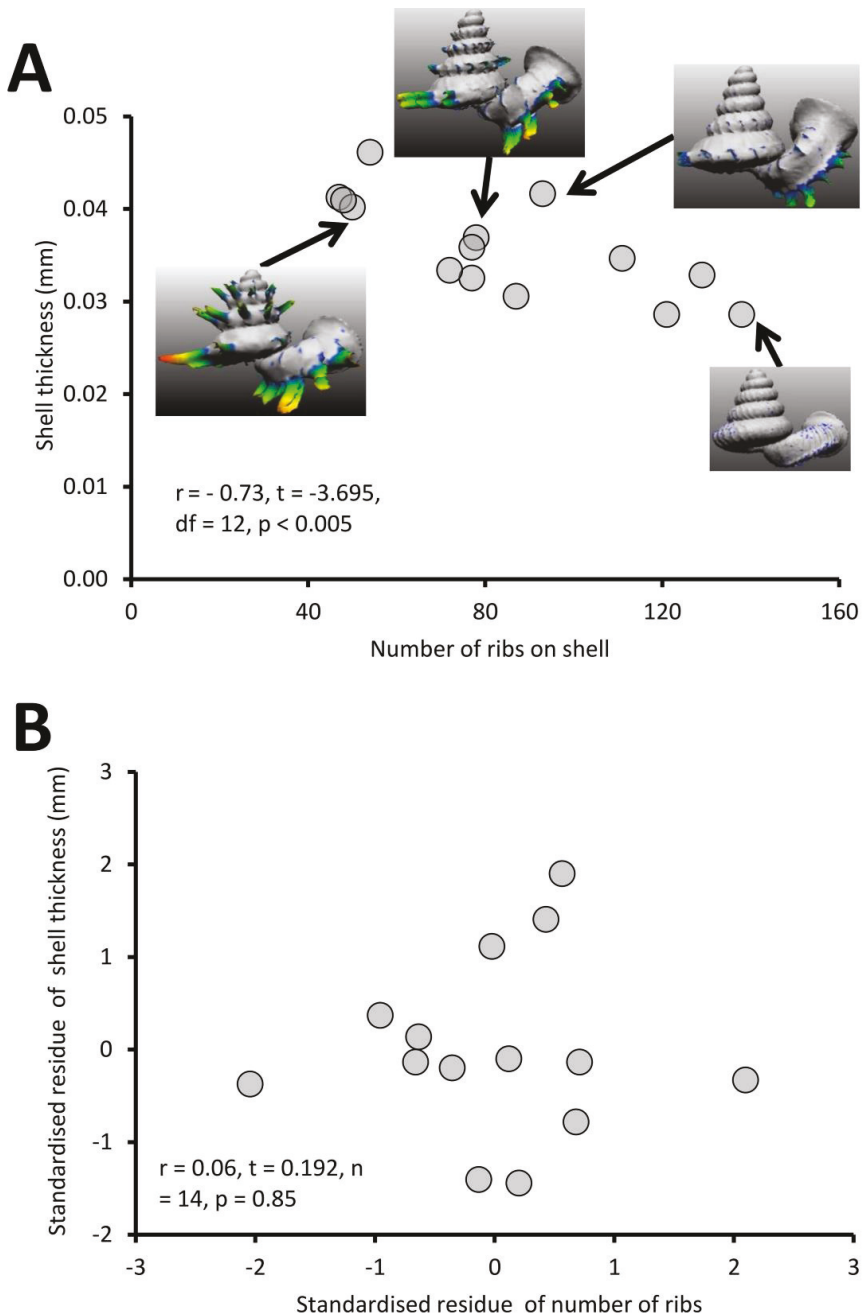


Figure 9. The graphs show the correlation between the number of ribs on the shell and shell thickness before and after controlling for shell size. (A) Correlation between the number of ribs on the shell and shell thickness ($r = -0.73, t = -3.7, df = 12, p < 0.005$). The shell thickness (mm) was measured from 14 shells, which belong to several *Plectostoma* species and populations that vary in rib number. The inset of four examples of shells. (B) The graph shows the partial correlation of number of the ribs on the shell and shell thickness after correcting for total shell material volume ($r = 0.06, t = 0.19, df = 14, p = 0.85$). The group mean values are represented by “0” on both axes.

Table 1. Data from Test 2 (a) – Predation behaviour in relation to prey shell morphology.

No.	<i>Atopos</i> slug ID	Observation starting time	Estimated starting and ending time of the predation by slug.	Duration (Hour: Minutes)	Snail survivorship of each shell form category*		
					Adult	Sub-adult	Juvenile
1	No. 7 of Table 1.	22:04, 18/01/2013	14:00 - 18:30, 19/01/2013	4:30	S	P**	P
3	No. 8 of Table 1.	11:50, 20/01/2013	22:00, 20/01 - 06:00, 21/01	8:00	S	p	S
5	No. 8 of Table 1.	06:30, 21/01/2013	13:00, 21/01 - 22:20:00, 21/01	9:20	S	p	p
7	No. 8 of Table 1.	22:22, 21/01/2013	22:22, 21/01/2013 - 06:45, 22/01/2013	9:07	S	p	p
8	No. 8 of Table 1.	06:45, 22/01/2013	21:50, 22/01/2013 - 05:30, 23/01/2013	9:20	S	p	p
9	No. 8 of Table 1.	05:30, 23/01/2013	15:00 - 18:00, 23/01/2013	3:00	S	p	Missing***
10	No. 8 of Table 1.	18:15, 23/01/2013	18:15, 23/01/2013- 10:55, 24/01/2013	16:40	S	p	p
11	No. 8 of Table 1.	11:00, 24/01/2013	18:15, 24/01/2013- 09:00, 25/01/2013	14:45	S	p	S
12	No. 8 of Table 1.	09:00, 25/01/2013	23:00, 25/01/2013 - 06:00, 25/01/2013	7:00	S	p	p

* “S” – snail survived after experiment, “P” – snail was preyed by *Atopos* slug in the experiment.

** Half of the animal was consumed

*** Specimen was lost during the handling and thus the status of survival of this individual was unknown.

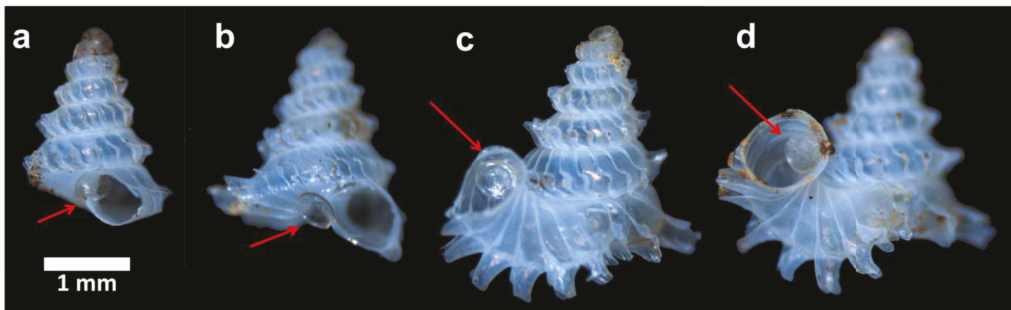


Figure 10. Four examples of shells after predation by apertural entry. Each of them has an intact operculum that is attached to the posterior side of the shell aperture (arrows).

Test 2 (b) – Effectiveness of resting behaviour of *Plectostoma* snails against *Atopos* shell-apertural entry predatory behaviour.

Our data show that the four sectors of the shell differ in their susceptibility to drilling by the slug (Figures 5A and 5B; $\chi^2 = 22.1$, $df = 3$, $p < 0.0001$; Supplementary materials File S2, Page 30: Figure S19). Drill hole frequency is highest in sectors A and B (both 35%), and lowest in sectors C and D (18% and 12%, respectively). The high frequency of drill holes in sector A suggests that the slug is capable of removing adult prey from the substrate. Prey shell rib densities are not significantly different among the four categories (Figure 5C;

Kruskal-Wallis $\chi^2 = 7.17$, $df = 3$, $p = 0.06$), which suggests that the slug's ability to drill the hole is not influenced by the prey rib density.

Test 2 (c) – Effectiveness of shell morphometrics against shell-apertural entry by the *Atopos* proboscis.

Radius of curvature (a proxy for whorl diameter) of the prey shell increases constantly with slight fluctuations throughout the shell ontogeny, apart from a few short but dramatic changes at the constriction (Figures 6A and 6B, 11; Supplementary materials File S2, Page 31: Figure S20). In addition, the predatory distance of the prey shell increases exponentially as the shell grows (Figures 6A, 6B, Supplementary materials File S2, Page 31: Figure S21). In addition to these two morphometric changes throughout shell ontogeny, there is a dramatic change in torsion between the spire whorls and the tuba whorl (Figure 11, Supplementary materials File S2, Page 32: Figure S22).

When the hypothetical slug proboscis morphometrics are plotted together with prey shell morphometrics, it becomes clear that a snail that has grown to at least five whorls would be safe from shell-apertural entry attacks by the smallest *Atopos* slug (green box in Figure 6A). Although the slug's proboscis could fit into the whorls (proboscis diameter < radius of curvature of prey shell, Figure 6A), it is too short to reach the soft body of an animal that has at least 5 spire whorls (slug proboscis length < predatory path distance of prey shell, Figure 6A).

However, a larger slug could attack and consume larger prey by shell-apertural entry. A larger slug could attack prey with more than 5 spire whorls and also prey with a partial tuba

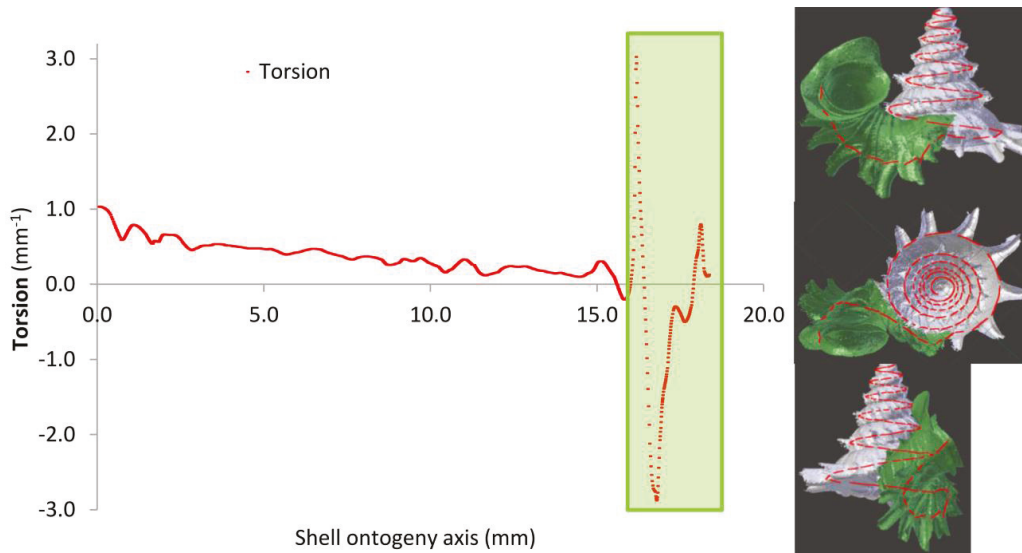


Figure 11. Shell whorl morphometric changes in torsion along the shell ontogeny. The tuba part undergoes dramatic changes in torsion during the shell growth.

because of the increase in its proboscis length and diameter (Figure 6B). Eventually, only fully-grown prey with a complete tuba would remain safe from shell-apertural attack of a fully-grown *Atopos* slug (green box in Figure 6B).

Discussion

Predatory behaviour of *Atopos* slugs toward *Plectostoma* micro-landsnails.

Atopos proved to be one of the main predators for *Plectostoma* in the two limestone hills in our small study area. Possibly, this is the case in general, because many shells of other *Plectostoma* species throughout the distribution area of the genus have the characteristic drill holes as our studied shells (Borneo, Kinabatangan region: Schilthuizen et al., 2006, and Peninsular Malaysia: Liew Thor-Seng, unpublished data; Supplementary materials File S2, Page 33 – 34: Figure S23). We are not sure whether the slugs in our case are generalist predators that also feed on other snail species, as is the case with other Rathousiidae slugs (Heude, 1882-1890; Kurozumi, 1985; Wu et al., 2006; Tan & Chan, 2009), because we have only recorded *Plectostoma* species as prey for *Atopos* in the field so far.

Predators need effective strategies to find, pursue, catch, and consume their prey (e.g., Vermeij, 1993; Alcock, 1998). Unfortunately, we were unable to study the behaviour leading up to prey attack, because we could obtain only a few live slugs, which are also very sensitive to experimental manipulation. At our two study sites, *Plectostoma* snails have high population density (i.e., Site A, 150 individuals per m², Liew Thor-Seng, personal observation, 18th January 2013; and Western slope of Batu Tomanggong Besar, 129 individuals per m², Schilthuizen et al., 2003). The abundance of *Plectostoma* snails in the vicinity of the places where *Atopos* slugs were found indicates that the slugs can easily find prey. In addition, we also suspect that the slug can effectively pursue their prey, because we observed that *Atopos* crawls faster than *Plectostoma*.

During the third stage of predation (prey capture), the prey would withdraw into the shell and adhere its shell aperture to the substrate (e.g. rock surface). The slug would attack by shell-apertural entry by removing the snail from its initial adherent position (Tests 2a & 2b), though we do not know exactly how the slug carries this out. Then, the slug holds the prey tightly in a distinctive posture (Figure 1C, Supplementary materials File S1, Page 1: Table S1). The same posture has also been observed in other Rathousiidae slugs (Heude, 1882-1890; Kurozumi, 1985; Wu et al., 2006; Tan & Chan, 2009). It adheres to the substrate with about two-thirds of the posterior part of the foot, and holds the prey shell with the remaining one-third, which straddles over and lays on the prey shell and pushes the shell against the substrate. On one end, the slug's head lies on the shell aperture or another part of the shell. The other end of the anterior part of the foot, which is slightly lifted from the substrate, has become thicker and might act as a pivot point. Thus, it seems to us unlikely that the snail could escape from the strong grip of *Atopos* after having been captured.

After the snail has been captured, the slug would attempt to reach the soft body by inserting its proboscis into the prey shell via the shell aperture (e.g. Heude, 1882-1890; Kurozumi, 1985; Wu et al., 2006; Tan & Chan, 2009). The slug is more likely to succeed by shell-apertural entry when the prey is not yet fully-grown (Test 2c). All other things being equal, when using the shell-apertural entry strategy, the slug would prefer to attack immature prey over prey with a fully-grown shell (Test 2a). If the slug can reach the deeply-withdrawn body of the snail (lying immediately behind the operculum) it would be able to consume it entirely (Test 2a). The slug may take more than three hours to attack and consume a juvenile snail by shell-apertural entry (Test 2a).

At the end of consumption, there is hardly any snail tissue left in the prey shell (Figure 10). However, the operculum that had withdrawn together with the soft body into the shell remains intact and has been moved to the outside of the shell (Test 2a). We did not observe how the slug extracts the soft body from the shell, but we suppose the slug may secrete digestive fluid to dissolve the snail's tissues and then ingesting this with its proboscis, like other Rathouisiidae (Heude, 1882-1890; Kurozumi, 1985; Wu et al., 2006; Tan & Chan, 2009). Interestingly, though, these digestive fluids then do not damage the operculum (made from corneous protein) (Figure 10; Test 2a). The operculum is free from physical damage as well.

The shell-apertural entry strategy would, however, fail if the slug's proboscis cannot reach the withdrawn soft body of snail (Test 2c; see also Kurozumi, 1985). In this situation, the slug uses shell-drilling to make a new opening directly on the part of the shell whorls where the snail is hiding (e.g. Kurozumi, 1985). We do not know how much time it takes for the slug to drill a hole on the prey shell. The holes made by the same slug individual have the same size (Supplementary materials File S1, Page 2) and this consistency is also known in other observations (Kurozumi, 1985; Wu et al., 2006). The exact drilling mechanism of the slug remains unknown, but it could be either mechanical or chemo-mechanical because of the narrow scraped rim on the hole margin (Figures 1E and 1F).

The slug is able to drill holes either directly on the shell whorl surface or through the ribs (Test 1a). Nevertheless, the slug prefers to drill its hole directly on the shell surface, especially in less densely-ribbed shells, and this tendency may not simply be due to a reduced chance of hitting a rib in a shell with larger rib spacing (Test 1a, Figure 7). Indeed, the tendency of the slug to avoid drilling holes through ribs on a less densely ribbed shell suggests that this is because ribs on a less densely ribbed shell are more "intense" (i.e., heavier; Test 1b, Figure 8). This agrees with observations in other drilling snail predators, which also choose the thinnest part of the prey shell for attack (Allmon, Nieh & Norris, 1990; Kelley & Hansen, 2003).

In summary, *Atopos* slugs might not encounter resistance from *Plectostoma* snails during the first stages of predation. In the final stage, the slug would first attempt its shell-apertural entry strategy to insert its proboscis, and then use the alternative shell-drilling strategy if the first strategy failed. Thus, we conclude that it is likely that *Atopos* slug predation of

Plectostoma snails is highly successful, even though the slug needs to spend more resources (e.g. time and energy) to neutralise the anti-predation shell traits of the prey. We note that *Atopos* predatory behaviour toward *Plectostoma* micro-landsnails agrees with predatory behaviours of Rathouisiidae slugs toward other snails (Heude, 1882-1890; Kurozumi, 1985; Wu et al., 2006; Tan & Chan, 2009). Hence, predatory behaviour appears to be conserved within the Rathouisiidae.

The effectiveness of anti-predation traits of *Plectostoma* against shell-apertural entry by *Atopos*.

A first line of defence of the *Plectostoma* snail against the *Atopos* slug predation is the snail's resting behaviour. When the snail is resting or disturbed, it withdraws its soft body into the shell and adheres its shell aperture firmly to the substrate. We found that the attachment of the *Plectostoma* shell aperture to the substrate may not be strong enough to resist manipulation by *Atopos*. The slug could remove the snail from the resting position and then approach the shell aperture. Hence, the resting behaviour of the snail is not an effective anti-predation trait against shell-apertural entry.

The tuba of a fully-grown shell, however, can act as a second line of defence, as it counteracts shell-apertural entry by creating a longer predatory path than the slug proboscis can traverse. However, our morphometric simulation (Figures 6A and 6B) suggests that survival chances of juvenile snails with incomplete tuba or no tuba at all are slim under shell-apertural attack. Indeed, we have not found any drill holes on the spire of juvenile shells (Test 2a). Our estimation of the *Atopos* proboscis dimensions (i.e. length 0.8 mm - 1.7 mm) agrees with those in other, similar-sized rathouisiids (Kurozumi, 1985: 20 mm long slug with an approximately 2-mm-long proboscis). We would like to point out that our analysis is readily re-evaluated when more data on the anatomy of *Atopos* become available, by simply changing the threshold lines of the proboscis morphometrics in Figures 6A and 6B (Supplementary materials File S4).

It is worth noting that Lampyridae beetle larvae also use shell-apertural entry to attack *Plectostoma* snails. Hence, the anti-predation properties of the snail tuba against *Atopos* attack might similarly defend against the lampyrid larvae. In addition to the increased predatory path as anti-predation property, it is possible that the twisted vacant tuba whorls also help obstruct the insertion of the feeding apparatus of the slug and beetle larva if these are not flexible enough to pass through the twists of the tuba. In short, this second line of defence posed by the snail tuba could force predators to use an alternative, more costly, predatory strategy.

Open-coiled and drastic torsion of the last shell whorl like the tuba in *Plectostoma* snails has evolved several times independently in recent and extinct land and marine snails (Vermeij, 1977; Gittenberger, 1996; Savazzi, 1996). Such shells have a longer and less direct predatory path as compared to tightly and regularly logarithmically-coiled shells. We showed that this could be an anti-predation adaptation to shell-apertural entry by the predator (see also Wada

& Chiba, 2013), which is opposed to the proposed association between open-coiled shell and low predation pressure (e.g. Vermeij, 1977; Seuss et al. 2012).

The effectiveness of *Plectostoma* anti-predation traits against *Atopos* shell-drilling predatory behaviour.

Upon failure of its first attempt at predation by shell-apertural entry, an *Atopos* slug will use the alternative shell-drilling strategy to consume the snail. The slug probably needs to expend more costs, in terms of time and energy, to drill a hole in the prey shell compared to the direct entry and consumption via the shell aperture. As suggested by our data (Test 2c), shell-drilling might be the only way in which *Atopos* can complete the consumption of a *Plectostoma* snail with a fully-grown shell. We did not find any signs of failed attempts of shell drilling (such as a scraped mark without a hole, or a repaired hole). Nevertheless, some of the *Plectostoma* anti-predation traits, namely, the tuba, the thickness of the shell wall, and the radial ribs could play a role in further increasing the predation cost to the shell-drilling predator.

In addition to the antipredation function towards preventing shell-apertural entry, the snail's tuba also acts as a diversionary defence against shell-drilling. When a snail has withdrawn its soft body into the spire, its tuba would be left vacant. We found evidence that the slug can be deceived, as it were, to drill a (useless) hole in the tuba (this happens rarely, though: 3% of the preyed shells in Test 1a, 8% - APO frequency in Table 1 of Schilthuis et al., 2006). Moreover, the slug would then drill a second hole in the spire (Test 1a) after the first drilling attempt at the tuba. Finally, the low error rates in drilling suggests that *Atopos* individuals that frequently feed on *Plectostoma* have learned (e.g. Kelley & Hansen, 2003), or their populations have evolved, to distinguish the dummy tuba and the “edible” spire of the prey shell.

The penultimate line of defence against shell drilling, where shell traits are concerned, is the shell thickness. We found that shell thickness is correlated with shell size (Test 1c, Figure 9). Although we did not experimentally test the anti-predation role of shell thickness, we suggest that a thicker shell may not fully protect the snail from shell-drilling by the slug, because we find drill holes on the shells regardless of their shell thickness. Nevertheless, *Atopos* slugs probably need to spend more energy and time to drill a hole through a thicker prey shell.

The *Plectostoma* snail's last line of defence is the rib intensity (i.e. amount of shell material in the ribs) and rib density on the shell whorls. We found that larger shells has low rib density (fewer ribs) than smaller shells, but the ribs of the larger shells are more intense (longer and thicker) than the ribs of smaller shells. Despite the variability in rib density, all of these snails are susceptible to drilling by the slug (Test 1a, Figure 7). Yet, *Atopos* avoids drilling through the more intense ribs on the less ribbed shells (Figure 7).

Nonetheless, we found a trade-off between rib intensity and rib density (see next section for more discussion about this). Thus, a snail with a shell of higher rib density does not necessarily have an anti-predation advantage over a snail with a shell of lower rib density.

Although we do not know if the slug would prefer prey that either have higher or lower rib density, the ribs on the prey shell do impose a greater cost for the slug because it needs to drill through these ribs before the drill hole breaches the shell wall. As suggested by Allmon, Nieh & Norris (1990), the sculpture of the shell is not a very effective adaptation to resist predation by drilling. Others have suggested that tall and strong ribs could make the shell effectively larger and therefore hinder the manipulation by a predator (Vermeij, 1977). These hypotheses still need to be tested in the *Atopos-Plectostoma* interaction.

To sum up, *Plectostoma* anti-predation traits might mainly act to delay the predator, which increases the time and energy requirement for *Atopos* to complete predation. The resistance exhibited by the snail in response to shell-drilling by the slug cannot ensure the survival of the preyed snail. Our results are in accordance with the general view that snail shells usually cannot resist drilling by their predators (Vermeij, 1982).

Why can't shell traits evolve to defend against both predatory strategies?

Atopos has two effective predatory strategies to neutralise the defences of *Plectostoma* during the last stage of predation. For both, it uses its digestive system (namely, its proboscis and digestive fluid in the shell-apertural entry strategy, and its proboscis, radula and digestive fluid in shell-drilling strategy). Thus, maintaining two predatory strategies that complement each other brings no additional cost to the slug development. By contrast, *Plectostoma* has to invest in two different sets of shell traits to deal with each of these predatory strategies. Yet, both sets of the shell traits have orthogonal growth directions, which indicate a possible trade-off between the shell traits.

In a hypothetical situation where predators are present that attack only by shell-apertural entry, snails can avoid predation by faster completion of a shell with a tuba, which means the snail would have to invest more resources (time and shell material) in the longitudinal growth of the shell. In the alternative situation where predators are present that attack only by shell-drilling, snails can avoid, or delay, predation by growing more thick flaring ribs, which means it would have to invest more resources in the transverse growth and more frequent shifts from a longitudinal whorl growing mode to a transverse rib growing mode. Due to the orthogonal growth modes of these two shell traits, a snail cannot attain adult shell form faster when it needs to grow more ribs, and vice versa. This developmental trade-off causes the functional trade-off in the anti-predation traits of the shell. Therefore, none of the shell traits of *Plectostoma* are at an optimal level to defend against both shell-apertural entry and shell-drilling strategies of the *Atopos* slug.

Besides the trade-off between the two sets of shells traits, we also found a trade-off within one of these shell traits. From a theoretical point of view, the snail's shell could have evolved to have very dense, protruded and thick ribs to hinder *Atopos*'s drilling strategy. However, we found a trade-off such that ribs of more densely ribbed shells are less intense than ribs of the less densely ribbed shells. The underlying factors that cause this trade-off were not determined, but it does appear to reflect a developmental constraint.

To date, the majority of the studies of adaptive evolution of antipredation shell traits have focused on the evolution of a single shell trait of the prey in response to a single predatory behaviour of one or more predators. However, in nature, a prey might possess several antipredation traits in response to several different predatory behaviours of a predator (e.g. Sih, Englund & Wooster, 1998; DeWitt & Langerhans, 2003; Relyea, 2003). Usually, a snail will counteract a particular predatory strategy with a single evolved anti-predation shell trait (Vermeij, 1993), but snails sometimes use a combination of more than one trait to defend against a predatory strategy (DeWitt, Sih & Hucko, 1999; Wada & Chiba, 2013). A few studies have shown that there may be a functional trade-off between such multiple anti-predation traits. For example, Hosoi (2012) demonstrated that two snail anti-predation traits evolved by changes in two different developmental mechanisms (shell coiling direction and foot structure) in response to two predation stages (capture and consumption) of the same predator. Here, we show another novel context of an anti-predation functional trade-off between two sets of anti-predation shell traits that are part of the same developmental mechanism (shell ontogeny), but in response to two different predatory behaviours within the same predation stage (consumption) by the same predator.

We found several correlations and trade-offs between and within the sets of anti-predation shell traits with each set having a specific function against a particular predatory strategy. However, more study is needed to clarify the exact causal relationships and to determine the underlying developmental biology of these shell anti-predatory traits. This could have important implications for our understanding of the evolutionary adaptability of shells under predation selection pressure in *Plectostoma* snail in particular and Gastropoda in general.

Conclusion

Our study has unravelled several aspects of the predator-prey interactions between the *Atopos* slug and *Plectostoma* snails in the limestone habitats of Borneo. Despite having several distinct anti-predation traits, such as protruding radial ribs and distorted coiling of the shell, *Plectostoma* snails have low resistance against predation by the slug with its two predatory strategies (shell-apertural entry and shell-drilling). Lastly, the effectiveness of the snail's anti-predation traits is probably limited by trade-offs imposed by ontogenetic constraints.

Acknowledgments

We are thankful to Effendi bin Marzuki, Heike Kappes, Angelique van Til, Mohd. Sobrin, and Samsudin's family for their assistance in the fieldwork. We are grateful to Willem Renema for introducing LTS to CT-Scan instrumentation. Finally, we would like to acknowledge Thomas DeWitt, Dany Garant and an anonymous reviewer for providing useful comments that improved the manuscript.

Supporting Information

File S1. Field observation and literature review of Rathousiidae slugs and Lampyridae beetle larvae predatory behaviours.

File S2. Raw data and supplementary information for results (Tables: S1 – S4, Figures: S1 – S23).

File S3. Raw data and R script for data analysis for all tests.

File S4. Raw data for Test 2 (c): Effectiveness of prey shell whorl morphometrics against shell-apertural entry by the *Atopos* proboscis.

Chapter 6

An ontogenetic perspective on the evolution of shell size and shell shape in the land snail genus *Plectostoma*

(unpublished manuscript)

Thor-Seng Liew and Menno Schilthuizen

1 Institute Biology Leiden, Leiden University, P.O. Box 9516, 2300 RA Leiden, The Netherlands.

2 Naturalis Biodiversity Center, P.O. Box 9517, 2300 RA Leiden, The Netherlands.

3 Institute for Tropical Biology and Conservation, Universiti Malaysia Sabah, Jalan UMS, 88400, Kota Kinabalu, Sabah, Malaysia.

Email: T-S L: thorsengliew@gmail.com

MS: Menno.Schilthuizen@naturalis.nl

Author Contributions

Conceived and designed the experiments: LTS. Performed the experiments: LTS. Analyzed the data: LTS. Contributed reagents/materials/analysis tools: LTS MS. Wrote the paper: LTS MS.

Supplementary Information

(<https://drive.google.com/a/naturalis.nl/#folders/0BwCpl3C2XSo9Zi1mQ0swal9xelU>)

Abstract

The rampant convergent and parallel evolution in shell form in the Gastropoda is well known. Many studies focus on the functional drivers which have been regarded as a major force in shell evolution. There is, however, a scarcity in studies that aim at understanding shell form evolution with respect to their ontogeny. Hence, we investigated the evolution of shell form in the micro-landsnail genus *Plectostoma* (Diplommatinidae) from the viewpoint of shell ontogeny. We examined the aperture ontogeny profiles that describe how aperture form and growth trajectory change along the shell ontogeny, and how the aperture ontogeny profiles relate to the observed shell forms. We also estimated the phylogeny of *Plectostoma* species, and examined patterns of character evolution for shell form. Our study revealed a general issue in the characterisation of shell shape and demonstrated how shell shape differences can be expressed as differences in the ontogeny of morphospace. It is clear that in *Plectostoma* the phylogenetic history does not prevent the course of shell ontogeny, and the resultant form. Finally, each species has a unique aperture ontogeny profile that determines its shell shape while retaining a conserved developmental program that maintains shell size.

Introduction

One of the central questions in the study of phenotypic evolution is why certain structures of a species evolve to obtain a certain form, whereas the same structure in other species does not. This disparity in phenotypic evolution generates the morphological variation that is the mainstay of biodiversity. Morphological diversity in organisms may be channelled by a combination of different evolutionary constraints, namely, phylogenetic, developmental, geometric and functional constraints (Seilacher, 1991; Arnold, 1992). However, it remains a challenge to unravel the evolutionary history of an organism's form because most organisms have very complex external forms consisting of many different structural modules.

The gastropod shell, however, is a single structure, which, across gastropod taxa, shares the same developmental process and similar functions since it first appeared during the Cambrian explosion. The shell is a product of accretionary growth where shell material is added at the existing aperture by the snail mantle edge (hereafter termed: aperture ontogeny). The aperture ontogeny consists of two major components: (1) the size and shape of the aperture and (2) the growth trajectories. Jointly, these components determine the shell form (**Chapter 3**). From a functional point of view, the shell is a solid exoskeleton in which the snail's soft body can fit to safeguard it against predators and, in the case of terrestrial snails, dehydration.

These characteristics produce similarity in the general form of the gastropod shell, despite a long evolutionary history and despite Gastropoda being an extremely speciose Molluscan class. Hence, shell form is prone to convergent evolution at various taxonomic levels (Wagner & Erwin, 2006). Phylogenetically closely related species, even within genus level, are known not to have similar shell size (Teshima et al., 2003; Parmakelis et al., 2003; Johnson et al., 2004; Ketmaier, Giusti & Caccone, 2006; Bichain et al., 2007; Kameda, Kawakita & Kato, 2007; Elejalde et al., 2008a; Fiorentino et al., 2008b; Puslednik et al.,

2009; Buckley et al., 2011; Stankowski, 2011; Criscione, Law & Koehler, 2012; Johnson et al., 2012; Koehler & Johnson, 2012; Lee, Lue & Wu, 2012; Criscione & Koehler, 2013; Du et al., 2013, but see Martinez-Orti et al., 2008; Kotsakiozi et al., 2013). Similarly, shell shape similarity does not usually translate to a close phylogenetic relationship between species (Boato, 1991; Emberton, 1995; Teshima et al., 2003; Tongkerd et al., 2004; Elejalde et al., 2005; Noshi & Sota, 2007; Elejalde et al., 2008a; Elejalde et al., 2008b; Stankowski, 2011; Johnson et al., 2012; Haase, Esch & Misof, 2013).

Studies of convergent evolution of shell form, as the works cited in the previous paragraph, quantify shell size and shape by treating the shell as a single entity. By convention, shell size is quantified by measuring the linear dimensions of the entire shell, such as shell height and width. Shell shape is obtained by taking ratios of shell dimensions or by geometric morphometrics, which are then used as criteria to assign the shell shape into shape categories, such as elongated, depressed, and flatted shells. While these entire-shell based characterisation approaches allow us to understand how the shell form could evolve under functional constraints, this approach does not allow us to understand the evolution of the aperture ontogeny that is fundamental in determining the shell form. Studies which take such an ontogenetic approach to understanding of shell form evolution are scarce (**Chapter 3**).

Here, we investigate the evolution of shell form in the micro-landsnail genus *Plectostoma* (Diplommatinidae) from the viewpoint of shell ontogeny. *Plectostoma* can be considered as one of the most diverse genera in terms of shell form (Vermeulen, 1994, **Chapter 2**). All species begin their shell ontogeny as a regular shell form, but some species change their coiling direction towards the end of the shell ontogeny. In this paper, we restrict our discussion to the evolutionary patterns in *Plectostoma* shell size and shape, and to what extent these patterns are related to the shell ontogeny. We will not discuss the possible functional drivers, most of which are still unknown, except anti-predation functions of the twisted tuba in a few species (Schilthuizen et al., 2006; **Chapter 5**).

First, we modified the conventional approaches so that both shell ontogeny and shape information could be characterised and analysed together with the phylogenetic data. For shell size, we quantified the inner volume of the entire shell, and obtained aperture size ontogeny profiles along the whorl accretionary length (i.e., the ontogeny axis). For shell shape, we adopt the approach of **Chapter 4** that divided the shell into five homologous developmental parts, for which each species was then characterised. In addition, we also quantified the shell shape in terms of its growth trajectories – curvature and torsion, and aperture shapes along the ontogeny axis. Next, we estimated the molecular phylogenetic relationships of selected *Plectostoma* species, covering most of the shell form diversity. Then, we examined the pattern of evolution for the shell size and shape based on the characterised shell traits for all six shell characters by phylogenetic signal tests and ancestral character estimates. Lastly, we explored the ontogeny of shell size based on the aperture size ontogeny profile and the ontogeny shell shapes based on the ontogenetic morphospace that was constructed from the three others aperture ontogeny profiles (curvature, torsion, and aperture shape).

Materials and Methods

Ethics Statement

The permissions for collecting specimens in Malaysia were given to LTS by the Economic Planning Unit, Prime Minister's Department (UPE: 40/200/19/2524), State Planning Unit, Chief Minister's Department, Sarawak ((47) UPN/S/G1/I/10.1 Vol.27), Forest Department Sarawak (Research Permit NPW.907.4.4(V)-19; Park Permit No. 07/2010; Export Permit No. 09003).

Ontogeny of shell size and shape

The relationship between the shell size, ontogeny axis length and aperture size

We examined whether there are associations between the shell size (internal volume in mm³), ontogeny axis length (corresponding to total whorl length in mm), and aperture size changes along the shell ontogeny. We obtained these three shell variables from 11 representative *Plectostoma* species (Table 1) by using the 3D approach as described in **Chapter 4**. Here, we only briefly describe this methodology.

First, 3D models of *Plectostoma* shells were obtained with CT-scanning. Then, we used the 3D modelling software Blender ver. 2.63 (www.blender.org) to retopologise the aperture outlines from the scanned 3D models and created retopologised shell models based on these aperture outlines. Next, we used custom written Python scripts to extract: (1) ontogeny axis data, in terms of the length, and growth trajectories for curvature and torsion, and (2) aperture form data, in terms of perimeter and shape, from the retopologised shell models in Blender. Finally, the growth trajectories and aperture form variables were analysed as they developed along the ontogeny (hereafter termed: aperture ontogeny profiles).

After that, we examined the pattern of aperture size changes along the shell ontogeny of each species. Then, we used Pearson correlation to test the correlation between the log-transformed shell volume and the log-transformed ontogeny axis length. In view of the strong correlation that we found (see Results), we also examined the pattern of aperture size changes of all 11 shells after their respective ontogeny axis length (mm) was rescaled by standardisation, which was done by dividing the ontogeny axis position of the apertures of each shell by axis length. All data analysis and exploration were done in R version 3.0.1 (R Core Team, 2013) (R scripts in Supplementary File 1).

Table 1. Specimen data for phylogenetic analysis.

Species	Collection number	18S	28S	16S	COI	Locality	Collection Date	Latitude, Longitude
<i>Plectostoma austeni</i> (Smith, 1894)	BOR 5546	#####	#####	#####	#####	Malaysia; Sarawak; Serian; Gunung Rimau near Kampung Benuk	19-Aug-2010	1.319, 110.291
<i>Plectostoma christae</i> (Maassen, 2001)	BOR 5572	KC420367	KC420316	KC420413	KC420271	Malaysia; Kelantan; Limestone in FELDA Ciku 5	17-Feb-2010	5.004, 102.2
<i>Plectostoma concinnum</i> (Fulton, 1901)	n.a.	#####	#####	#####	#####	Malaysia; Sabah; Sandakan; limestone hill 'Keruak'	16-Dec-2010	5.518, 118.291
<i>Plectostoma crassipupa</i> (van Benthem Jutting, 1952)	BOR 5512	KC420400	KC420353	KC420451	KC420304	Malaysia; Kelantan; ; Limestone hill near Kampung Paloh, on the right hand side of the road no 8 to	16-Jun-2011	4.992, 102.228

The evolution of shell form

						Gua Musang		
<i>Plectostoma davisoni</i> Liew, Vermeulen, Marzuki & Schilthuizen 2014	BOR 5508	KC250938	KC250963	KC250913	KC250872	Malaysia; Kelantan; Limestone hill on the right hand side of the road D29, km 17 from Jelawang to Gua Musang	28-May-2011	4.985, 101.965
<i>Plectostoma grandispinosum</i> (Godwin Austen, 1889)	BOR 5590	KC250946	KC250971	KC250921	KC250879	Malaysia; Sarawak; Miri; along the trail to the Bukit Kasut, Niah National Park	12-Jun-2010	3.804, 113.78
<i>Plectostoma ikanensis</i> Liew, Vermeulen, Marzuki & Schilthuizen 2014	BOR 5504	KC250929	KC250954	KC250903	KC250862	Malaysia; Kelantan; ; Limestone hills 'Ciku 2'. In the FELDA plantation Ciku 2	28-May-2011	4.924, 102.177
<i>Plectostoma kubuensis</i> Liew, Vermeulen, Marzuki & Schilthuizen 2014	BOR 5519	KC420366	KC420315	KC420412	KC420270	Malaysia; Perlis; Bukit Kubu. Loc 3	21-May-2011	6.404, 100.144
<i>Plectostoma tenggekensis</i> Liew, Vermeulen, Marzuki & Schilthuizen 2014	BOR 5596	KC420380	KC420332	KC420431	n.a.	Malaysia; Pahang; loc. 14 Bukit Tenggek (c. 45 km NW of Kuantan)	27-Jun-1997	4.014, 103.159
<i>Plectostoma laidlawi</i> (Sykes, 1902)	BOR 5510	KC420372	KC420323	KC420421	KC420279	Malaysia; Kelantan; ; Limestone hill in Kampung Bayu. About 337 km from Kuala Lumpur by road no. 8	28-May-2011	5.09, 102.22
<i>Plectostoma pulchellum</i> (Godwin Austen, 1890)	BOR 5563	KC250924	KC250949	KC250898	KC250857	Malaysia; Sarawak; Mulu National Park, Moon Cave	24-Sep-2010	4.044, 114.815
<i>Plectostoma pumilio</i> (Smith, 1894)	BOR 5550	#####	#####	#####	#####	Malaysia; Sarawak; Serian; Unnamed limestone hill near Kg. Sematan, along the new road to Bau	19-Aug-2010	1.296, 110.274
<i>Plectostoma relauensis</i> Liew, Vermeulen, Marzuki & Schilthuizen 2014	BOR 5511	KC420370	KC420321	KC420419	KC420277	Malaysia; Kelantan; Taman Negara, Sungai Relau Station. Gua Gajah	15-Jun-2011	4.642, 102.063
<i>Plectostoma retrovertens</i> (Tomlin, 1938)	BOR 5559	KC420392	KC420345	KC420443	KC420297	Malaysia; Pahang; Karak; Bukit Chintamanis	29-Aug-2010	3.446, 102.014
<i>Plectostoma salpidomon</i> (van Benthem Jutting, 1952)	BOR 5569	KC250934	KC250959	KC250909	KC250868	Malaysia; Pahang; Kuala Lipis; Gua Bama	16-Feb-2010	4.194, 101.967
<i>Plectostoma senex</i> (van Benthem Jutting, 1952)	BOR 5575	KC250926	KC250951	KC250900	KC250859	Malaysia; Pahang; Kuantan; Gua Charas	20-Feb-2010	3.908, 103.147
<i>Plectostoma sinyumensis</i> (Maassen, 2001)	BOR 5537	KC250936	KC250961	KC250911	KC250870	Malaysia; Pahang; Gunung Jebak Puyuh, near Gunung Senyum	16-Jul-2010	3.7, 102.453
<i>Plectostoma siphonostomum</i> (van Benthem Jutting, 1952)	BOR 5557	KC250932	KC250957	KC250906	KC250865	Malaysia; Pahang; Chegar Perah; Limestone hill on the left hand side of the road no. 8 toward Kuala Lipis. Near Kampung Chegar Perah I and II FELDA	27-Aug-2010	4.487, 101.976
<i>Plectostoma stellasubis</i> (Vermeulen, 1994)	BOR 5588	KC250925	KC250950	KC250899	KC250858	Malaysia; Sarawak; Miri; Location near the Great Cave. Niah National Park	11-Jun-2010	3.804, 113.78
<i>Plectostoma umbilicatum</i> (van Benthem Jutting, 1952)	BOR 5503	KC420374	KC420325	KC420423	KC420281	Malaysia; Pahang; Gua Tongkat	29-May-2011	3.891, 102.473
<i>Plectostoma wallacei busauense</i> (Smith, 1893)	BOR 5545	KC250941	KC250966	KC250916	KC250875	Malaysia; Sarawak; Serian; Gunung Baru near Kampung Benuk	19-Aug-2010	1.323, 110.3

Shell shape ontogeny in aperture ontogenetic morphospace

In addition to the shell shape and size, we examined the remaining aperture ontogeny profiles for curvature, torsion and aperture shape (for the latter, we used the first principal component, which explained 46 % of the variation) of the 11 shells along the standardised ontogeny axis. To remove the size component from the morphospace, we standardised the curvature and torsion profiles by multiplying them with the aperture size profile, because the raw aperture curvature and torsion estimates may be related to the aperture size (Okamoto, 1988).

Then, we visualised the aperture ontogenetic morphospace by plotting the three aperture ontogeny profiles, namely: (1) aperture shape scores; (2) standardised torsion, and (3) standardised curvature. Finally, each of the apertures in the morphospace was labelled with its species identity and its standardised ontogeny position (%) in two separate panels.

To explore this ontogenetic morphospace, we first identified the outlier aperture ontogeny in the morphospace, defined as the apertures with ontogeny profiles larger than quartile 3, and smaller than quartile 1, by at least 1.5 times the interquartile range. This range was selected for the sake of convenience so that the outliers can be identified within and between species ontogenetic morphospace. After the region of ontogenetic morphospace with outliers was identified, the remaining occupied ontogenetic morphospace was examined. We investigated whether the occupancy of ontogeny morphospace was associated with the shell shape categories (see below) and whether it was specific to species or to a particular ontogeny stage. All data explorations and analyses were done in R (R scripts in Supplementary File 1).

Evolution of shell size and shape

Molecular Phylogenetics

We included 21 *Plectostoma* species in our molecular phylogenetic analysis, seven endemic to Borneo and 14 to Peninsular Malaysia. These species form a fair representation for *Plectostoma* shell diversity (Vermeulen, 1994; **Chapter 2**). In addition to these ingroup taxa, four outgroup taxa were included in the phylogenetic analysis. Sequence data for these outgroup taxa, which include three genera of the Diplommatinidae and a species of the Cochlostomatinae, were obtained from Webster et al. (2012). The details of these specimens and the Genbank accession numbers are listed in Table 1.

We extracted DNA from one specimen (entire animal and its shell) for each species by using the E.Z.N.A. Mollusc DNA kit (OMEGA bio-tek) and the manufacturer's extraction protocol. After extraction, PCR was carried out to amplify four regions, namely, 16S (mitochondrial, Palumbi 1996), COI (mitochondrial, Folmer et al. 1994), 28S (nuclear, Park and Foighil 2000), and 18S (nuclear, Stothard et al. 2000). We followed the PCR protocols of Webster et al. (2012). After that, positive PCR products were sequenced by MacroGen sequencing service (MacroGen Inc., Europe).

Alignment of sequences was done with Bioedit ver 7.1.3 (Hall 1999) and adjusted manually. The final aligned data matrix consists of 2,234 positions (Supplementary File 2). We divided the dataset into six partitions which represent the three separate codon positions of COI and

the remaining three sequenced genetic regions. We inferred a phylogeny using both Bayesian and maximum likelihood analyses.

For Bayesian analysis, we used jModelTest 2.1.4 (Darriba et al., 2012) to select the most appropriate model, based on the Akaike Information Criterion (AICc) for each of the six partitions. The best fits were: the HKY+I+G model for 16S; GTR+I+G for 28S, COI(1st codon); GTR+I for COI(2nd codon); HKY + G for COI(3rd codon); and JC for 18S. Bayesian inference was run in MrBayes ver. 3.2.1 (Huelsenbeck and Ronquist 2001) with the following setting: mcmc ngen=1,000,000; nchains=4; samplefreq=100; average deviation of split frequencies < 0.01; and a burn-in value of 25%. We retained the consensus tree for further analysis. Maximum likelihood analysis was done in RAxML v8.0.0 (Stamatakis, 2014) via the CIPRESS portal v3.3 (Miller, Pfeiffer and Schwartz, 2010). We set the GTRGAMMA model for the concatenated six partitions and 1,000 bootstrap replicates.

Ancestral state reconstructions

We scored shell shape as five discrete characters representing five subsequent phases in shell ontogeny, namely, apex shape, apical spire shapes, basal spire shape, tuba coiling type, and aperture opening orientation. The detailed description of these shell parts from the developmental and morphological points of view can be found in **Chapter 2**, with the addition of one extra category for apical spire shape, namely equal lateral, when the ratio of apical spire height and width is equal to one (Supplementary File 3).. For this reason, five species that had previously been categorised as oblong were moved to this new category. In addition, four of the shells that were categorised into moderately convex/slightly convex apex were now categorised as moderately convex; and one *Plectostoma laidlawi* was now in the distinctly convex apex category (cf. Table 3 in **Chapter 2**).

Then, we reconstructed ancestral states of the five discrete shell shape characters and the continuous shell size variable on the Bayesian estimated consensus tree. The ancestral state reconstructions were done with both maximum likelihood using the ‘ace’ function in R package ‘ape’ (Paradis, Claude & Strimmer, 2004), and maximum parsimony using MESQUITE 2.75 (Maddison & Maddison, 2011).

Phylogenetic signal

We investigated whether closely related species are more likely to have similar shell traits than expected by chance by examining the phylogenetic signal with two approaches, namely, maximum likelihood in terms of lambda (λ) (Pagel, 1999), and maximum parsimony in terms of randomisation tests. As required by lambda analysis, we transformed the Bayesian consensus tree into an ultrametric tree by using Sanderson's semi-parametric penalized likelihood approach (Sanderson, 2002) as implemented in the R package ‘ape’ (i.e., ‘chronopl’ function). All data analysis and exploration was done in R version 3.0.1 (R Core Team, 2013) (R scripts in Supplementary File 1).

We estimated λ and its model likelihood score of each shell trait (i.e. alternative model) on the basis of the *Plectostoma* phylogenetic tree by using the “*fitContinuous*” function for shell

size and the “*fitDiscrete*” function for the five shell shape characters, in the “Geiger” package (Harmon et al., 2008) via R (R Core Team, 2013). After that, we repeated the analysis for a null model, for which the *Plectostoma* phylogenetic tree was transformed to a total basal polytomy tree (i.e. $\lambda = 0$, no phylogenetic signal) by using the “*transform*” function. Lastly, we examined whether there was a significant phylogenetic signal in each of the shell traits by running a likelihood ratio test for both alternative and null model likelihood scores.

In addition to the likelihood method above, we performed a randomisation test for the five discrete shell shape characters based on the parsimony method implemented in Mesquite (Maddison & Maddison, 2011). First, we created a null model that consists of 999 random trees for each shell trait by reshuffling terminal taxa. The null model is a distribution of steps in character for all random trees, and has percentile boundary of 0.05. Then, we obtained the steps value for each shell trait and compared the value with the respective null model. Shell traits were considered to have significant phylogenetic signal if the steps value fell outside the percentile boundary. In addition, we tested the phylogenetic signal in shell size with K of Blomberg et al. (2003) by using the ‘*phylosig*’ function in R package ‘*phytools*’ (Revell, 2012).

Results

Ontogeny of shell size and shape

The relationship between the shell size, ontogeny axis length and aperture size

There are associations among shell volume, ontogeny axis length and aperture size profile (Figure 1A). Figure 1C shows a strong correlation between the log-transformed shell volume and the log-transformed ontogeny axis length ($r = 0.91$, $t = 6.6805$, $df = 9$, $p = 0.000$). In addition, the larger shells always have larger aperture sizes than smaller shells at the same point of their standardised ontogeny axis (Figure 1B).

All species, with the exception of *Plectostoma grandispinosum*, have similar patterns in aperture size changes along the standardised shell ontogeny axis (Figure 1D). Initially, aperture size increases constantly before it reaches the first plateau at about 70 – 75 % of the shell ontogeny. Then, aperture size decreases toward the shell’s constriction around 80 – 90 % of the shell ontogeny. After the constriction phase, the aperture size increases until the end of the shell ontogeny. *P. grandispinosum*, on the other hand, has its first aperture size plateau at 50 % and its constriction at about 60 % of the shell ontogeny. We found that *P. grandispinosum* has a *ca.* 30 % longer ontogeny axis during the tuba phase as compared to the rest of the species, if the standardised ontogeny axis of *P. grandispinosum* was rescaled until its constriction phase – a developmental homology matched with the other species.

Shell shape ontogeny in aperture ontogenetic morphospace

Figure 2 shows the aperture ontogeny profiles for the 11 *Plectostoma* species on the standardised ontogeny axis (raw data: Supplementary File 4). The modest changes in curvature and torsion profile of the shells are generally in accord with their regularly coiled conical (i.e., logarithmically spiralling) shell before the constriction phase and tuba phase of

the ontogeny (raw curvature and torsion in Figures 2A and 2B; standardised curvature and torsion in Supplementary File 5: Figures S1-S5).

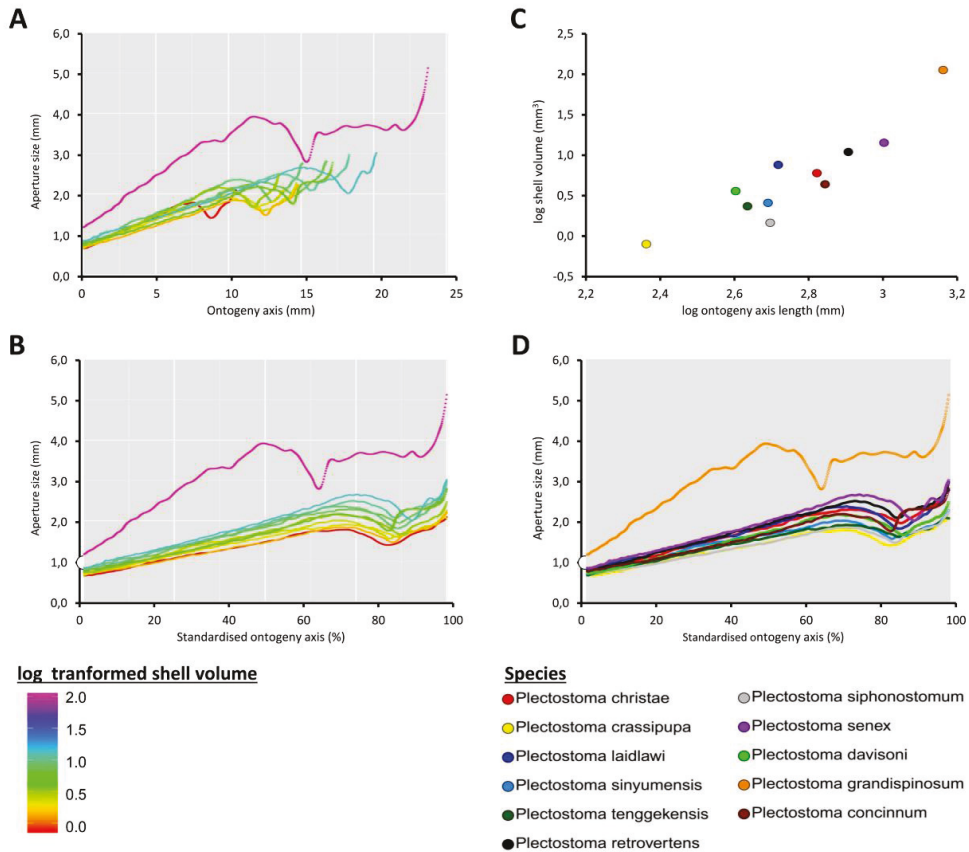


Figure 1. The ontogeny analysis of shell size of the 11 *Plectostoma* species. (A) Plot of aperture size ontogeny profile vs. ontogeny axis, and each profile annotated by its size. (B) Plot of aperture size ontogeny profile vs. standardised ontogeny axis, and each species profile annotated by its size. (C) Correlation between log-transformed shell volume and log-transformed ontogeny axis length. (D) Same as C, but each profile annotated by the species identity.

Figure 3 shows the ontogenetic morphospace of the 11 species. The outliers of the aperture shape changes along the ontogeny always are located either at the very beginning of the shell ontogeny (before 10%) or at the later phase of the ontogeny (after 60%) (Figure 3B). Nine of the 11 species occupied the outlier aperture shape space, either at the beginning or at the later stage of shell ontogeny, but never both (Figure 3E).

The outliers of the aperture standardised torsion always are located at the end of the ontogeny (after 80%) and some of these outliers are also outliers in the standardised curvature (Figure 3A). This space is occupied by the species with a twisted tuba, namely, *P. laidlawi*, *P. tenggekensis*, *P. retrovertens*, *P. davisoni*, *P. grandispinosum*, and *P. concinnum* (Figure 3D).

When the non-outlier ontogenetic morphospace in Figure 4 was examined closely, the species that share similar shell shapes as far as the five shell characters are concerned, do not necessarily share the same ontogenetic morphospace (see also Supplementary File 5: Figure S6-S8). Most species occupy a species-specific region in the aperture shape and standardised curvature morphospace in the first half of shell ontogeny (0 % – ca. 50 %) (Figure 4B and Figure 4E).

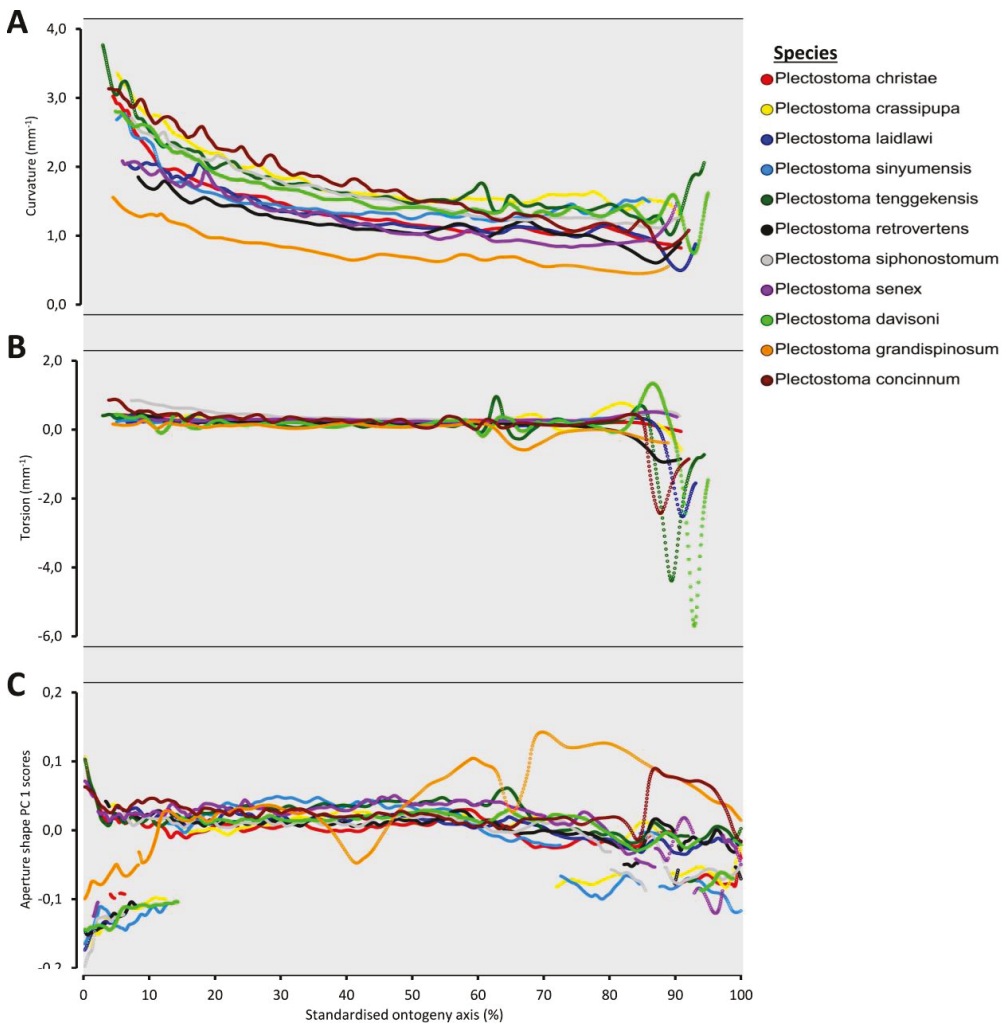


Figure 2. Aperture ontogeny profiles of the 11 *Plectostoma* species. (A) Plot of curvature vs. standardised ontogeny axis. (B) Plot of torsion vs. standardised ontogeny axis. (C) Plot of aperture shape scores vs. standardised ontogeny axis.

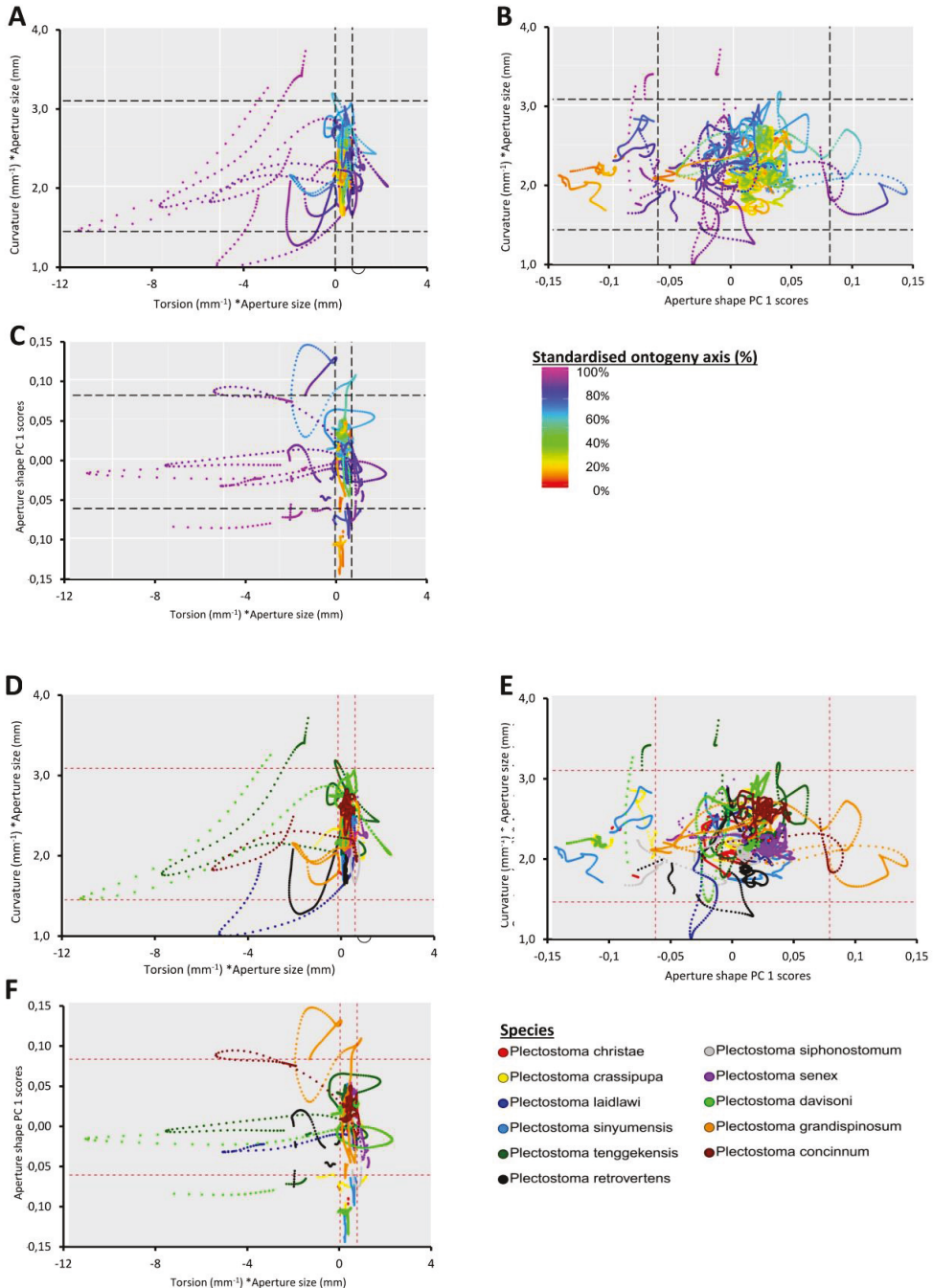


Figure 3. Shell ontogenetic morphospace of the 11 *Plectostoma* species. (A) – (C) Three panels that show each dimension of the ontogenetic morphospace, and each aperture annotated by its position along the standardised ontogeny axis. (D) – (E) Three panels that show each dimension of the ontogenetic morphospace and each aperture annotated by its species identity. The dashed line marks the outlier values for each ontogenetic morphospace axis.

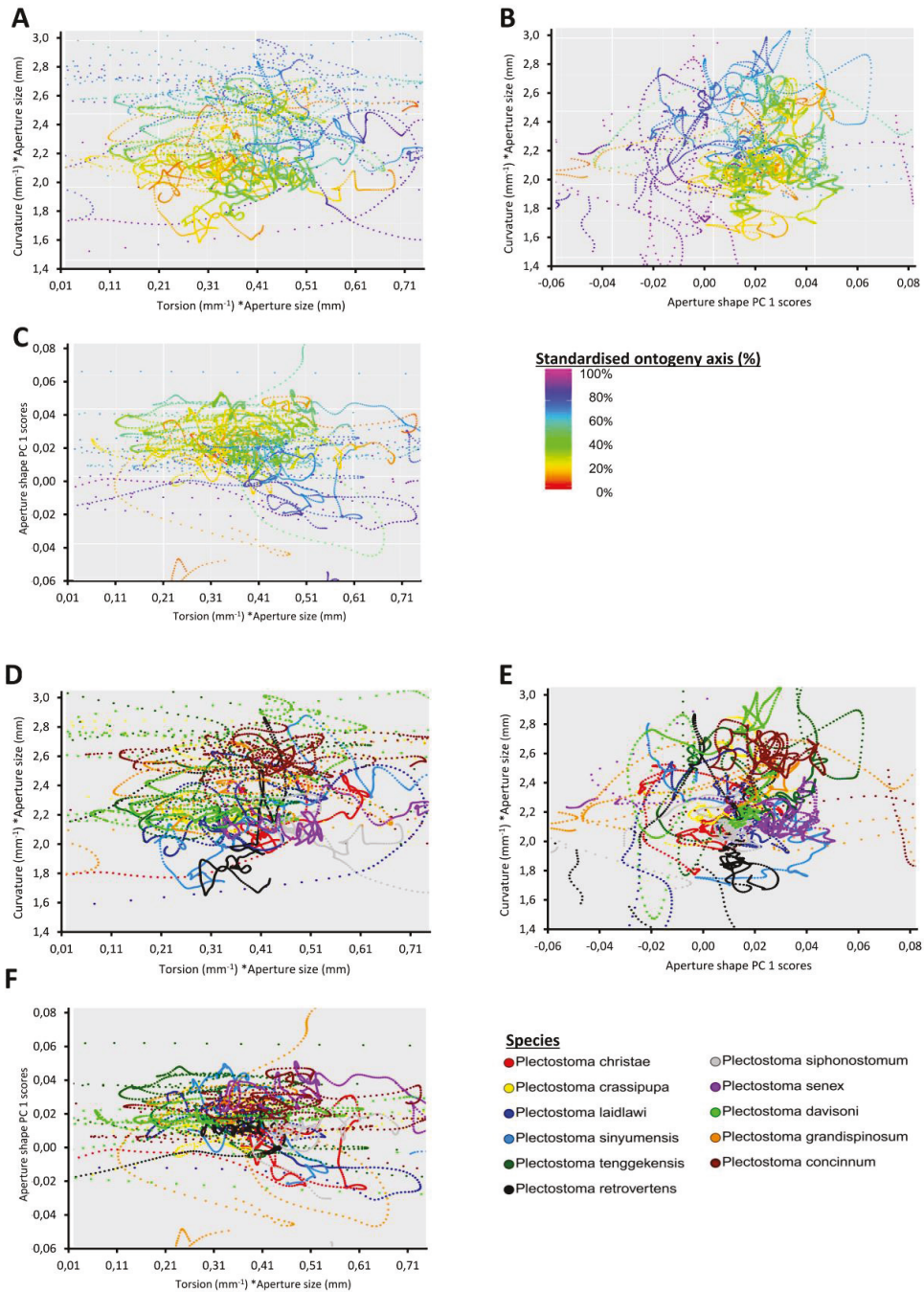


Figure 4. Shell ontogenetic morphospace of the 11 *Plectostoma* species after exclusion of the outlier region (see Figure 3). (A) – (C) Three panels that show each dimension of the ontogenetic morphospace, and each aperture annotated by its position along the standardised ontogeny axis. (D) – (E) Three panels that show each dimension of the ontogenetic morphospace and each aperture annotated by its species identity.

Evolution of shell size and shape

Molecular Phylogenetics

The phylogenetic relationships among *Plectostoma* species can be seen in Figure 5. The monophyly of the *Plectostoma* clade and the majority of its internal nodes are well supported by Bayesian posterior probabilities (> 0.95). Similarly, the monophyly of *Plectostoma* and the four major clades are also well supported in the maximum likelihood analysis (bootstrap $> 85\%$) (Supplementary File 6). Each of the major clades consists of species that are diverse in shell form.

Ancestral state reconstructions

Figure 6 shows the results from maximum likelihood ancestral state reconstruction for the shell shapes and shell size. The results are consistent with the reconstruction based on maximum parsimony (Supplementary File 7). The ancestral shell size is estimated to be about 2.5 mm^3 – an intermediate size for *Plectostoma* species (95% CI: 1.7 – 3.2) (Figure 6F). The ancestral shapes of the three shell spire parts are present in almost all deep nodes (i.e. backbone nodes for the four clades) in the phylogeny. The different apex and spire shapes have been derived from their respective ancestral states multiple times in all four major clades during the radiation of *Plectostoma* (Figure 6A, 6B, and 6C).

Figure 6D shows that a twisted tuba is an ancestral trait for *Plectostoma*, backbone nodes, and its clades 1, 2 and 3. The transition from twisted tuba to the other two tuba types does not occur in clade 1. There, a regularly coiled tuba has been derived from the twisted tuba independently from those in clades 3 and 4; and a distorted tuba has been derived from a twisted tuba independently in clades 2 and 3. There is a single case of secondary gain of a twisted tuba in clade 4 after it was lost. The ancestral *Plectostoma* shell had a leftward aperture (Figure 6E). This ancestral apertural state has been retained in the ancestral shell of clades 1 and 2, but there are several transitions to other aperture inclinations in the remaining backbone nodes and particularly in clade 3.

Phylogenetic signal

Shell size, the shapes of all shell spire parts (apex, apical spire, and basal spire), tuba coiling type, and aperture opening orientation show no significant phylogenetic signal, based on likelihood and parsimony methods (Table 2).

Table 2. Phylogenetic signal test results obtained from likelihood method (λ) and randomisation method (Steps in character).

Shell Traits	Lambda (λ)	Likelihood score (alternative model)	Likelihood score (null model, $\lambda=0$)	p-value	Steps in Character	95% confidence interval of steps
Size ¹	0.84	-35.86	-37.15	0.109	-	-
Apex	0.92	-13.80	-14.56	0.219	5	4 – 10
Apical spire	0.88	-16.34	-16.72	0.387	4	3 – 6
Basal spire	0.53	-20.73	-22.16	0.091	7	5 – 11
Tuba	1	-16.03	-16.72	0.239	4	4 – 6
Apertural view	0.00	-26.62	-26.62	1.000	8	8 – 11

¹ randomisation method cannot be done on size, thus Blomberg et al.'s K was done (K = 0.92, p = 0.062).

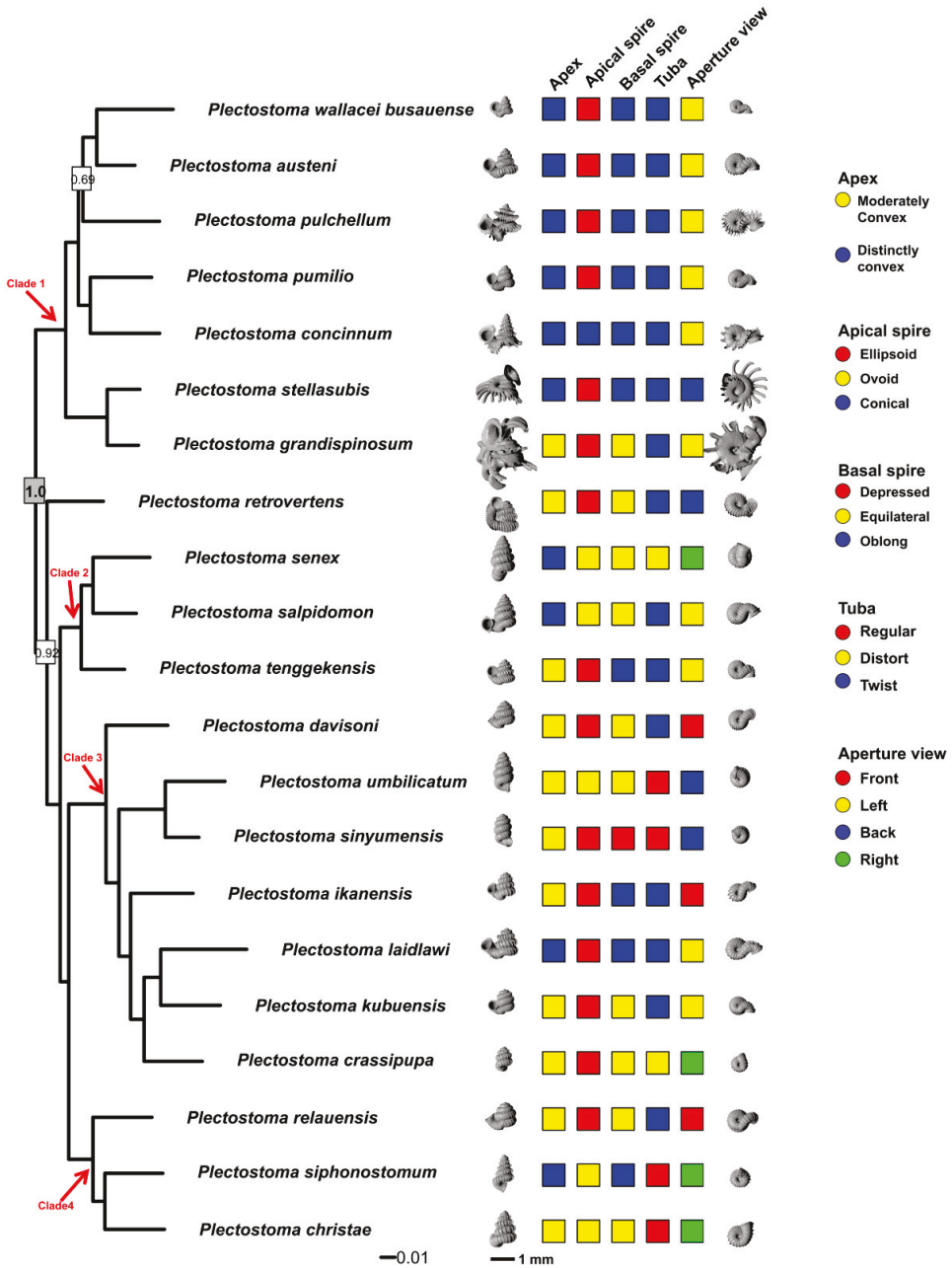


Figure 5. Phylogenetic tree and character states for each shell part for 21 *Plectostoma* species. The Bayesian estimated consensus phylogenetic tree, in which the monophyly of *Plectostoma* was well supported (grey box, posterior probability >95%) consists of four major clades. All nodes were well supported, except the two nodes that are annotated in the white box. The character states of five shell parts were annotated by different colours, and the left lateral and bottom views of the shell are shown.

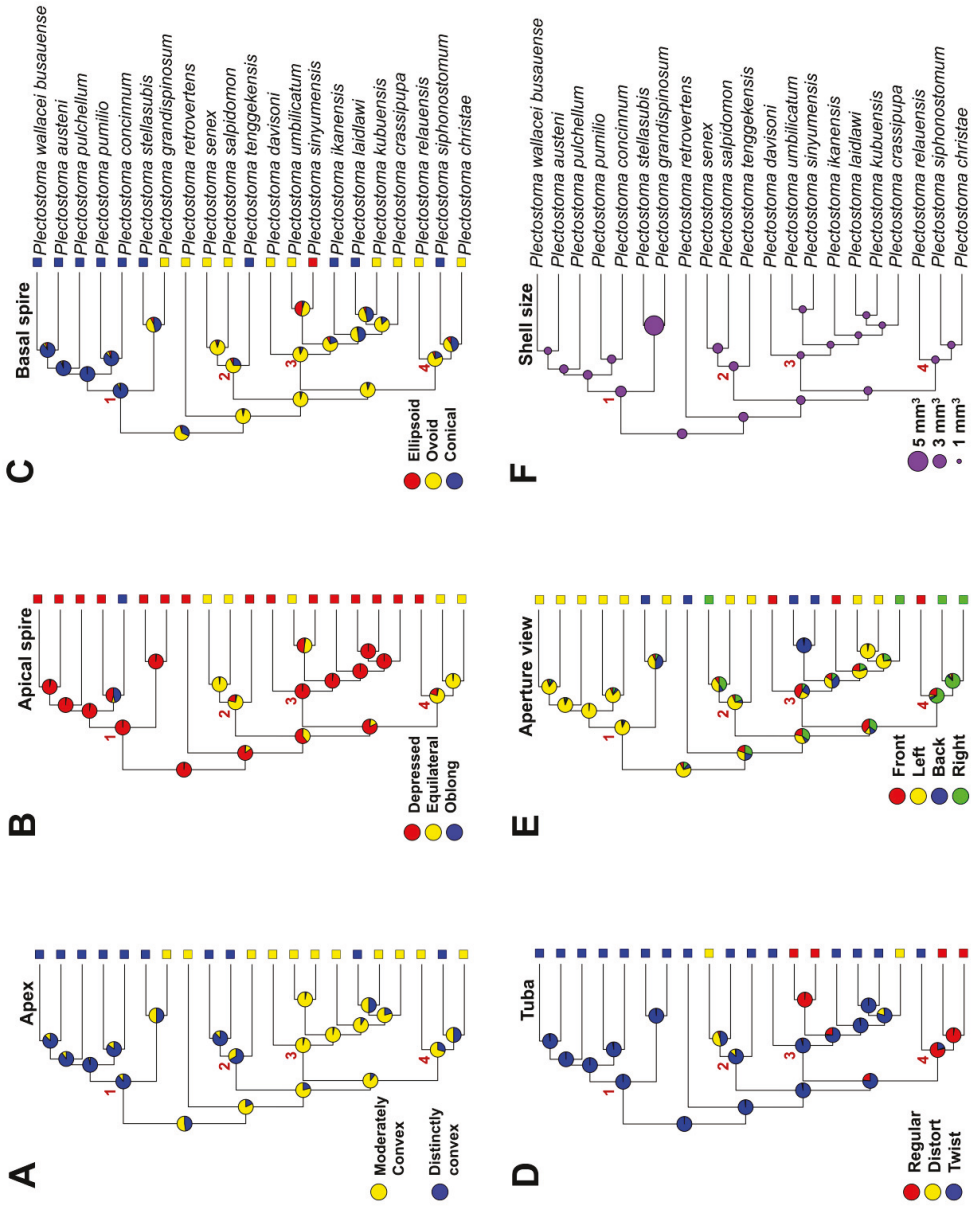


Figure 6. Ancestral state reconstructions for shell shape and size, using the maximum likelihood method. (A) Shell apex shapes. (B) Shell apical spire shapes. (C) Shell basal spire shapes. (D) Tuba coiling types. (E) Direction of aperture view. (F) Shell size.

Discussion

Shell size ontogeny and evolution

From a developmental point of view, we may expect a snail to grow a shell into which its entire soft body fits when it withdraws into the shell. From functional and developmental points of view, the shell volume is a more accurate measurement of shell size than linear dimensions such as shell height and width (see also Gould, 1984). Conventional linear measurements are extremely effective for size comparisons between shells of similar shape. However, they have limitations when comparison is made between shells that are of different shape. For example, shell height comparison between a discoidal shell and a fusiform shell tells very little about the size differences because the dimensional measurements are tied to shell shapes that result from different coiling strategies. Similarly, the whorl count that is often used in conjunction with the shell dimensional measurements has the same problem when dealing with shells that are very different in shape (Cain, 1980). These two issues are particularly relevant to *Plectostoma* shells, where comparison between diverse shell forms cannot be easily carried out with such conventional shell size measurements.

Shell size is controlled by the shell growth rate, which, in turn has both genetic and environmental components (see review by Goodfriend, 1986; and others: Baur & Raboud, 1988; Baur, Baur & Froberg, 1994; d'Avila & Bessa, 2005; Miereles et al., 2008; Martin & Bergey, 2013) that are hard to disentangle. In the case of *Plectostoma*, we do not know to what extent environmental factors may impact the, presumably genetically determined, aperture size ontogeny profiles in a species. Nevertheless, all *Plectostoma* species have identifiable shell-developmental homologies – the constriction before the tuba and differentiated peristome and aperture, which allows for reference points in the ontogeny and to define the end of shell ontogeny.

The evolution of *Plectostoma* shell size (shell volume) is not constrained by phylogeny. This finding confirms the results of most previous studies in which shell size (estimated by other metrics) tends to be as dissimilar between closely related species within a genus, as between more distantly related species (Teshima et al., 2003; Parmakelis et al., 2003; Johnson et al., 2004; Ketmaier, Giusti & Caccone, 2006; Bichain et al., 2007; Kameda, Kawakita & Kato, 2007; Elejalde et al., 2008b; Fiorentino et al., 2008; Puslednik et al., 2009; Buckley et al., 2011; Stankowski, 2011; Criscione, Law & Koehler, 2012; Johnson et al., 2012; Koehler & Johnson, 2012; Lee, Lue & Wu, 2012; Criscione & koehler, 2013; Du et al., 2013; but see Martinez-Orti et al., 2008; Kotsakiozi et al., 2013).

A general developmental program may exist that governs the length of the ontogeny axis and size changes of the aperture profile in the final determination of shell size. In general, the larger shells of *Plectostoma* is result from shell growth in which the aperture size is larger and the ontogeny axis (more or less equal to total whorl length) is longer than in the smaller *Plectostoma* shells (Figures 1B and 1C). A few previous studies have suggested that larger shell size tends to correspond with larger whorl size (an estimation for aperture size), but smaller whorl number (Cameron, 1981; Goodfriend 1983 cited in Goodfriend, 1986; Gould,

1984, Gould, 1989). However, all these studies used different measurements for shell size (shell weight in Cameron, 1981; shell diameter in Goodfriend, 1983; and linear measurement of shell dimensions in Gould, 1989). Thus, how the shell size is exactly determined by aperture size changes and total number of whorls added along the ontogeny remains unresolved.

In addition to the strong relationships among shell size, ontogeny axis length, and aperture size along the shell ontogeny, there is a consistent pattern of size changes along the standardised ontogeny axis; for example, the constriction occurs at approximately the same point in the standardised shell ontogeny in all species. Both the shell size relationships and the aperture size ontogenetic pattern are quite conserved among *Plectostoma* species, regardless of shell shape. However, a few species with an extremely long tuba, such as *P. grandispinosum*, deviate slightly from these rules by having a 30% longer ontogeny axis in the tuba phase of the ontogeny.

In brief, we showed that comparing shell size in terms of aperture size ontogeny and the ontogeny axis length may help to gain a better understanding of development and evolution of gastropod shell size. In *Plectostoma*, the size of the shell is determined by a conserved aperture size ontogeny and total shell ontogeny length. It is likely that ontogeny axis length and aperture size are strongly tied in the shell ontogeny. Hence, the parallel evolution of shell size in *Plectostoma* is a reflection of parallel evolution of ontogeny length and aperture size along the shell ontogeny, and does not involve significant changes in the pattern of the aperture size ontogeny profile.

Shell shape ontogeny and evolution

In contrast to the shell size, which can be characterised in a standard metric, shell shape analysis is more challenging because shape is much more difficult to characterise. Thus, shell shape has often been characterised semi-quantitatively, as it was in our study. Besides, shell form is usually treated as a single, functionally significant entity (see Introduction). Hence, the parallel evolution of shell shape in different lineages would imply the parallel evolution of the shell's adaptive function in these lineages; however, this does not need to imply a parallel evolution of the shell ontogeny.

As the shell is essentially a petrified ontogeny of the organ that secretes this exoskeleton (i.e., the mantle and the aperture ontogeny), the evolvability and heritability of aperture ontogeny can be examined on the basis of shell shape. The unidirectional accretionary growth of the shell may suggest that seemingly large shape differences between two shells may actually be caused by small differences in the aperture ontogeny; and also that shell whorls produced early in the ontogeny could have an influence on the subsequent aperture ontogeny and hence the subsequent shell form (Gould, 1984; Hutchinson, 1989). Hence, it is important to understand the evolution of shell form in view of the aperture ontogeny, growth trajectories, and aperture shape, which could provide further insight into the evolutionary lability of shell form.

We show the spire shape of *Plectostoma* shells not to be constrained by phylogeny. This result is mirrored in other studies that examined the relationship between the phylogeny and shell shapes among species within a genus (Boato, 1991; Emberton, 1995; Teshima et al., 2003; Tongkerd et al., 2004; Noshi & Sota, 2007; Elejalde et al., 2008a; Elejalde et al., 2008b; Elejalde et al., 2009; Stankowski, 2011; Johnson et al., 2012; Haase, Esch & Misof, 2013). Tuba coiling type in *Plectostoma* also is not constrained by phylogeny; similar results were obtained in studies of convergent evolution of the irregular coiling of the last whorl in other micro-snail taxa in Southeast Asia (Tongkerd et al., 2004). Homoplasy of shell traits at such a low taxonomic level, across different taxa, raises the question whether shell shapes that evolve in parallel could have the same shell ontogeny; or, in other words, occupy the same ontogenetic morphospace. To answer this question, we discuss the evolution of shell spire and tuba shape, respectively, based on the occupancy of ontogenetic morphospace.

Spire

The shell spire of all *Plectostoma* species has a regular shape, coiled around an imaginary axis. The shape differences between shell spires can be detected from a geometric perspective, for example height and width ratio and diameter differences between shell whorls. Although small spire shape differences between species are detectable by our qualitative approach, all *Plectostoma* species have a conical spire and live in a vertical limestone habitat. Hence, the slight differences in spire shape may not change the shell's adaptation to the inclination of the habitat (for similar results in other land snails, see review in Goodfriend, 1986; Okajima & Chiba, 2009; Okajima & Chiba, 2011; Noshita, Asami & Ubukata, 2012; Okajima & Chiba, 2012; Stankowski, 2013). The lack of adaptive differences could be one of the explanations for the lack of phylogenetic signal in *Plectostoma* spire shape.

For the ontogenetic point of view, similarly-shaped shell spires do not have the same aperture ontogeny profiles or occupy the same region in ontogenetic morphospace. In fact, the ontogenetic morphospace dimensions of the standardised curvature and aperture shape during the intermediate phase of shell ontogeny (*ca.* 20 – 60 %) are species-specific (Figure 4E). Neighbouring species in this part of ontogenetic morphospace do not necessarily have similar apical spire shapes (Figures 4B, 4E, and Supplementary File 5: Figures S6-S8). This suggests that two species may obtain similar spire shape with unique but different aperture ontogeny profiles. This also highlights the fact that our semi-quantitative spire shape categories which are similar to the conventional approach in the determination of shell shape (based on dimensional ratios) cannot effectively capture the ontogenetic differences between species (see also Haase, Esch & Misof, 2013).

Tuba

In contrast to the majority of gastropod, in which the last shell whorl is usually coiled in the same way as the preceding whorls, the shells of many species in Diplommatinidae, Streptaxidae, and Vertiginidae deviate from this generality. Although this character state is obviously derived, the opposite appears to be the case within the genus *Plectostoma*: a

twisted tuba is the ancestral state, whereas a distorted and a regularly coiled tuba are derived character states. It is clear that the magnitude of change in the aperture ontogeny profile in *Plectostoma* is related to the degree of distortion in tuba coiling (Figures 3A, 3D, 4A and 4D).

The twisted tuba occupies a larger ontogenetic morphospace than a regular or distorted tuba. The aperture ontogeny profiles for standardised torsion and curvature of the shells change drastically when forming the twisted tuba at the end of the *Plectostoma* shell ontogeny (after ca. 80 %) (Figure 3A). In addition, the aperture shape changes drastically as well for the species with a long tuba, such as *P. grandispinosum* and *P. retrovertens*. It is clear that the aperture ontogeny needs to undergo drastic changes to accomplish the transition from the regular spire to the twisted tuba, and therefore occupy a larger region in ontogenetic morphospace, as compared to species with a regular or slightly distorted tuba.

Conclusions

Our study has revealed a methodological issue in shell shape characterisation, and has shown an alternative to describing measurable differences between shell shapes in view of geometry and ontogeny. We support the concern of Haase et al. (2013) that using shell dimensional ratio as a proxy for shell shape may be oversimplified and inaccurate in the determination of similarity between shells, especially when the differences are small. We have also revealed that each species has a unique aperture ontogeny profile that is responsible for its shape while retaining a conserved shell size developmental program to gain its size. It is clear that the phylogeny does not limit changes in shell ontogeny. Further studies are needed to assess how other evolutionary processes and constraints, geometrical as well as functional, could have driven the parallel evolution of *Plectostoma* shell forms.

Acknowledgments

We thank Heike Kappes for fruitful discussion and Willem Renema for permission to use the CT-scanner outside of working hours. LTS thanks the Economic Planning Unit, Prime Minister's Department (UPE: 40/200/19/2524), State Planning Unit, Chief Minister's Department, Sarawak ((47) UPN/S/G1/I/10.1 Vol.27), Forest Department Sarawak (Research Permit NPW.907.4.4(V)-19; Park Permit No. 07/2010; Export Permit No. 09003) permissions to collect specimens in Malaysia.

Supplementary Information

Supplementary File 1. R scripts and data.

Supplementary File 2. Sequence data for 21 *Plectostoma* species and 4 outgroup taxa in nexus format for MrBayes analysis.

Supplementary File 3. Character matrix.

Supplementary File 4. Aperture ontogeny profiles for 11 *Plectostoma* species raw data.

Supplementary File 5. Aperture ontogeny profiles for 11 *Plectostoma* species, in which each was labelled by respective shell shape.

Supplementary File 6. Phylogenetic tree inferred by maximum likelihood analysis.

Supplementary File 7. Ancestral state reconstructions for shell shape and size, and rib form, as derived by the maximum parsimony method.

References

- Abel RL, Laurini CR, Richter M. 2012. A palaeobiologist's guide to 'virtual' micro-CT preparation. *Palaeontologia Electronica* 15(2):1-16.
- Ackerly SC. 1989a. Kinematics of accretionary shell growth, with examples from brachiopods and molluscs. *Paleobiology* 15(2):147-164.
- Ackerly SC. 1989b. Shell coiling in gastropods: analysis by stereographic projection. *Palaios* 4:374-378
- Adam H. 1865a. Description of a new genus of land-shells from the Island of Labuan, Borneo. *The Annals and Magazine of Natural History, including Zoology, Botany and Geology* 3(15): 177. <http://www.biodiversitylibrary.org/item/90412#page/859/mode/1up>.
- Adam H. 1865b. Descriptions of a new genus and some new species of mollusks. *Proceedings of the Zoological Society of London* 1865: 753-755. <http://www.biodiversitylibrary.org/item/90954#page/543/mode/1up>.
- Ahmed M, Raut SK. 1991. Influence of temperature on the growth of the pestiferous land snail *Achatina fulica* (Gastropoda: Achatinidae). *Walkerana* 5(13):33-62.
- Alcock J. 1998. *Animal Behavior: An Evolutionary Approach* (6th edition). Sunderland, Mass.: Sinauer Associates, Inc.
- Alexander RR, Dietl GP. 2003. The Fossil Record of Shell-Breaking Predation on Marine Bivalves and Gastropods. In: Kelley PH, Kowalewski M, Hansen TA, ed. *Predator-prey interactions in the fossil record* (Vol. 20). Springer US, 141-176.
- Ali JH, Taakob A. 2001. Diversity and importance of gastropods in Wang Kelian, Perlis. In: Faridah-Hanum I, Osman K, Latiff (Eds) *Kepelbagaian Biologi dan Pengurusan Taman Negeri Perlis: Persekitaran Fizikal dan Biologi Wang Kelian*. Jabatan Perhutanan Perlis, Malaysia, 139-147.
- de Almeida MN, de Almeida Bessa EC. 2001a. Growth and reproduction of *Leptinaria unilamellata* (d'Orbigny) (Mollusca, Subulinidae) in laboratory conditions. *Revista Brasileira de Zoologia* 18(4):1107-1113.
- de Almeida MN, de Almeida Bessa EC. 2001b. Growth and reproduction of *Bradybaena similaris* (Férussac) (Mollusca, Xanthonychidae) in laboratory conditions. *Revista Brasileira de Zoologia* 18(4):1115-1122.
- Allmon WD, Nieh JC, Norris RD. 1990. Drilling and peeling of turrnelline gastropods since the Late Cretaceous. *Palaeontology* 33(3):595-611.
- Allmon WD. 2011. Natural history of turrnelline gastropods (Cerithioidea: Turritellidae): a status report. *Malacologia* 54(1-2):159-202.
- Ancey CF. 1887. Nouvelles contributions malacologiques. *Bulletins de la Société Malacologique de France* 4: 273-288. <http://www.biodiversitylibrary.org/item/54677#page/303/mode/1up>.

References

- Andrei RM, Callieri M, Zini MF, Loni T, Maraziti G, Pan MC, Zoppè M. 2012. Intuitive representation of surface properties of biomolecules using BioBlender. *BMC Bioinformatics*, 13(Suppl 4):S16.
- Archangelsky M, Branham MA. 1998. Description of the preimaginal stages of *Pyraetomena borealis* (Randall, 1838) (Coleoptera: Lampyridae) and notes on its biology. *Entomological Society of Washington* 100:421-430.
- Arnold SJ. 1992. Constraints on phenotypic evolution. *American Naturalist* 140:S85-S107.
- Atwood JW, Sumrall CD. 2012. Morphometric investigation of the Pentremites fauna from the Glen Dean formation, Kentucky. *Journal of Paleontology* 86(5):813-828.
- D'Avila S, de Almeida Bessa EC. 2005. Influence of substrate on growth of *Subulina octona* (Brugüière) (Mollusca, Subulinidae), under laboratorial conditions. *Revista Brasileira de Zoologia* 22(1):205-211.
- Barker GM. 2004. *Natural enemies of terrestrial molluscs*. CABI.
- Baur B. 1984. Shell size and growth rate differences for alpine populations of *Arianta arbustorum* (L.) (Pulmonata: Helicidae). *Revue suisse de zoologie* 91(1):37-46.
- Baur B, Raboud C. 1988. Life history of the land snail *Arianta arbustorum* along an altitudinal gradient. *The Journal of Animal Ecology* 57(1):71-87.
- Baur A, Baur A, Froberg L. 1994. Herbivory on calcicolous lichens: different food preferences and growth rates in two co-existing land snails. *Oecologia* 98(3-4):313-319.
- Bayer U. 1978. Morphogenetic programs, instabilities and evolution: a theoretical study. *Neues Jahrbuch für Geologie und Paläontologie. Abhandlungen* 156:226-261.
- van Benthem-Jutting WSS. 1932. Notes on land Mollusca of the Malay Archipelago. *Journal of Conchology* 19(7): 196-210.
- van Benthem-Jutting WSS. 1952. The Malayan species of *Opisthostoma* (Gastropoda, Prosobranchia, Cyclophoridae), with a catalogue of all the species hitherto described. *The Bulletin of the Raffles Museum* 24(5): 5-61. <http://rmbr.nus.edu.sg/rbz/biblio/24/24brm005-062.pdf>.
- van Benthem-Jutting WSS. 1960. Non-marine Mollusca of the limestone hills in Malaya. *Proceedings of the Centenary and Bicentenary Congress of Biology*: 63-68.
- van Benthem-Jutting WSS. 1961. Additional new species and new localities of the family Vertiginidae and the genera *Oophana* and *Opisthostoma* from Malaya. *The Bulletin of the National Museum* 26: 34-48. <http://rmbr.nus.edu.sg/rbz/biblio/26/26brm034-048.pdf>.
- van Benthem-Jutting WSS. 1962. Coquilles Terrestres Nouvelles de Quelques Collines Calcaires du Cambodge et du Sud Vietnam. *Journal de Conchyliologie* 102(2): 3-15.

References

- Berry AJ. 1961. The habitats of some minute cyclophorids, hydrocenids and vertiginids on a Malayan limestone hill. *The Bulletin of the National Museum* 30: 101-105. <http://rmbn.nus.edu.sg/rbz/biblio/30/30bnm101-105.pdf>.
- Berry AJ. 1962. The growth of *Opisthostoma (Plectostoma) retrovertens* Tomlin, a minute cyclophorid from a Malayan limestone hill. *Journal of Molluscan Studies* 35: 46-49. <http://mollus.oxfordjournals.org/content/35/1/46.full.pdf>.
- Berry AJ. 1963. Growth and variation of the shell in certain Malayan limestone hill snails. *Journal of Molluscan Studies* 35: 203-206. <http://mollus.oxfordjournals.org/content/35/5/203.full.pdf>.
- Berry AJ. 1964. The reproduction of the minute cyclophorid snail *Opisthostoma (Plectostoma) retrovertens* from a Malayan limestone hill. *Proceedings of the Zoological Society of London* 142: 655-664. <http://dx.doi.org/10.1111/j.1469-7998.1964.tb04633.x>.
- Berry AJ. 1966. Population structure and fluctuations in the snail fauna of a Malayan limestone hill. *Journal of Zoology* 150: 11-27. <http://dx.doi.org/10.1111/j.1469-7998.1966.tb02996.x>.
- Benson DA, Boguski MS, Lipman DJ, Ostell J. 1997. GenBank. *Nucleic Acids Research* 25(1): 1-6. <http://dx.doi.org/10.1093/nar/gkq1079>.
- Bichain J-M, Boisselier-Dubayle M-C, Bouchet P, Samadi S. 2007. Species delimitation in the genus *Bythinella* (Mollusca : Caenogastropoda : Rissooidea): A first attempt combining molecular and morphometrical data. *Malacologia* 49(2):293-311.
- Bieler R. 1992. Gastropod phylogeny and systematic. *Annual Review of Ecological Systems* 23:311-338.
- Blanford WT, Blanford HF. 1860. Contributions to Indian Malacology. *Journal of the Asiatic Society of Bengal* 29: 117-127. <http://www.biodiversitylibrary.org/item/124448#page/141/mode/1up>.
- Blanford WT. 1866. On *Opisthostoma*, H. Blanford, with description of a new species from the neighbourhood of Bombay, and of the animal and operculum. *Proceedings of the Zoological Society of London* 1866: 447-451. <http://www.biodiversitylibrary.org/item/90954#page/545/mode/1up>.
- Blanford WT. 1867. On the Genus *Plectostoma* H. Adam, and the animal of *Diplommatina* Benson. *The Annals and Magazine of Natural History, including Zoology, Botany and Geology* 3(19): 305-307. <http://www.biodiversitylibrary.org/item/72153#319>.
- Bloch CP, Willig MR. 2009. Effects of competition on size and growth rates of *Caracolus caracolla* (L.) in Puerto Rico. *Journal of Molluscan Studies* 75:133-138.
- Blomberg SP, Garland T, Ives AR. 2003. Testing for phylogenetic signal in comparative data: behavioral traits are more labile. *Evolution* 57(4):717-745.

References

- Boata A. 1991. Allozyme versus discrete morphological characters in the phylogenetic analysis of the land snail *Solatopupa* (Pulmonata, Chondrinidae). *Bollettino Di Zoologia* 58(4):345-354.
- Van Bocxlaer B, Schultheiß R. 2010. Comparison of morphometric techniques for shapes with few homologous landmarks based on machine-learning approaches to biological discrimination. *Paleobiology* 36(3):497-515.
- Boeters HD, Knebelberger T. 2012. Revision of selected species of *Bythinella* Moquin-Tandon 1856 from Central Europe using morphology, anatomy and DNA barcodes (Caenogastropoda: Risssooidea). *Archiv für Molluskenkunde* 141(1): 115-136. doi: <http://dx.doi.org/10.1127/arch.moll/1869-0963/141/115-136>.
- Boettger A, Ermentrout B, Oster G. 2009. The neural origins of shell structure and pattern in aquatic mollusks. *Proceedings of the National Academy of Sciences* 106(16):6837-6842.
- Boettger O. 1893. Drei neue Pneumonopomen aus Borneo. *Nachrichtsblatt der Deutschen Malakozoologischen Gesellschaft* 25: 194-197.
<http://www.biodiversitylibrary.org/item/53280#page/202/mode/1up>.
- Bookstein, F. L. 1977. The study of shape transformation after D'Arcy Thompson. *Mathematical Biosciences* 34:177-219.
- Bookstein, F. L. 1980. When one form is between two others: an application of biorthogonal analysis. *American Zoologists* 20:627-641.
- Bookstein FL. 1991. *Morphometric Tools for Landmark Data: Geometry and Biology*. Cambridge University Press.
- Brandmaier AM. 2012a. *Permutation Distribution Clustering and Structural Equation Model Trees*. Fakultät 6 - Naturwissenschaftlich-Technische Fakultät I, Universität des Saarlandes.
- Brandmaier AM. 2012b. *pdcc: Permutation Distribution Clustering. R package version 0.3*.
<http://CRAN.R-project.org/package=pdcc>
- Brown AC, Trueman ER. 1982. Muscles that push snails out of their shells. *Journal of Molluscan Studies* 48:97-98.
- Brusca RC, Brusca GJ. 2003. *Invertebrates*. 2nd edition. Sunderland, MA: Sinauer Associates, Inc.
- Buckley TR, Stringer I, Gleeson D, Howitt R, Attanayake D, Parrish R, Sherley G, Rohan MA. 2011. A revision of the New Zealand *Placostylus* land snails using mitochondrial DNA and shell morphometric analyses, with implications for conservation. *New Zealand Journal of Zoology* 38(1):55-81.
- Cain AJ. 1977. Variation in the spire index of some coiled gastropod shells, and its evolutionary significance. *Philosophical Transactions of the Royal Society of London. B, Biological Sciences* 277:377-428

References

- Cain A. 1980. Whorl number, shape, and size of shell in some pulmonate faunas. *Journal of Conchology* 30(3):209-221.
- Cameron R. 1981. Functional aspects of shell geometry in some British land snails. *Biological Journal of the Linnean Society* 16(2):157-167.
- Carbayo F, Marques AC. 2011. The costs of describing the entire animal kingdom. *Trends in Ecology and Evolution* 26(4): 154-155. <http://dx.doi.org/10.1016/j.tree.2011.01.004>.
- Cardini A, Loy A. 2013. On growth and form in the "computer era": from geometric to biological morphometrics. *Hystrix, the Italian Journal of Mammalogy*, 24(1), 1-5.
- Cassola, VF, de Melo Lima VJ, Kramer R, Khoury HJ. 2010. FASH and MASH: female and male adult human phantoms based on polygon mesh surfaces: I. Development of the anatomy. *Physics in Medicine and Biology* 55(1):133.
- Chaplin TA, Yu HH, Rosa MG. 2013. Representation of the visual field in the primary visual area of the marmoset monkey: Magnification factors, point-image size, and proportionality to retinal ganglion cell density. *Journal of Comparative Neurology* 521(5):1001-1019.
- Chacon R. 2012. Using Jacobian elliptic functions to model natural shapes. *International Journal of Bifurcation and Chaos* 22(1):1230005.
- Checa A. 1991. Sectorial expansion and shell morphogenesis in molluscs. *Lethaia* 24(1):97-114.
- Checa A, Aguado R. 1992. Sectorial-expansion analysis of irregularly coiled shells: application to the recent gastropod *Distorsio*. *Palaeontology* 35:913-925.
- Checa AG, Jiménez- Jiménez AP, Rivas P. 1998. Regulation of spiral coiling in the terrestrial gastropod *Sphincterochila*: an experimental test of the road-holding model. *Journal of Morphology* 235:249-257.
- Chirat R, Moulton DE, Goriely A. 2013. Mechanical basis of morphogenesis and convergent evolution of spiny seashells. *Proceedings of the National Academy of Sciences* 110(15):6015-6020.
- Chow V. 1987. Patterns of growth and energy allocation in northern California populations of *Littorina* (Gastropoda: Prosobranchia). *Journal of Experimental Marine Biology and Ecology* 110:69-89.
- Cignoni P, Corsini M, Ranzuglia G. 2008. Meshlab: an open-source 3d mesh processing system. *Ercim news* 73:45-46.
- Clarke RK, Grahame J, Mill PJ. 1999. Variation and constraint in the shells of two sibling species of intertidal rough periwinkles (Gastropoda: *Littorina* spp.). *Journal of Zoology* 247(2):145-154.
- Claude J. 2008. *Morphometrics with R*. Springer.

References

- Clench WJ, Jacobson MK. 1968. Monograph of the Cuban genus *Viana* (Mollusca: Archaeogastropoda: Helicinidae). *Breviora* 298:1-25.
- Clements GR. 2007. Conservation biogeography of terrestrial molluscs on tropical limestone karsts. MSC thesis. National University of Singapore.
- Clements R, Ng PKL, Lu XX, Ambu S, Schilthuizen M, Bradshaw CJA. 2008. Using biogeographical patterns of endemic land snails to improve conservation planning for limestone karsts. *Biological conservation* 141: 2751–2764.
<http://dx.doi.org/10.1016/j.biocon.2008.08.011>.
- Clements R, Liew T-S, Schilthuizen M, Vermeulen JJ. 2008. Further twists in gastropod shell evolution. *Biology Letter* 4:179-182.
- Clements R. 2009a. *Opisthostoma sciaphilum*. In: IUCN 2013. IUCN Red List of Threatened Species. Version 2013.2. <www.iucnredlist.org>. Downloaded on 26 November 2013.
- Clements R. 2009b. *Opisthostoma senex*. In: IUCN 2013. IUCN Red List of Threatened Species. Version 2013.2. <www.iucnredlist.org>. Downloaded on 26 November 2013.
- Clements R. 2009c. *Opisthostoma retrovertens*. In: IUCN 2013. IUCN Red List of Threatened Species. Version 2013.2. <www.iucnredlist.org>. Downloaded on 26 November 2013.
- Cock PJ, Antao T, Chang JT, Chapman BA, Cox CJ, Dalke A, Friedberg I, Hamelryck T, Kauff F, Wilczynski B, de Hoon MJ. 2009). Biopython: freely available Python tools for computational molecular biology and bioinformatics. *Bioinformatics* 25(11): 1422-1423.
<http://dx.doi.org/10.1093/bioinformatics/btp163>.
- Cortie MB. 1989. Models for mollusk shell shape. *South African Journal of Science* 85(7):454-460.
- Cortie MB. 1993. Digital seashells. *Computers & graphics* 17(1):79-84.
- Cracraft J. 1983. Species concepts and speciation analysis. *Current Ornithology* 1: 159-187.
- de Crespigny CC. 1865. Note on a shell from Labuan. *The Natural History Review* 5(20): 599. <http://www.biodiversitylibrary.org/page/9749440#page/609/mode/1up>.
- Criscione F, Koehler F. 2013. Conserved shell disguises diversity in *Mesodontrachia* land snails from the Australian Monsoon Tropics (Gastropoda: Camaenidae). *Zoologica Scripta* 42(4):389-405.
- Criscione F, Law ML, Koehler F. 2012. Land snail diversity in the monsoon tropics of Northern Australia: revision of the genus *Exiligada* Iredale, 1939 (Mollusca: Pulmonata: Camaenidae), with description of 13 new species. *Zoological Journal of the Linnean Society* 166(4):689-722.

References

- Crosse H. 1892. Études malacologiques sur les genres nouveaux ou peu connus. *Journal de Conchyliologie* 32: 279-292.
<http://www.biodiversitylibrary.org/page/25234590#page/292/mode/1up>.
- D'ávila S, Bessa E. 2005. Influence of substrate on reproduction of *Subulina octona* (Brugüière)(Mollusca, Subulinidae), under laboratorial conditions. *Revista Brasileira de Zoologia* 22(1):197-204.
- Darriba D, Taboada GL, Doallo R, Posada D. 2012. jModelTest 2: more models, new heuristics and parallel computing. *Nature Methods* 9(8):772-772.
- Davison A, Blackie RL, Scothern GP. 2009. DNA barcoding of stylommatophoran land snails: a test of existing sequences. *Molecular Ecology Resources* 9(4): 1092-1101.
<http://dx.doi.org/10.1111/j.1755-0998.2009.02559.x>.
- Davison GWH, Kiew R. 1990. *Survey of Flora and Fauna of Limestone Hills in Kelantan, with Recommendations for Conservation, Kuala Lumpur*. Worldwide Fund for Nature Malaysia.
http://repository.wwf.org.my/technical_reports/S/1990_SurveyOfFloraAndFaunaOfLimestoneHillsInKelantanWithRecommendationsForConservation_GWHDavidson_RKiew.pdf.
- Dautzenberg P, Fischer H. 1905. Liste des mollusques récoltés par M.H. Mansuy en Indo-Chine et au Yunnan et description d'espèces nouvelles. *Journal de Conchyliologie* 53: 343-471. <http://www.biodiversitylibrary.org/item/55051#page/379/mode/1up>.
- Davoli E, Russo F. 1974. Una metodologia paleontometrica basata sul modello di Raup: Verifica sperimentale su rappresentanti follili del gen. *Subula* Schumacher. *Bollettino della Societa Paleontologica Italiana* 13:108-121.
- Deans AR, Yoder MJ, Balhoff JP. 2012. Time to change how we describe biodiversity. *Trends in Ecology and Evolution* 27(2): 78-84. <http://dx.doi.org/10.1016/j.tree.2011.11.007>
- Dera G, Eble GJ, Neige P, David B. 2009. The flourishing diversity of models in theoretical morphology: from current practices to future macroevolutionary and bioenvironmental challenges. *Paleobiology* 34 (3):301-317.
- DeWitt TJ, Sih A, Hucko JA. 1999. Trait compensation and cospecialization in a freshwater snail: size, shape and antipredator behaviour. *Animal Behaviour* 58(2):397-407.
- DeWitt TJ, Langerhans RB. 2003. Multiple prey traits, multiple predators: keys to understanding complex community dynamics. *Journal of Sea Research* 49:143-155.
- Du L, Yang J, von Rintelen T, Chen X, Aldridge D. 2013. Molecular phylogenetic evidence that the Chinese viviparid genus *Margarya* (Gastropoda: Viviparidae) is polyphyletic. *Chinese Science Bulletin* 58:2154-2162.
- Edwards JL. 2004. Research and societal benefits of the Global Biodiversity Information Facility. *BioScience* 54(6): 486-487.
[http://dx.doi.org/10.1641/0006-3568\(2004\)054\[0486:RASBOT\]2.0.CO;2](http://dx.doi.org/10.1641/0006-3568(2004)054[0486:RASBOT]2.0.CO;2).

References

- Ekaratne SUK, Crisp DJ. 1983. A geometric analysis of growth in gastropod shells, with particular reference to turbinate forms. *Journal of the Marine Biological Association of the United Kingdom* 63(4):777-797.
- Elejalde M, Munoz B, Arrebola J, Gomez-Moliner B. 2005. Phylogenetic relationships of *Iberus gualtieranus* and *I. Alonensis* (Gastropoda : Helicidae) based on partial mitochondrial 16S rRNA and COI gene sequences. *Journal of Molluscan Studies* 71(4):349-355.
- Elejalde MA, Madeira MJ, Arrebola JR, Munoz B, Gomez-Moliner BJ. 2008a. Mitochondrial DNA diversity and taxa delineation in the land snails of the *Iberus gualtieranus* (Pulmonata, Helicidae) complex. *Zoological Journal of the Linnean Society* 154(4):722-737.
- Elejalde MA, Madeira MJ, Arrebola JR, Munoz B, Gomez-Moliner BJ. 2008b. Molecular phylogeny, taxonomy and evolution of the land snail genus *Iberus* (Pulmonata: Helicidae). *Journal of Zoological Systematics and Evolutionary Research* 46(3):193-202.
- Elkarmi AZ, Ismail NS. 2007. Growth models and shell morphometrics of two populations of *Melanoides tuberculata* (Thiaridae) living in hot springs and freshwater pools. *Journal of Limnology* 66(2):90-96.
- Emberton K. 1994. Polygyrid land snail phylogeny: external sperm exchange, early North American biogeography, iterative shell evolution. *Biological Journal of the Linnean Society* 52(3): 241-271.
- Emberton K. 1995. Cryptic, genetically extremely divergent, polytypic, convergent, and polymorphic taxa in Madagascan *Tropidophora* (Gastropoda: Pomatiasidae). *Biological Journal of the Linnean Society* 55(3):183-208.
- Evans AR. 2013. Shape descriptors as ecometrics in dental ecology. *Hystrix, the Italian Journal of Mammalogy*, 24(1), 8.
- Faghih Shojaei M, Mohammadi V, Rajabi H, Darvizeh A. 2012. Experimental analysis and numerical modeling of mollusk shells as a three dimensional integrated volume. *Journal of the Mechanical Behavior of Biomedical Materials* 16:38-54.
- Faulwetter S, Vasileiadou A, Kouratoras M, Dailianis T, Arvanitidis C. 2013. Micro-computed tomography: Introducing new dimensions to taxonomy. *ZooKeys* 263: 1-45. <http://dx.doi.org/10.3897/zookeys.263.4261>.
- Fiorentino V, Salomone N, Manganelli G, Giusti F. 2008. Phylogeography and morphological variability in land snails: the *Sicilian Marmorana* (Pulmonata, Helicidae). *Biological Journal of the Linnean Society* 94(4):809-823.
- Fischer PH. 1963. Mollusques terrestres de l'Indo-Chine et du Yunnan conservés dans la collection de l'École des Mines de Paris. *Journal de Conchyliologie* 103: 32-37.
- Folmer O, Black M, Hoeh W, Lutz RA, Vrijenhoek RC. 1994. DNA primers for amplification of mitochondrial Cytochrome Oxidase Subunit I from diverse metazoan invertebrates. *Molecular Marine Biology and Biotechnology* 3:294-299.

References

- Foote M, Cowie RH. 1988. Developmental Buffering as a Mechanism for Stasis: Evidence from the Pulmonate *Theba pisana*. *Evolution* 42(2):396-399.
- Fournié J, Chétail M. 1984. Calcium dynamics in land gastropods. *American Zoologist* 24:857-870.
- Fowler DR, Meinhardt H, Prusinkiewicz P. 1992. Modeling seashells. *ACM SIGGRAPH Computer Graphics* 26(2):379-387.
- Frescura M, Hodson AN. 1992. The fine structure of the collumellar muscle of some gastropod mollusks. *Veliger* 35(4):308-315.
- Fryda J, Ferrová L. 2011. The oldest evidence of non-coaxial shell heterostrophy in the Class Gastropoda. *Bulletin of Geosciences* 86(4):765-776.
- Fulton HC. 1901. Descriptions of some supposed new species of *Diplommatina*, *Opisthostoma*, and a new variety of *Alycaeus* from N. Borneo, Banguay Island, and Darjeeling. *The Annals and Magazine of Natural History, including Zoology, Botany and Geology* 7(8): 242-245. <http://biodiversitylibrary.org/item/94923#page/270/mode/1up>.
- Galbraith C, Prusinkiewicz P, Wyvill B. 2002. Modeling a *Murex cabritii* sea shell with a structured implicit surface modeler. *The Visual Computer* 18(2):70-80.
- Ghosh E. 1913. XV. Mollusca, I: Rathouisiidae. *Records of the Indian Museum* 8:209-227.
- Giam X, Scheffers BR, Sodhi NS, Wilcove DS, Ceballos G, Ehrlich PR. 2011. Reservoir of richness: least disturbed tropical forests are centres of undescribed species diversity. *Proceedings of the Royal Society B: Biological Sciences* 279(1726): 67-76. <http://dx.doi.org/10.1098/rspb.2011.0433>.
- Gittenberger E. 1996. Adaptations of the aperture in terrestrial gastropod-pulmonate shells. *Netherlands Journal of Zoology* 46(3-4):191-205.
- Godefroy JE, Bornert F, Gros CI, Constantinesco A. 2012. Elliptical Fourier descriptors for contours in three dimensions: A new tool for morphometrical analysis in biology. *Comptes rendus biologiques* 335(3):205-213.
- Godwin-Austen HH. 1889. On a collection of land-shells made in Borneo by Mr. A. Everett, with descriptions of supposed new species. *Proceedings of the Zoological Society of London* 1889: 332-355. <http://www.biodiversitylibrary.org/item/96894#462>.
- Godwin-Austen HH. 1890. On a collection of land-shells made in Borneo by Mr. A. Everett, with descriptions of supposed new species. Part 1: Cyclostomacea. *The Annals and Magazine of Natural History, including Zoology, Botany and Geology* 6(6): 244-246. <http://biodiversitylibrary.org/item/63336#page/271/mode/1up>.
- Goodfriend GA. 1983. Some new methods for morphometric analysis of gastropod shells. *Malacological Review* 16:79-86.

References

- Goodfriend GA. 1986. Variation in land-snail shell form and size and its causes: a review. *Systematic Biology* 35(2):204-223.
- Gould SJ. 1968. Ontogeny and the explanation of form: an allometric analysis. *Paleontological Society Memoir* 2:81-98.
- Gould SJ. 1969. Ecology and functional significance of uncoiling in *Vermicularia spirata*: an essay on gastropod form. *Bulletin of Marine Science* 19(2):432-445.
- Gould SJ. 1984. Morphological channeling by structural constraint: convergence in styles of dwarfing and gigantism in *Cerion*, with a description of two new fossil species and a report on the discovery of the largest *Cerion*. *Paleobiology* 10(2):172-194.
- Gould SJ. 1989. A developmental constraint in *Cerion*, with comments of the definition and interpretation of constraint in evolution. *Evolution* 43(3):516-539.
- Graus RR. 1974. Latitudinal trends in the shell characteristics of marine gastropods. *Lethaia*, 7(4):303-314.
- Gwinn NE, Rinaldo C. 2009. The Biodiversity Heritage Library: sharing biodiversity literature with the world. *International Federation of Library Associations Journal* 35:25-34. <http://dx.doi.org/10.1177/0340035208102032>.
- Haase M, Esch S, Misof B. 2013. Local adaptation, refugial isolation and secondary contact of Alpine populations of the land snail *Arianta arbustorum*. *Journal of Molluscan Studies* 79:241-248.
- Hall TA .1999. BioEdit: a user-friendly biological sequence alignment editor and analysis program for Windows 95/98/NT. *Nucleic acids symposium series* 41: 95-98. <http://www.mbio.ncsu.edu/bioedit/bioedit.html>.
- Hammer Ø. 2000. A theory for the formation of commarginal ribs in mollusc shells by regulative oscillation. *Journal of Molluscan Studies* 66(3):383-392.
- Harary G, Tal A. 2011. The natural 3D spiral. *Computer Graphics Forum* 30(2):237-246).
- Hardy OJ, Pavoine S. 2012. Assessing phylogenetic signal with measurement error: a comparison of Mantel tests, Blomberg et al.'s K, and phylogenetic distograms. *Evolution* 66:2614-2621
- Harmon LJ, Weir JT, Brock CD, Glor RE, Challenger W. 2008. GEIGER: investigating evolutionary radiations. *Bioinformatics* 24(1):129-131.
- Haug JT, Maas A, Waloszek D. 2009. Ontogeny of two Cambrian stem crustaceans, †*Gotiscaris longispinosa* and †*Cambropachycope clarksoni*. *Palaeontographica A* 289:1-43.
- Haug JT, Waloszek D, Haug C, Maas A. 2010. High-level phylogenetic analysis using developmental sequences: The Cambrian †*Martinssonina elongata*, †*Musacaris gerdgeyeri* gen. et sp. nov. and their position in early crustacean evolution. *Arthropod Structure & Development* 39(2):154-173.

References

- Haug C, Haug JT, Fayers SR, Trewin NH, Castellani C, Waloszek D, Maas A. 2012. Exceptionally preserved nauplius larvae from the Devonian Windyfield chert, Rhynie, Aberdeenshire, Scotland. *Palaeontologia Electronica* 15:2-24.
- Heath DJ. 1985. Whorl overlap and the economical construction of the gastropod shell. *Biological Journal of the Linnean Society* 24:165-174.
- Hebert PDN, Ratnasingham S, deWaard JR. 2003. Barcoding animal life: cytochrome oxidase subunit 1 divergences among closely related species. *Proceedings of the Royal Society of London. Series B: Biological Sciences* (Suppl.) 270: S96-S99. <http://dx.doi.org/10.1098/rsbl.2003.0025>.
- Hedgpeth JW. 1961. *Taxonomy: Man's Oldest Profession*. 11th Annual University of the Pacific Faculty Lecture, Stockton, California, USA. 19 pp.
- Heller J. 2001. Life History Strategies. In Barker GM (Ed) *The Biology of Terrestrial Molluscs*. CABI Publishing, Oxon, UK, 413-445.
- Hemmen J, Hemmen C. 2001. Aktualisierte Liste der terrestrischen Gastropoden Thailands. *Schriften zur Malakozoologie - aus dem Haus der Natur Cismar* 18: 35-70.
- Henry PY, Jarne P. 2007. Marking hard-shelled gastropods: tag loss, impact on life-history traits, and perspectives in biology. *Invertebrate Biology* 126(2):138-153.
- Heude PM. 1882-1890. Notes sur les mollusques terrestres de la vallee du Fleuve Bleu. *Mémoires concernant l'histoire naturelle de l'Empire Chinois*: 1-179.
- Heywood VH. 1974. Systematics – the stone of Sisyphus. *Biological Journal of the Linnean Society* 6: 169-178. <http://dx.doi.org/10.1111/j.1095-8312.1974.tb00721.x>.
- Hoekstra P, Schilthuizen M. 2011. Phylogenetic relationships between isolated populations of the limestone-dwelling microsnail *Gyliotrachela hungerfordiana* (Gastropoda: Vertiginidae). *Journal of Zoological Systematics and Evolutionary Research* 49(4): 266-272. <http://dx.doi.org/10.1111/j.1439-0469.2011.00623.x>.
- Hoso M. 2012. Cost of autotomy drives ontogenetic switching of anti-predator mechanisms under developmental constraints in a land snail. *Proceedings of the Royal Society B: Biological Sciences* 279(1748):4811-4816.
- Hoso M, Hori M. 2008. Divergent shell shape as an antipredator adaptation in tropical land snails. *The American Naturalist* 172(5):726-732.
- Hoso M, Kameda Y, Wu S P, Asami T, Kato M, Hori M. 2010. A speciation gene for left-right reversal in snails results in anti-predator adaptation. *Nature communications* 1: 133.
- Huelsenbeck JP, Ronquist F. 2001. MRBAYES: Bayesian inference of phylogenetic trees. *Bioinformatics* 17(8): 754-755. <http://dx.doi.org/10.1093/bioinformatics/17.8.754>.
- Hutchinson JMC. 1989. Control of gastropod shell shape; the role of the preceding whorl. *Journal of Theoretical Biology* 104:431-444.

References

- Hutchinson JMC. 1999. But which morphospace to choose?: Theoretical Morphology by GR McGhee, Jr. *Trends in Ecology & Evolution* 14:414.
- Iller C. 1983. The mathematics of gnomonic seashells. *Mathematical Biosciences* 63:21-56.
- Illert C. 1987. Formulation and solution of the classical seashell problem. *II Nuovo Cimento D*. 9: 791–814. <http://dx.doi.org/10.1007/BF02453750>.
- Illert C, Pickover CA. 1992. Generating irregularly oscillating fossil seashells. *Computer Graphics and Applications, IEEE* 12(3):18-22.
- Im CH, Park JH, Shim M, Chang WH, Kim YH. 2012. Evaluation of local electric fields generated by transcranial direct current stimulation with an extracephalic reference electrode based on realistic 3D body modeling. *Physics in Medicine and Biology* 57(8):2137.
- Ito Y, Jenkins R, Ichikawa T, Sasaki T, Tanabe K. 2009. *Catalogue of Type and Cited Specimens in the Department of Historical Geology and Paleontology of the University Museum*. The University of Tokyo.
- IUCN Standards and Petitions Subcommittee. 2013. *Guidelines for Using the IUCN Red List Categories and Criteria*. Version 10.1. Prepared by the Standards and Petitions Subcommittee.
- Johnson DS. 1964. A question of nomenclature. *Malayan Nature Journal* 18: 68–69.
- Johnson M, Black R. 1991. Growth, survivorship, and population size in the land snail *Rhagada convicta* Cox, 1870 (Pulmonata: Camaenidae) from a semiarid environment in Western Australia *Journal of Molluscan Studies* 57(3):367-374.
- Johnson M, Hamilton Z, Murphy C, MacLeay C, Roberts B, Kendrick P. 2004. Evolutionary genetics of island and mainland species of *Rhagada* (Gastropoda : Pulmonata) in the Pilbara Region, Western Australia. *Australian Journal of Zoology* 52(4):341-355.
- Johnson MS, Hamilton ZR, Teale R, Kendrick PG. 2012. Endemic evolutionary radiation of *Rhagada* land snails (Pulmonata: Camaenidae) in a continental archipelago in northern Western Australia. *Biological Journal of the Linnean Society* 106(2):316-327.
- Johnston MR, Tabachnick RE, Bookstein FL. 1991. Landmark-based morphometrics of spiral accretionary growth. *Paleobiology* 17(1):19-36.
- Kaesler RL, Waters JA. 1972. Fourier analysis of the ostracode margin. *Geological Society of America Bulletin* 83(4):1169-1178.
- Kado Y. 1960. Studies on shell formation in molluscs. *Journal of science of the Hiroshima University Series B Div. I (Zool)* 19:163-210.
- Kameda Y, Kawakita A, Kato M. 2007. Cryptic genetic divergence and associated morphological differentiation in the arboreal land snail *Satsuma* (Luchuhadra) largillierti (Camaenidae) endemic to the Ryukyu Archipelago, Japan. *Molecular Phylogenetics and Evolution* 45(2):519-533.

References

- Kawaguchi Y. 1982. A morphological study of the form of nature. *Computer Graphics* 16:223-232.
- Kelley PH, Hansen TA. 2003. The fossil record of drilling predation on bivalves and gastropods. In: Kelley PH, Kowalewski M, Hansen TA, ed. *Predator-prey interactions in the fossil record* (Vol. 20). Springer US, 113-139.
- Kemp P, Bertness MD. 1984. Snail shape and growth rates; evidence for plastic shell allometry in *Littorina littorea*. *Proceedings of the National Academy of Sciences* 81:811-813.
- Ketmaier V, Giusti F, Caccone A. 2006. Molecular phylogeny and historical biogeography of the land snail genus *Solatopupa* (Pulmonata) in the peri-Tyrrhenian area. *Molecular Phylogenetics and Evolution* 39(2):439-451.
- Kier W. 1988. The arrangement and function of molluscan muscle. In: Trueman E, Clarke M, ed. *The Mollusca* (Volume 11), *Form and Function*. Academic Press, New York, 211-252
- Kimura M. 1980. A simple method for estimating evolutionary rate of base substitutions through comparative studies of nucleotide sequences. *Journal of Molecular Evolution* 16:111-120.
- Klingenberg CP. 2013. Visualizations in geometric morphometrics: how to read and how to make graphs showing shape changes. *Hystrix, the Italian Journal of Mammalogy*, 24(1), 10.
- Kobayashi SR, Hadfield MG. 1996. An experimental study of growth and reproduction in the Hawaiian tree snails *Achatinella mustelina* and *Partulina redfieldii* (Achatinellinae). *Pacific Science* 50(4):339-354.
- Koehler F, Johnson MS. 2012. Species limits in molecular phylogenies: a cautionary tale from Australian land snails (Camaenidae: Amplirhagada Iredale, 1933). *Zoological Journal of the Linnean Society* 165(2):337-362.
- Köhler F, Johnson MS. 2012. Species limits in molecular phylogenies: a cautionary tale from Australian land snails (Camaenidae: Amplirhagada Iredale, 1933). *Zoological Journal of the Linnean Society* 165(2): 337-362. <http://dx.doi.org/10.1111/j.1096-3642.2011.00810.x>.
- Kohn AJ, Riggs AC. 1975. Morphometry of the *Conus* shell. *Systematic Zoology* 24:346-359.
- Konumu J, Chiba S. 2007. Trade-Offs between Force and Fit: Extreme Morphologies Associated with Feeding Behavior in Carabid Beetles. *The American Naturalist* 170(1):90-100.
- Kotsakiozi P, Rigal F, Valakos E, Parmakelis A. 2013. Disentangling the effects of intraspecies variability, phylogeny, space, and climate on the evolution of shell morphology in endemic Greek land snails of the genus *Codringtonia*. *Biological Journal of the Linnean Society* 110(4):796-813.
- Kowalewski M, Dulai A, Fürsich FT. 1998. A fossil record full of holes: the Phanerozoic history of drilling predation. *Geology* 26(12):1091-1094.

References

- Kramarenko SS, Popov VN. 1999. Specific features of reproduction and growth of the terrestrial mollusk *Eobania vermiculata* (Müller, 1774) (Gastropoda; Pulmonata; Helicidae) under laboratory conditions. *Russian Journal of Ecology* 30(4):269-272.
- Kuhl FP, Giardina CR. 1982. Elliptic Fourier features of a closed contour. *Computer Graphics and Image Processing* 18(3):236-258.
- Kurozumi T. 1985. Evidence of slug predation on land snail eggs. *Applied Entomology and Zoology* 20(4):490-491.
- Kuźnik-Kowalska E, Lewandowska M, Pokryszko BM, Proćków M. 2013. Reproduction, growth and circadian activity of the snail *Bradybaena fruticum* (OF Müller, 1774) (Gastropoda: Pulmonata: Bradybaenidae) in the laboratory. *Central European Journal of Biology* 8(7):693-700.
- Laidlaw FF. 1928. A list of the land and fresh-water Mollusca of the Malay peninsula with notes. *Journal of the Malaysian Branch of the Royal Asiatic Society* 6: 25-37.
- Laxton JH. 1970. Shell growth in some New Zealand Cymatiidae (Gastropoda: Prosobranchia). *Journal of Experimental Marine Biology and Ecology* 4(3):250-260.
- Lazaridou-Dimitriadou M. 1995. The life-cycle, demographic-analysis, growth and secondary production of the snail *Helicella (Xerothracia) Pappi* (Schutt, 1962) (Gastropoda Pulmonata) in E. Macedonia (Greece). *Malacologia* 37(1):1-11.
- Lee Y-C, Lue K-Y, Wu W-L. 2012. The Phylogeny and Morphological Adaptations of *Cyclotus taiwanus* ssp. (Gastropoda: Cyclophoridae). *Malacologia* 55(1):91-105.
- Lewiner T, Gomes Jr JD, Lopes H, Craizer M. 2005. Curvature and torsion estimators based on parametric curve fitting. *Computers & Graphics* 29(5):641-655.
- Liew T-S, Schilthuizen M, Vermeulen JJ. 2009. Systematic revision of the genus *Everettia* Godwin-Austen, 1891 (Mollusca: Gastropoda: Dyakiidae) in Sabah, northern Borneo. *Zoological Journal of the Linnean Society* 157(3): 515-550. <http://dx.doi.org/10.1111/j.1096-3642.2009.00526.x>.
- Linsley RM. 1977. Some "laws" of gastropod shell form. *Paleobiology* 3:196-206.
- Linsley RM (1978) Shell form and the evolution of gastropods. *American Scientist* 66:432-441.
- Linsley RM, Javidpour M. 1980. Episodic growth in Gastropoda. *Malacologia* 20(1):153-160.
- Løvtrup S, von Sydow B. 1974. D'Arcy Thompson's theorems and the shape of the molluscan shell. *Bulletin of Mathematical Biology* 36:567-575.
- Lv Z, Tek A, Da Silva F, Empereur-mot C, Chavent M, Baaden M. 2013. Game On, Science-How Video Game Technology May Help Biologists Tackle Visualization Challenges. *PLoS ONE* 8(3):e57990.

References

- Maassen WJM. 2001. Four new Diplommatinidae (Gastropoda, Prosobranchia, Diplommatinidae) from southern Thailand and northern Peninsular Malaysia. *Basteria* 65(1-3):51-56.
- Maassen WJM. 2002. Remarks on the Diplommatinidae from Sumatra, Indonesia, with descriptions of eleven new species (Gastropoda, Prosobranchia). *Basteria* 66: 163-182.
- Maddison DR, Guralnick R, Hill A, Reysenbach AL, McDade LA. 2012. Ramping up biodiversity discovery via online quantum contributions. *Trends in Ecology and Evolution* 27(2): 72-77. <http://dx.doi.org/10.1016/j.tree.2011.10.010>.
- Maddison WP, Maddison DR. 2011. *Mesquite: a modular system for evolutionary analysis*. Version 2.75 <http://mesquiteproject.org>
- Madruga Rios O, Hernández Quinta M. 2010. Larval Feeding Habits of the Cuban Endemic Firefly *Alecton discoidalis* Laporte (Coleoptera: Lampyridae). *Psyche: A Journal of Entomology* 2010:Article ID 149879, 5 pages, doi:10.1155/2010/149879
- Malayan Nature Society. 1991. *A conservation assessment of limestone hills in the Kinta Valley*. 210 pages.
- von Martens E, Thiele J. 1908. Beschreibung einiger im östlichen Borneo von Martin Schmidt gesammelten Land und Süßwasser-Conchylien. *Mitteilungen aus dem Zoologischen Museum in Berlin* 4: 251-294.
<http://www.biodiversitylibrary.org/item/44411#page/272/mode/1up>.
- Martin R, Bergey E. 2013. Growth plasticity with changing diet in the land snail *Patera appressa* (Polygyridae). *Journal of Molluscan Studies* 79(4):364-368.
- Martinez-Orti A, Arantzazu Elejalde M, Jose Madeira M, Gomez-Moliner B. 2008. Morphological and DNA-based taxonomy of *Tudorella* P. Fischer, 1885 (Caenogastropoda : Pomatiidae). *Journal of Conchology* 39(5):553-567.
- Maxted N. 1992. Towards defining a taxonomic revision methodology. *Taxon* 41: 653-660.
- Mayer G, Haug J, Maas A, Waloszek D. 2012. Functional aspects of the gammaridean mandibles with special reference to the lacinia mobilis (Crustacea, Amphipoda). *Zoologischer Anzeiger-A Journal of Comparative Zoology* 252:536-547.
- Mayr E. 1942. *Systematics and the Origin of Species: From the Viewpoint of a Zoologist*. Harvard University Press.
- McGhee GR. 1978. Analysis of the shell torsion phenomenon in the Bivalvia. *Lethaia* 11(4):315-329.
- McGhee GR. 1999. *Theoretical Morphology: the Concept and Its Applications*. Columbia University Press.
- McGhee GR. 2007. *The Geometry of Evolution: Adaptive Landscapes and Theoretical Morphospaces*. New York: Cambridge University Press.

References

- Meinhardt H. 2009. *The Algorithmic Beauty of Sea Shells*. Springer.
- Meireles LM, Silva LC, Junqueira FO, Bessa EC. 2008. The influence of diet and isolation on growth and survival in the land snail *Bulimulus tenuissimus* (Mollusca: Bulimulidae) in laboratory. *Revista Brasileira de Zoologia* 25(2):224-227 .
- Mesibov R. 2012. Known unknowns, Google earth, plate tectonics and Mt Bellenden Ker: some thoughts on locality data. *Zookeys* 247: 61-67.
<http://dx.doi.org/10.3897/zookeys.247.4195>.
- Miller J, Dikow T, Agosti D, Sautter G, Catapano T, Penev L, Zhang Z-Q, Pentcheff D, Pyle R, Blum S, Parr C, Freeland C, Garnett T, Ford LS, Muller B, Smith L, Strader G, Georgiev T, Bénichou L. 2012. From taxonomic literature to cybertaxonomic content. *BMC Biology* 10: 87. <http://dx.doi.org/10.1186/1741-7007-10-87>.
- Miller MA, Pfeiffer W, Schwartz T. 2010. *Creating the CIPRES Science Gateway for inference of large phylogenetic trees*. In Gateway Computing Environments Workshop (GCE), 2010: 1-8. <http://www.phylo.org/index.php/portal/>.
- von Moellendorff O. 1902. Binnenmollusken aus Hinterindien:1. Landschnecken von Kelantan, Ostküste der Halbinsel Malacca. *Nachrichtsblatt der Deutschen Malakozoologischen Gesellschaft* 34: 135-149.
<http://www.biodiversitylibrary.org/page/15598866#page/525/mode/1up>.
- Monnet C, Zollikofer C, Bucher H, Goudemand N. 2009. Three-dimensional morphometric ontogeny of mollusc shells by micro-computed tomography and geometric analysis. *Paleontologia Electronica* 12(3/12A):1-13.
- Mora C, Tittensor DP, Adl S, Simpson AGB, Worm B. 2011. How many species are there on earth and in the ocean? *PLoS Biology* 9(8): e1001127.
<http://dx.doi.org/10.1371/journal.pbio.1001127>.
- Moreno-Rueda G. 2009. Disruptive selection by predation offsets stabilizing selection on shell morphology in the land snail *Iberus g. gualtieranus*. *Evolutionary Ecology* 23(3):463-471.
- Morita R. 1991a. Finite element analysis of a double membrane tube (DMS-tube) and its implication for gastropod shell morphology. *Journal of Morphology* 207:81-92.
- Morita R. 1991b. Mechanical constraints on aperture form in gastropods. *Journal of Morphology* 207:93-102.
- Morita R. 1993. Development mechanics of retractor muscles and the “Dead Spiral Model” in gastropod shell morphogenesis. *Neues Jahrbuch für Geologie und Palaöontologie Abhandlungen* 190:191-217.
- Morita R. 2003. Why do univalve shells of gastropods coil so tightly? A head-foot guidance model of shell growth and its implication on developmental constraints. In: Sekimura T, Noji S, Ueno N, Maini PK, editors. *Morphogenesis and pattern formation in biological systems: experiments and models*. Tokyo: Springer. p 345–354.

References

- Moseley H. 1838. On the geometrical forms of turbinated and discoid shells. *Philosophical Transactions of the Royal Society of London* 128:351-370.
- Moulton DE, Goriely A. 2012. Surface growth kinematics via local curve evolution. *Journal of Mathematical Biology*: 1-28.
- Moulton DE, Goriely A, Chirat R. 2012. Mechanical growth and morphogenesis of seashells. *Journal of Theoretical Biology* 311:69-79.
- Nabhitabhata J. 2009. *Checklist of Molluscan Fauna in Thailand*. Office of Natural Resources and Environmental Policy and Planning, Bangkok, Thailand. 576 pages.
- Nakazawa M. 2012. *fmsb: Functions for Medical Statistics Book with Some Demographic Data. R package version 0.4.1*. <http://CRAN.R-project.org/package=fmsb>
- Newkirk GF, Doyle RW. 1975. Genetic analysis of shell-shape variation in *Littorina saxatilis* on an environmental cline. *Marine Biology* 30(3):227-237.
- Nishi H, Sota T. 2007. Geographical divergence in the Japanese land snail *Euhadra herklotsi* inferred from its molecular phylogeny and genital characters. *Zoological Science* 24(5):475-485.
- Norhanis MR, Aileen Tan SH, Zulfigar Y, Panha S, Sutcharit C, Tongkerd P. 2010. An annotated checklist of micro-landsnails from limestone areas in Langkawi Islands, Kedah, Peninsular Malaysia. *Malayan Nature Journal* 62(3): 307-313.
- Noshita K. 2010. Spiral Shell Form: A computer software package for theoretical morphological analysis of spiral shell form. *Geoscience reports of Shizuoka University* 37:57-73. (In Japanese)
- Noshita K, Asami T, Ubukata T. 2012. Functional constraints on coiling geometry and aperture inclination in gastropods. *Paleobiology* 38(2):322-334.
- Nylander JAA. 2004. MrModeltest 2.3 (program distributed by the author) Evolutionary Biology Centre. Uppsala University, Sweden.
<http://www.ebc.uu.se/systzoo/staff/nylander.html>.
- Okajima R, Chiba S. 2009. Cause of bimodal distribution in the shape of a terrestrial gastropod. *Evolution* 63(11):2877-2887.
- Okajima R, Chiba S. 2011. How does life adapt to a gravitational environment? The outline of the terrestrial gastropod shell. *The American Naturalist* 178(6):801-809.
- Okajima R, Chiba S. 2012. Adaptation from restricted geometries: the shell inclination of terrestrial gastropods. *Evolution* 67:429-437.
- Okamoto T. 1988. Analysis of heteromorph ammonoids by differential geometry. *Palaeontology* 31(1):35-52.

References

- Oliphant TE. 2007. Python for scientific computing. *Computing in Science & Engineering* 9(3):10-20.
- Olson SL, Hearty PJ. 2010. Predation as the primary selective force in recurrent evolution of gigantism in *Poecilozonites* land snails in Quaternary Bermuda. *Biology letters* 6(6):807-810.
- Oosterhoff LM. 1977. Variation in growth rate as an ecological factor in the landsnail *Cepaea nemoralis* (L.). *Netherlands Journal of Zoology* 27(1):1-132.
- Padial JM, Miralles A, De la Riva I, Vences M. 2010. The integrative future of taxonomy. *Frontiers in Zoology* 7: 16. <http://dx.doi.org/10.1186/1742-9994-7-16>.
- Page RDM. 2011. Extracting scientific articles from a large digital archive: Biostor and the Biodiversity Heritage Library. *BMC Bioinformatics* 12: 187. <http://dx.doi.org/10.1186/1471-2105-12-187>.
- Pagel M. 1999. Inferring the historical patterns of biological evolution. *Nature* 401:877-884.
- Palumbi SR. 1996. Nucleic acids II: the polymerase chain reaction. In Hillis DM, Moritz C, Mable BK (Eds.) *Molecular systematics*. Sunderland, MA, Sinauer Associates: 205-247.
- Panha S. 1996. A new species of *Opisthostoma* from Thailand (Prosobranchia: Cyclophoroidea: Diplommatinidae). *Malacological Review* 29: 133-134.
- Paradis E, Claude J, Strimmer K. 2004. APE: analyses of phylogenetics and evolution in R language. *Bioinformatics* 20(2):289-290.
- Park JK, Foighil DO. 2000. Sphaeriid and corbiculid clams represent separate heterodont bivalve radiations into freshwater environments. *Molecular Phylogenetics and Evolution* 14:75-88.
- Parmakelis A, Spanos E, Papagiannakis G, Louis C, Mylonas M. 2003. Mitochondrial DNA phylogeny and morphological diversity in the genus *Mastus* (Beck, 1837): a study in a recent (Holocene) island group (Koufonisi, south-east Crete). *Biological Journal of the Linnean Society* 78(3):383-399.
- Parmakelis A, Kotsakiozi P, Rand D. 2013. Animal mitochondria, positive selection and cyto-nuclear coevolution: insights from pulmonates. *PloSone*, 8(4): e61970. <http://dx.doi.org/10.1371/journal.pone.0061970>.
- Parr CS, Guralnick R, Cellinese N, Page RD. 2012. Evolutionary informatics: unifying knowledge about the diversity of life. *Trends in Ecology and Evolution* 27(2): 94-103. <http://dx.doi.org/10.1016/j.tree.2011.11.001>.
- Penev L, Agosti D, Georgiev T, Catapano T, Miller J, Blagoderov V, Roberts D, Smith VS, Brake I, Rycroft S, Scott B, Johnson NF, Morris RA, Sautter G, Chavan V, Robertson T, Remsen D, Stoev P, Parr C, Knapp S, Kress WJ, Thompson FC, Erwin T. 2010. Semantic tagging of and semantic enhancements to systematics papers: ZooKeys working examples. *ZooKeys* 50: 1-16. <http://dx.doi.org/10.3897/zookeys.50.538>.

References

- Penev L, Lyal CHC, Weitzman A, Morse DR, King D, Sautter G, Georgiev T, Morris RA, Catapano T, Agosti D. 2011. XML schemas and mark-up practices of taxonomic literature. *Zookeys* 150: 89-116. <http://dx.doi.org/10.3897/zookeys.150.2213>.
- Picado J. 2009. Seashells: the plainness and beauty of their mathematical description. *MAA Mathematical Sciences Digital Library*: 1-18.
- Price RM. 2003. Columellar muscle of neogastropods: muscle attachment and the function of columellar folds. *The Biological Bulletin* 25:351-366
- Puillandre N, Modica MV, Zhang Y, Sirovich L, Boisselier MC, Cruaud C, Holford M, Samadi S. 2012. Large-scale species delimitation method for hyperdiverse groups. *Molecular Ecology* 21(11): 2671-2691. <http://dx.doi.org/10.1111/j.1365-294X.2012.05559.x>.
- Puslednik L, Ponder WF, Dowton M, Davis AR. 2009. Examining the phylogeny of the Australasian Lymnaeidae (Heterobranchia: Pulmonata: Gastropoda) using mitochondrial, nuclear and morphological markers. *Molecular Phylogenetics and Evolution* 52(3):643-659.
- Pyka M, Hertog M, Fernandez R, Hauke S, Heider D, Dannlowski U, Konrad C. 2010. fMRI data visualization with BrainBlend and Blender. *Neuroinformatics* 8(1):21-31.
- Pyle RL, Michel E. 2008. ZooBank: Developing a nomenclatural tool for unifying 250 years of biological information. *Zootaxa* 1950: 39-50.
- Quensen III JF, Woodruff DS. 1997. Associations between shell morphology and land crab predation in the land snail *Cerion*. *Functional Ecology* 11(4):464-471.
- R Core Team. 2013. *R: A Language and Environment for Statistical Computing*. R Foundation for Statistical Computing, Vienna, Austria. URL <http://www.R-project.org>.
- Ratnasingham S, Hebert PD. 2007. BOLD: The Barcode of Life Data System (<http://www.barcodinglife.org>). *Molecular Ecology Notes* 7(3): 355-364.
- Raup DM. 1961. The geometry of coiling in gastropods. *Proceedings of the National Academy of Sciences of the United States of America* 47(4):602.
- Raup DM. 1966. Geometry analysis of shell coiling: general problems. *Journal of Paleontology* 40(5):1178-1190.
- Raup DM. 1967. Geometric analysis of shell coiling: coiling in ammonoids. *Journal of Paleontology* 41(1):43-65.
- Raup DM, Graus RR. 1972. General equations for volume and surface area of a logarithmically coiled shell. *Journal of the International Association for Mathematical Geology* 4:307-316.
- Raup DM, Michelson A. 1965. Theoretical morphology of the coiled shell. *Science* 147(3663):1294-1295.

References

- Relyea RA. 2003. How prey respond to combined predators: a review and an empirical test. *Ecology* 84(7):1827-1839.
- Revell LJ. 2012. phytools: an R package for phylogenetic comparative biology (and other things). *Methods in Ecology and Evolution* 3(2):217-223.
- Rice SH. 1998. The bio-geometry of mollusc shells. *Paleobiology* 24(1):133-149.
- Rodrigues ASL, Gray CL, Crowter BJ, Ewers RM, Stuart SN, Whitten T, Manica A. 2010. A global assessment of Amphibian taxonomic effort and expertise. *Bioscience* 60(10): 798-806. <http://dx.doi.org/10.1525/bio.2010.60.10.6>.
- Rohlf FJ, Archie JW. 1984. A comparison of Fourier methods for the description of wing shape in mosquitoes (Diptera: Culicidae). *Systematic Biology* 33(3):302-317.
- Rohlf FJ, Slice D. 1990. Extensions of the Procrustes method for the optimal superimposition of landmarks. *Systematic Biology* 39(1):40-59.
- RStudio. 2012. *RStudio: Integrated Development Environment for R* (Version 0.97.336), Boston, MA. URL <http://www.rstudio.org/>.
- Ruthensteiner B, Hess M. 2008. Embedding 3D models of biological specimens in PDF publications. *Microscopy Research and Technique* 71(11): 778-786. <http://dx.doi.org/10.1002/jemt.20618>.
- Salas C, Marina P, Checa AG, Rueda JL. 2012. The periostracum of *Digitaria digitaria* (Bivalvia: Astartidae): formation and structure. *Journal of Molluscan Studies* 78:34-43.
- Samadi S, David P, Jarne P. 2000. Variation of shell shape in the clonal snail *Melanoides tuberculata* and its consequences for the interpretation of fossil series. *Evolution* 54(2):492-502.
- Sanderson MJ, Donoghue MJ, Piel WH, Eriksson T. 1994. TreeBASE: a prototype database of phylogenetic analyses and an interactive tool for browsing the phylogeny of life. *American Journal of Botany* 81(6): 183.
- Sanderson MJ. 2002. Estimating absolute rates of molecular evolution and divergence times: a penalized likelihood approach. *Molecular Biology and Evolution* 19(1):101-109.
- Sarkar D. 2008. *Lattice: Multivariate Data Visualization with R*. Springer.
- Sasaki T. 2010. *Malacology*. University of Tokyo Press.
- Saunders WB, Shapiro EA. 1986. Calculation and simulation of ammonoid hydrostatics. *Paleobiology* 12(1):64-79.
- Saurin E. 1953. Coquilles nouvelles de l'Indochine. *Journal de Conchyliologie* 93: 113-120.
- Savazzi E. 1985. SHELLGEN: A BASIC program for the modeling of molluscan shell ontogeny and morphogenesis. *Computers & Geosciences* 11(5):521-530.

References

- Savazzi E. 1990. Biological aspects of theoretical shell morphology. *Lethaia* 23(2):195-212.
- Savazzi E. 1992. Shell construction, life habits and evolution in the gastropod *Velates*. *Palaeogeography, Palaeoclimatology, Palaeoecology* 99(3):349-360.
- Savazzi E. 1993. C++ classes for theoretical shell morphology. *Computers & Geosciences* 19(7): 931-964.
- Savazzi E. 1995. Theoretical shell morphology as a tool in construction morphology. *Neues Jahrbuch für Geologie und Paläontologie. Abhandlungen* 195:229-240.
- Savazzi E. 1996. Adaptations of Vermetid and Siliquariid gastropods. *Palaeontology* 39(1):157-177.
- Schilthuizen M. 2003. Sexual selection on land snail shell ornamentation: a hypothesis that may explain shell diversity. *BMC Evolutionary Biology* 3: 13. doi: 10.1186/1471-2148-3-13.
- Schilthuizen M, Rosli R, Ali AMM, Salverda M, van Oosten H, Bernard H, Ancrenaz M, Lackman-Ancrenaz I. 2003. The ecology and demography of *Opisthostoma (Plectostoma) concinnum* s.l. (Gastropoda: Diplommatinidae) on limestone outcrops along the Kinabatangan river. In: Maryati M, Takano A, Goossens B, Indran R, eds. *Lower Kinabatangan scientific expedition*. Kota Kinabalu: Universiti Malaysia Sabah. 55-71.
- Schilthuizen M, Chai HN, Kimsin TE, Vermeulen JJ. 2003b. Abundance and diversity of land-snails (Mollusca: Gastropoda) on limestone hills in Borneo. *Raffles Bulletin of Zoology* 51: 35-42. <http://rmbr.nus.edu.sg/rbz/biblio/51/51rbz035-042.pdf>.
- Schilthuizen M, Liew TS, Elahan BB, Lackman-Ancrenaz I. 2005. Effects of karst forest degradation on pulmonate and prosobranch land snail communities in Sabah, Malaysian Borneo. *Conservation Biology* 19: 949-954. <http://dx.doi.org/10.1111/j.1523-1739.2005.00209.x>.
- Schilthuizen M, Til A, Salverda M, Liew TS, James SS, Elahan B, Vermeulen JJ. 2006. Microgeographic evolution of snail shell shape and predator behavior. *Evolution* 60: 1851-1858. <http://dx.doi.org/10.1554/06-114.1>.
- Schilthuizen M, Clements R. 2008. Tracking extinction from space. *Tentacle* 16: 8-9.
- Schilthuizen M, Liew T-S. 2008. The slugs and semislugs of Sabah, Malaysian Borneo (Gastropoda, Pulmonata: Veronicellidae, Rathouisiidae, Ariophantidae, Limacidae, Philomycidae). *Basteria* 72(4-6):287-306.
- Schindel DE. 1990. Unoccupied morphospace and the coiled geometry of gastropods: architectural constraint or geometric covariation. In Ross, R. M. and Allmon W. D. (eds) *Causes of Evolution: A Paleontological Perspective*. University of Chicago Press, Chicago. Page 270-304.
- Seilacher A. 1991. Self-organizing mechanisms in morphogenesis and evolution. In: Schmidt-Kittler N, Vogel K, ed. *Constructional Morphology and Evolution*. Springer, 251-271.

References

- Seuss B, Nützel A, Scholz H, Frýda J. 2012. The Paleozoic evolution of the gastropod larval shell: larval armor and tight coiling as a result of predation-driven heterochronic character displacement. *Evolution & Development* 14(2):212-228.
- Signor PW, Kat PW. 1984. Functional significance of columellar folds in turrotelliform gastropods. *Journal of Paleontology* 58(1):210-216.
- Sih A, Englund G, Wooster D. 1998. Emergent impacts of multiple predators on prey. *Trends in Ecology & Evolution* 13(9):350-355.
- Silva L, Meireles L, Vargas Té, Junqueira FO, de Almeida Bessa EC. 2009. Life history of the land snail *Habroconus semenlini* (Stylommatophora: Euconulidae) under laboratory conditions. *Revista de Biologia Tropical* 57(4):1217-1222.
- Silva L, Meireles L, D'ávila S, Junqueira FO, de Almeida Bessa EC. 2013. Life history of *Bulimulus tenuissimus* (D'Orbigny, 1835) (Gastropoda, Pulmonata, Bulimulidae): effect of isolation in reproductive strategy and in resources allocation over their lifetime. *Molluscan Research* 33(2):75-79.
- Silva EC, Molozzi J, Callisto M. 2010. Size-mass relationships of *Melanoides tuberculatus* (Thiaridae: Gastropoda) in a eutrophic reservoir. *Zoologia* 27(5):691-695.
- Sluys R. 2013. The unappreciated, fundamentally analytical nature of taxonomy and the implications for the inventory of biodiversity. *Biodiversity and Conservation* 22(4): 1095-1105. <http://dx.doi.org/10.1007/s10531-013-0472-x>.
- Smith EA. 1893a. Note on the Genera *Geothauma* and *Gyrostropha*. *The Annals and Magazine of Natural History, including Zoology, Botany and Geology* 6(11): 284-285. <http://www.biodiversitylibrary.org/page/24344618#page/332/mode/1up>.
- Smith EA. 1893b. Descriptions of new species of land-shells from Borneo. *Journal of the Proceedings of the Linnean Society Zoology* 24: 341-352. <http://www.biodiversitylibrary.org/item/98716#page/361/mode/1up>.
- Smith EA. 1894. A list of the Bornean species of the genus *Opisthostoma* and descriptions of four new species. *The Annals and Magazine of Natural History, including Zoology, Botany and Geology* 6(14): 269-273. <http://biodiversitylibrary.org/item/78508#page/295/mode/1up>.
- Smith EA. 1904. Description of a new species of *Opisthostoma* from Borneo. *Proceedings of the Malacological Society of London* 6: 105. <http://www.biodiversitylibrary.org/item/52315#page/135/mode/1up>.
- Smith EA. 1905a. Description of a new species of *Opisthostoma* from North Borneo. *The Annals and Magazine of Natural History, including Zoology, Botany and Geology* 7(15): 360. <http://biodiversitylibrary.org/item/63423#page/404/mode/1up>.
- Smith EA. 1905b. Descriptions of three new species of *Opisthostoma* from Sarawak, North Borneo. *Proceedings of the Malacological Society of London* 6: 189-190. <http://biodiversitylibrary.org/item/52315#page/231/mode/1up>.

References

- Smith VS, Rycroft SD, Harman KT, Scott B, Roberts D. 2009. Scratchpads: a data-publishing framework to build, share and manage information on the diversity of life. *BMC Bioinformatics* 10: S6. <http://dx.doi.org/10.1186/1471-2105-10-S14-S6>.
- Solem A. 1966. Sacks of exotic dirt. *Bulletin Field Museum of Natural History* 37(6): 3-4. <http://www.biodiversitylibrary.org/page/4188033#page/36/mode/1up>.
- Solem A, Solem BK. 1976. Endodontoid land snails from Pacific Islands (Mollusca : Pulmonata : Sigmurethra). *Fieldiana. Zoology. Special Publications*. Part 1: 536. <http://www.biodiversitylibrary.org/item/20377#page/49/mode/1up>.
- Spight T, Lyons A. 1974. Development and functions of the shell sculpture of the marine snail *Ceratostoma foliatum*. *Marine Biology* 24(1):77-83.
- Stamatakis A. 2006. RAxML-VI-HPC: maximum likelihood-based phylogenetic analyses with thousands of taxa and mixed models. *Bioinformatics* 22(21): 2688-2690. <http://dx.doi.org/10.1093/bioinformatics/btl446>.
- Stamatakis A. 2014. RAxML Version 8: A tool for Phylogenetic Analysis and Post-Analysis of Large Phylogenies. *Bioinformatics* doi: 10.1093/bioinformatics/btu033
- Stankowski S. 2011. Extreme, continuous variation in an island snail: local diversification and association of shell form with the current environment *Biological Journal of the Linnean Society* 104(4):756-769.
- Stankowski S. 2013. Ecological speciation in an island snail: evidence for the parallel evolution of a novel ecotype and maintenance by ecologically dependent postzygotic isolation. *Molecular Ecology* 22:2726-2741.
- Stępień C. 2009. An IFS-based method for modelling horns, seashells and other natural forms. *Computers & Graphics* 33(4):576-581.
- Stone JR. 1996. Computer-simulated shell size and shape variation in the Caribbean land snail genus *Cerion*: a test of geometrical constraints. *Evolution* 50(1):341-347.
- Stone JR. 1997. Mathematical determination of coiled shell volumes and surface areas. *Lethaia* 30:213-219.
- Stone JR. 1999. Using a mathematical model to test the null hypothesis of optimal shell construction by four marine gastropods. *Marine Biology* 134:397-403.
- Stone JR. 2004. Nonoptimal shell forms as overlapping points in functional and theoretical morphospaces. *American Malacological Bulletin* 18:129-134.
- Stothard JR, Bremond P, Andriamaro L, Loxton NJ, Sellin B, Sellin E, Rollinson D. 2000. Molecular characterization of the freshwater snail *Lymnaea natalensis* (Gastropoda: Lymnaeidae) on Madagascar with an observation of an unusual polymorphism in ribosomal small subunit genes. *Journal of Zoology* 252:303-315.

References

- Sulikowska-Drozd A. 2011. Population dynamics of the Carpathian Clausiliid *Vestia gulo* (E. A. Bielz 1859) (Pulmonata: Clausiliidae) under various climatic conditions. *Journal of Conchology* 40(4):462-470.
- Suvorov AN. 1993. Problems of Functional Morphology of Ostium in Pupillacea Snails (Gastropoda Pulmonata). *Ruthenica* 3(2):141-152.
- Suvorov AN. 1999a. Functional Relations between Shell Structures and Soft Body in Lower Geophila. 1. Pupillina, Oleacinina. *Zoologicheskyy Zhurnal* 78(1):5-15.
- Suvorov AN. 1999b. Functional Relations between Shell Structures and Soft Body in Lower Geophila. 2. Achatinina. *Zoologicheskyy Zhurnal* 78(5):528-538.
- Suvorov AN. 2002. Prospects for studies of morphological variability of land pulmonate snails. *Biology Bulletin of the Russian Academy of Sciences* 29(1):455-467.
- Swofford D. 1998. *PAUP 4.0: phylogenetic analysis using parsimony*. Smithsonian Institution.
- Sykes ER. 1902a. Descriptions of six new land shells from the Malay Peninsula. *Journal of Malacology* 9: 22-23. <http://www.biodiversitylibrary.org/item/89648#page/202/mode/1up>.
- Sykes ER. 1902b. On a collection of land and fresh water shells from Kelantan, Malay Peninsula. *Journal of Malacology* 9: 60-63. <http://www.biodiversitylibrary.org/item/89648#page/240/mode/1up>.
- Sykes ER. 1903. On the land operculate Mollusca collected during the "Skeat Expedition" to the Malay Peninsula in 1899-1900. *Proceedings of the Zoological Society of London* 1903: 194-199. <http://www.biodiversitylibrary.org/item/98587#258>.
- Takano A, Goossens B, Indran R, ed. *Lower Kinabatangan scientific expedition*. Universiti Malaysia Sabah, Kota Kinabalu, 55-71.
- Tamura K, Peterson D, Peterson N, Stecher G, Nei M, Kumar S. 2011. MEGA5: molecular evolutionary genetics analysis using maximum likelihood, evolutionary distance, and maximum parsimony methods. *Molecular Biology and Evolution* 28(10): 2731-2739. doi: 10.1093/molbev/msr121.
- Tan SK, Chan SY. 2009. New records of predatory slugs from Singapore with notes on their feeding behaviour. *Nature in Singapore* 2:1-7.
- Terhivuo J. 1978. Growth, reproduction and hibernation of *Arianta arbustorum* (L.) (Gastropoda, Helicidae) in southern Finland. *Annales Zoologici Fennici* 15:8-16
- Teshima H, Davison A, Kuwahara Y, Yokoyama J, Chiba S, Fukuda T, Ogimura H, Kawata M. 2003. The evolution of extreme shell shape variation in the land snail *Ainohelix editha*: a phylogeny and hybrid zone analysis. *Molecular Ecology* 12(7):1869-1878
- Thompson D. 1917. *On growth and form*. Cambridge University Press, Cambridge.

References

- Thompson JT, Lowe AD, Kier WM. 1998. The columellar muscle of prosobranch gastropods: morphological zonation and its functional implication. *Invertebrate Biology* 117(1):45-56.
- Thornton IW. 1997. *Krakatau: the destruction and reassembly of an island ecosystem*. Harvard University Press.
- Tissot BN. 1988. Geographic variation and heterochrony in two species of cowries (genus *Cypraea*). *Evolution* 42(1):103-117.
- le Tomlin JRB. 1938. New Malay land shells. *Journal of Conchology* 21: 73-75.
- le Tomlin JRB. 1948. New Malay land-shells. *Proceedings of the Malacological Society of London* 27: 224-225.
- Tongkerd P, Lee T, Panha S, Burch J, Foighil D. 2004. Molecular phylogeny of certain Thai gastrocoptine micro land snails (Stylommatophora : Pupillidae) inferred from mitochondrial and nuclear ribosomal DNA sequences. *Journal of Molluscan Studies* 70(2):139-147.
- Ubukata T. 2001. Stacking increments: a new model and morphospace for the analysis of bivalve shell growth. *Historical Biology: A Journal of Paleobiology* 15(4):303-321.
- Umiński T. 1975. Life cycles in some Vitrinidae (Mollusca, Gastropoda) from Poland. *Annales Zoologici Fennici* 33(2):1-16.
- Urduy S, Goudemand N, Bucher H, Chirat R. 2010. Allometries and the morphogenesis of the molluscan shell: a quantitative and theoretical model. *Journal of Experimental Zoology Part B: Molecular and Developmental Evolution* 314(4):280-302.
- Urduy S, Goudemand N, Bucher H, Chirat R. 2010. Growth-dependent phenotypic variation of molluscan shells: implications for allometric data interpretation. *Journal of Experimental Zoology Part B: Molecular and Developmental Evolution*, 314B:303-326.
- Urduy S, Wilson LA, Haug JT, Sánchez-Villagra MR. 2013. On the Unique Perspective of Paleontology in the Study of Developmental Evolution and Biases. *Biological Theory* 8(3):293-311.
- Venables WN, Ripley BD. 2002. *Modern Applied Statistics with S*. Springer.
- Verduin A. 1982. How complete are diagnoses of coiled shells of regular build? A mathematical approach. *Basteria* 45(6):127-142.
- Vermeij GJ. 1971. Gastropod evolution and morphological diversity in relation to shell geometry. *Journal of Zoology* 163(1):15-23.
- Vermeij GJ. 1977. The Mesozoic marine revolution: evidence from snails, predators and grazers. *Paleobiology* 3(3):245-258.
- Vermeij GJ, Covich AP. 1978. Coevolution of freshwater gastropods and their predators. *American Naturalist* 112:833-843.

References

- Vermeij GJ. 1980. Gastropod shell growth rate, allometry, and adult size: environmental implications. In: Rhoads DC, Lutz RA, ed. *Skeletal growth of aquatic organisms: biological records of environmental change*. Plenum Publishing Corporation, New York., 379-394.
- Vermeij GJ. 1982. Unsuccessful predation and evolution. *American Naturalist* 120(6):701-720.
- Vermeij GJ. 1987. *Evolution and Escalation*. Princeton University Press, Princeton.
- Vermeij GJ. 1993. *A natural history of shells*. Princeton University Press, Princeton.
- Vermeij GJ. 2002. Characters in context: molluscan shells and the forces that mold them. *Paleobiology* 28(1):41-54.
- Vermeulen JJ. 1991. Notes on the non-marine molluscs of the island of Borneo 2. The genus *Opisthostoma* (Gastropoda Prosobranchia: Diplommatinidae), part 1. *Basteria* 55: 139-163.
- Vermeulen JJ. 1994. Notes on the non-marine molluscs of the island of Borneo. 6. The genus *Opisthostoma* (Gastropoda Prosobranchia: Diplommatinidae), part 2. *Basteria* 58(3-4): 73-191.
- Vermeulen JJ, Clements R. 2008. Another twist in the tale: a new species of *Opisthostoma* (Gastropoda, Diplommatinidae) from Peninsular Malaysia. *Basteria* 72: 263-266.
- Wada S, Chiba S. 2013. The Dual Protection of a Micro Land Snail against a Micro Predatory Snail. *PloS one* 8(1):e54123.
- Wägele H, Klussmann-Kolb A, Kuhlmann M, Hasprunar G, Lindberg D, Koch A, Wägele JW. 2011. The taxonomist – an endangered race. A practical proposal for its survival. *Frontiers in Zoology* 8: 25. <http://dx.doi.org/10.1186/1742-9994-8-25>.
- Wagge LE. 1951. The activity of amoebocytes and of alkaline phosphatases during the regeneration of the shell in the snail, *Helix aspersa*. *Quarterly Journal of Microscopical Science* 92:307-321.
- Wagner P, Erwin D. 2006. Patterns of convergence in general shell form among Paleozoic gastropods. *Paleobiology* 32(2):316-337.
- Wang Y, Fu X, Lei C, Jeng ML, Nobuyoshi O. 2007. Biological Characteristics of the Terrestrial Firefly *Pyrocoelia pectoralis* (Coleoptera: Lampyridae). *The Coleopterists Bulletin* 61(1):85-93.
- Warburton K. 1979. Variation in shell geometry in the genus *Lacuna* (Prosobranchia: Lacunidae). *Journal of Natural History* 13(3):385-391.
- Waterstradt J. 1902. Kelantan and my trip to Gunong Tahan. *Journal of the Straits Branch of the Royal Asiatic Society* 37(4): 1-27.
<http://www.biodiversitylibrary.org/item/130392#page/24/mode/lup>.

References

- Webb CO, Slik JWF, Triono T. 2010. Biodiversity inventory and informatics in Southeast Asia. *Biodiversity and Conservation* 19: 955-972. <http://dx.doi.org/10.1007/s10531-010-9817-x>.
- Webster NB, van Dooren TJM, Schilthuizen M. 2012. Phylogenetic reconstruction and shell evolution of the Diplommatinidae (Gastropoda: Caenogastropoda). *Molecular Phylogenetics and Evolution* 63: 625-638. <http://dx.doi.org/10.1016/j.ympev.2012.02.004>.
- Wheeler QD, Knapp S, Stevenson DW, Stevenson J, Blum SD, Boom BM, Borisy GG, Buizer JL, de Carvalho MR, Cibrian A, Donoghue MJ, Doyle V, Gerson EM, Graham CH, Graves P, Graves SJ, Guralnick RP, Hamilton AL, Hanken J, Law W, Lipscomb DL, Lovejoy TE, Miller H, Miller JS, Naeem S, Novacek MJ, Page LM, Platnick NI, Porter-Morgan H, Raven PH, Solis MA, Valdecasas AG, van Der Leeuw S, Vasco A, Vermeulen N, Vogel J, Walls RL, Wilson EO, Woolley JB. 2012. Mapping the biosphere: exploring species to understand the origin, organization and sustainability of biodiversity. *Systematics and Biodiversity* 10(1): 1-20. <http://dx.doi.org/10.1080/14772000.2012.665095>.
- Wilbur KM, Owen G. 1964. Growth. In: Wilbur KM, Yonge CM, ed. *Physiology of Mollusca*. Academic Press, New York, 211-242.
- Wilson EO. 2003. The encyclopedia of life. *Trends in Ecology and Evolution* 18(2): 77-80. [http://dx.doi.org/10.1016/S0169-5347\(02\)00040-X](http://dx.doi.org/10.1016/S0169-5347(02)00040-X).
- Wilson EO. 2004. Taxonomy as a fundamental discipline. *Philosophical Transactions of the Royal Society of London. Series B: Biological Sciences* 359(1444): 739-739. <http://dx.doi.org/10.1098/rstb.2003.1440>.
- Winston JE. 1999. *Describing species: practical taxonomic procedure for biologists*. Columbia University Press.
- Wu M, Guo JY, Wan FH, Qin QL, Wu Q, Wiktor A. 2006. A preliminary study on the biology of the predatory terrestrial mollusk *Rathouisia leonina*. *Veliger* 48(2):61-74.
- Yesson C, Brewer PW, Sutton T, Caithness N, Pahwa JS, Burgess M, Gray WA, White RJ, Jones AC, Bisby FA, Culham A. 2007). How global is the global biodiversity information facility? *PLoS one* 2(11): e1124. <http://dx.doi.org/10.1371/journal.pone.0001124>.
- Zhang ZQ. 2008. Contributing to the progress of descriptive taxonomy. *Zootaxa* 1968: 65-68.

Curriculum Vitae

Liew Thor Seng was born on the 19th of December, 1980 in Johor Bahru, Johor, Malaysia. He received his early education in Kulai, Johor. After he obtained his Malaysian Higher School Certificate, he enrolled in a Conservation Biology undergraduate course at Universiti Malaysia Sabah (UMS), Kota Kinabalu. Up until that point, he was ignorant about biodiversity, though he grew up in one of Earth's biodiversity hotspots. After he completed the undergraduate course in September 2004, he started his Master of Science in Tropical Biology and Conservation Institute, UMS later that year. In September 2006, he completed his Master of Science with a dissertation *Analytical Biogeography of Land Snails of Mount Kinabalu*, under the supervision of Dr. Menno Schilthuizen. Since then, he succumbed to his scientific curiosity and started his journey exploring, investigating, and learning about tropical biodiversity. He worked as a part-time tutor and a research assistant at UMS between 2006 and 2008. During the same period, he stayed a total of six months in the Netherlands and worked in Naturalis Biodiversity Center under the Martin Fellowship. In June 2008, he worked as a tutor in the Tropical Biology and Conservation Institute in UMS. In March 2010, he started his PhD in Institute for Biology at Leiden University and obtained a Rubenstein Fellowship (Encyclopedia of Life) to support his project. His PhD project was supervised by Prof. Dr. Menno Schilthuizen and was supported by Netherlands Organisation for Scientific Research (NWO, ALW 819.01.012). The results he obtained during his candidature are documented in this thesis. He will continue his career in Malaysia with the Tropical Biology and Conservation Institute in UMS.

Publications

Liew TS, Schilthuizen M. 2014. Association between shell morphology of micro-land snails (genus *Plectostoma*) and their predator's predatory behaviour. *PeerJ* 2:e329.

Liew TS, Vermeulen JJ, bin Marzuki ME, Schilthuizen M. 2014. A cybertaxonomic revision of the micro-land snail genus *Plectostoma* Adam (Mollusca, Caenogastropoda, Diplommatinidae), from Peninsular Malaysia, Sumatra and Indochina. *ZooKeys* 393:1–107.

Schilthuizen M, **Liew TS**, Liew TH, Berlin P, King JP, Lakim M. 2013. Species diversity patterns in insular land snail communities of Borneo. *Journal of the Geological Society* 170(3):539-545.

Koene JM, **Liew TS**, Montagne-Wajer K, Schilthuizen M. 2013. A Syringe-Like Love Dart Injects Male Accessory Gland Products in a Tropical Hermaphrodite. *PloS one* 8(7):e69968.

Liew TS, Schilthuizen M, Lakim M. 2010. The determinants of land snail diversity along a tropical elevational gradient: insularity, geometry and niches. *Journal of Biogeography* 37(6):1071-1078.

Liew TS, Schilthuizen M, Vermeulen JJ. 2009. Systematic revision of the genus *Everettia* Godwin-Austen, 1891 (Mollusca: Gastropoda: Dyakiidae) in Sabah, northern Borneo, *Zoological Journal of the Linnean Society* 157(3):515-550.

Curriculum Vitae

Schilthuizen M, **Liew TS**. 2008. The slugs and semislugs of Sabah, Malaysian Borneo (Gastropoda, Pulmonata: Veronicellidae, Rathouisiidae, Ariophantidae, Limacidae, Philomycidae). *Basteria* 72(4-6):287-306.

Liew TS, Clements R, Schilthuizen M. 2008. Sampling micromolluscs in tropical forests: one size does not fit all. *Zoosymposia* 1:271-280.

Clements R, **Liew TS**, Vermeulen JJ, Schilthuizen M. 2008. Further twists in gastropod shell evolution. *Biology Letters* 4(2):179-182.

Schilthuizen M, Til, A van, Salverda M, **Liew TS**, James SS, Elahan BB, Vermeulen JJ. 2006. Microgeographic evolution of snail shell shape and predator behaviour. *Evolution* 60(9):1851-1858.

Schilthuizen M, **Liew TS**, Elahan BB, Lackman-Ancrenaz I. 2005. Effects of karst forest degradation on pulmonate and prosobranch land snail communities in Sabah, Malaysian Borneo. *Conservation Biology* 19(3):949-954.

